GEOLOGY, GEOCHEMISTRY AND GOLD MINERALIZATION IN THE MADRID CORRIDOR, HOPE BAY VOLCANIC BELT, NUNAVUT, CANADA

(Spine title: Geology of the Madrid Gold Deposit, Hope Bay Volcanic Belt)

by
Ronnie Therriault
Department of Earth Sciences

Submitted in partial fulfillment
of the requirements for the degree of
Master of Geology

Faculty of Graduate Studies
The University of Western Ontario
London, Ontario
February, 2006

ABSTRACT

The Hope Bay Volcanic Belt (HBVB) is a north-south striking mafic volcanic greenstone belt in the northeastern Slave Province. Mineralized mafic flows divide into two lithotectonic packages. Komatiitic basalts exhibit elevated Fe-Ti-Cr-Ni, incompatible element enrichment and a within-plate basalt signature. High-Fe tholeiitic basalts have lower Fe-Ti-Cr-Ni values and a primitive tholeiitic island arc signature. Together, these two packages represent a plume influenced subduction environment.

The interface between these two units was the focus of early deformation giving rise to the Hope Bay Deformation Zone (HBDZ). The HBDZ controls the distribution of gold mineralization at Madrid with all deposits occurring adjacent to the structure. An early high-temperature alteration event syn/predating the intrusion of the 2686 Ma Wolverine Porphyry is characterized by K-metasomatism, phengite formation and magnesite/ankerite blastesis. Early alteration softened the rocks, making them amenable to late D_2 mineralization. This corresponds to the main Au event characterized by Na-metasomatism, paragonite growth, and Au-W enrichment.

Keywords: Madrid, Hope Bay Volcanic Belt, hydrothermal gold, komatiite, plume influenced subduction zone, white mica, porphyry, deformation zone

ACKNOWLEDGEMENTS

The author wishes to thank the numerous people and organizations that have offered support toward the construction of this thesis.

I wish to thank my family for their moral and financial support over the course of the last two years. Their understanding and encouragement have not gone unappreciated. I would like to thank my friends within the Earth Sciences department at UWO. Specifically Jeff Cormier and Sarah Johnston kept me entertained but driven over the past two years. I wish to thank my advisor, Dr. Norm Duke. Time spent pouring over core, chats over beers concerning 'what the hells a komatiite anyway?' and critical draft reviews went a long way to improving the final copy of this thesis. Dr. Howard Poulson and Mike Young are thanked for their time spent in the field deciphering various aspects of the Madrid deposit and for a great many additions to the Madrid geology map. Much gratitude is expressed toward Peter Kleespies for the tremendous amount of time he spent with me studying drillcore, printing out sections and maps and chatting about Madrid geology. Richard Beck, Josh Gladstone, Frank Ratte, Stacey Lopson, Al Turner and many other Miramar personnel are thanked for their input on Naartok and Suluk geology as well as their receptiveness and friendliness during my time at Windy Lake. Forgive me for not naming you all! Dr. Ross Sherlock is thanked for his input on several important facets of my thesis. Despite the fact that we don't agree on certain aspects, your critical comments kept me focused and forced me to improve. Dr. Robert Carpenter is thanked for the time he spent with me looking at core, walking the hills of Madrid and discussions on lithogeochemistry. Darren Lindsay is thanked for providing me with sections and maps over the course of my thesis. The Miramar Mining Corporation is thanked for their financial support as well as providing me with abundant lithogeochemical, drillcore and cartographic data. NSERC is acknowledged for their financial contribution toward the project. Finally, CNGO is thanked for their financial and logistical support in the first summer of my thesis.

CHAPTER 3

MADRID CORRIDOR GEOLOGY

CHAPTER 4

LITHOGEOCHEMISTRY

CHAPTER 5

MINERAL CHEMISTRY

CHAPTER 6

DISCUSSION

CHAPTER 7

CONCLUSIONS

LIST OF PHOTOGRAPHIC PLATES

LIST OF FIGURES

LIST OF TABLES

LIST OF APPENDICIES

CHAPTER 1

INTRODUCTION

1.1 – General Statement and Purpose of Thesis

The recent upward trend in metal prices and the closure of several northern Canadian mines (Lupin, Polaris, Nanisivik, Con and Giant) has lead to a flurry of gold, base metal and diamond exploration in the Northwest Territories and Nunavut. Most of the gold exploration is focused on mesothermal quartz-carbonate shear/vein hosted Au deposits occurring in various Archean greenstone belts and in banded iron formation hosted gold within granite-metasedimentary terranes.

One of the most promising new gold targets of northern Canada lies within the Hope Bay Volcanic Belt (HBVB) in northwestern Nunavut. The Miramar-owned HBVB has been intensely explored over the past decade and as a result is nearing production stage. Three major gold deposits (Doris, Madrid and Boston) have been identified in the belt. The northernmost Doris deposit has measured and indicated reserves of 763 000 tonnes at 23.9 g/t with a total contained gold content of 586 000 oz. (Miramar Mining Corporation, 2003). The southernmost Boston deposit has measured and indicated reserves totaling 1 387 000 t at 15.4 g/t gold amounting to 687 000 oz. (Miramar Mining Corporation, 2003). The Madrid deposit, which is the topic of this thesis, is located approximately 10 km south of Doris and 50 km north of the Boston deposits. The Madrid system consists of quartz-carbonate-albite-pyrite veins and stockworks which overprint ankerite-sericite altered Fe-Ti rich komatiites and komatiitic basalts. At Madrid several mineralized zones (Naartok, Perrin, Rand, Suluk) occur adjacent to a major

mylonitic schist shear zone here called the Hope Bay Deformation Zone (HBDZ). Measured and indicated resources total 4 703 000 tonnes grading 5.5 g/t for a total of 838 000 oz. of gold (Miramar Mining Corporation, 2003).

The Miramar Mining Corporation has spent considerable effort over the past four years on understanding the geology of the Madrid deposits, however; this is the first M.Sc. thesis to be completed on the deposit. The intent of this thesis is to characterize features of the HBDZ that are relevant to Au mineralization. This will entail detailed petrology of volcanic hostrocks, stratigraphy, associated hydrothermal alteration and gold mineralization. Special focus is placed on the type, distribution and geochemical signatures of the alteration assemblages associated with the Au mineralization.

1.2 – Sources of Data and Methodology

Outcrop mapping, diamond drillcore logging and rock sampling followed by petrographic examination supported by bulk rock lithogeochemical analyses and mineral chemistry constitute the database for this thesis. Geological mapping, core logging and sampling were conducted during the summers of 2003 and 2004. A total of 130 thin sections were prepared from collected samples for petrographic study. Description of primary igneous and secondary alteration assemblages, mineral paragenesis and ore mineral relationships were described and form the bulk of Chapter 3. The majority of whole rock data was provided courtesy of the Miramar Mining Corporation and this was supplemented by 26 samples collected by the author. The former dataset was completed by ALS Chemex in Vancouver. Major elements were calculated by XRF (geochemical package ME-XRF06) and trace elements by ICP-MS (geochemical package ME-MS81).

The latter analyses were determined by fusion ICP and ICP-MS at Activation Laboratories (Code 4E-Research package). Major and trace element lithogeochemistry is discussed in Chapter 4. A number of thin-section samples were analyzed by WDS and EDS on a JEOL JXA 8600 electron microprobe directed by Dr. Menghua Liu at The University of Western Ontario. Mineral chemistry of white mica, carbonate, chlorite, clinopyroxene, amphibole, epidote, feldspar and sulphides are presented in Chapter 5.

1.3 – Exploration History

Exploration in the HBVB was initiated following the reconnaissance mapping at 1:560 880 in 1962 by Fraser (1964) of the Geological Survey of Canada. The following brief summary of exploration within the belt relies heavily on the chronologies provided by Reid (1987), Gebert (1993; 1999) and Agnerian (2003) and also includes information from other informal internal reports. Past exploratory activities include:

1964-1966: Exploration by the Robert's Mining Company (RMC) in the northern part of the HBVB resulted in the detection of the Discovery and Ida Point gold showings and the Ida Bay silver showing. International Mine Services staked the CIC claim group.

1967-1969: In 1967, Radiore Uranium Mines (RUM) staked the Rad showing, a high-grade quartz vein with up to 2.0 oz/ton Au over approximately 0.5 meters. The Hope Bay Syndicate acquired all of RMC's claims and initiated a three-year belt-wide prospecting program. Fifty drillholes were completed by the syndicate on the Ida Bay, Ida Point and Robert's Lake showings.

1972-1974: The Hope Bay Mining Company acquired a four-year lease from the Hope Bay Syndicate and RMC on 121 adjoining claims and initiated mine development at the

Ida Bay silver showing in 1973. Disappointing results led the company to shift mining activities to the Robert's Lake showing where a 400-foot decline was driven. Approximately ten tons of hand-cobbled ore were extracted, grading at 4.863 oz/ton silver. A 50 to 75 tons-per-day mill was constructed in 1974 and production proceeded at 14 tons/day until September. Total production was reported to be in excess of 100 000 oz. of silver.

1976: Perry River Nickel Mines reported >1 oz/ton Au in quartz veins on the Lahti showing.

1977: Noranda commenced a reconnaissance VMS exploration program in the belt.

1980-1981: Ida Point minerals and RMC entered into an agreement to reassess existing claims, stake more ground and carry out drilling on the Ida Bay silver showing. Noranda flew 2 809 km of airborne EM and magnetic surveys over the belt. This was followed up by geological mapping, ground magnetic/HLEM surveys and claim staking where anomalies were identified. Drilling by Noranda on the Cope base metal showing produced results of 0.53% Cu, 1.8% Zn, 0.16 oz/ton Ag and 0.008 oz/ton Au over 3.5 m.

1982-1983: Noranda entered into a joint venture agreement with Ida Point Mineral and Lynx Canada Exploration to follow up work on Ida Point's claims. Noranda carried out gravity profiles over promising EM targets and tested these with 450 m of BQ drilling.

1987: The Abermin Corporation obtained a 100% interest in RMC mining and RUM's Mining Lease and surrounding properties. They staked all known gold showings in the belt and began exploration in the north part of the belt.

1988-1989: Abermin staked the SPYDER claims over a large carbonated shear zone and McSPOT claims over the previously identified Doris Lake quartz vein. BHP Minerals

Canada Ltd. conduced a small reconnaissance program, exploring unstaked portions of the belt to evaluate the potential for gold mineralization. Abermin discontinued exploration in the belt in 1989.

1990: Norex (Noranda) completed an I.P. survey over the Granite and Wombat showings. Three holes were drilled on the Wombat showing later that year. Hole WBT-90-3 encountered a three-meter interval grading between 50-69 g/ton Au. Despite this, Noranda decided to abandon the property. BHP staked the KAMIK claims, covering a carbonate altered zone toward the middle of the belt.

1991: CSA Management Ltd. and Goldcorp Investments Ltd. acquired Abermin's KOIG/WOG properties as well as the Robert's Mining Lease. Several holes were drilled on the Wombat showings late in the season. BHP staked the SANTIAGO, HAVANA, MADRID and BOSTON (1-7) claims. They began geological mapping and sampling on the BOSTON property and continued exploration on unclaimed areas in the HBVB and the Elu Inlet Volcanic Belt (EIVB).

1992: BHP carried out an 11 week exploration program on properties within the belt. They initiated a drilling program on the BOSTON claims, targeting a carbonated shear zone with anomalous gold. Additional BOSTON claims (8-13) were staked.

1993: BHP staked the AMAROK, BUFFALO, CHICAGO, QUITO and BOSTON (14-17) claims. Mapping of newly acquired claims and continued drilling on the BOSTON claims was completed. Southern Copper Corporation staked the SY claims to the south and east of BOSTON and initiated mapping and sampling to assess the potential for gold and diamonds.

1994: BHP continued drilling at BOSTON and initiated drilling on the MADRID

property. Promising results were obtained from MADRID, but strike length was poor. BHP staked the UMINGMAK, TOK (1-4) and BOSTON (18-20) claims and completed a partial airborne aeromagnetic survey over their properties. BHP entered into a five year joint venture agreement with CSA Goldcorp to explore the KOIG/WOG claims.

1995: BHP staked the AKUNGANI (1-9), Engine (1-2) and AMAROK (9-13) claims. Additional airborne aeromagnetic surveys were flown to complete coverage over all claims. Mapping and sampling continued on the AMAROK, TOK, KOIG and AKUNGANI claims, and drilling was completed at the BOSTON, KOIG, KAMIK, MADRID and TOK claims. Early drilling on the Doris Lake property yielded very promising results. William Jopson staked the KNIFE claim NE of Boston.

1996: BHP drove a decline at BOSTON in order to obtain a bulk sample. Drilling continued at TOK and MADRID and began at AMAROK. Reinterpretation of MADRID geology gave rise to better placed drillholes and increased potential for the claims. Gopher drilling commenced on the KOIG 4, BUFFALO and UMINGMAK claims. Mapping and sampling continued on the TOK, UMINGMAK and AKUNGANI claims. A regional till sampling program completed by BHP revealed anomalous gold under the southwest arm of Patch Lake. BHP staked the PJ, BOSTON (21-22) and TOK (5-6) claims.

1997: BHP continued and completed the bulk sampling project at BOSTON, removing a 26 761 ton sample. Drilling continued at BOSTON, TOK, MADRID, KOIG and AKUNGANI. Discovery holes were drilled in the Central Doris and South Patch Shear Zone. The regional till sampling program was completed and the area between the Doris Deposit and UMINGMAK was mapped in detail. Gopher drilling was carried out on the

AKUNGANI 1, QUITO, and TOK claims. BHP staked the TOK 7 claim. Navigator Resources staked the ORO claims in the northern part of the belt, encompassing RBM's lapsed claims.

1998: 10 500 m of drilling was completed in the Boston area and 25 000 m were completed in the north part of the belt (Madrid and Doris) including 6,100 m of RC drilling. The Northern and Central resources of Doris were connected indicating approximately 3 km of strike length. A 5 534 km aeromagnetic survey was flown between Boston and Doris.

1999: Cambiex Exploration Inc. optioned the Hope Bay project from BHP. Miramar acquired a 50% interest in the Hope Bay Project from Cambiex and formed the Hope Bay Joint Venture (HBJV). The HBJV completed approximately 40 000 m of drilling in the Doris and Boston area. Cambiex changed its name to the Hope Bay Gold Corp Inc.

2000: A total of 44 643 m of drilling was completed by HBJV in the Boston and Doris area including 7 944 m of exploration drilling.

2001: 39 829 m of exploration drilling was conducted resulting in the discovery of the Naartok and Suluk deposits adjacent to the Madrid system.

2002: Miramar Hope Bay Ltd. merged with Hope Bay Gold Corp. Inc. placing control of the belt in MHBL. A total of 25 796 m of drilling was conducted on the South Patch, Madrid, Doris South and Twin Peaks areas. The Marianas trend was discovered north of South Patch. Reverse circulation drilling was carried out on the Twin Peaks, Nexus, Amarok 5 and Gas Cache claims. Smaller drilling/sampling projects were carried out in the North Patch area on the northern limit of the Patch system, on the QSP trend to assess

the potential for Au enriched VMS systems and on the Twin Peaks-Clover Lake area to test the theory of a Temiskaming type Au setting.

2003: Significant Au intercepts were discovered below existing resources at Boston. Infill drilling at Suluk increased strike length and depth extent of known mineralized lenses. Less intense drilling was conducted along the HBDZ south of Suluk (Patch Lake South) and at Rand and Perrin. Regional mapping and prospecting was conducted at numerous showings south of Madrid and along the granite contact northeast of Madrid. Reverse circulation drilling programs were carried out at prospective overburden covered areas (QSP, and Gas-Cache).

2004: Expansion and infill drilling focused on the Naartok area of the Madrid deposit was accompanied by additional expansion and exploration drilling at Boston to better define resources. The Doris project proposal was submitted to the Nunavut Impact Review Board. Additional work was completed in the Doris North area in anticipation of a near-future mine. Mapping and sampling programs were carried out at Madrid, Maximus, Boston and Chicago.

2005: Drilling was focused on the Naartok area of the Madrid system where approximately 15 533 m of drillcore from 58 holes were completed. Focus was placed on confirming and expanding a high-grade mineralization zone (11.5 g/t over 64.2 m) identified in a single drill hole earlier in the year. 11 370 m of core were drilled to infill and expand the Naartok deposit. The eastern part of the Naartok system was expanded 200 m to the north. Meetings in August between Miramar and the Nunavut Impact Review Board were held to review issues and concerns regarding the Doris North project proposal in preparation for the final Environmental Impact Statement.

1.4 – Previous Work

The majority of information on the HBVB is in the form of internal reports completed by company and contract geologists. A number of recent government reports and two theses have also been completed in the belt. Countless year-end reports and site-specific studies have been completed, many of which are not relevant to this study. The most significant of these documents are included below:

The general geology of the belt has been described by Fraser (1964), Gibbons (1987), Gebert (1989a/b, 1990a/b, 1992, 1993, 1999), Poulson (2002c, 2003b), Sherlock and Lindsay (2002), Sherlock *et al.* (2003), and Sherlock and Carpenter (2003). Alteration and mineralization have been discussed by Getsinger (1997), Reid and Gerakiteys (1998), Carpenter and Sherlock (2001), Kleespies and Mercer (2001), Sherlock *et al.* (2002), Poulson (2002c, 2003a), Carpenter *et al.* (2003) and Mann (2003). The structural geology has been addressed by Gebert (1993, 1999), Simpson (2001), Stubley (2002), Poulson (2002b, 2004), Sherlock *et al.* (2002, 2003) and Sherlock and Carpenter (2003). Relevant lithogeochemistry studies of the volcanic flows and alteration assemblages are discussed by Gebert (1993, 1999), Hebel (1999), Carpenter and Sherlock (2001), Kleespies and Mercer (2001) and Poulson (2002a, 2003a). Geochronology studies of the felsic volcanic rocks and flanking granites have been completed by Bevier and Gebert (1991), Hebel (1999) and unpublished internal data. Marginal granitic rocks have been studied by Thompson (1996, 1997). Studies of the Doris deposit have been completed by Tyler (1997) and Carpenter *et al.* (2003) and the Boston deposit by Gebert (1993, 1999), Clark (1996), Stemler (2000) and Sherlock and Sandeman (2004a/b). The Ida Point showing has been discussed by LeClair (1990a/b/c,

1991, 1992). The Madrid deposit has been reported on by Getsinger (1997), Lindsay (1997), Reid and Gerakiteys (1998), Carpenter (2001), Carpenter and Sherlock (2001), Kleespies and Mercer (2001), Sherlock *et al.* (2002), Sherlock and Carpenter (2003) and Poulson (2004), as well as various other internal progress and year-end reports.

1.5 – Location, Access and Physiography

The Hope Bay Volcanic Belt (HBVC) is located in the northeast part of the Slave Structural Province along the Arctic coast in the northwest part of Nunavut (Fig. 1.1). It is situated approximately 750 km northeast of the city of Yellowknife and 150 km southwest of Cambridge Bay. The belt covers NTS areas 76 O/9, 10, 15, 16; and 77 A/2, 7, 10 (Gebert, 1993). The property that is the focus of this thesis is located in the north part of the belt approximately 15 km from the coast.

Granitic and gneissic rocks on the margins of the HBVB define a relatively rugged and elevated terrain in contrast to the rather subdued topography interior to the belt. Mafic and felsic volcanic rocks interior to the HBVB define north-trending ridges separated by low-lying areas of glacial deposits overgrown by shrubs and grass, terrain typical of the tundra. Mafic intrusives including Franklin aged diabase dykes and sills define a distinct positive topography, whereas areas of strong alteration and deformation are markedly recessive. Outcrop averages approximately 25% within the Madrid corridor excluding the area directly above the HBDZ which is completely till covered.

During the summer months the belt is accessible by barge via Melville Sound and Robert's Bay. As the Doris deposit nears production, it is likely that Robert's Bay will become increasingly important, facilitating the transport of supplies to the various

properties. The primary method of access during the summer months is by floatplane, typically from Yellowknife or Cambridge Bay. An airstrip completed at Boston in 1997 is capable of handling wheeled Twin Otters and Caravans. Helicopters are generally used for intrabelt transportation between properties.

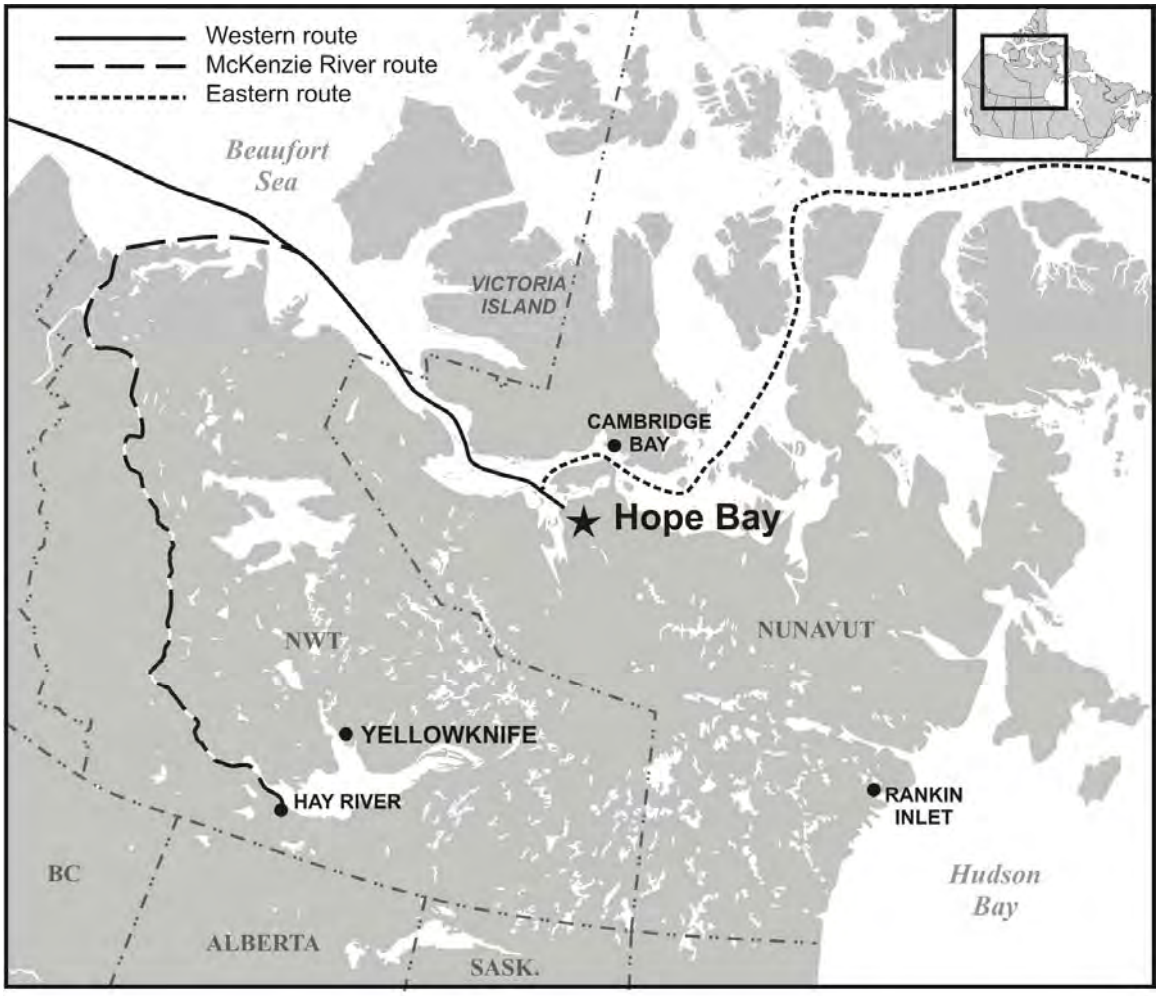

Fig. 1.1 Location of the Hope Bay Volcanic Belt, Nunavut (modified from Miramar Mining Corporation figure).

Access by aircraft during the winter months is made possible by the construction of ice-strips on property-adjacent lakes. Snow machine and winter roads also allow transportation between properties between freeze-up in October and break-up in June.

CHAPTER 2

REGIONAL GEOLOGY

2.1 – Geology of the Slave Structural Province

Numerous authors have recently reported on various geological aspects of the Slave Structural Province (SSP) in the wake of intense study following the discovery of diamonds in the central Slave Lac des Gras area. It is now one of the best documented Archean cratons on record.

The Slave Province is one of approximately 35 Archean cratons preserved worldwide (Bleeker, 2003). As in many Archean terranes the SSP is composed of deformed and metamorphosed supracrustal volcano-sedimentary assemblages intruded by syn to post kinematic granitoids (Fig. 2.1). In contrast to other Archean Shields, the Slave Province supracrustal assemblages are dominated by thick greywacke-mudstone turbidites and abundant highly evolved granitoids and is lacking in significant komatiite sequences (Padgham, 1992). The eastern margin of the SSP is bordered by the Paleoproterozoic Thelon Orogen (2.02-1.91 Ga) which separates it from the Archean Rae Province (Thompson and Henderson, 1983; van Breeman *et al*., 1987; Hoffman, 1988). The craton is separated from the Bear Province in the west by the Wopmay Orogen (1.95-1.84 Ma; Hoffman and Bowring, 1984; Hoffman, 1988).

The SSP has been divided into eastern and western domains based on geochronological and isotopic evidence. In the west, 3.2 Ga polymetamorphic tonalitic gneisses of the Mesoarchean Central Slave Basement Complex form the basement to overlying volcanic and sedimentary assemblages of the Yellowknife Supergroup

(Henderson, 1970; Bleeker and Ketchum, 1998; Bleeker *et al*., 1999a/b; Ketchum *et al*., 2004). Although these rocks have not been identified in the eastern portion of the SSP, it has been suggested that similarly aged basement rocks may underlie the Hope Bay-Elu Inlet volcanic belts in the northeastern part of the province (Bleeker, 2004). Evidence for a central Slave suture was provided by Thorpe (1972; 1982) and Thorpe *et al*. (1992). VMS-related galena from the eastern Slave are more juvenile than those found in the west, the higher Pb^{207}/Pb^{204} ratios in the west suggest a different source (older, more evolved crust) - the boundary possibly corresponding to a major tectonic break (Padgham, 1992; Padgham and Fyson, 1992).

The Central Slave Basement Complex is overlain by a 2.9-2.8 Ga sedimentary cover termed the Central Slave Cover Group (Bleeker *et al*., 1999a/b; Ketchum and Bleeker, 2000). From oldest to youngest this unit consists of quartz pebble conglomerate, fuchsitic sandstone and banded iron formation. This unit is interpreted to represent an Archean platformal succession formed during the initial stages of plume induced rifting (Bleeker *et al*., 1999a; Ketchum *et al*., 2004; Mueller *et al*., 2005; Mueller and Pickett, 2005).

Volcanic belts and turbidite basins dating between 2.73-2.60 Ga overlie the Central Slave Basement Complex and have been grouped into the Yellowknife Supergroup (Henderson, 1970). Padgham (1992) divided the Slave greenstone belts into two types: Yellowknife- type consist of thick packages of predominately tholeiitic basalts overlain by calc-alkaline felsic rocks where as Hackett River-type is characterized by intermediate to felsic calc-alkaline volcaniclastic rocks. Yellowknife type greenstone belts occur throughout the western Slave and are believed to be older (2.73-2.70 Ga), whereas the

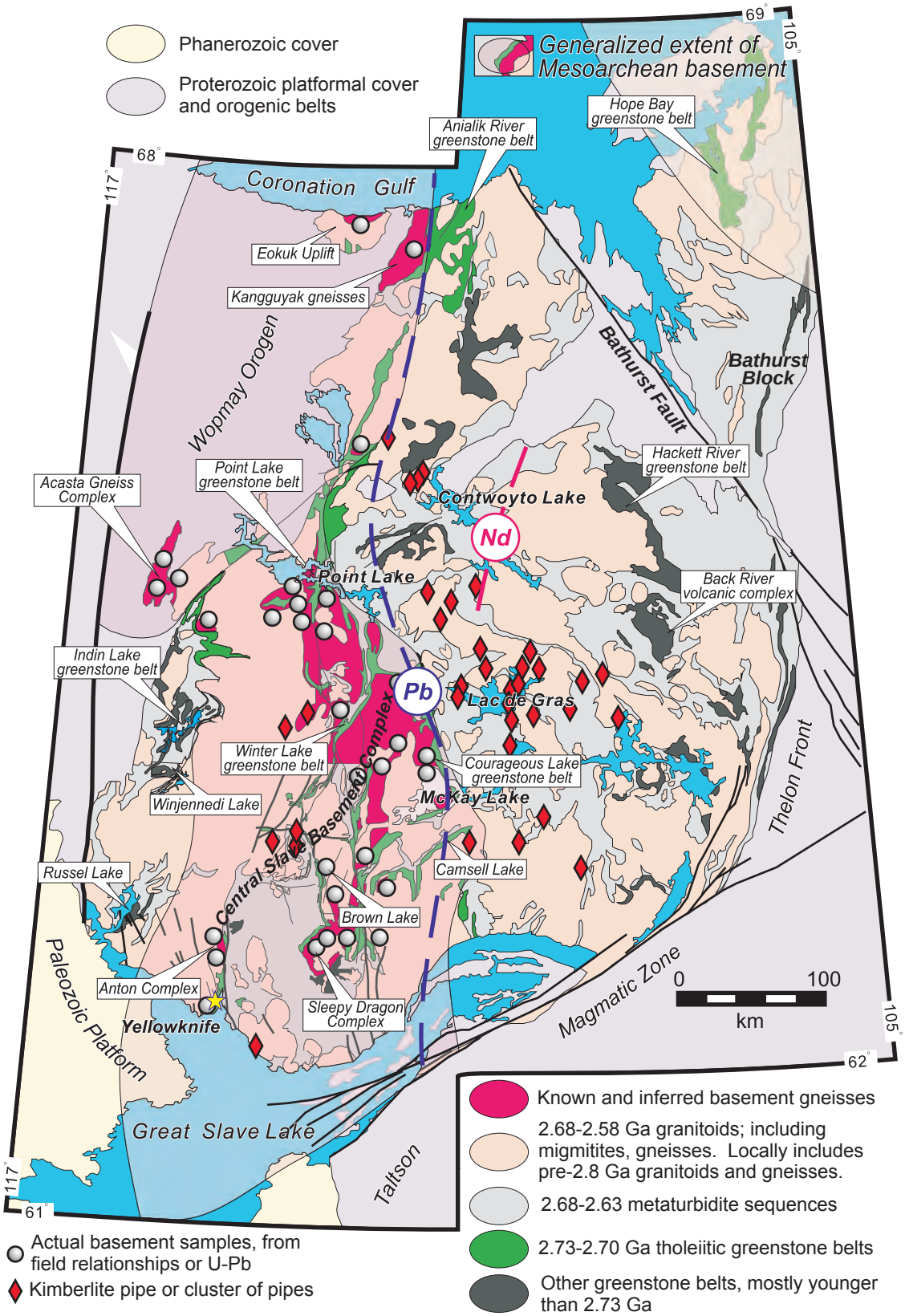

Fig. 2.1 Geology of the Slave Structural Province (Modified from Davis and Bleeker, 1999 and Bleeker *et al*., 2004). Pb isotope line from Thorpe *et al*. (1992). Nd isotope boundary from Davis and Hegner (1992).

Hackett River type are younger (post 2.70 Ga) and constrained to the eastern part of the SSP (Padgham and Fyson, 1992; Isachsen and Bowring, 1997; Bleeker *et al*., 2004). Associated synvolcanic subvolcanic intrusions span a period of 2.695-2.650 Ga (van Breeman *et al*., 1992). The volcanism which formed these belts was followed by extensive turbidite sedimentation between 2.68-2.66 Ga (Davis and Bleeker, 1999; Bleeker *et al*., 2004). Orogenesis and D_1 folding began with the closure of sedimentary basins between 2.65-2.63 Ga and is likely related to the earliest phase of syntectonic granites (the Defeat Suite in the Yellowknife Domain) which date between 2.625-2.595 Ga (van Breeman *et al*., 1992; Davis and Bleeker, 1999). Peak plutonism was concomitant with peak metamorphism between 2.610-2.590 Ga (van Breeman *et al*., 1992). Continued crustal shortening post 2.6 Ga gave rise to D_2 folding with predominately north-south axes. Moderate crustal thickening led to high temperature low pressure metamorphism, migmitization and anatectic melting, resulting in syn-D_2 megacrystic biotite granodiorite and two mica granite plutonism between 2.605-2.580 Ga culminating with an extensional phase of orogeny at 2.59 Ga (Thompson, 1978; van Breeman *et al*., 1992; Davis and Bleeker, 1999; Bleeker *et al*., 2004).

Several alternative geotectonic models have been proposed to explain the origin of the SSP and are briefly described below. McGlynn and Henderson (1970; 1972) and Henderson (1981; 1985) suggested that volcano-sedimentary rocks were deposited into intracratonic rift basins with volcanism occurring predominately along basin margins. Kusky (1989) suggested the SSP is comprised of four accreted terranes; the Anton (Archean microcontinent), Sleepy Dragon (exhumed portion of Anton?), Contwoyto (turbidite dominated accetionary prism to volcanic arc) and Hackett River (volcanic arc).

The Hackett River arc and associated Contwoyto prism presumably formed above an east-dipping subduction zone and were subsequently accreted onto the Anton-Sleepy Dragon microcontinent. Helmstaedt *et al*. (1986) and Fyson and Helmstaedt (1988) have proposed pre-3.0 Ga rifting of sialic basement followed by mafic volcanism. Ocean closure by means of an east-dipping subduction zone resulted in calc-alkaline volcanism to produce the Hackett River-type belts common in the eastern Slave. Mafic volcanic rocks were eventually transported onto the sialic basement as ophiolite-style slivers.

2.2 – The Northeastern Slave Province: Geology of the Bathurst Block

The Bathurst Block of the northeast SSP is bound to the east by the Thelon Front, the western edge of the Thelon Tectonic Zone (Wright, 1957; 1967; Thompson and Henderson, 1983; Henderson *et al*., 1990; Thompson *et al*., 1985, 1986), to the west by the Bathurst Fault, which bounds the eastern edge of the Paleoproterozoic Kilohigok basin (Campbell and Cecile, 1976a/b; 1981), and by undeformed Proterozoic sedimentary rocks to the north (Campbell, 1978; 1979). The northern portion of the Bathurst Block consists of volcanic rocks (Hope Bay and Elu Inlet volcanic belts) surrounded by granitoid plutons and gneisses of various ages (Thompson, 1997; Gebert, 1993). Thompson and Ashton (1984) and Thompson *et al*. (1985; 1986) have divided the southern portion of the Bathurst Block into the western Bathurst Terrane and the eastern Ellis River Terrane. The two terranes are separated by a metadiabase swarm and shear zone. The Bathurst Terrane is predominately composed of migmatites derived from Yellowknife Supergroup sedimentary rocks. Subordinate amounts of muscovite-biotite leucogranite/granodiorite, tourmaline bearing pegmatites and silicate-sulphide facies iron

formation are also present (Thompson *et al*., 1985; 1986; Therriault, 2003). The eastern Ellice River Terrane consists of amphibolite and granulite facies gneisses, migmatites and mylonites of mostly plutonic and less commonly sedimentary origin. Linear shaped homogenous metaplutonic bodies occur in lesser amounts throughout the area (Thompson *et al*., 1985; 1986).

2.3 – Geology and Mineral Potential of the Hope Bay Volcanic Belt

The north-south trending Hope Bay Volcanic Belt is situated in the northern part of the Bathurst Block. Pillowed mafic volcanic rocks are the dominant lithology with lesser felsic volcaniclastic rocks and sedimentary assemblages, especially toward the western part of the belt (Fig. 2.2). Granitic and gneissic rocks of various ages occur at the margins of the HBVB and separate it from the Elu Inlet Volcanic Belt to the east. Major gold targets are hosted in mafic volcanic rocks as veins and stockworks, whereas lower potential targets include Temiskaming/syenite associated Au and intrusive tonalite-trondjemite-granodiorite hosted Au. Felsic volcanic rocks have been explored for base metal potential with limited success.

2.3.1 – Mafic Rocks

Mafic volcanic rocks constitute a package of pre 2.7 Ga rocks that comprise approximately 70% of the HBVB. Pillowed tholeiitic basalts are the most common mafic volcanic rocks in the belt and they generally preserve primary volcanic textures including varioles, amygdules, peperitic textures, gas escape structures and hyaloclastic rims. Commonly, massive flow bases grade into thick pillowed portions capped by

flow/pillow breccias with or without an argillite drape. A broad subdivision of mafic volcanic rocks can be made between Fe-Ti-rich suites and normal to high-Fe basalts and basaltic andesites. Gebert (1999) has suggested the mafic volcanic rocks may form two distinct sequences: a pre 2.7 Ga mafic volcanic event and a 2.66 Ga event synchronous with turbidite sedimentation in the western part of the belt. Ultramafic bodies locally intrude the mafic volcanic units, forming sill-like bodies up to 200 m thick. Three swarms of post-Archean dikes intrude the HBVB: the ca. 2000 Ma Beechey dykes, the 1267 ± 2 Ma Mackenzie dykes, and the 723 ± 4 Ma Franklin Diabase (Gebert, 1993). Mafic volcanic rocks in the Madrid area are discussed in greater detail in subsequent chapters.

Three Au deposits (Doris, Madrid, Boston) and numerous showings are hosted within the mafic volcanic rocks of the HBVB. The northernmost Doris deposit occurs as a continuous (3 km) meter-scale quartz-carbonate vein system which hosts multigram gold as coarse flecks associated with tourmaline-sericite-pyrite septa at wallrock contacts (Carpenter *et al*, 2003). Marginal variolitic and amygdular basalts exhibit an alteration assemblage of ankerite-sericite-paragonite and pyrite. The quartz vein and surrounding basalts and gabbros have been folded into a tight doubly plunging D_2 anticlinal structure. The presence of unoriented foliated wall rock clasts suggests vein emplacement occurred syn to post D_2 where veining developed preferentially in dilational zones created during folding (Carpenter *et al*, 2003). The southernmost Boston deposit is a mafic volcanic hosted multistage mesothermal quartz-ankerite-sulphide vein system (Stemler, 2000). As at Doris, mafic units have been altered to quartz-ankerite-sericite-paragonite and pyrite.

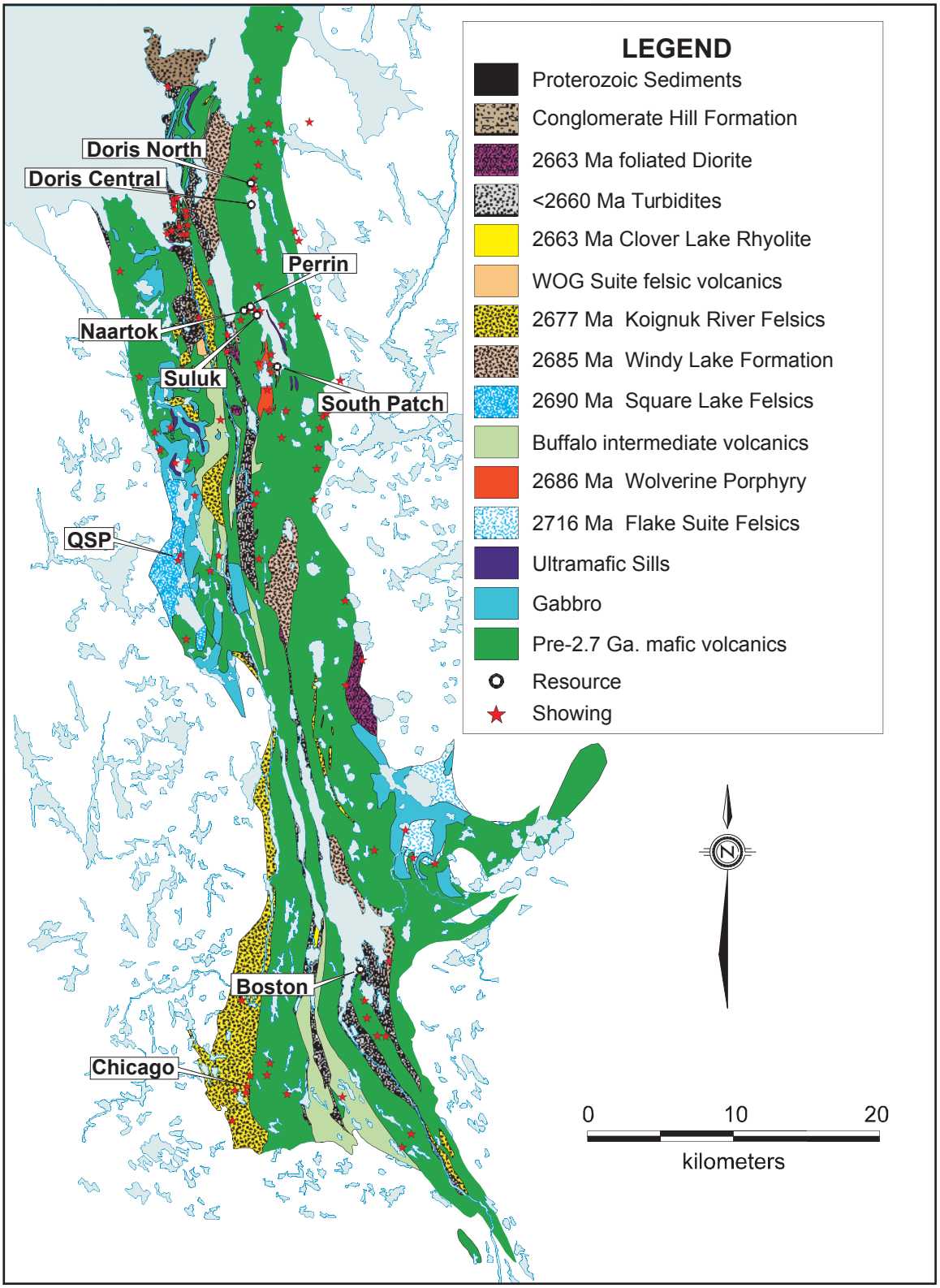

Fig. 2.2 General geology of the Hope Bay Volcanic Belt (modified after Miramar compilation map).

Mafic volcanic rocks and interflow sedimentary rocks are folded into a synformal anticline. Gold mineralization occurs in pillowed mafics in the core of the structure and is controlled by anastomozing axial planar shear zones (Sherlock and Sandeman, 2004b). Numerous other mafic hosted gold showings in the belt are of similar style but smaller in size than the deposits discussed above.

2.3.2 – Felsic Volcanic Rocks

Felsic volcanic rocks preferentially occur in the western half of the belt and have been subdivided into six major suites. These suites span a period of 53 Ma and include the turbidite-bound Clover Lake suite (U-Pb, 2663 Ma; Hebel, 1999), the dacitic Koignuk River suite (U-Pb, 2677 +3/-1 Ma; Hebel, 1999), the dacitic Windy Lake suite (U-Pb, 2685 +3.3/-1.9 Ma; Hebel, 1999), the quartz-feldspar phyric Wolverine Porphyry (U-Pb, 2686 Ma; Sherlock, unpublished data), the Square Lake suite (U-Pb, 2690 +1.4/-1.2 Ma; Hebel, 1999) and the rhyolitic Flake Lake suite (U-Pb, 2716 +4.3/-3.4 Ma; Hebel, 1999). Felsic rocks are typically volcaniclastic (crystal-lithic tuffs, volcanic conglomerates, etc) and commonly epiclastic with rarer examples of massive flows or sills. Intrusive phases include the Wolverine Porphyry and smaller units interlayered with volcaniclastic rocks (Gebert, 1993, 1999; Sherlock *et al*., 2002; Sherlock and Carpenter, 2003). Intermediate (predominately dacitic) lapilli tuff and quartz-plagioclase phyric volcanic flows of the Buffalo suite are thought to postdate the main phase of mafic volcanism (pre 2.7 Ga) and predate the onset of voluminous felsic volcanism which gave rise to the Windy Lake suite (Gebert, 1999).

Although the HBVB is mafic dominated, felsic volcanic rocks may be prospective

for base metal deposits. At least two base metal showings have been identified (Cope and UK/Chicago, Fig 2.2), both of which lie within intermixed sedimentary and felsic volcanic rocks of the Koignuk Suite (Gebert, 1993, 1999). Syngenetic sulphides are often bedded/laminated and include pyrite, chalcopyrite, pyrrhotite and sphalerite. Recent surface sampling and drilling in the Square Lake felsics (QSP showing) and Koignuk felsics (Chicago area) has identified Cu enriched gold systems comparable with Quebec's Bousquet District (Stone, 1988; Tourigny *et al*., 1993; Sherlock and Lindsay, 2002; Lindsay *et al*, 2003). The rhyolitic flows of the Flake Lake Suite are also considered to be prospective for base metals (Sherlock, personal communication). Ongoing exploration to identify primary pyroclastic deposits, felsic centers, appropriate alteration patterns and multiple cycles of volcanism is warranted, but considered secondary to gold exploration (Gebert, 1999; Lindsay *et al*., 2002).

2.3.3 – Sedimentary Rocks

Sedimentary rocks are found throughout the HBVB interlayered with both mafic and felsic units. Mafic volcanic flows locally contain interflow cherty to graphitic argillite-siltstone packages and are discussed in greater detail in Chapter 3. Greywacke-mudstone turbidites are common in the central and western part of the belt. Detrital zircon ages gave a maximum depositional age of 2675 Ma (Hebel, 1999). This age conveniently falls within the bracket of pan-Slave turbidite sedimentation (2.68-2.66 Ga) as defined by Davis and Bleeker (1999) and Bleeker (2004). Interestingly, Hebel (1999) reports two pre 2.7 ages (2804 and 3281 Ma) from detrital zircons that show no evidence for prolonged transport.

Two late conglomeratic units have been identified in the HBVB: the Conglomerate Hill Formation and the Hope Bay Formation. These two conglomerates may not be facies variations of the same stratigraphic unit.

The Hope Bay Formation, occupying a small island north of Discovery Bay immediately west of Doris Lake, unconformably overlies the greenstone belt. It consists of interbedded greywacke and conglomerate with mafic volcanic, gabbroic and granitoid clasts. Two granitoid clasts from this unit have been dated at 2686 Ma and 2701 Ma whereas a detrital zircon from the wacke unit yielded a maximum age of deposition at 2647 Ma (U-Pb, Hebel, 1999). The 2686 Ma granite clasts indicate plutonism was synchronous with felsic volcanism associated with the Windy Lake Felsics (Hebel, 1999; Gebert, 1999). Although the maximum age of the Hope Bay Formation is older than that of the <2.6 Ga Jackson Lake Formation, it is believed the two are comparable in tectonic setting (Hebel, 1999; Bleeker, 2002; Isachsen and Bowring, 1994).

The Conglomerate Hill Formation occurs as a linear fault-bounded unit west and north of Windy Lake. It consists of bedded fluvial-alluvial sequences of argillite-wacke-conglomerate unlike the turbidite sequences seen throughout the SSP (Stubley, 2002). In contrast to the Hope Bay Formation, the Conglomerate Hill conglomerates are dominated by felsic porphyry and sedimentary clasts while lacking the granitoid component (Gebert, 1999). The Conglomerate Hill Formation has been intruded by a late-stage xenolithic diorite suite which forms a large sill-like complex within the sedimentary strata (Stubley, 2002). The bounding faults commonly exhibit strong carbonate +/- sericite alteration envelopes with quartz-ankerite-sulphide stockworking. Late kinematic (D_2) fluvial-alluvial fault-bound basins with spatially (and temporally?) associated monazite-syenite-

diorite intrusives are key characteristics of the Temiskaming/syenite associated Au model (Robert, 2001; Stubley, 2002). Similar settings in the Abitibi Belt (Robert, 1997; 2001) suggest that the Conglomerate Hill area may be a smaller-scale analogue of a Temiskaming-type basin and a prospective Au target (Gebert, 1999; Stubley, 2002).

2.3.4 – Plutonic Rocks

Granitic rocks predominately occur on the margins of the HBVB and the Elu Inlet Volcanic Belt (Fig. 2.3). These rocks have been briefly discussed by Gebert (1993, 1999), however, the majority of work has been completed by Thompson (1996, 1997), who has divided the granitic rocks into three groups based on degree of heterogeneity, inferred age relative to the volcanics and degree of deformation and metamorphism.

Plutonic rocks in Group 1 are designated as metagranitoid-migmatite-gneiss and are described as being "homogenous in their heterogeneity". Three main characteristics are responsible for the heterogeneity: deformation (producing a foliation or lineation), migmitization (through in-situ partial melting or injection of younger granitoid phases) and gneissification (flattening or shearing of migmatites or magma injection parallel to an existing foliation). Thompson (1997) suggests that this unit represents old basement onto which the volcanics were deposited, or the lower crustal level of the orogenic event that metamorphosed the supracrustal rocks. A titanite age of 2589 Ma has been reported by Hebel (1999) and is thought to represent peak metamorphism.

Group 2 intrusives have been subdivided into three lithological varieties based on composition and timing of emplacement. They are believed to be broadly synvolcanic, pre to syn dating the earliest stage of crustal thickening. Group 2 granites are interpreted

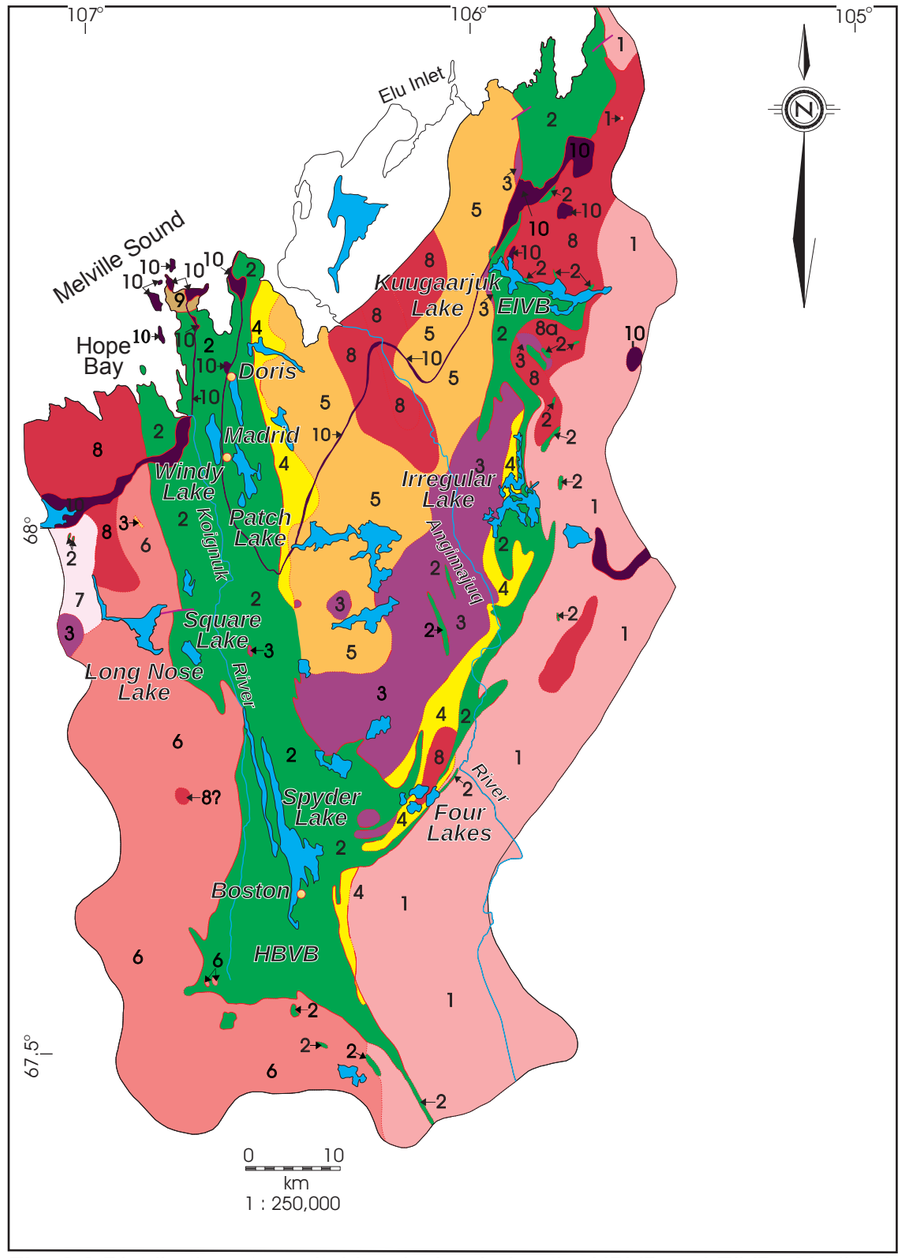

Fig. 2.3 Distribution of granitoid rocks bordering the HBVB and EIVB. Modified after Thompson (1997).

LEGEND

PROTEROZOIC

10 Franklin diabase dykes and sills

9 Sedimentary rocks

ARCHEAN

MASSIVE HOMOGENEOUS GRANITOIDS (GROUP III)

8 Biotite granite suite: biotite granite to granodiorite, K-feldspar megacrysts typical; weakly foliated locally; 8a - relatively fine-grained, inclusions of granitoid migmatite, quartzofeldspathic gneiss, foliated metatonalite, mafic metavolcanic rocks, and/or metagabbro.

7 Biotite tonalite: granodiorite to tonalite; schistose to gneissic metasedimentary and metavolcanic inclusions which define a foliation.

6 Monzodiorite suite: biotite-hornblende quartz monzodiorite, monzodiorite, granodiorite, diorite; typically foliated and recrystallized with lenticular inclusions of metavolcanic rocks near contact with Unit 2; mafic and ultramafic inclusions (most cm scale)

VARIABLY FOLIATED METAMORPHOSED HOMOGENEOUS GRANITOIDS (GROUP II)

5 Pitted metatonalite: hornblende/biotite tonalite, minor granodiorite; massive to moderately foliated, variably recrystallized; differential weathering of coarse-grained biotite forms pits.

4 Metatonalite suite: biotite/hornblende tonalite, some granodiorite;intensely foliated and recrystallized, dykes intrude Unit 2.

3 Mafic metaplutonic suite: biotite/hornblende diorite, tonalite to quartz diorite, leucogabbro, gabbro, anorthosite; massive to moderately foliated, variably recrystallized.

METAMORPHOSED VOLCANIC AND RELATED ROCKS

2 Volcanic, volcanoclastic, and sedimentary rocks, gabbro sills,quartzo-feldspar porphyries.

HETEROGENEOUS METAGRANITOIDS (GROUP I)

1 Metagranitoid-migmatite-gneiss complex: foliated, recrystallized granite to tonalite, granitic to tonalitic granitoid migmatite, quartzofeldspathic gneiss, (layered rocks), minor granitic pegmatite, amphibolite gneiss and migmatitic metagabbro.

Geological contact; approximate, inferred
(for volcanic belts in part after 1997 BHP map)

to be the plutonic component of the magmatic event that produced the volcanic rocks of the HBVB. The mafic metaplutonic suite is the first unit of Group 2 granites and consists of gabbro, leucogabbro, diorite and tonalite. Intrusive relationships indicate this unit was emplaced into previously undeformed mafic volcanic rocks. A preliminary age of 2701 Ma (Thompson, 1997; Hebel, 1999) supports the conclusion that mafic metaplutonic magmatism overlapped with mafic volcanism.

Strongly deformed lensoidal shaped metatonalite bodies (second unit of Group 2 granitoids) parallel regional structures along the eastern contact of the HBVB and the western boundary of the EIVB. Contact relationships indicate that this unit intrudes the mafic metaplutonic suite. Biotite altered hornblende and recrystallized plagioclase indicates that this unit predates peak metamorphism, whereas a U-Pb date of 2672 +4/-1 Ma (Bevier and Gebert, 1991) suggests a syn to slightly post volcanic age (Thompson, 1997). Bevier and Gebert (1991) suggest that the latest felsic volcanism could have been related to this suite of granites.

Pitted metatonalite defines the third unit within Group 2 granitoids, forming a large U-shaped body between the northern portion of the HBVB and EIVB. Contact relationships with the metatonalite are obscure and appear to be transitional; consequently the two are thought to be co-magmatic (Thompson, 1997).

Group 3 granites are predominately massive and homogenous with only local evidence for recrystallization and deformation. They are interpreted to be late to post kinematic. Group 3 granites have been divided into three units. A suite of monzodiorites occurs along the southern and western margins of the belt. Deformation and recrystallization of this suite is confined to a meter scale zone at the greenstone contact.

This unit is interpreted by Thompson (1997) to be a bridge compositionally and temporally between the pre-orogenic granites of Group 2 and the syn to post tectonic granites of Group 3. Biotite tonalite forms a relatively small body west of the HBVB. The unit is weakly to moderately foliated, and best identified by the presence of gneissic metasedimentary and metavolcanic inclusions aligned with the foliation. The metavolcanic inclusions exhibit a greenschist facies assemblage yet the granite shows no evidence of recrystallization. This indicates that the tonalite intruded post-peak metamorphism, but before the end of deformation (Thompson, 1997).

K-feldspar megacrystic monzogranites are widely distributed in the map area. Overall, these are massive and homogenous with only local zones of deformation. Blocks and lenses of metamorphosed granite, basalt and gabbro indicate these are late to post kinematic granites. Bevier and Gebert (1991) have obtained a U-Pb date of 2608 Ma from a monzogranite with foliated mafic inclusions. This places an upper limit on the main phase of metamorphism and deformation in the area (Bevier and Gebert, 1991; Thompson, 1997).

A direct link between granite magmatism and gold mineralization is not apparent in the HBVB. Group 1 and 2 granites both appear to predate mineralization as they are cut by gold-bearing veins whereas Group 3 granites appear to postdate regional metamorphism and gold mineralization. Despite this, several tonalite-hosted showings occur on the eastern margins of the belt within deformed intrusions. The deposits are small but similar to other tonalite-trondhjemite-granodiorite hosted deposits in other Archean cratons (eg. Renabie Mine: Callan and Spooner, 1989; Jemiellta *et al.*, 1988). Deposits along the eastern margin of the belt are characterized by narrow quartz veins

controlled by shear zones or north/northeast trending lineaments. The veins have narrow selvedges of Au enrichment and higher silver values than veins within the metavolcanics. It is believed that the granite-greenstone contact was preferentially exploited by late mineralizing hydrothermal fluids. Thompson (1997) also suggest that deformation of the ductile supracrustal rocks of the HBVB around the more rigid Group 1 and 2 granites would have resulted in complex structures which may have controlled the location and distribution of gold within the belt.

2.3.5 – Metamorphism and Deformation

Regional low grade metamorphism and seafloor alteration in the HBVB is characterized by a lower greenschist facies assemblage of quartz-chlorite-plagioclase-calcite +/- amphibole, hematite and epidote. Evidence presented later in this thesis suggests a higher (epidote-actinolite) metamorphic grade based on samples from the Madrid area. Amphibolite facies conditions prevail towards the belt margins where chlorite is replaced by amphibole and a biotite-garnet assemblage is developed in the metasedimentary rocks (Gebert, 1993).

Deformation events in the HBVB are complex and not entirely resolved. D_1 structures are difficult to recognize in the belt, however, Gebert (1999) outlines several possible D_1 thrusts where older rocks were tectonically juxtaposed against younger lithologies. A locally preserved, approximately bedding parallel spaced cleavage is interpreted as an S_1 fabric as it is clearly crosscut by S_2 (Sherlock *et al.*, 2003). East-west shortening and associated D_2 deformation produced tight to isoclinal folds with a penetrative north-trending axial planar cleavage. One such fold is seen at the Doris

deposit and can be traced south of Patch Lake (Sherlock and Carpenter, 2003). Possible D_3 open folds are discussed by Gebert (1999). Gentle flexes of the D_2 fabric on a belt-wide scale may be a result of D_3 deformation. Crenulation of the D_2 cleavage is common in areas where D_2 deformation was preferentially focused (eg. the HBDZ). Zones of high strain (including shear zones) parallel the regional S_2 fabric. Late brittle faults are locally delineated in outcrop by offset stratigraphy.

CHAPTER 3

GEOLOGY OF THE MADRID AREA

3.1 – Introduction

The Madrid deposit is located in the northern part of the Hope Bay Volcanic Belt (HBVB) approximately10 km south of the Doris and 45 km north of the Boston deposits (Fig. 2.2). Gold is situated within quartz-ankerite-sericite-albite-pyrite altered and quartz vein stockworked high-Ti komatiitic basalts bordering a mylonitic schist shear zone termed the Hope Bay Deformation Zone (HBDZ). The research for the present study focused on the lithogeochemistry and mineral chemistry of the Au-bearing mafic volcanic units to characterize the alteration mineral assemblages associated with Au. The immediate Madrid area has been subdivided into several informal lithological units on the basis of petrology and bulk rock geochemical signatures. For the sake of clarity field terminology is retained but combined with more formal terminology developed throughout the thesis. Although rocks within the Madrid area have been metamorphozed to epidote-actinolite facies, the prefix *meta* is omitted for brevity.

3.2 – Structure and Stratigraphy

The first section of this chapter introduces the lithological units present within the Madrid Corridor and characterizes the structural events which have deformed them. The stratigraphic relationships between these units are of central importance in delineating the structural history of the area and so are also discussed below.

The various lithological units in the Madrid Corridor are summarized in Table

3.1. Volcanological features and stratigraphic relationships of these units are illustrated on a simplified cross-section in Fig. 3.1. This cross-section accompanies Fig. 3.2 which illustrates the detailed geology of the Madrid area. Mafic volcanic rocks outcropping in the Madrid corridor have been subdivided into six groups based on petrography, stratigraphic position and lithogeochemistry. Felsic rocks consist of the Wolverine Porphyry, a quartz-feldspar phyric intrusive phase, and the Windy Lake Felsics, composed of reworked volcaniclastic crystal-lithic tuffs. At least two varieties of dykes

	Lithotype	**Characteristics**
1)	Ti-rich komatiitic basalts *(Patch A)*	Pillowed to massive, commonly brecciated, black to dark green flows. Peperitic, harrisitic and pseudocumulate textures common. Host to the majority of Au mineralization at Madrid.
2)	High Fe-Ti transitional basalts *(Patch B)*	Pillow and flow breccia units, medium-dark green with large white coalescing varioles. Typically unmineralized.
3)	Variolitic (high-Fe) tholeiitic basalts *(Windy Lake Mafics)*	Large, strongly variolitic pillows, medium green with black chloritic selvedges. Located north of HBDZ.
4)	Non-variolitic (high-Fe) tholeiitic basalts *(Wolverine Mafics)*	Pillowed and flow brecciated non-variolitic flows south of the HBDZ.
5)	Gabbroic textured mafic rocks *(Naartok Gabbros)*	Medium-coarse grained medium-dark green massive intrusives and flow bases to 3) and sometimes 4).
6)	Basaltic andesites *(Pale Green Pillows: PGP)*	Light earthy gray-green coloured massive to pillowed often peperitic flows.
7)	Windy Lake Felsics	Volcaniclastic crystal-lithic tuffs and massive flows, dacitic.
8)	Wolverine Porphyry	Quartz-feldspar phyric dacitic intrusive. Main constituent of the HBDZ.
9)	I-dykes	Thin, rare intermediate dykes, post mineralization.
10)	Franklin diabase	Coarse massive mafic dyke in western Madrid, N-S trending.

Table 3.1 Summary of major lithological units in the Madrid corridor.

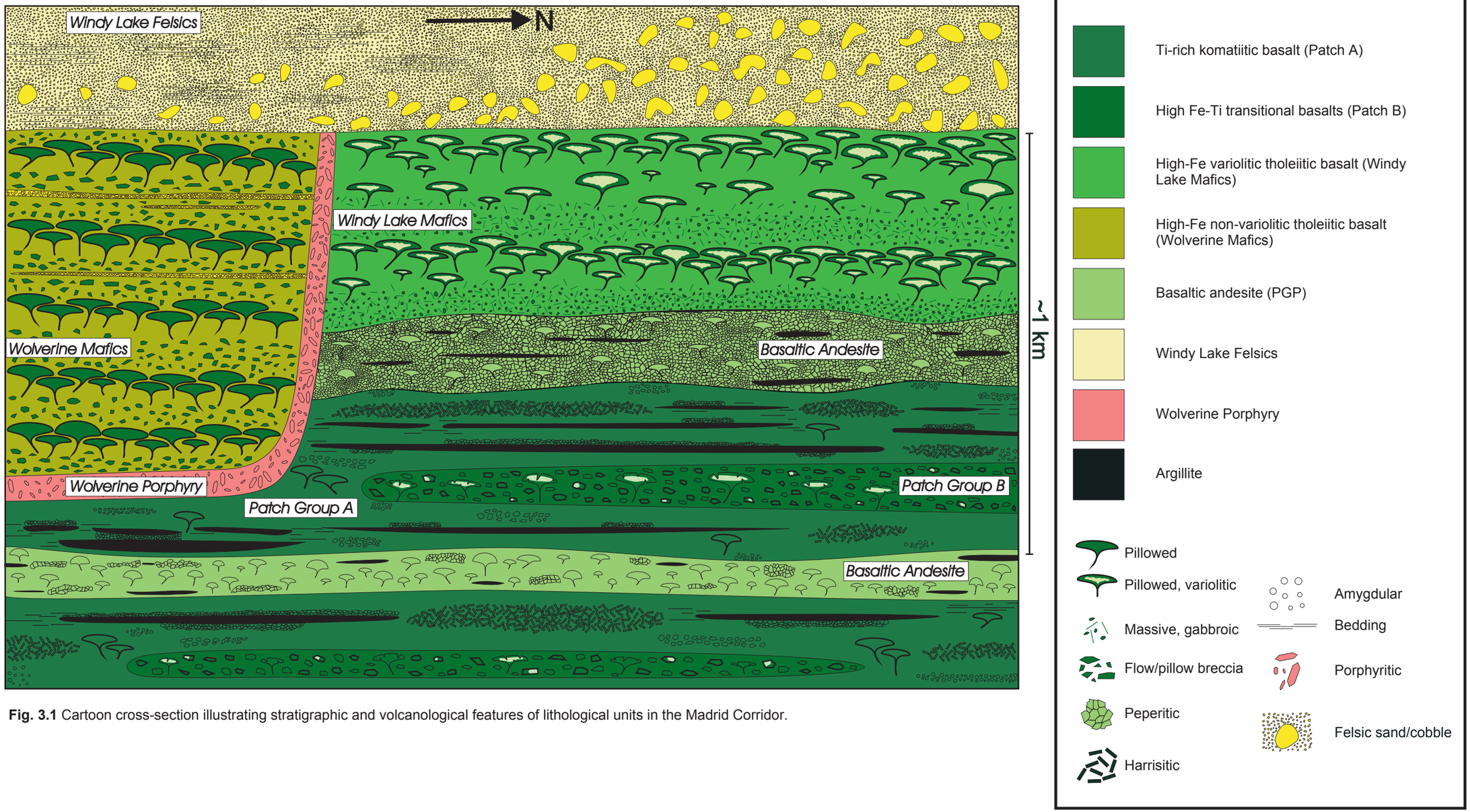

Fig. 3.1 Cartoon cross-section illustrating stratigraphic and volcanological features of lithological units in the Madrid Corridor.

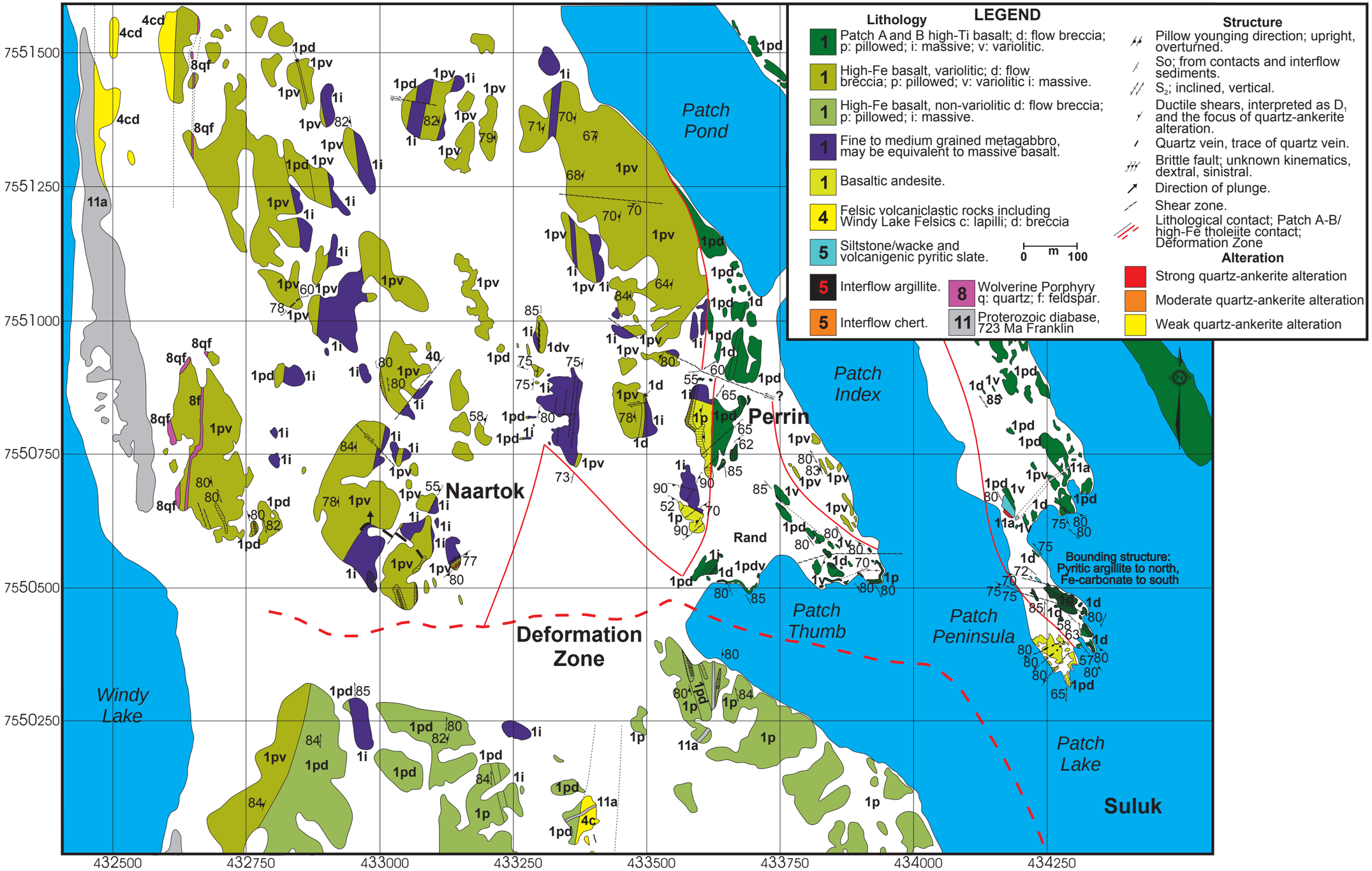

Fig. 3.2 Geology of the Madrid Corridor.

occur in the Madrid area. Thin (1-2 m), aphanitic intermediate to mafic dykes occur rarely at Madrid and postdate Au mineralization. A coarse grained Franklin-aged (723 Ma; Gebert, 1993) diabase dyke occurs along the contact between the Windy Lake Mafics and Windy Lake Felsics.

The structural framework presented here derives substantially from discussions with Dr. Howard Poulson and Mike Young. Their contribution is graciously acknowledged and greatly appreciated. The main structural feature in the area is the HBDZ, a major mylonitic shear zone which trends north-south through the Suluk area, rotating counterclockwise into an east-west orientation at the north end of Patch Lake, and trending to the eastern shore of Windy Lake (Fig. 3.2). Similar changes in lithology occur across both the N-S and E-W segments of the HBDZ. The HBDZ is truncated by a N-S trending break at the NW end of the map area. This break marks the transition from mafic flow dominated volcanic rocks to dacitic volcanic rocks of the Windy Lake Felsics.

At least four structural events have been imposed on the rocks at Madrid, and are briefly discussed below:

D_0: Primary sedimentary/volcanic bedding can be measured utilizing the orientation of interflow argillite and chert horizons within the mafic volcanics or drainage cavities in pillows. Stratigraphy in the Madrid area has an overall N-S strike and youngs to the west. A number of structural complexities proximal to the HBDZ has resulted in reorientation of this stratigraphy and is discussed below. Sherlock *et al*. (2003) suggests that the HBDZ is a synvolcanic (D_0) growth fault. This conclusion is based on the juxtaposition of different mafic flow series - the variolitic and non-variolitic high-Fe

tholeiitic basalts. Also, felsic volcaniclastic units found on the south side of the east-west segment of the HBDZ cannot be traced northward across the structure.

D_1: The earliest phase of deformation is difficult to observe as it is strongly overprinted by an S_2 fabric. Sherlock *et al*. (2002; 2003) identified a fabric approximately parallel to bedding and consider it a composite S_0/S_1 transposition fabric. Poulson (2004) describes a number of D_1 shear zones crosscutting the mafic volcanic rocks in the Madrid area. These structures strike at approximately 110^o and have been overprinted by the regional S_2 fabric. On Patch Lake Peninsula a package of siltstone-sulphidic argillite-pillow breccia is truncated to the south by one of these early structures (Fig. 3.2). This boundary also separates strongly ankeritized rocks to the south from weakly altered rocks in the north. There is also a change in the strike of stratigraphy from NW in the Patch A basalts to NE in the basaltic andesites on the south end of the peninsula. In the Rand/Patch Thumb area a northwest striking interflow argillite package can be traced south to approximately 50 m north of the shore. Beyond this point stratigraphy takes on an approximately east-northeast trend based on a cherty argillite horizon and bedding in volcanic units (Plate 3.1). The bounding structure at Patch Thumb may in fact be the extension of the one at Patch Peninsula. Furthermore, this larger structure may be a subsidiary splay off of the HBDZ suggesting it is D_1 in origin (Poulson, 2004). One example of a possible D_1 structure suggests dextral displacement (Plate 3.2). Evidence is presented later in the thesis to link D_1 with the intrusion of the Wolverine Porphyry.

D_2: The dominant fabric in the Madrid area is a steep bedding-parallel, north-trending foliation which deviates slightly either clockwise or anticlockwise. This fabric is the dominant regional foliation seen throughout the belt and is designated as S_2. The S_2

fabric is best developed within the HBDZ, in Patch A rocks, along lithlogical contacts, in pillow/flow breccia and peperitic units, and in areas that have undergone early carbonate sericite alteration. A first order F_2 isoclinal anticline occurs east of Patch Lake and can be traced northward through the Doris deposit (Sherlock and Carpenter, 2003). It is a doubly plunging east verging structure with an approximately north-south trending axis. Asymmetrical Z-shaped folds in the Madrid area attest to being on the west limb of this F_2 structure. F_2 folding has resulted in a north-trending axial planar cleavage and folding of quartz-ankerite veins (Plate 3.2, 3.3). In addition to discrete shear zones, many domains at Madrid exhibit a strong spaced S_2 cleavage that show no signs of displacement. These so-called "cleavage zones" are common in the hangingwall portion of the HBDZ in the Naartok region (Plate 3.3). The S_2 fabric overprints a mafic dyke that crosscuts mineralization in the Naartok area (Plate 3.4), providing information for constraining the timing of mineralization relative to deformation. A clast of quartz-ankerite veined basalt within the 2686 Ma Windy Lake Felsics is also useful for this same purpose (Plate 3.5). Its presence suggests an alteration-veining event which pre/syn dates the intrusion of the Wolverine Porphyry.

D_3: D_3 deformation is predominately expressed as a localized asymmetrical S-shaped sinistral crenulation cleavage rotated clockwise of S_2 (Plate 3.4). S_3 is localized in areas with a strong S_2 fabric and is well expressed on the southeast side of Patch Lake. It is likely that much of the S_2 warping interior to the HBDZ over its east-west segment is a result of this D_3 overprint.

Drillcore and geophysical data have outlined a significant NW trending fault in the Naartok area (Fig. 3.2) which can be traced north to where it offsets the Windy Lake

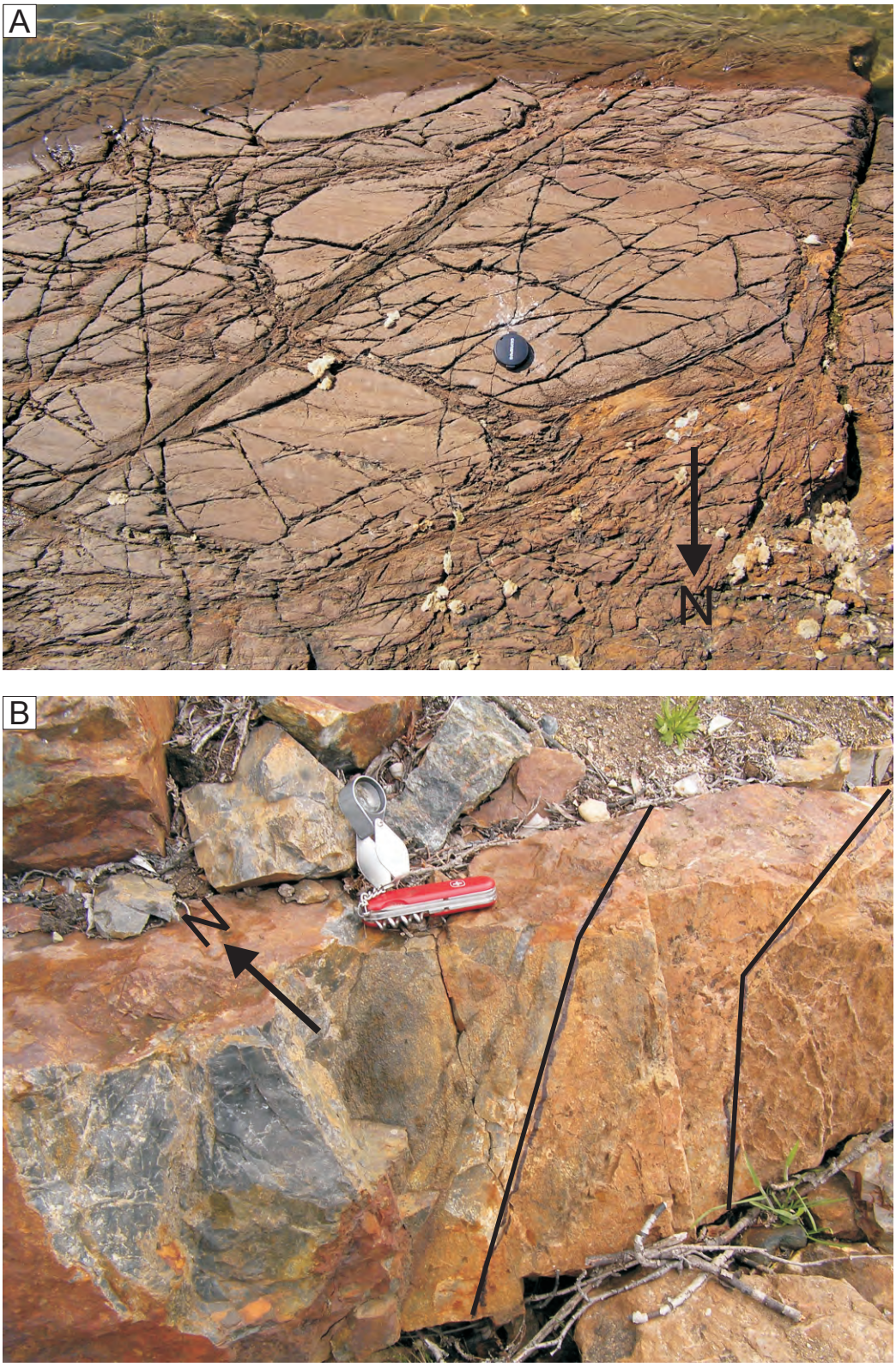

Plate 3.1 (A) Pillowed komatiitic basalt flows (Patch A) suggesting tops to the south, Patch Thumb area; (B) Chert-argillite horizon in komatiitic basalts striking approximately east-west, Patch Thumb area. Approximate direction of north indicated.

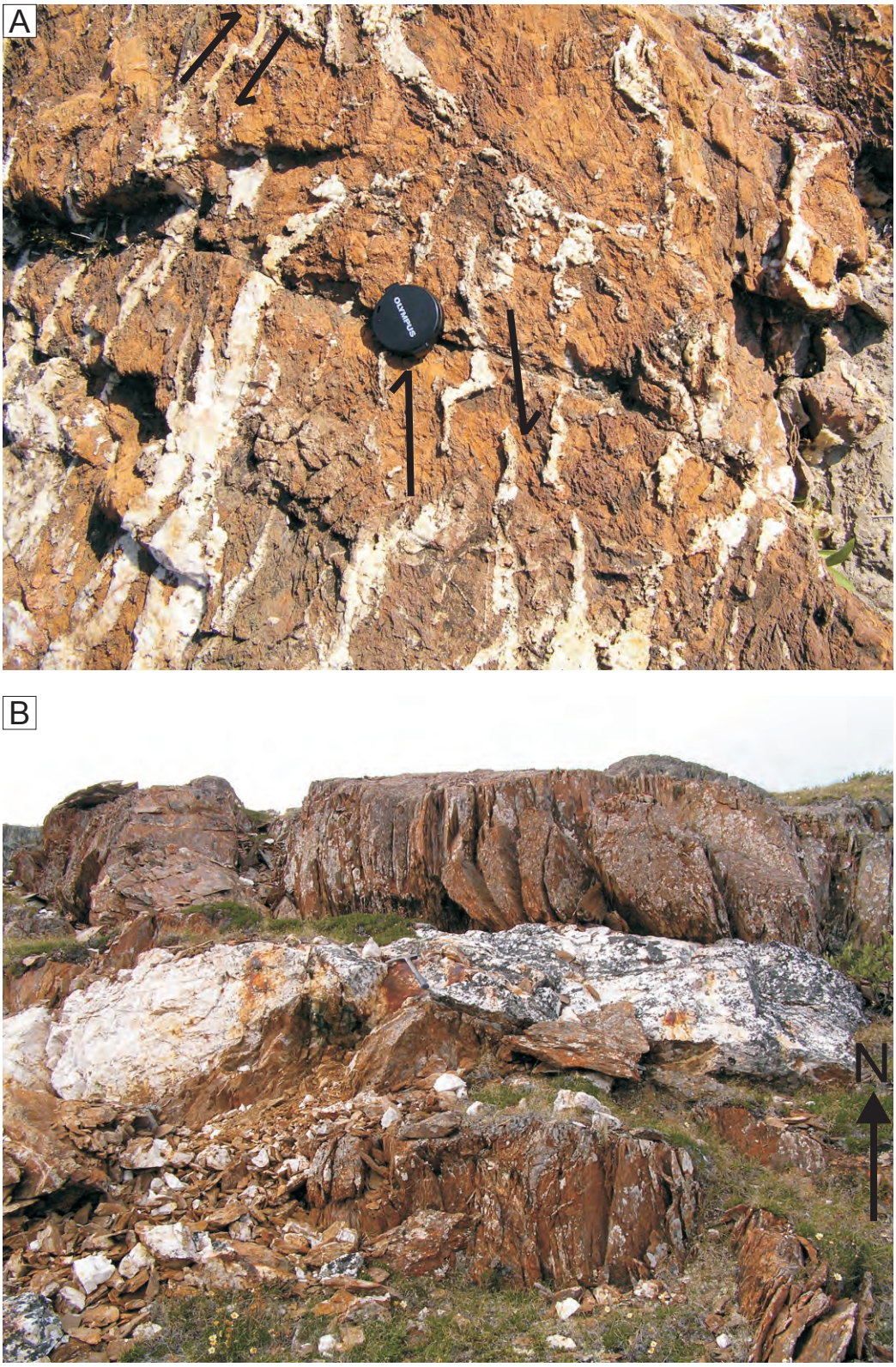

Plate 3.2 (A) Komatiitic basalts exhibiting strong carbonate alteration and quartz-ankerite veining with a dextral sense of shear possibly related to D_1; (B) F_2 folded quartz-ankerite vein trending at 290^0 and plunging to the north, Naartok. Enveloping basalt exhibits N-S axial planar S_2 cleavage.

Plate 3.3 (A) Quartz-ankerite vein folded by F_2 fold with associated axial planar S_2 cleavage; (B) "Poker-chip" style S_2 cleavage zone overprinting strong carbonate-sericite alteration zone, Naartok area.

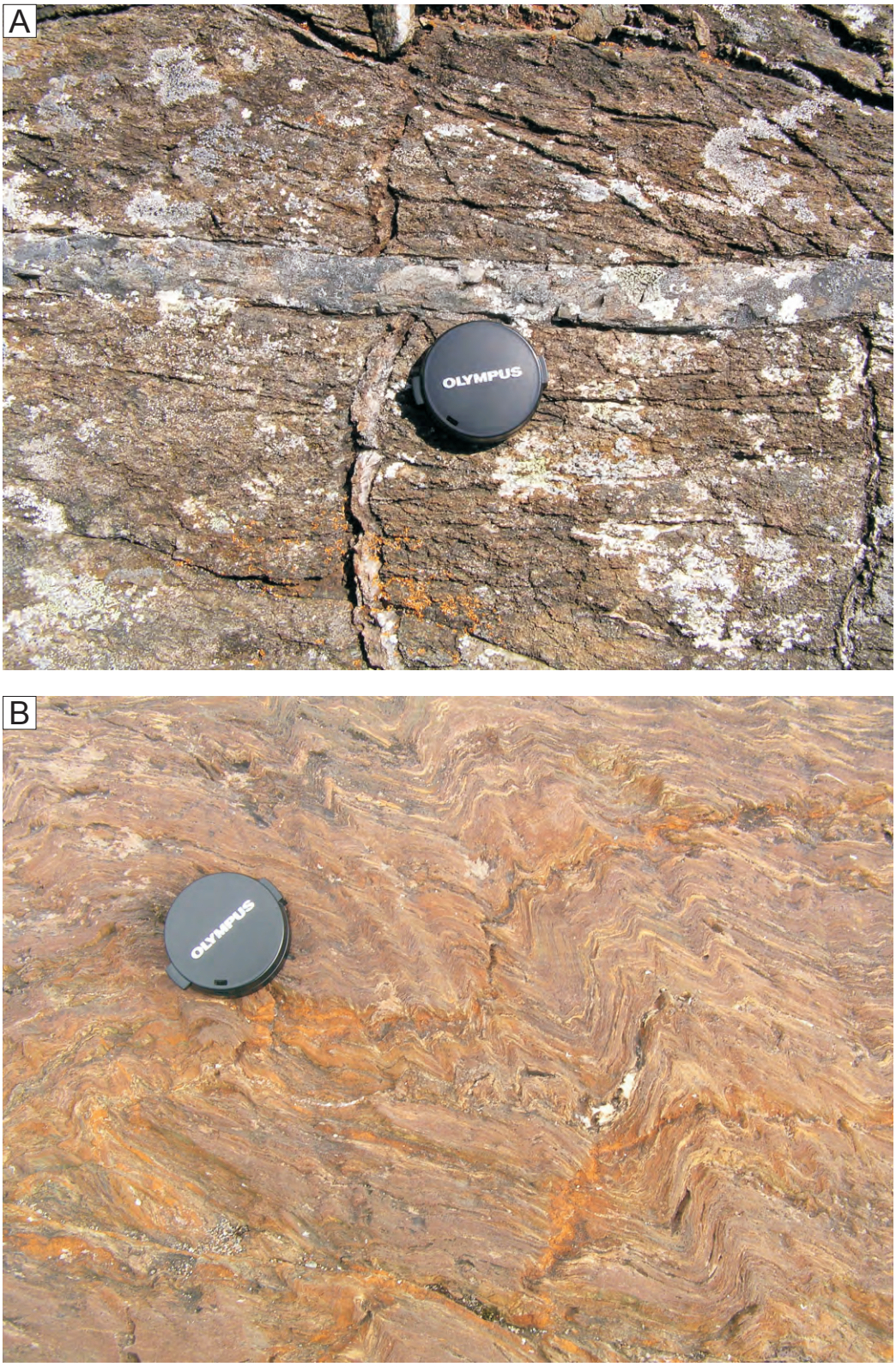

Plate 3.4 (A) Mafic dyke crosscutting quartz-ankerite alteration and veining but displaying an S_2 fabric, Naartok area; (B) S_2 fabric crenulated by S_3 in komatiitic basalts proximal to the HBDZ, Suluk area.

Plate 3.5 (A) Quartz-ankerite veined fragment interior to the 2686 Ma Windy Lake Felsics, northern HBVB; (B) Closeup of above showing truncation of quartz-ankerite vein at clast margin.

Felsics on the northeast shore of Windy Lake. This fault is responsible for dextrally offsetting a mineralized triangular shaped block of Patch A and B rocks toward the west. This block is bound to the south by the HBDZ and to the west by the (faulted) contact against the variolitic high-Fe tholeiitic basalts. A displacement of approximately 350 m is suggested based on drillcore correlations. Structural contour maps within the displaced block suggest approximately N-E trending stratigraphy. The exact timing of this fault is unclear, but it predates the regional D_2 deformation.

The origin of the HBDZ still remains quite controversial. However it is clear that it predates D_2 deformation as the 2686 Ma Wolverine Porphyry, overprinted by both S_2 and S_3 intrudes into the structure. Furthermore, pre-D_2 sericite-carbonate alteration enveloping the Wolverine Porphyry is preferentially deformed by D_2. This identifies the HBDZ as either a D_0 or D_1 structure which has been subsequently modified during D_2 and D_3 deformation.

Several lithological transects have been completed through the Madrid area including the Naartok (Fig. 3.4), Perrin (Fig. 3.5) and Suluk (Fig. 3.6) deposits. The precise location of these cross-sections and their associated drillholes are shown in Fig. 3.3. The purpose of these cross-sections are to reconcile some of the structural and stratigraphic complexities in the Madrid area and to map the distribution and extent of alteration and associated Au mineralization.

Section A-A' (Fig 3.3, 3.4) is a north-south transect across the western part of Naartok and illustrates a moderately north-dipping volcanic stratigraphy. This package forms the hangingwall of the Wolverine Porphyry-intruded HBDZ which also dips northward at approximately 60^{o}. From youngest to oldest, the upright stratigraphy

progresses from pillowed variolitic high-Fe tholeiites and interlayered gabbro (Windy Lake Mafics) to peperitic basaltic andesites to high-Ti komatiitic and transitional basalts (Patch A and B) with interlayered argillite and peperitic textures. Non-variolitic high-Fe basalts (Wolverine Mafics) make up the footwall of the HBDZ. Gold bearing sericite-ankerite-pyrite altered Patch A basalts occur parallel to the HBDZ hangingwall.

A similar stratigraphic sequence can be seen in the eastern part of Naartok along section B-B' (Figs 3.3 & 3.4). In this case the section transects a faulted contact (Fig 3.1). The exact orientation of the fault is unknown but adjacent drillholes suggest it is NNE trending and NW dipping. Movement along this fault is indicated by the truncation of two argillite beds and a thick layer of Patch B basalts. Furthermore, a thin sequence of basaltic andesites in the footwall cannot be traced across the fault. In addition to the mineralized zone adjacent to the HBDZ, another mineralized lens occurs higher up in stratigraphy near the contact with overlying basaltic andesites.

Stratigraphy in the northern part of the Perrin Zone (Section C-C'; Fig 3.3 & 3.5) is approximately north-striking and steeply west-dipping. As at Naartok, Windy Lake mafics overlie peperitic basaltic-andesites which overlie high-Ti komatiitic basalts with interflow argillite and variolitic high Fe-Ti transitional basalts. The thickest mineralized lens occurs in the hangingwall of the Patch A - Patch B basalt contact. Other mineralized horizons occur along lithological contacts and proximal to argillite horizons.

Section D-D' transects the southern part of the Perrin Zone (Fig 3.3 & 3.5). The transect crosses a NW-trending NE-dipping fault at the eastern edge of the dextrally displaced high-Ti suite basalt block. A small wedge of Windy Lake Mafics (basalt and gabbro) are bound in the west by this fault and in the east by the high-Ti komatiitic basalt

contact. Volcanic units on the east side of the fault strike approximately N-S and dip steeply west. Gold-bearing horizons occur throughout the high-Ti komatiitic basalts and interstratified argillite, especially in the hangingwall of the variolitic high Fe-Ti interstratified argillite, transitional basalt contact.

Section E-E' transects N-S striking volcanic units at the Suluk deposit (Figs 3.3 & 3.6). The HBDZ occurs at the boundary between the Wolverine Mafics and Patch A/B basalts. This package of rocks is interrupted by a unit of light green coloured pillowed basaltic andesites. The bulk of the mineralization is situated in the footwall of the HBDZ in a package of high-Ti komatiitic basalts with abundant interstratified argillite.

3.3 – Petrography

This section is intended to describe the various textural features related to primary igneous processes and the changes which occurred during hydrothermal alteration and mineralization. Descriptions of the different types of veining, styles of alteration and siting of Au mineralization are described after the main lithological units.

3.3.1 – Primary Textures and Mineralogy

Primary igneous textures, well preserved at the outcrop, handsample and thin section scales, are abundant and varied. More often than not they can be confidently used to identify the various lithological units. Despite their well-preserved state, most of the primary mineralogy has been destroyed by metamorphism and/or alteration.

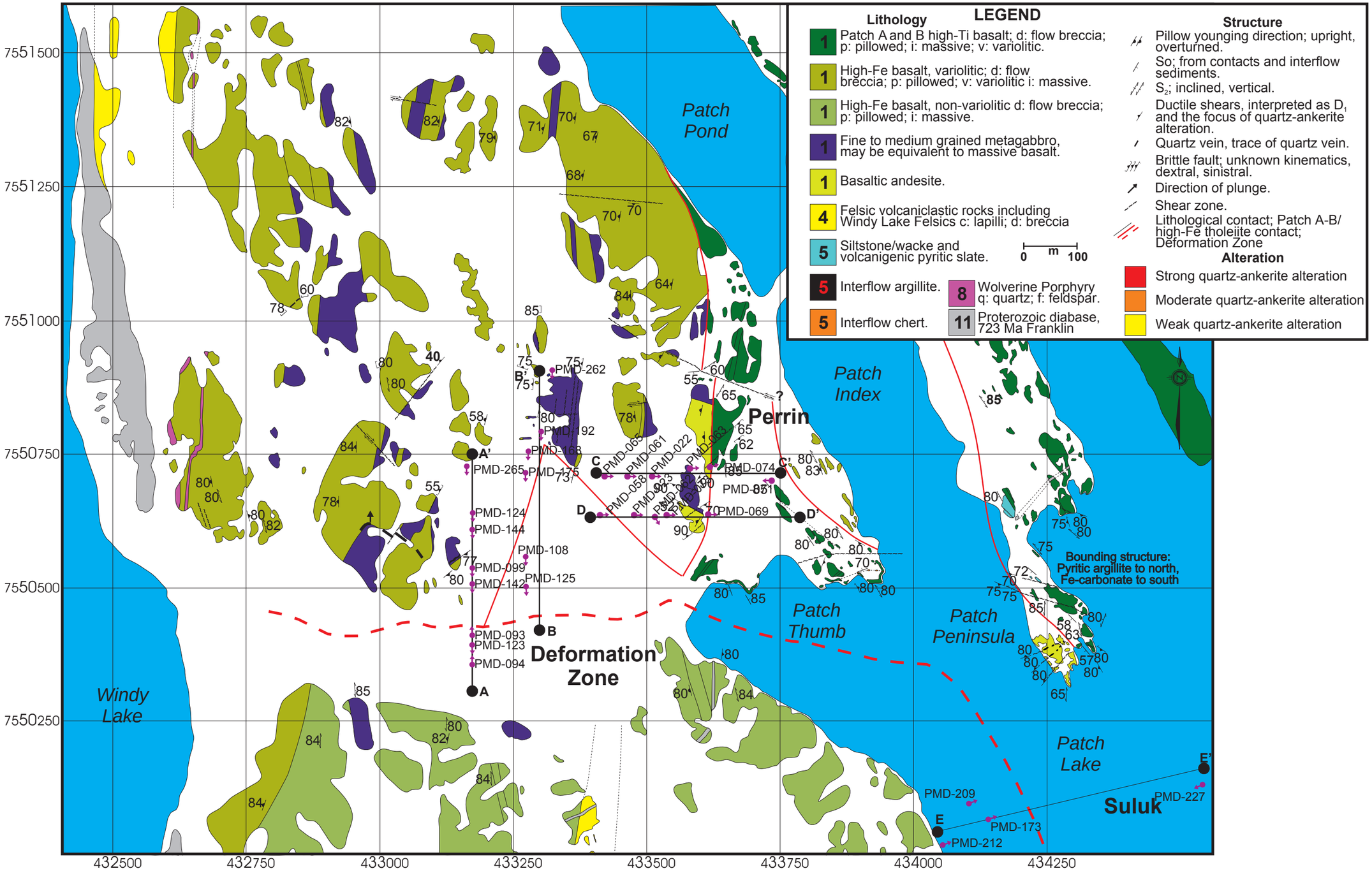

Fig. 3.3 Location of drillholes (purple dots) and cross sections (black lines) shown in Figs. 3.4-3.6.

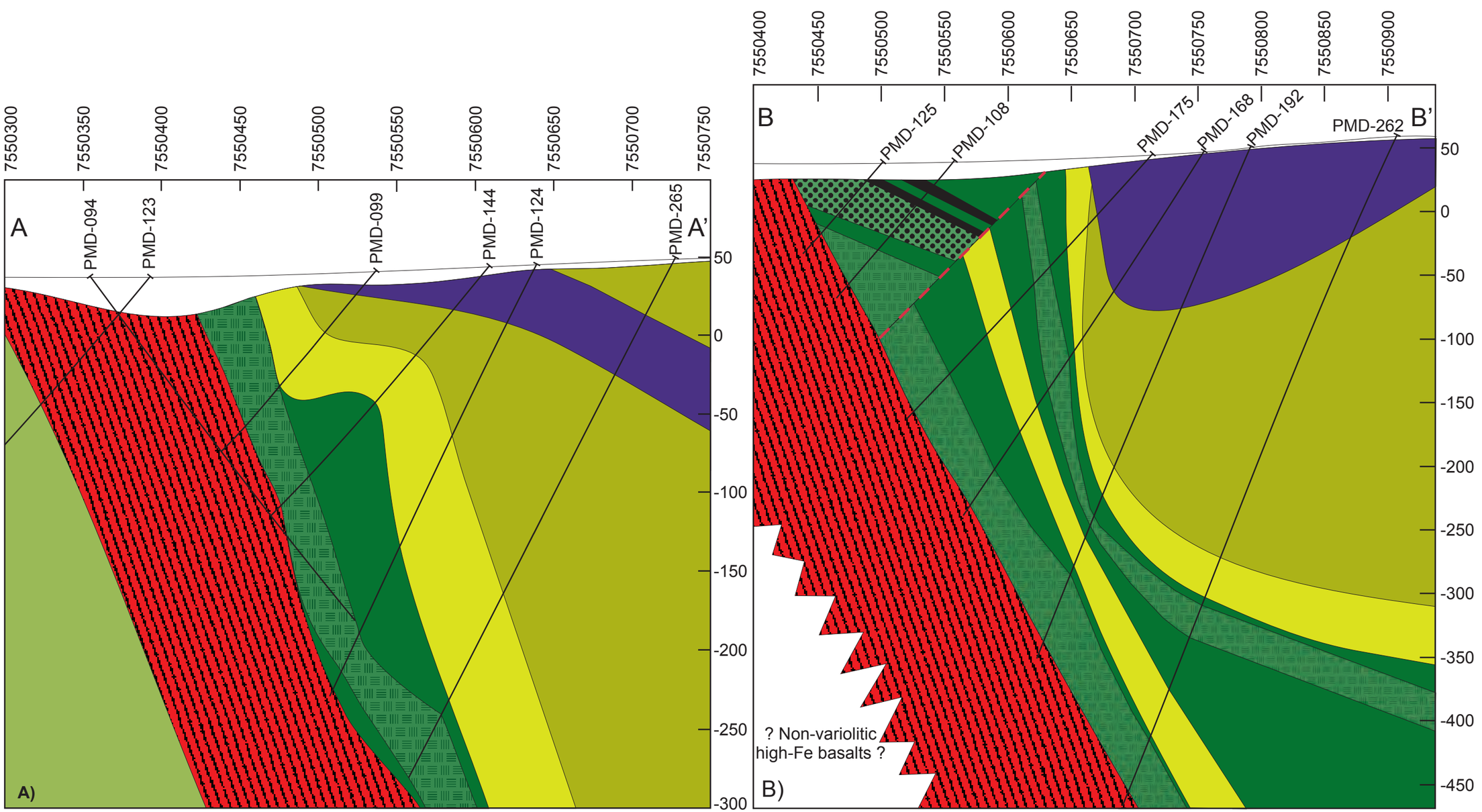

Fig. 3.4 Cross-sections through the Naartok area: (A) Western Naarok; B) Eastern Naartok. Location of cross-section is shown on Fig. 3.3 and legend on Fig. 3.6. Black lines are drillholes. Depth is in meters.

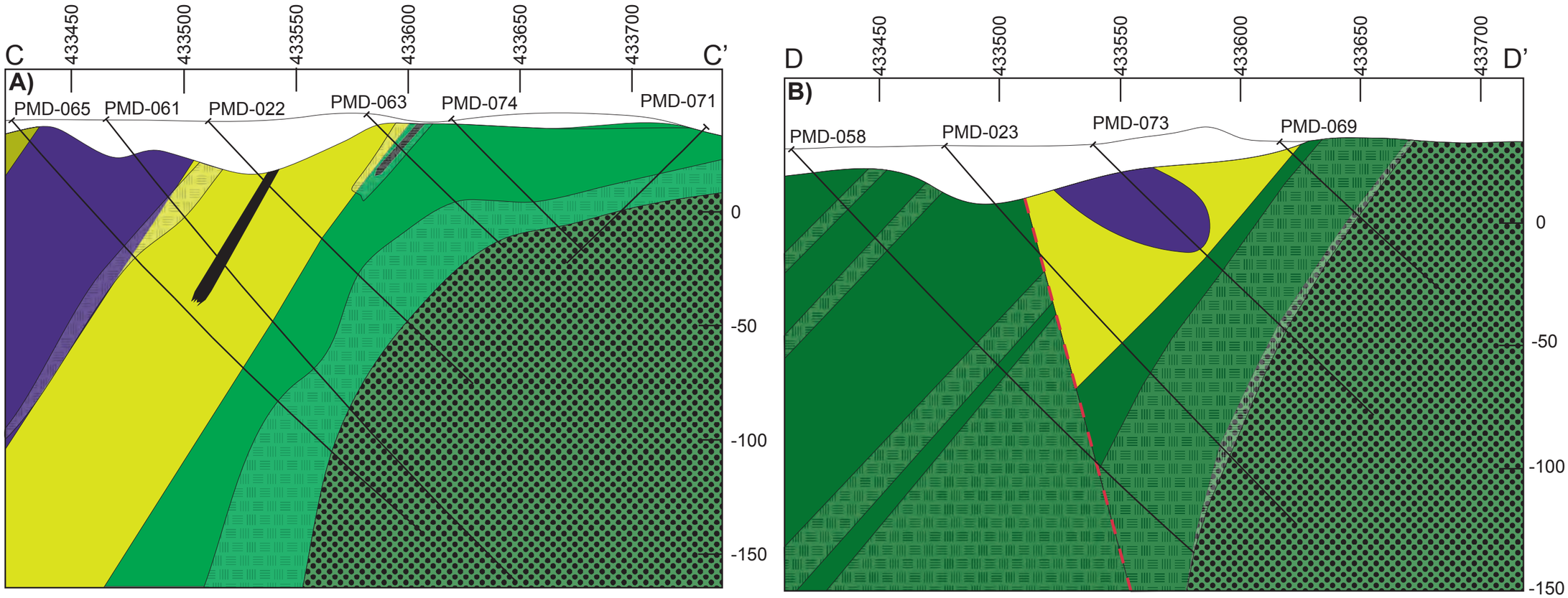

Fig. 3.5 Cross sections through the Perrin deposit: A) Northern Perrin; B) Southern Perrin. Location of sections shown of Fig. 3.3 and legend on Fig. 3.6. Black lines are drillholes. Depth is in meters.

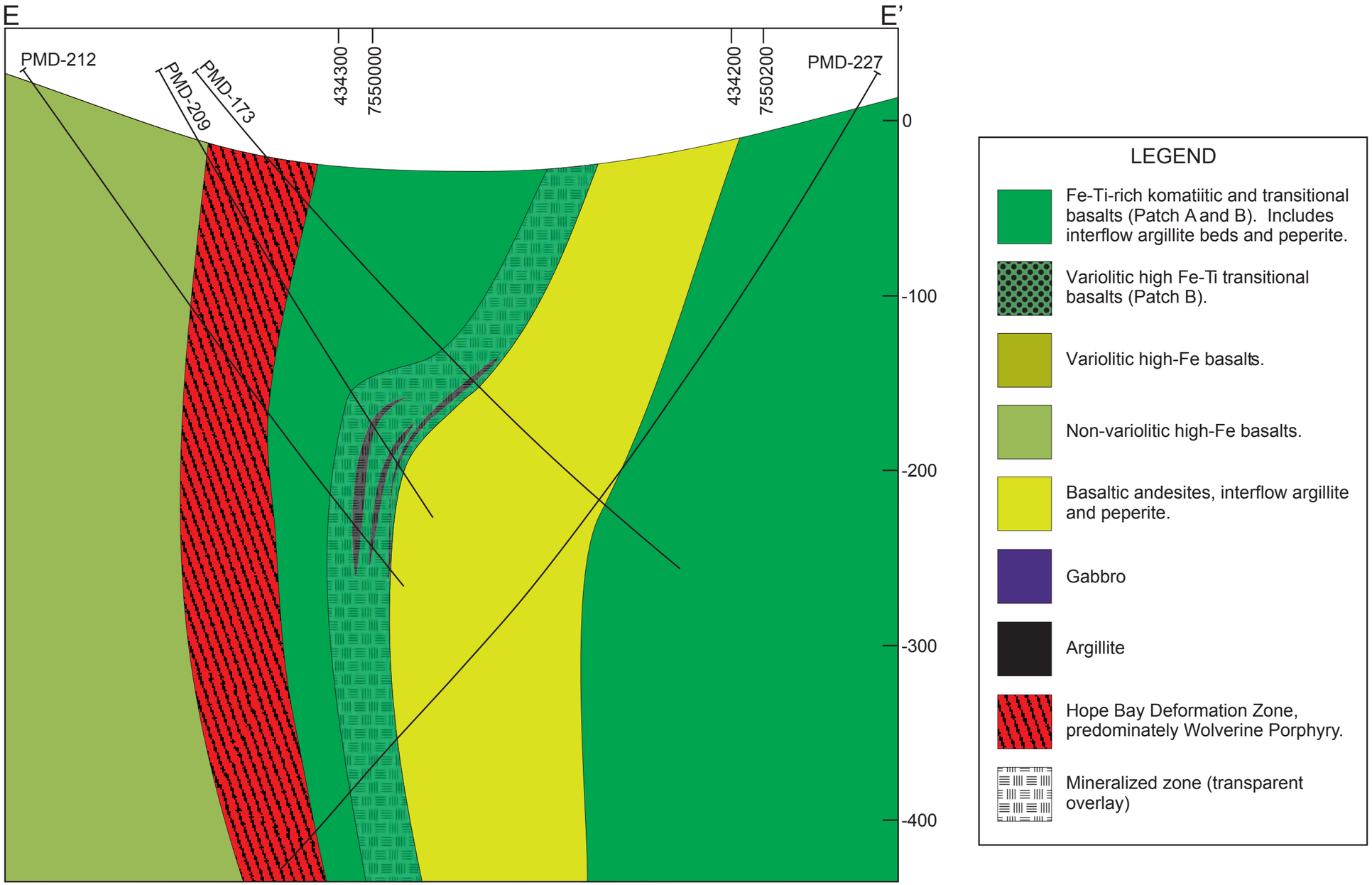

Fig. 3.6 Cross-section through the Suluk Deposit. Location of cross-section shown on Fig. 3.3. Black lines are drillholes. Depth is in meters.

Ti-rich komatiitic basalts (Patch A)

This unit of black to dark green flows form the stratigraphically lowermost unit in the Madrid corridor. Interlayering with overlying tholeiitic basalts occurs at the upper contact whereas interstratification with Patch B occurs throughout. Despite small variations in major element geochemistry, least altered samples from the Madrid area plot as (high-Ti) komatiitic basalts on a Jensen cation diagram (Jensen, 1976; Grunsky *at al*., 1992). The unique geochemistry of these rocks will be addressed more completely in Chapter 4.

Individual flow units within Patch A can often be delineated in outcrop by basal and flow top breccia zones which bound poorly formed pillows, pillow breccia or massive flows (Plate 3.6). Single flow units are also recognized in core, but are more difficult to identify. Flow thicknesses are typically <10 m, but may be greater. Minor but significant amounts of argillite or chert interrupt flow successions. The fine-grained black argillite members are typically <1 m, but may be up to a few meters thick. Argillite also occurs as matrix material within peperitic textured flows. Quenched juvenile basalt clasts (jigsaw-textured breccia), rounded "fingers" of basalt surrounded by argillite and argillite filled hairline cracks all attest to hot lava mingling with wet, unconsolidated sediment (Skilling *et al.,* 2002). The occurrence of interflow sediment and recognition of peperitic textures within flows indicates that either background sedimentation rates were greater as compared with rates during overlying volcanism and/or that komatiitic basalt volcanism was more sporadic. The pillowed flows and presence of argillite also points to a subaqueous oceanic setting. The peperitic textured Patch A basalts are commonly the preferred host for gold at Madrid. This relationship is described in more detail below.

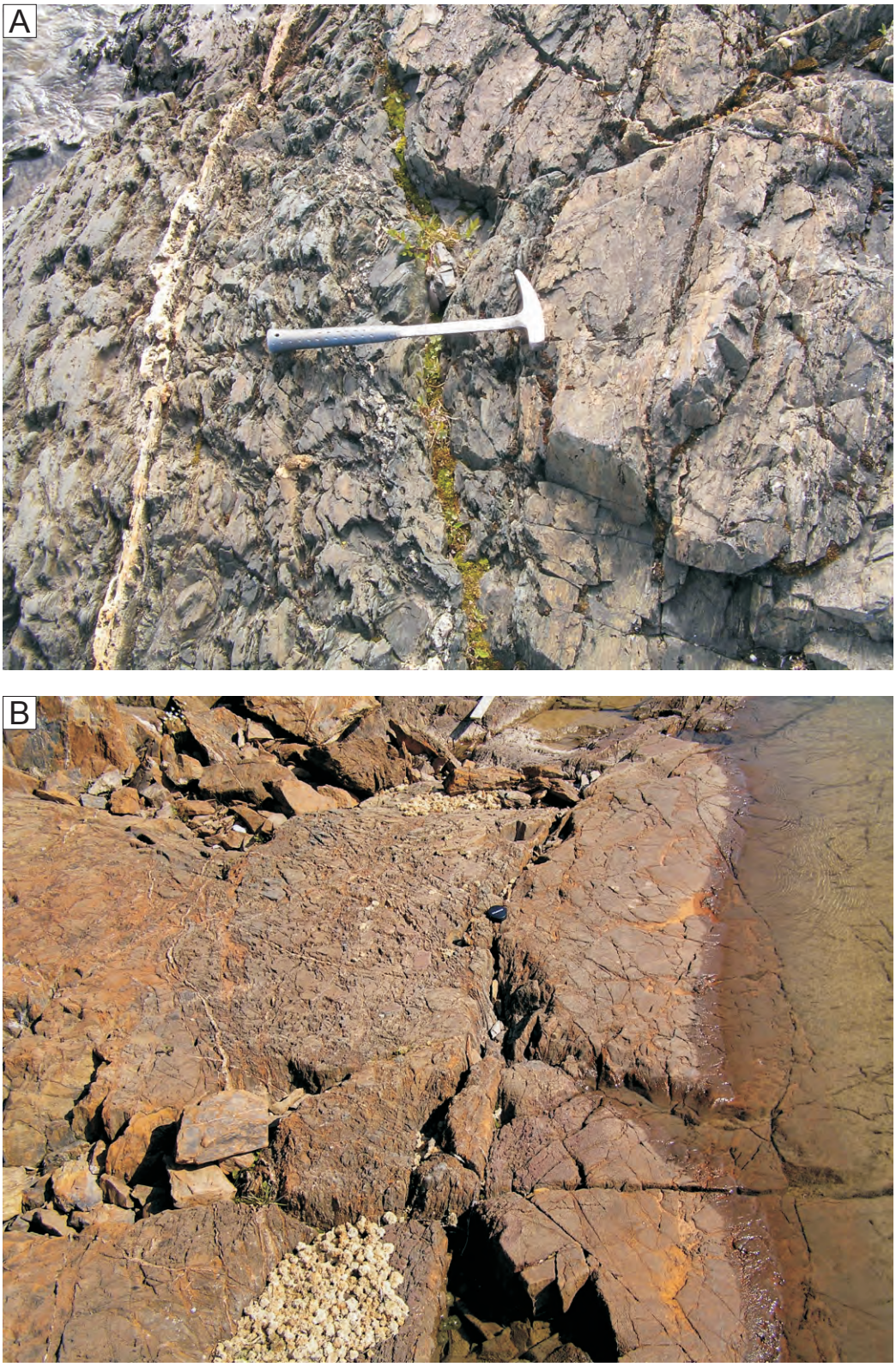

Plate 3.6 (A) Contact between flow breccia and massive flow in komatiitic basalts; (B) Ankerite altered massive komatiitic basalt flow with a flow breccia cap.

Individual high-Ti komatiitic basalt pillows contrast with those of tholeiitic basalt composition by being smaller (<1 m), more brecciated, darker in colour, and more poorly formed with thick, often indistinct selvedges. When present, mm-scale amygdule clusters are fairly diagnostic of the komatiitic basalt suite. Varioles are sporadically present within Patch A flows and are typically darker in colour and less coalescing than in Patch B rocks and the variolitic units of the tholeiitic basalts. Thin cm-scale interflow chert horizons are common and provide means for determining bedding.

Coarse clinopyroxene crystals are a clear diagnostic feature of Patch A rocks. The clinopyroxenes typically occur in overlapping mats composed of mm-scale (< 5mm) stubby unoriented carbonate-sphene-oxide-sericite/chlorite altered crystals. There are two main textural varieties:

1) Rare true spinifex textured flows which exhibit bundles of parallel pyroxene plates. These flows show evidence of layering analogous to the subunits of a true komatiite (Pyke *et al*., 1973; Arndt *et al*., 1977). Chilled and fractured flow top breccia (zone A_1) overlies quench-textured plate spinifex (zone A_3) which overlies knobby cumulate textured pyroxene/olivine (zone B_3)

2) More commonly, short (<5 mm) stubby unoriented clinopyroxenes occur as overlapping mat textured layers and pods which occur down into the flow. This texture has been traditionally described as harrisitic by exploration geologists at Madrid. However, the lack of oriented branching, arborescent or fern like forms characteristic of harristic textures (Wadsworth, 1961; Blackburn and Dennen, 1969; Nesbitt, 1971; Theriault and Fowler, 1995;) suggest the term may be inappropriate. Despite this, the definition of Donaldson (1982a/b) is much broader, including elongate, randomly

oriented olivine/pyroxene as a variety of harrisitic texture. The textures observed in the high-Ti komatiitic basalts of the Madrid area more closely resemble the "radiating spinifex" of Nesbitt (1971). It should be noted that despite the name, radiating spinifex is randomly oriented and does not radiate. It is beyond the scope of this chapter to further debate the contradictory terminology and petrogenesis of this texture, however, it is further discussed within the context of other textural features of these rocks in Chapter 6. The term 'harrisitic' is retained recognizing that it is not simply a classical plate spinifex or cumulate texture but may be the product of quench crystallization or late nucleation interior to a cooling flow.

The primary mineralogy of the komatiitic basalts is pervasively overprinted by chlorite-carbonate-amphibole-epidote-sphene-magnetite-ilmenite alteration. Euhedral randomly overlapping pyroxene splays are pseudomorphed by fine grained carbonate (magnesite and ankerite) and/or coarse chlorite laths (Plate 3.7). Dusty iron oxides (magnetite, ilmenite, hematite and leucoxene) and sphene occur on crystal outlines, along cleavage surfaces and as inclusions in magnesitic carbonate. Fine-grained green pleochroic acicular actinolite and feathery epidote are regularly found replacing the margins of pyroxene blades. Individual pyroxenes may be bound and crosscut by coarse chlorite stringers. Interpyroxene material is entirely overprinted by carbonate-chlorite-epidote-amphibole-Fe-Ti oxide alteration.

Pyroxene also occurs as rounded magnesite pseudomorphed cumulate-style grains bound by coarse chlorite laths (Plate 3.8). Pseudocumulate textured komatiitic basalts also contain coarse (1-2mm) subhedral magnetite grains which may be a replacement of olivine. Ilmenite exsolution lamellae in magnetite and sphene near the

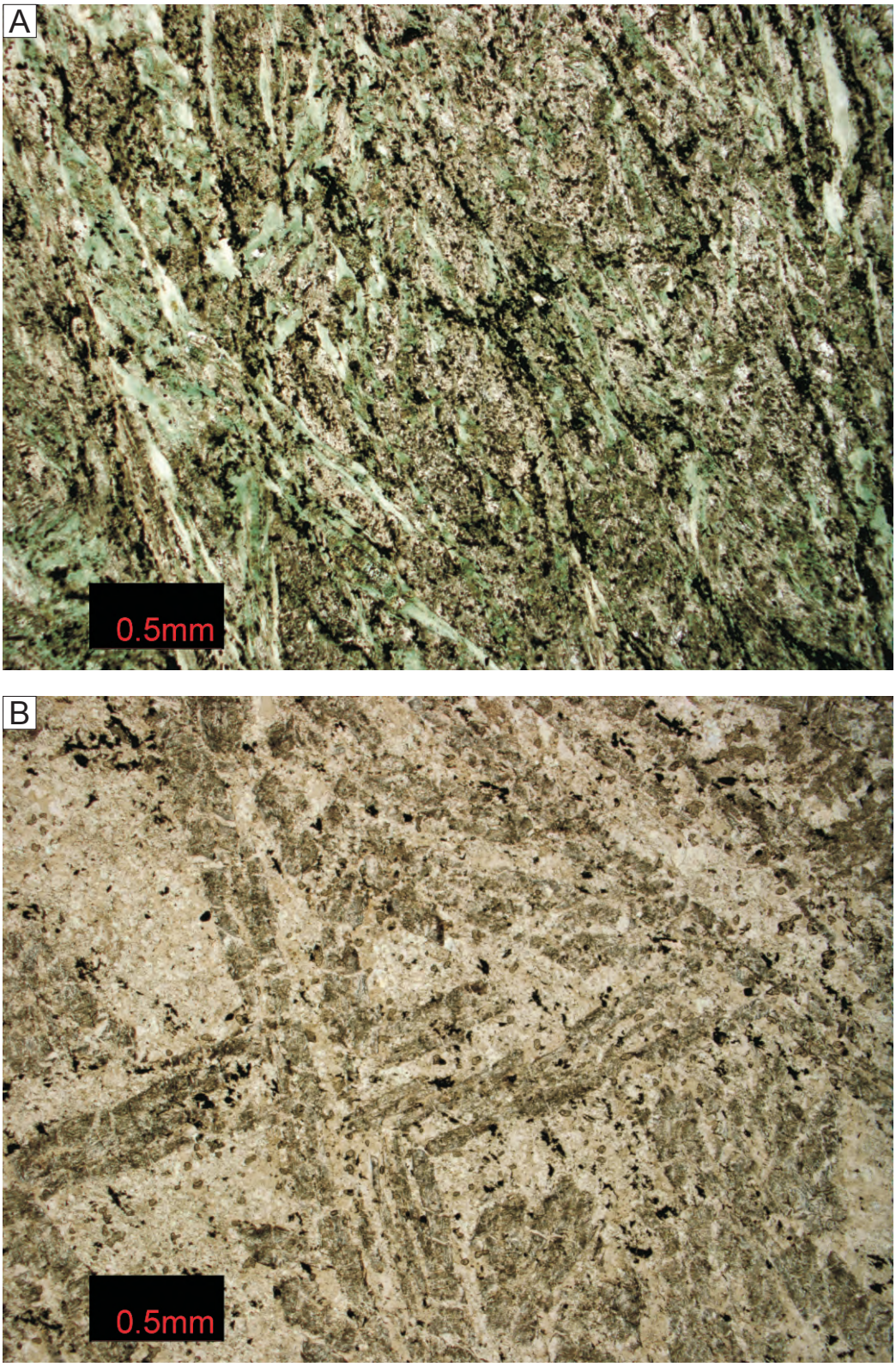

Plate 3.7 (A) Chlorite-carbonate-sphene altered harrisitic textured komatiitic basalt; (B) Strongly altered pyroxene needles replaced by sphene, Fe-Ti oxides and ankerite. Interpyroxene material is predominately ankerite.

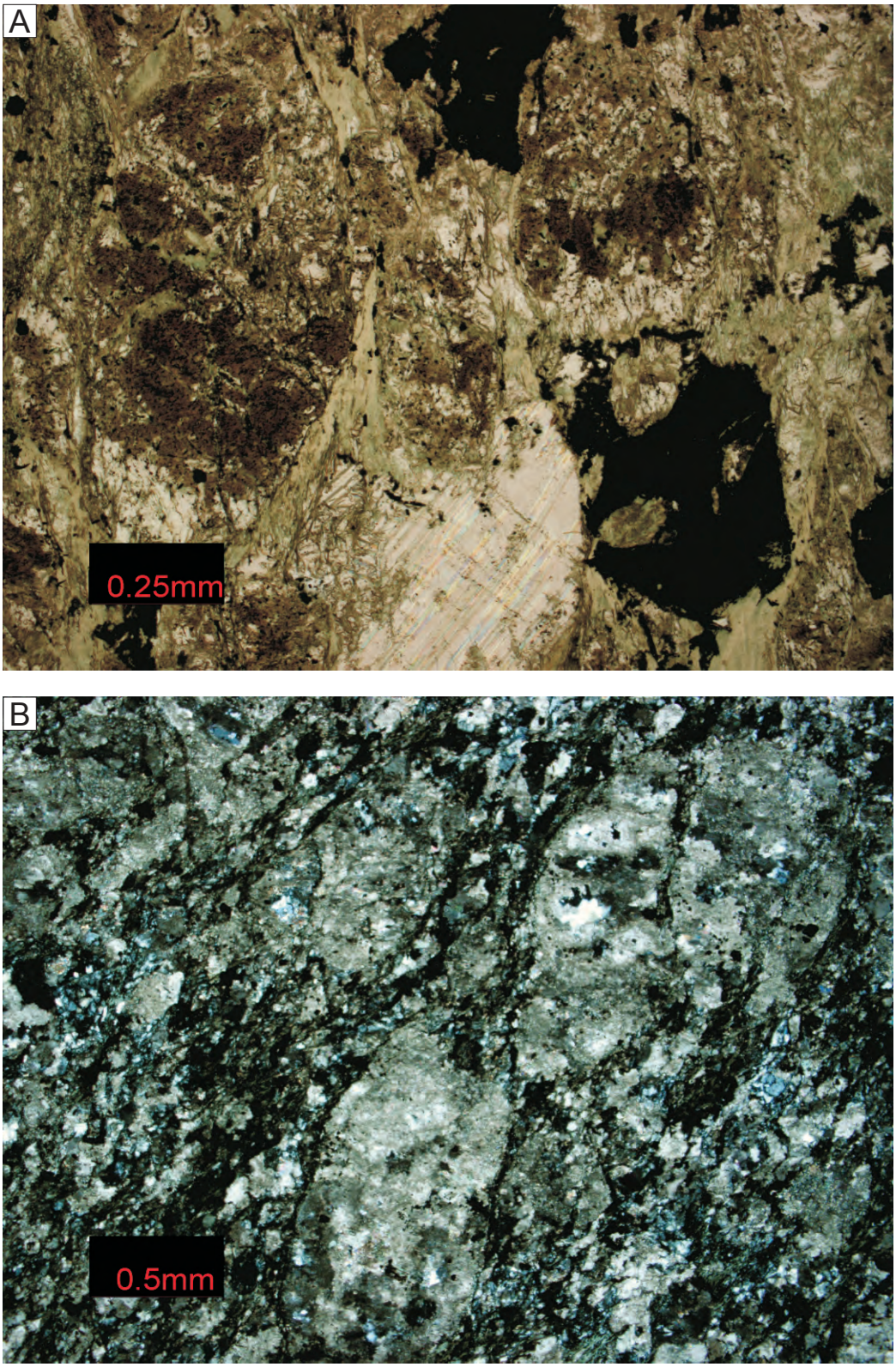

Plate 3.8 (A) Rounded pseudocumulate textured pyroxene grains altered to fine grained magnesite and Fe-Ti oxides, bound by coarse chlorite laths. Opaque grains are subhedral magnetite, an alteration product of olivine; (B) Strong quartz-carbonate-sericite altered equivalent of (A).

margins of former pyroxene grains are commonly present.

With increased intensity of alteration this low-grade assemblage is upgraded to quartz-ankerite-sericite-pyrite alteration (Plate 3.7 & 3.8). This alteration assemblage is closely associated with Au-mineralization and is discussed in more detail below.

High Fe-Ti transitional basalts (Patch B)

High Fe-Ti transitional basalts comprise a lithologically and chemically distinct unit that forms a distinct marker in the Perrin-Naartok area. The unit is observed at surface and in core, forming the footwall to the Perrin deposit. Medium green coloured flow top/pillow breccias exhibit cm-scale chilled clasts within a fine flow top/pillow hyaloclastic matrix composed of shards of quenched basalt surrounded by what was likely basaltic glass (Plate 3.9). This matrix has been subsequently overprinted by strong chlorite-calcite-hematite-amphibole-epidote alteration similar in style to the komatiitic basalts. The key identifying feature of this unit is large (cm-scale), white, round to oval shaped strongly coalescing varioles (Plate 3.9). Notably, this unit is not commonly mineralized but its upper contact has been hydrothermally altered adjacent to the overlying mineralized Ti-rich komatiitic basalts along the north-south trending Perrin zone.

The bulk of the Patch B volcanic rocks have experienced variable chlorite-calcite facies alteration, which has helped to preserve primary volcanic textures and minerals. Euhedral clinopyroxene microphenocrysts and feathery plagioclase mats can be extremely fresh (Plate 3.10). The sub-mm clinopyroxene crystals exhibit marginal chlorite-sphene-amphibole-epidote-oxide alteration. The aphanitic groundmass is

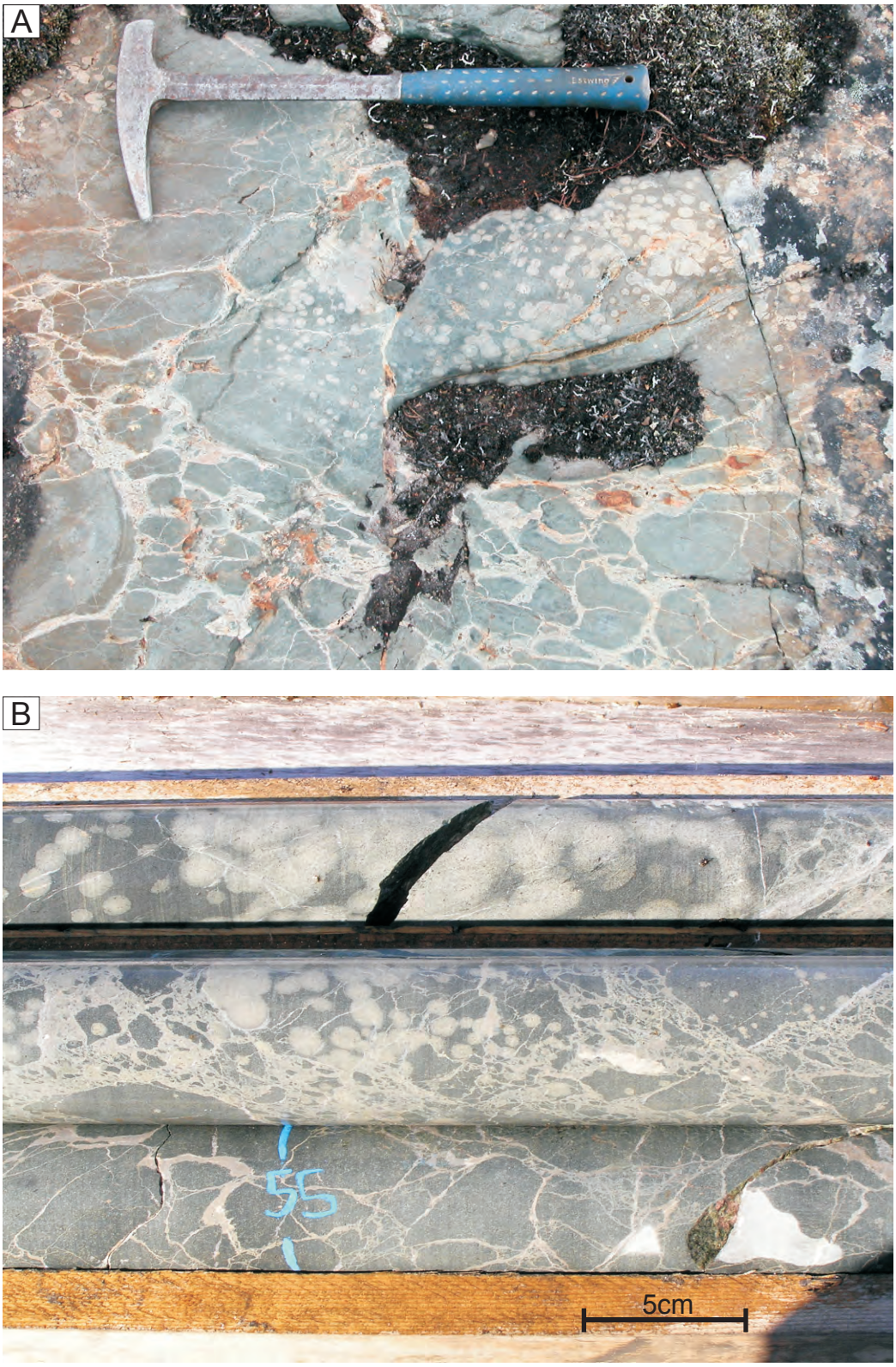

Plate 3.9 (A; B) Chlorite-calcite-hematite-epidote-amphibole altered pillowed/flow brecciated strongly variolitic high Fe-Ti transitional basalt.

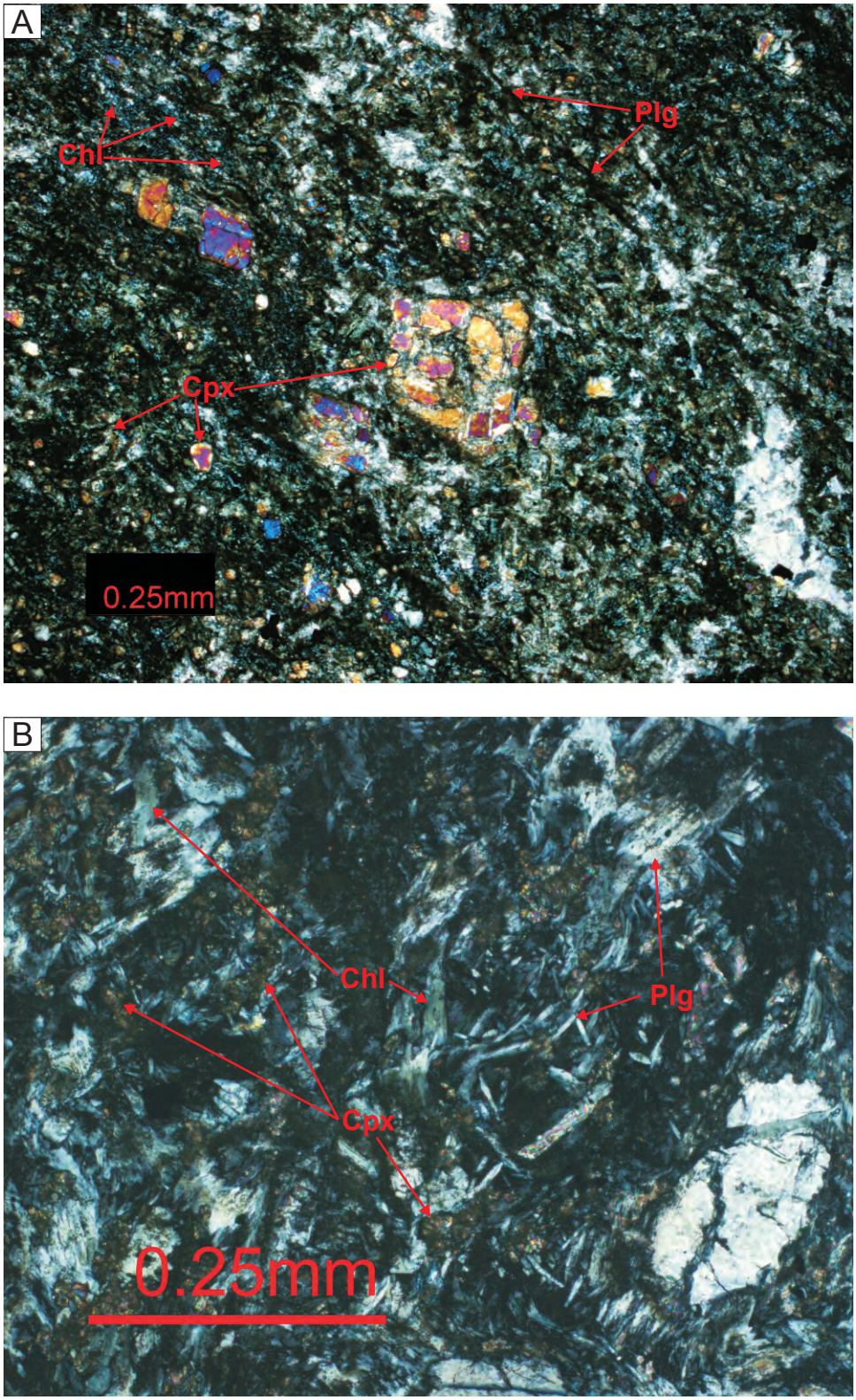

Plate 3.10 (A) Primary igneous clinopyroxene microphenocrysts in a groundmass of plagioclase and pyroxene altered to chlorite, amphibole, epidote, carbonate and Fe-Ti oxides; (B) Feathery textured plagioclase and fine-grained chlorite-Fe-oxide altered clinopyroxenes.

composed of clinopyroxene and plagioclase pervasively overprinted by coarse strongly pleochroic green chlorite-amphibole and patches of fine grained Fe-Ti oxides, sphene and carbonate (calcite/ankerite).

Tholeiitic (high-Fe) basalts, variolitic (Windy Lake Mafics)

A strongly variolitic tholeiitic basalt series outcrops immediately east of Windy Lake (Fig. 3.1). This stratigraphic package can be traced several km's north to the coast, but is truncated to the south by the HBDZ. A fault-bound wedge reappears on the south side of the HBDZ near the eastern shore of Windy Lake. Individual flows are more difficult to recognize than in the Patch Group rocks, however, massive coarse-grained flow bases can occasionally be observed to grade upward into variolitic pillows. Pillows of this unit consistently indicate younging to the west in the Madrid area. Individual pillows contrast with those of the Patch Group by being larger (generally >50 cm, commonly 1-2 m and rarely >2 m), more distinctly formed with thinner rusty weathered selvedges and abundant, strongly coalesced varioles (Plate 3.11 & 3.12). Varioles are typically pea-sized but may be as large as 2 cm. They coalesce strongly toward the pillow core, and more rarely, toward pillow rims. Several examples of epidotized pillow cores ("epidote hearts") were observed in the Madrid area.

The fine-grained groundmass of plagioclase, quartz and pyroxene and the variolitic domains have been overprinted by different alteration types. Darker green areas in handsample consist of strong chlorite-amphibole-epidote alteration in the form of fine-grained light green pleochroic patches. Lighter green to white coloured areas correspond to variolitic zones and vein margins. Chlorite is generally absent, whereas

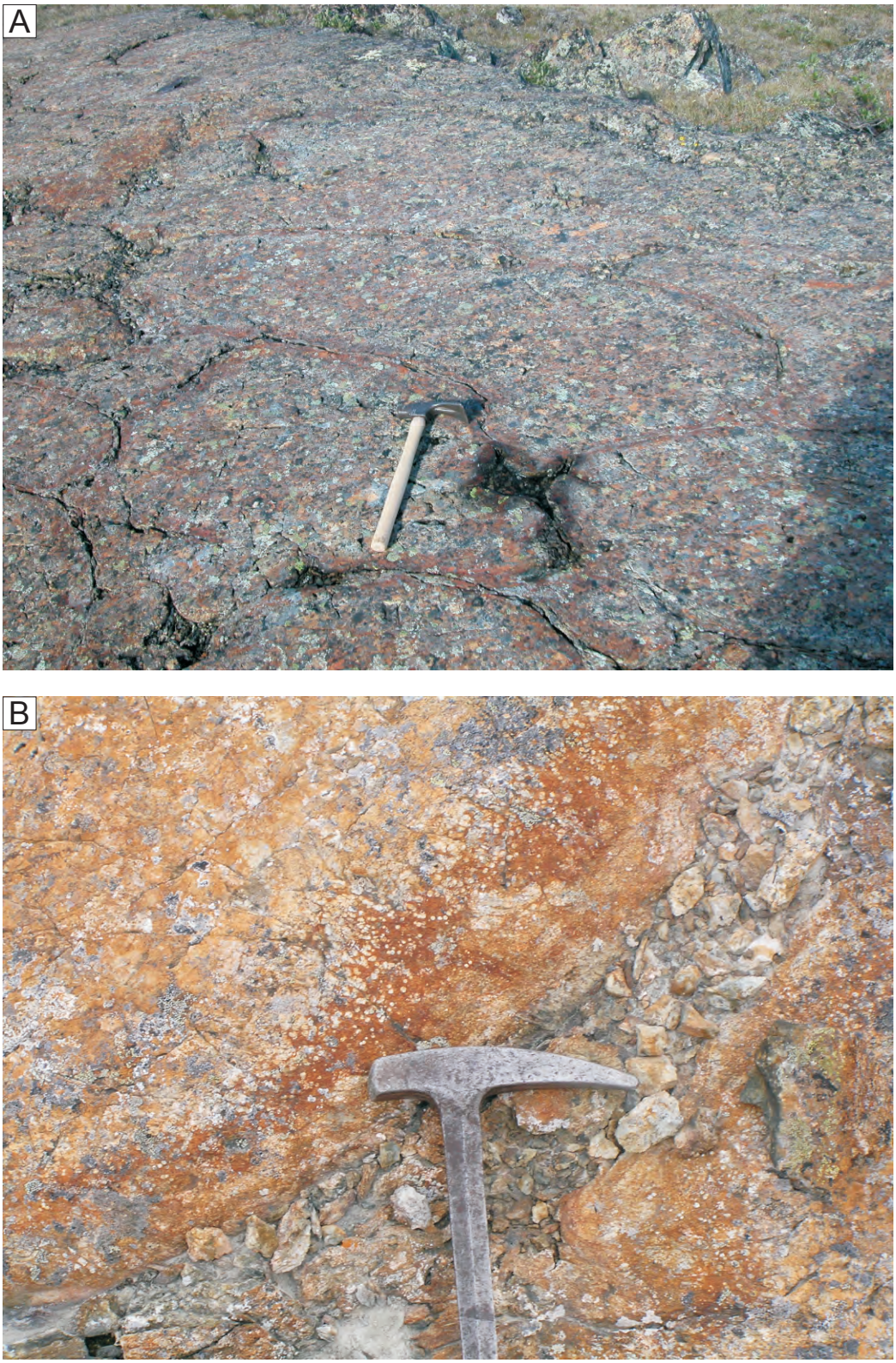

Plate 3.11 (A) Large well-formed strongly variolitic pillowed high-Fe tholeiitic basalts; (B) Strongly variolitic pillow cores giving rise to rusty coloured pillow rims with small scattered varioles.

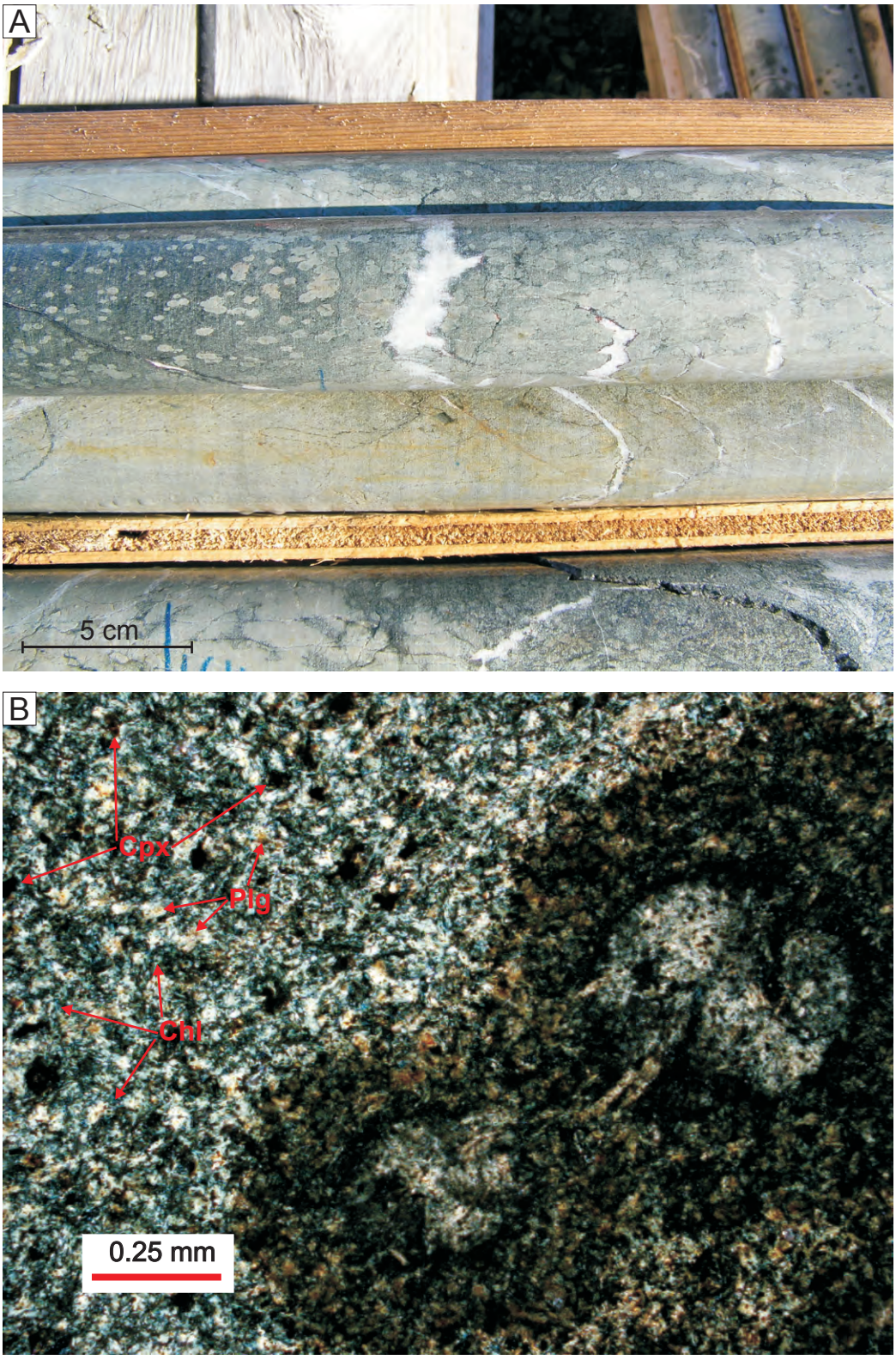

Plate 3.12 (A) Light green pillow cores composed entirely of coalesced varioles bordered by chloritic pillow selvedges; (B) Feathery mats of chlorite altered feldspar and fine grained clinopyroxene crystals. Round varioles contain outward radiating feldspars in the core and carbonate-oxide rims.

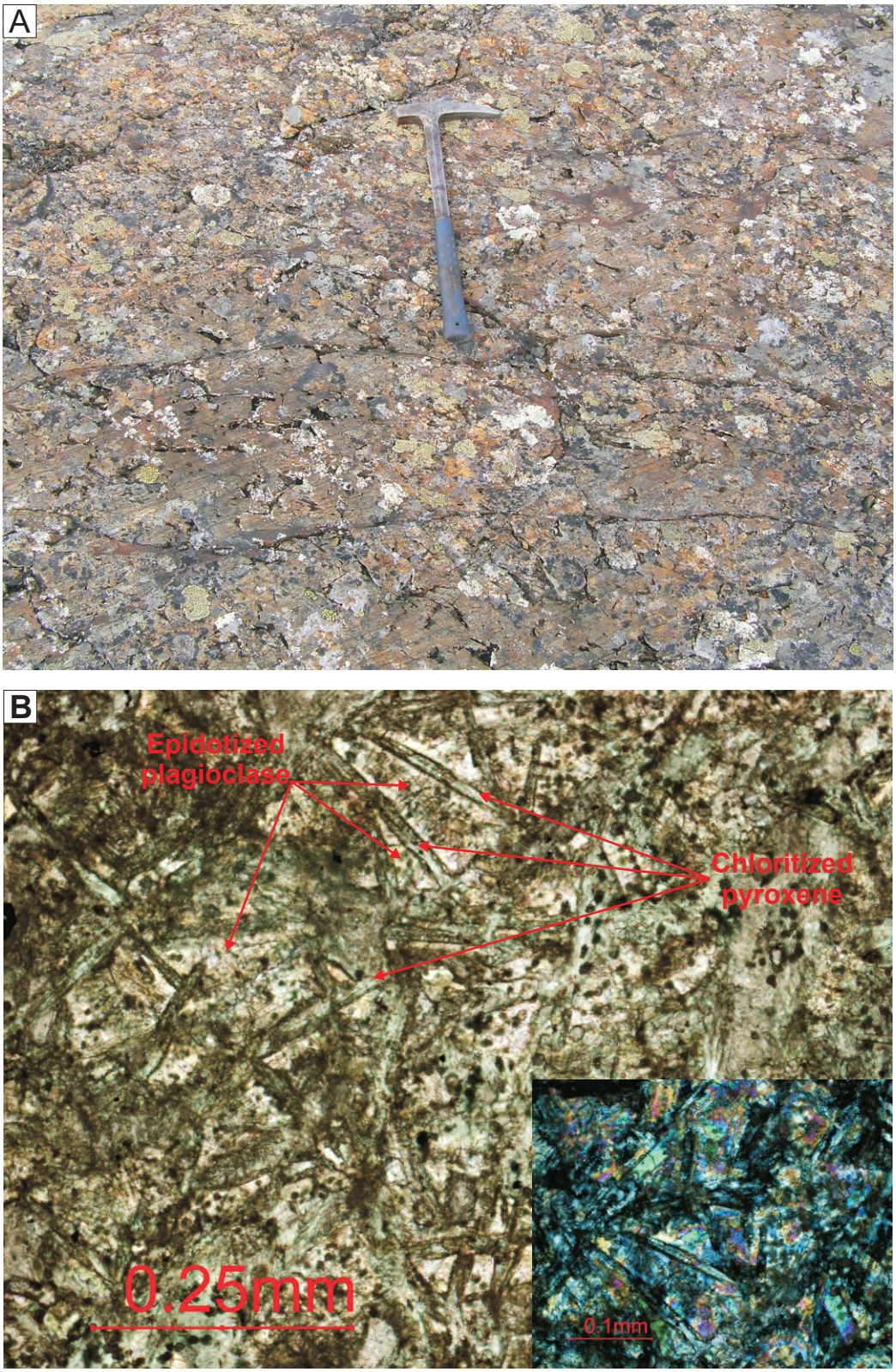

Plate 3.13 (A) Non-variolitic pillowed flows from south of the HBDZ; (B) Intergranular textured epidote altered plagioclase surrounded by chlorite altered pyroxene.

fine grained dark coloured carbonate and Fe-Ti oxides predominate (Plate 3.12).

Tholeiitic (high-Fe) basalt, non-variolitic (Wolverine Mafics)

Sherlock *et al.* (2002) noted that pillow basalts on the south size of the HBDZ lacked significant concentrations of varioles and as a result treated them as a separate volcanic unit (Plate 3.13). Geochemically this unit is nearly identical to the variolitic tholeiitic basalts north of the HBDZ, however, they do vary somewhat in volcanological features. Flow breccia is more common and pillows are commonly more brecciated than on the north side of the HBDZ. Darker green to black melanobasalt flows are observed to be interlayered with this package in core. Furthermore, this unit is interlayered with felsic volcaniclastic rocks - a feature not seen in the basalts north of the HBDZ. Limited petrographic work on this unit has identified a primary mineral assemblage of clinopyroxene, plagioclase and possibly orthopyroxene which has been strongly overprinted by chlorite-amphibole-epidote-carbonate alteration. Textures such as lath shaped chloritized/amphibolitized pyroxene enclosing epidotized feldspar (Plate 3.13) and feathery plagioclase laths surrounded by cloudy chlorite-oxide altered basaltic glass were documented.

Massive tholeiitic basalt/gabbro (Naartok Gabbros)

Interlayered with the variolitic tholeiitic basalts are massive coarse grained bases to the pillowed flows and homogenous medium grained gabbro sills. Contacts with pillowed flows vary from sharp to gradational, however, chilled margins are rarely observed. Surface mapping and subsurface correlations suggest some of these bodies are

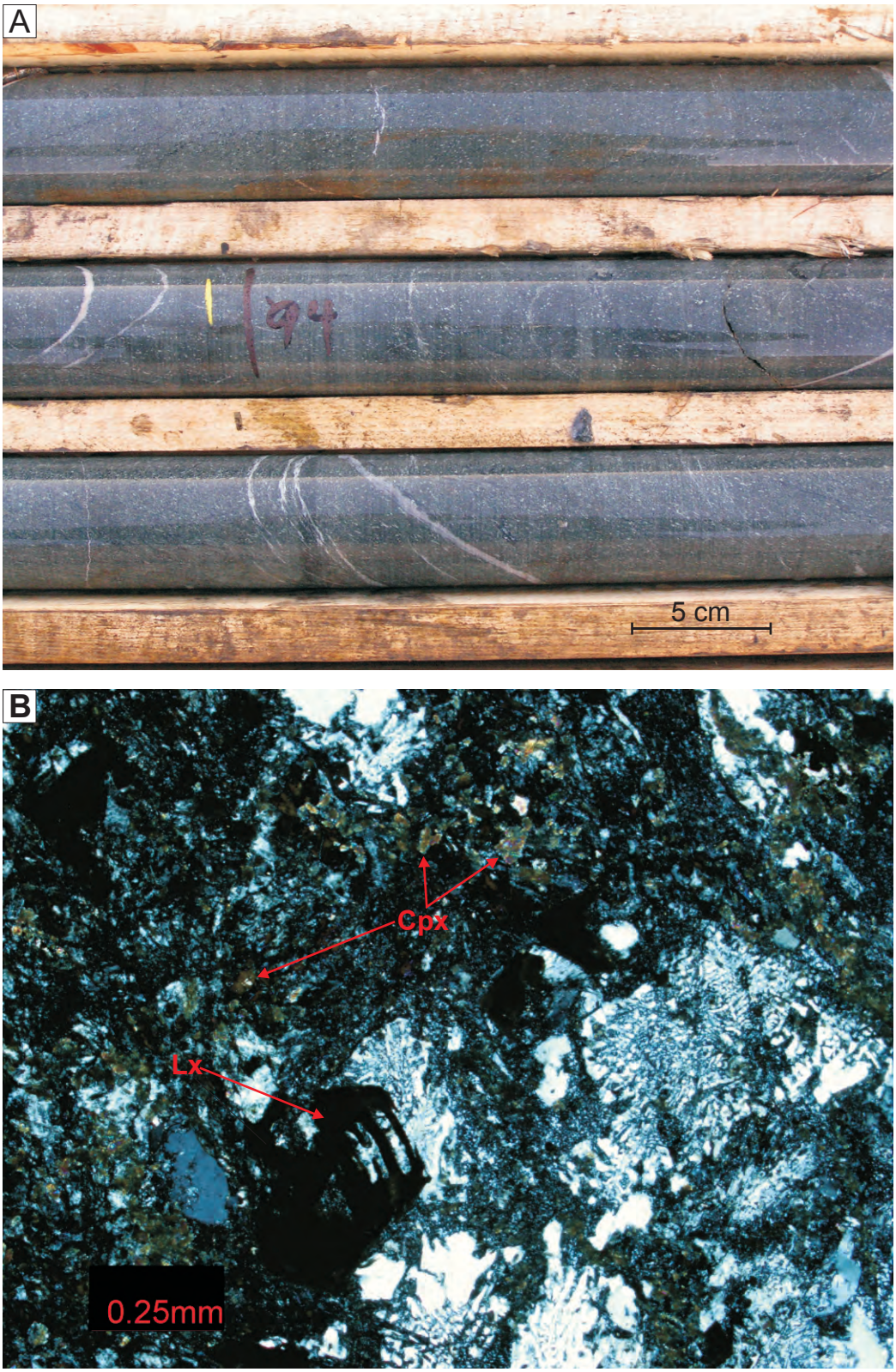

Plate 3.14 (A) Massive homogenous medium grained gabbro with pervasive leucoxene; (B) Myrmekitic textured quartz-plagioclase interstitial to granular clinopyroxene crystals and skeletal leucoxene in gabbro.

concordant with stratigraphy while others crosscut. Texturally and geochemically the two varieties are indistinguishable. Fine grained 1-2 mm light coloured skeletal leucoxene crystals are invariably present within the gabbros (Plate 3.14). Primary clinopyroxene and orthopyroxene can both be readily identified, however, most grains are strongly overprinted by Fe-Ti oxides and chlorite. Altered 1-3 mm plagioclase laths are commonly identifiable and these exhibit an ophitic to subophitic texture with included sub-mm pyroxenes. Intergrowths of 1-2 mm quartz crystals with plagioclase (myrmekitic textures) are well preserved as only the feldspar component has been altered (Plate 3.14).

Basaltic andesite (Pale Green Pillows: PGP)

Basaltic andesite flow sequences occur stratigraphically below the variolitic (high-Fe) basalts at Naartok-Perrin and are sandwiched between two komatiitic basalt packages on the east side of the HBDZ at Suluk. Small light green silicified pillows are typical at Suluk and earthy grey-green peperitic pillowed (~25 cm) to massive flows are characteristic of Naartok-Perrin (Plate 3.15). The pillowed flows at Suluk commonly exhibit 1-2mm white coalescing spots and patches. This texture may correspond to small poorly formed varioles as the shape and alteration in thin section is similar in style to altered varioles in other volcanic units. Coarse (1-2mm) albite-chlorite filled amygdules are also present. Basaltic andesite flows in the Naartok-Perrin area often show a slightly coarser-grained base which grades upward into aphanitic peperitic flow tops. The peperitic units are characterized by angular shaped jigsaw-fit juvenile clasts of basalt within a chlorite-rich argillite matrix (Plate 3.15 & 3.16). Examples of rounded basalt clasts in an argillite matrix suggest either fluidal peperitic textures (Skilling *et al.*, 2002)

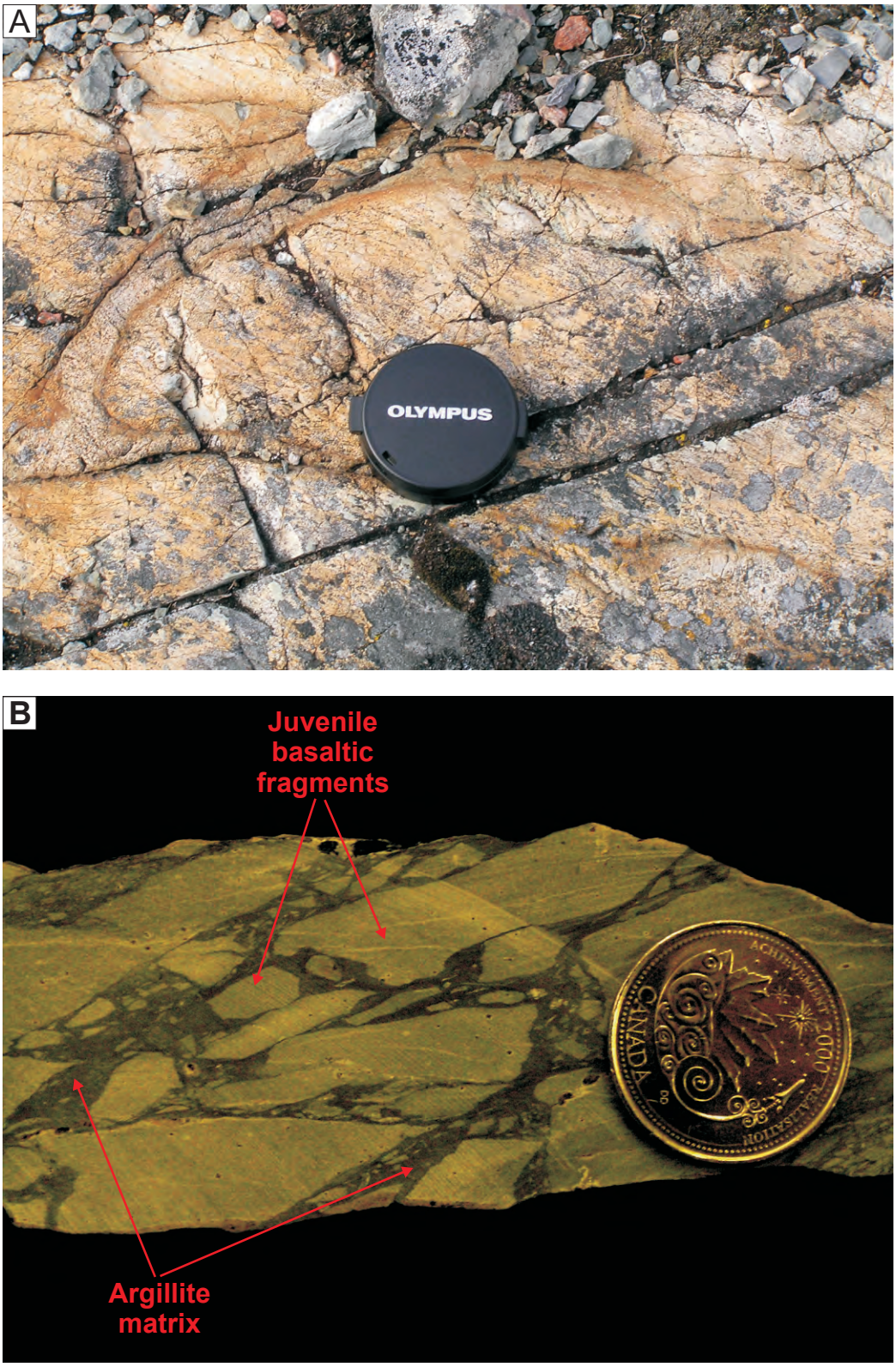

Plate 3.15 (A) Small pale green basaltic andesite pillows; (B) Pale grey-green coloured brittle peperitic textured basaltic andesite.

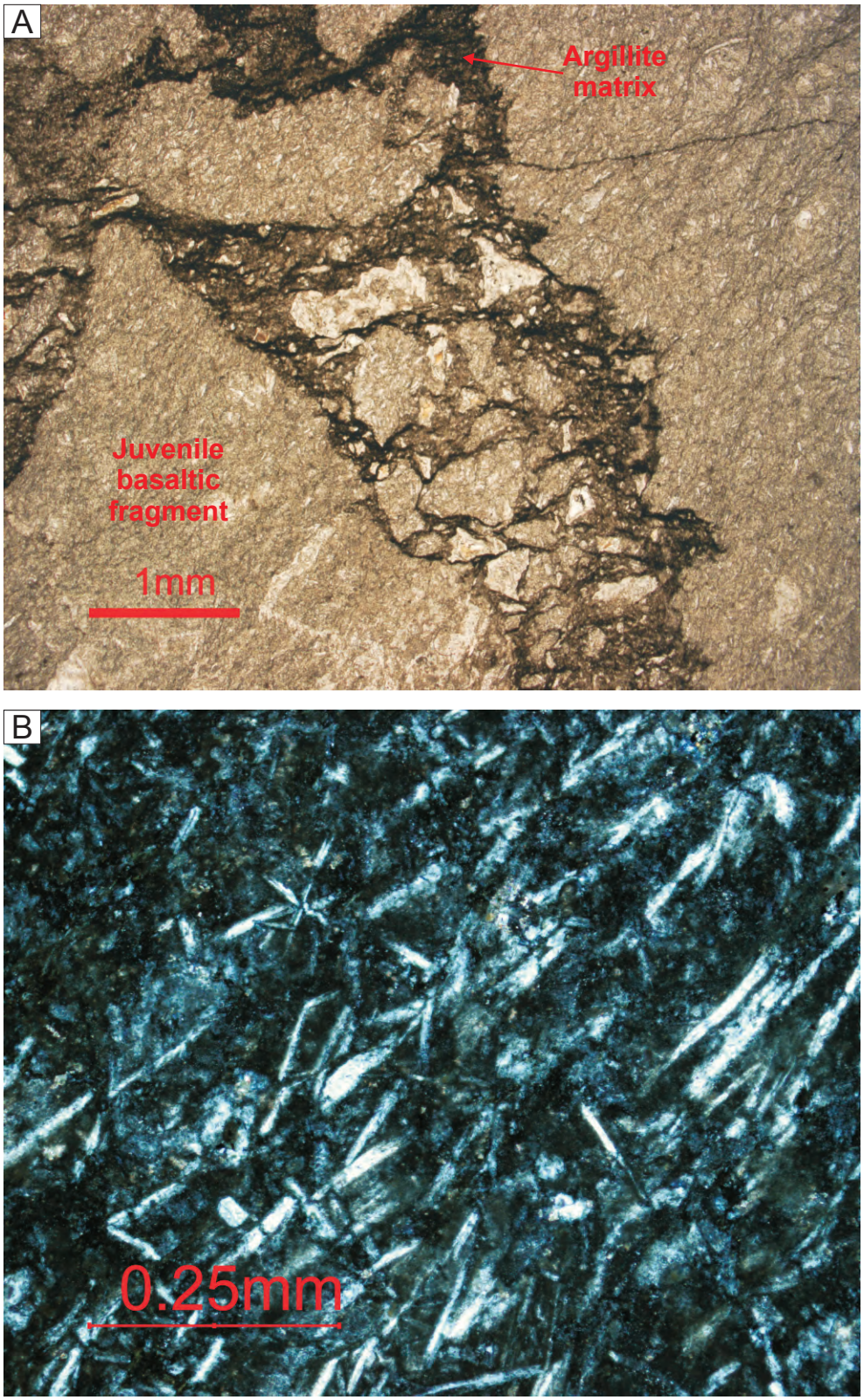

Plate 3.16 (A) Peperitic textured basaltic andesite; (B) Flow oriented plagioclase in basaltic andesite.

or epiclastic reworking. The amount of argillite varies from 0-75%. Thin linear strands of argillite anastamozing through the basaltic host are common and indicate fluidization and sediment remobilization along basalt fragment margins. Matrix argillite is composed of fine-grained quartz-feldspar overprinted by chlorite/sericite and carbonate. Carbonitization of the argillite can impart a greyish colour which can be mistaken for quartz-ankerite veining. Unlike the peperitic komatiitic basalts, these units are typically unmineralized.

In both occurrences of basaltic andesites sub-mm lath-shaped feldspar crystals show flow orientation and weak microglomeroporphyritic textures (Plate 3.16). Sub-mm relict clinopyroxene can be observed in least-altered samples. Very light green weakly pleochroic chlorite, calcite, euhedral epidote and various oxides pervasively overprint this assemblage. With increasing alteration intensity toward the high-Ti komatiitc basalts there is near complete replacement by sericite and ankerite.

Felsic volcanics and intrusives

The immediate thesis area is host to at least three differing series of felsic rocks: 1) The Windy Lake Felsics occur to the west of Madrid and can be traced northward to the coast. They are composed of variable amounts of volcaniclastic (pyroclastic and epiclastic), sedimentary and massive extrusive dacitic flows. In the immediate Madrid area the Windy Lake Felsics are composed of fine to medium grained epiclastic crystal-lithic tuffs (Plate 3.17). Sherlock and Carpenter (2003) noted that this package becomes thicker and coarser to the north suggesting a possible source center for felsic volcanism in this direction. Hebel (1999) obtained a U-Pb date of 2685 +3.3/-1.9 Ma from a dacite

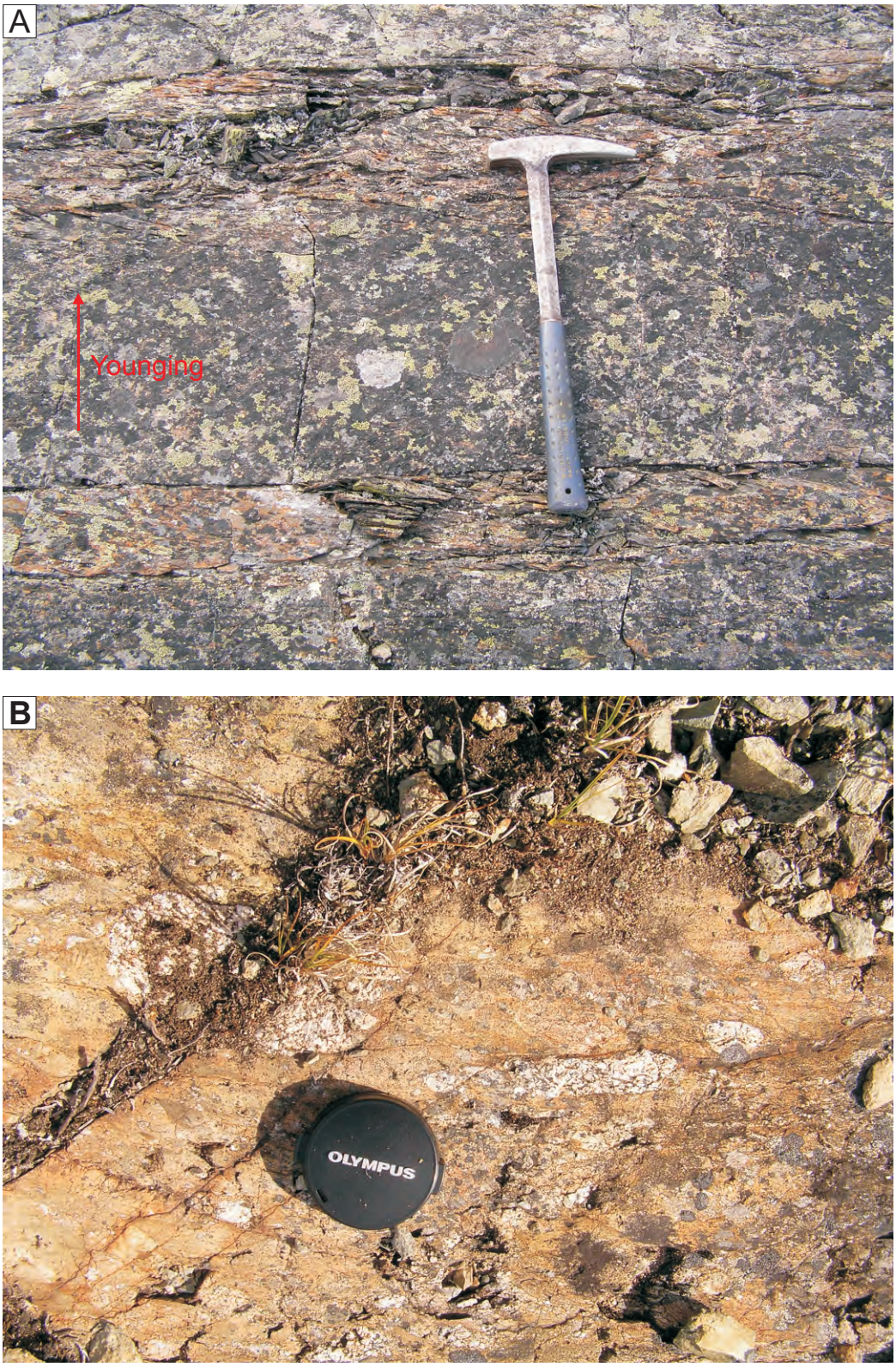

Plate 3.17 (A) Graded bedding in volcanigenic sandstones of the Windy Lake Felsics south of the HBDZ; (B) Dacitic crystal-lithic tuff horizon in non-variolitic high-Fe tholeiitic basalts south of the HBDZ

lapilli tuff in the center of the Windy Lake felsics.

2) Thin (<10m) felsic volcaniclastic rocks (dacite tuffs) locally occur as traceable beds within the mafic flows (Plate 3.17). These units have only been identified interlayered with the non-variolitic high-Fe tholeiites, being truncated to the north by the HBDZ. Their presence indicates that felsic volcanism had begun before mafic volcanism had ended (Sherlock and Carpenter, 2003). A U-Pb age of 2689.4 +4.0/-3.6 has been obtained from one of these interbeds south of the HBDZ (Sherlock and Carpenter, 2003).

3) The Wolverine Porphyry, a quartz-feldspar phyric intrusive body can be found surrounding the shores of Wolverine Lake, approximately 4 km south of Madrid. Thin north-south trending dykes of the Wolverine Porphyry also occur north of Wolverine Lake and in the western part of Madrid, east of Windy Lake. Drilling has indicated it is the primary lithology in the HBDZ. A U-Pb date of 2686 Ma has been obtained from the porphyry (Sherlock, unpublished data). Sherlock and Carpenter (2003) have suggested that the HBDZ was used as a magma conduit by the Wolverine Porphyry, which vented and gave rise to the overlying Windy Lake Felsics. Fresh Wolverine porphyry consists of abundant 2-5 mm feldspar crystals (albite and K-feldspar) with a subordinate amount of 1-2 mm embayed quartz phenocrysts in a fine quartzo-feldspathic groundmass. This unit will be discussed in more detail later in the chapter.

3.3.2 – Alteration

Identification of early seafloor hydration (spilitization) in less hydrothermally altered basaltic andesite packages is suggested by an early albite-chlorite-hematite assemblage and elevated Na_2O values within light green basaltic andesite pillowed flows

(Fiala, 1974; Leow, 1985). Albite-chlorite filled amygdules are also present and have been used as an indication of spilitization (Amstutz, 1968). Regional metamorphism to upper greenschist facies has produced an assemblage of chlorite + epidote + actinolite in the mafic volcanic rocks. Basalts bordering Franklin aged diabase dykes are typically strongly steatitized (talc-serpentine-magnetite altered) for intervals of a few meters.

The varying intensity of alteration overprinting different lithological units produces several distinct alteration styles. Hydrothermal alteration assemblages within and outside mineralized horizons are strongly dependant on parent lithology. Petrographic studies of alteration assemblages are consistently supported by mass gain/loss calculations (Chapter 4) and alteration mineral chemistry (Chapter 5). Although all units in the Madrid corridor show varying types and degrees of alteration, emphasis is placed on gold-bearing assemblages.

Ti-rich komatiitic basalts (Patch A)

Primary coarse grained textures (harrisitic and pseudocumulate) are commonly preserved in the komatiitic basalts at Madrid. With increasing alteration these textures become masked at the handsample scale but can be resolved in thin section. Less altered samples outside mineralized zones consist of coarse chlorite laths and fine grained magnesitic to ankeritic carbonate which overprint harrisitic and coarse textured pyroxene crystals. The elongate (<1 cm) chlorite laths commonly contain rounded islands of magnesite-oxide-sphene-amphibole-epidote altered, quartz-cored pseudomorphed pyroxenes. Intergrown feathery textured epidote + actinolite is a common assemblage in least altered komatiitic basalts. Coarse (2-3 mm) rounded chlorite altered pyroxene

grains coexist with large (2 mm) magnetite crystals, most likely an alteration product of olivine. With increased alteration magnesite blasts become progressively replaced by ankerite and/or siderite in part related to quartz-ankerite veining and stockworking.

Carbonate minerals constitute the most abundant alteration phase at Madrid forming as much as 60% of the rock. Several species have been identified and show considerable interspecies variation based on electron microprobe work. Ankeritic carbonate is by far the most common variety occurring with quartz as pervasive fine-medium grained crystals with dusty Fe-oxide inclusions. Sidero-magnesite grains are also a common constituent of background carbonate alteration. This form of carbonate commonly zones outward to a more Fe-rich assemblage (Plate 3.18). Ankerite also occurs as coarser polycrystalline grains pseudomorphing mafic minerals. Ankerite-siderite intergrowths are relatively common, overprinting the fine to medium grained background ankeritic-sideromagnesite alteration (Plate 3.18). Magnesitic carbonate occurs as fine grains replacing mafic minerals. It is most abundant in samples with fuchsitic phengitic muscovites and is overprinted by ankerite +/- siderite. High-Ti komatiitic basalts have been crosscut by a number of different vein types which typically contain coarse clear ankeritic carbonate intergrown with quartz +/- albite.

White mica in komatiitic basalts is a weakly paragonitic phengitic muscovite. It occurs as fine to medium grained (<1 mm) plates forming thin foliation-aligned anastamosing and bifurcating strands with fine grained Fe-Ti oxides and pyrite. These segregations wrap around and sometimes crosscut sub-mm blasts of carbonate, which are interpreted to pseudomorph mafic minerals (Plate 3.19). When mica is abundant it occurs in thick bands composed of coarse intergrown and aligned flecks which grade

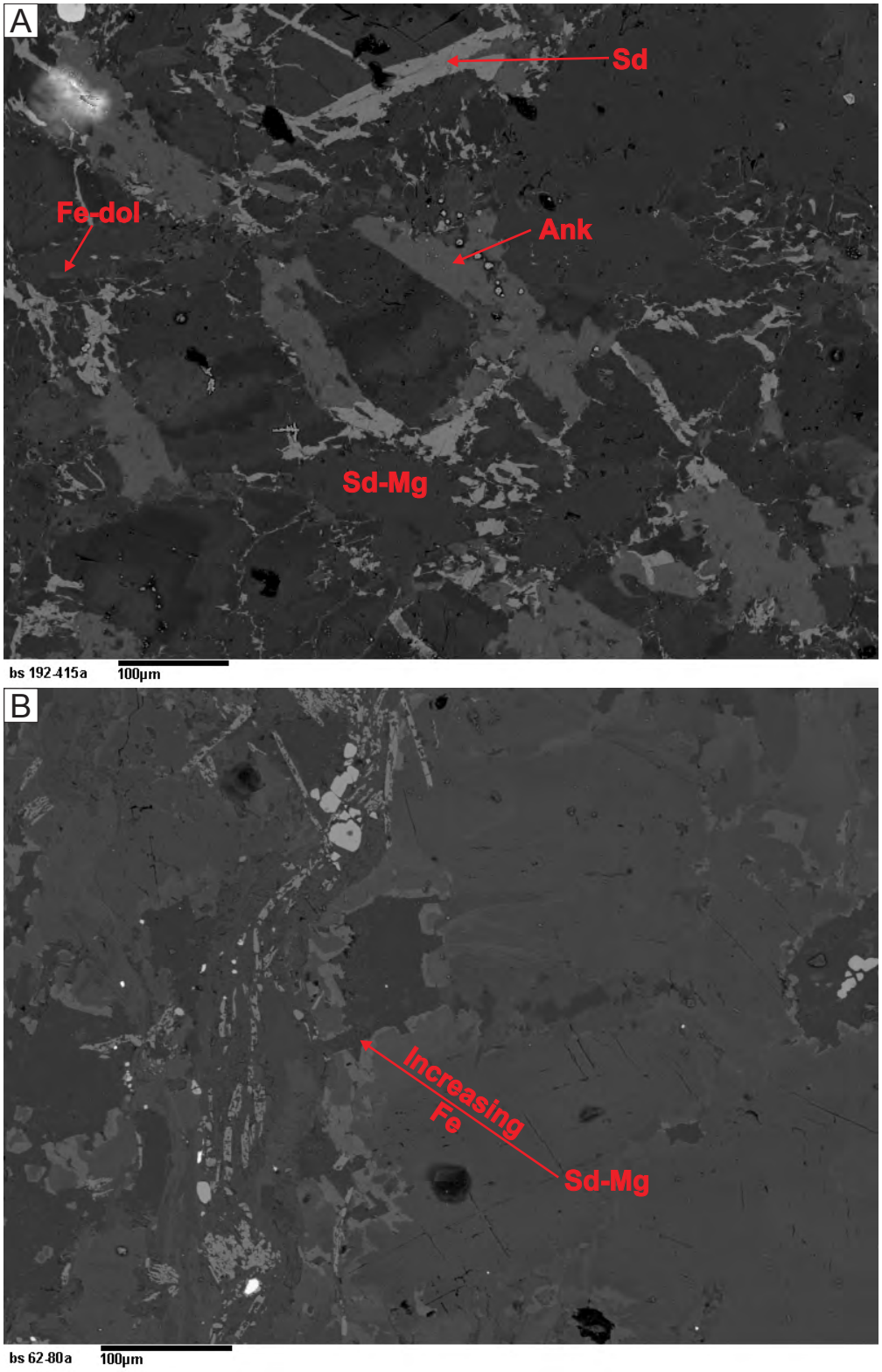

Plate 3.18 Backscatter image illustrating carbonate relationships in altered komatiitic basalts (A) Sidero-magnesite (breunnerite) overprinted by ankerite, siderite and minor Fe-dolomite; B) Zoned sidero-magnesite grain, increasing in Fe towards the rim.

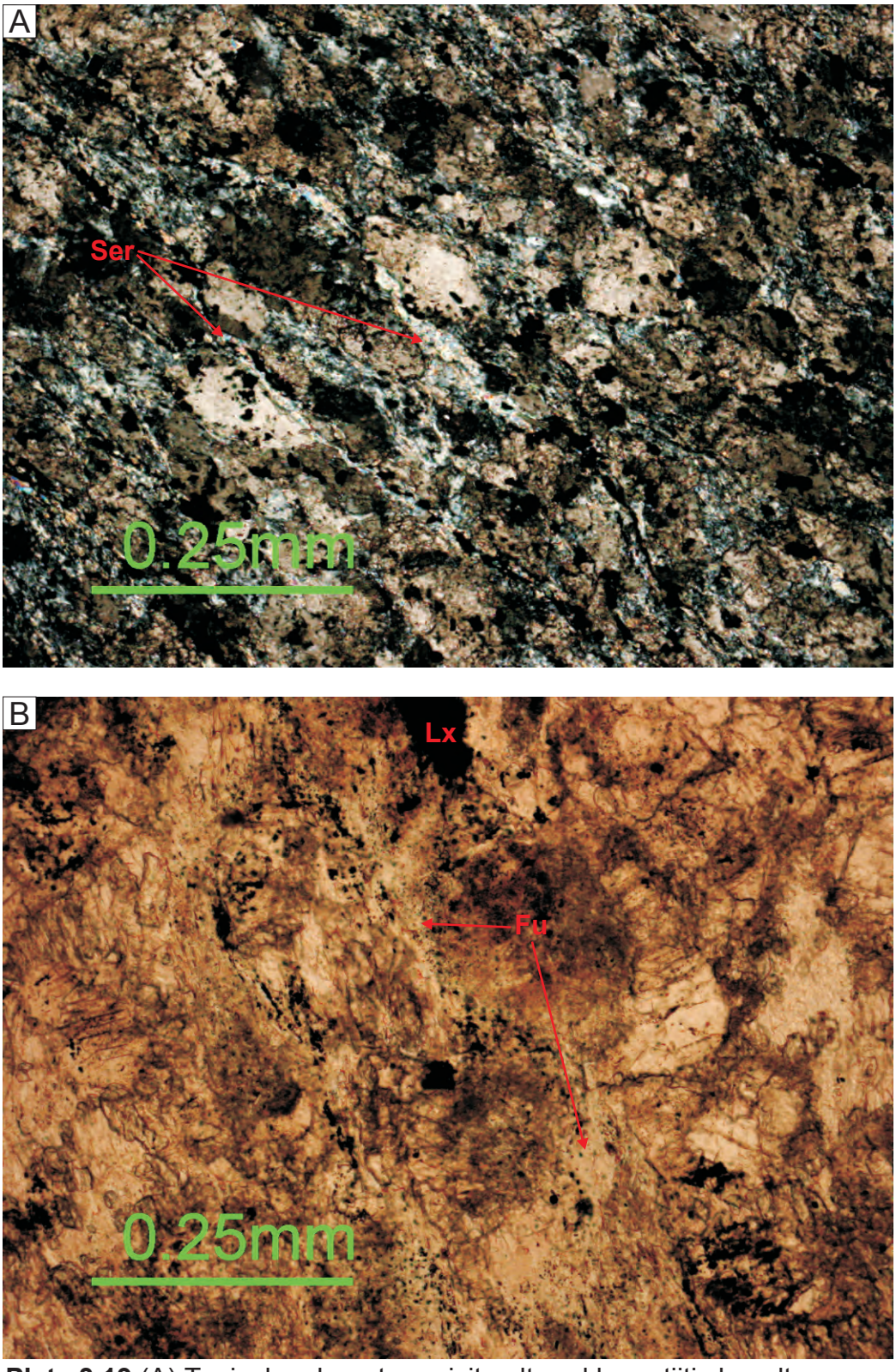

Plate 3.19 (A) Typical carbonate-sericite altered komatiitic basalt. Magnesite-ankerite blasts pseudomorph mafic minerals. Carbonate blasts are rinded and crosscut by thin sericite bands; (B) Light green coloured fuchsite rinding carbonate porphyroblasts. Opaque grains are leucoxene.

away from the band core to finer slightly more random grains. Thicker bands generally contain less Fe-Ti oxides and are separated by ankerite-quartz rich bands. When mica is not abundant it occurs as very fine grained weakly oriented slips between quartz and carbonate grains. Modal percentages of mica range from 5% to 30%. Light green coloured Cr-bearing mica (fuchsitic phengites) are relatively common, especially at Naartok-Perrin and shows similar textural relationships as the non fuchsitic varieties (Plate 3.19). Chlorite occurs as a relict phase as well as thin laminae intergrown with white micas.

Fe-Ti rich transitional basalts (Patch B)

The majority of the Fe-Ti rich transitional basalts exhibit an alteration assemblage of chlorite + calcite/ankerite + epidote + amphibole (Plate 3.20). In this facies coarse strongly pleochroic green (Fe-rich) chlorite laths, and pervasive calcite overprint basalt and interclast hyaloclastic material. Epidote and amphibole occur as stubby to elongate feathery masses adjacent to and intermixed with chloritic domains (Plate 3.20). Less commonly this group of basalts display sericite-ankerite facies alteration, especially when in contact with Patch A basalts. It is important to note that strongly altered Patch A and Patch B basalts are difficult to distinguish from each other. The only effective method is through the use of 'alteration lines' where altered samples plot on the same line as their least altered equivalent. This is discussed in more detail in Chapter 4.

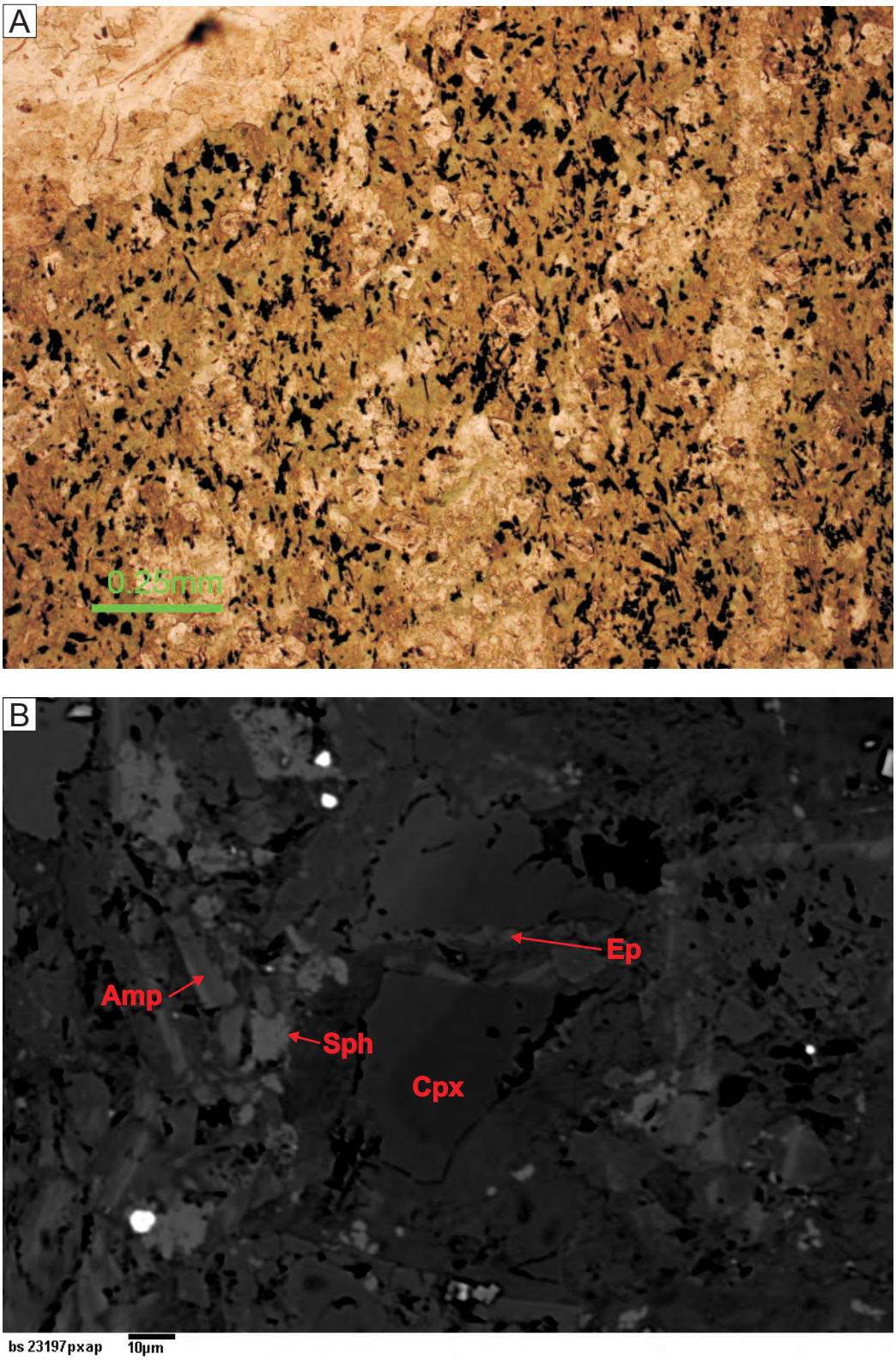

Plate 3.20 (A) Strong chlorite-amphibole alteration and patchy calcite alteration and veining. Abundant aligned Fe-Ti oxides including sphene, ilmenite and magnetite; (B) Primary clinopyroxene crystals altered to amphibole epidote and sphene.

Tholeiitic (high-Fe) basalts, gabbros and basaltic andesites

The variolitic and non-variolitic component of the tholeiitic Fe-basalts, gabbros and andesitic basalts exhibit similar styles of alteration and will be discussed under the same section. In the distal regions of the deposit these rocks are dominated by fine-grained weakly green pleochroic aligned chlorite laths and pervasive fine-medium grained calcite alteration. Deep green to black coloured chlorite is especially common in pillow selvedges, between clasts in brecciated units and within the argillaceous component of peperitic units. Andesitic basalts often show stronger and more consistent silicification, and evidence of spilitization (Plate 3.21). Fine grained Fe-Ti oxides invariably overprint primary mafic minerals producing a cloudy or patchy alteration texture. Fine to medium grained light coloured leucoxene slips are common in massive phases, especially gabbroic rocks.

Sharp boundaries occur between calcite and dolomite (ankerite) altered rocks. These boundaries also approximate the transition from chlorite to sericite alteration (Plate 3.21 & 3.22). Pervasive ankerite alteration ranges from fine grained disseminated crystals to 0.5 mm blasts with abundant dusty oxide inclusions. The Fe-oxide inclusions allow this phase of carbonate alteration to be easily distinguished from clear inclusion-free vein/stockwork related carbonate. Carbonate porphyroblasts are commonly wrapped and sometimes crosscut by thin sericite strands suggesting carbonate blastesis predates sericite formation (Plate 3.22). Sericite rims on chlorite laths and strands indicate the progressive replacement of chlorite by sericite. Larger bands of sericite may contain islands of carbonate, providing further evidence that sericite alteration postdates the carbonate. As alteration strengthens, sericite bands become thicker, coarser and better

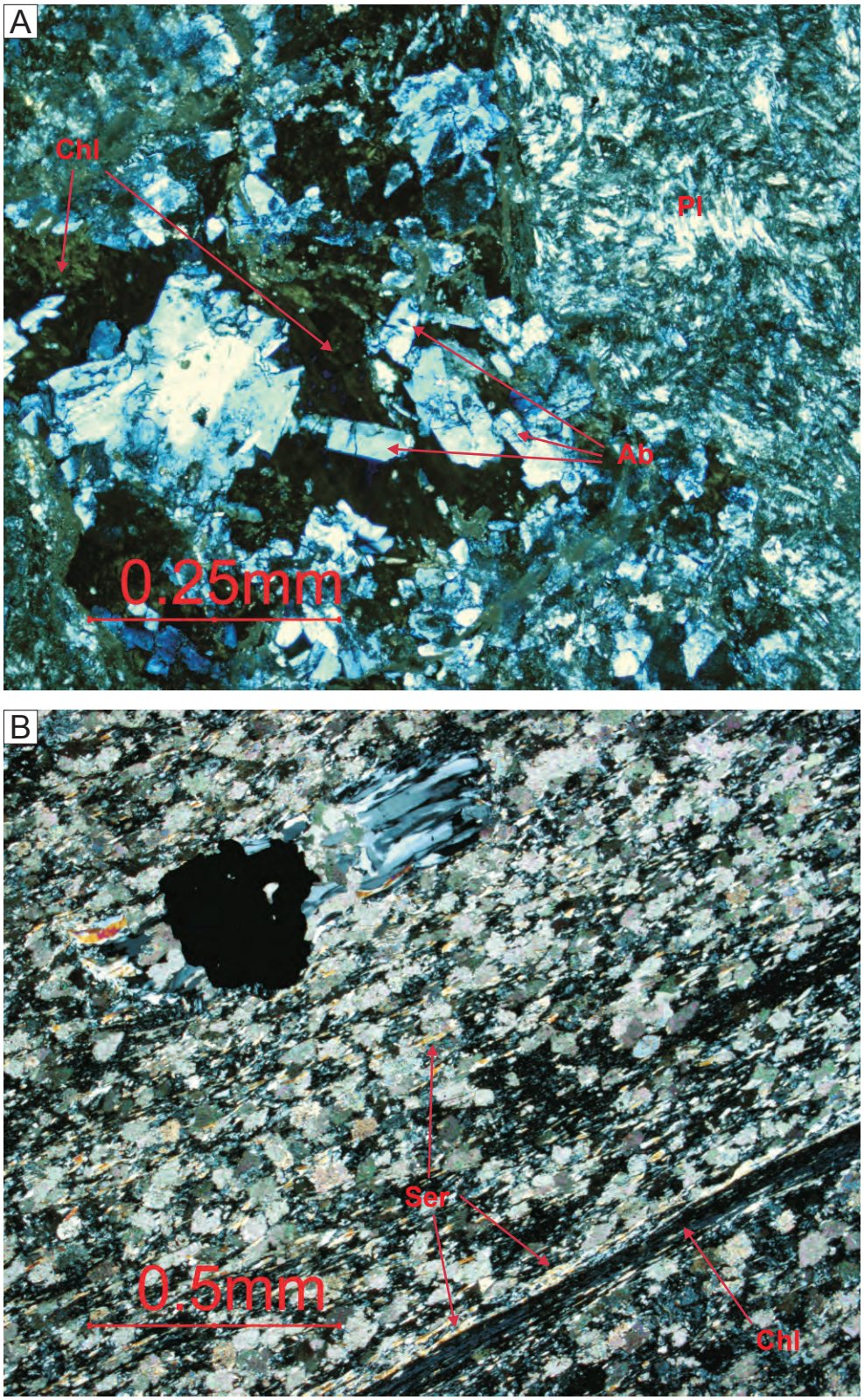

Plate 3.21 (A) Albite-chlorite-quartz filled amygdules likely related to spilitization of basaltic andesite pillows; (B) Sericite-carbonate altered tholeiitic basalt. Sericite replaces the margins of relict chlorite stringers (lower right). Pyrite with foliation-aligned pressure shadows.

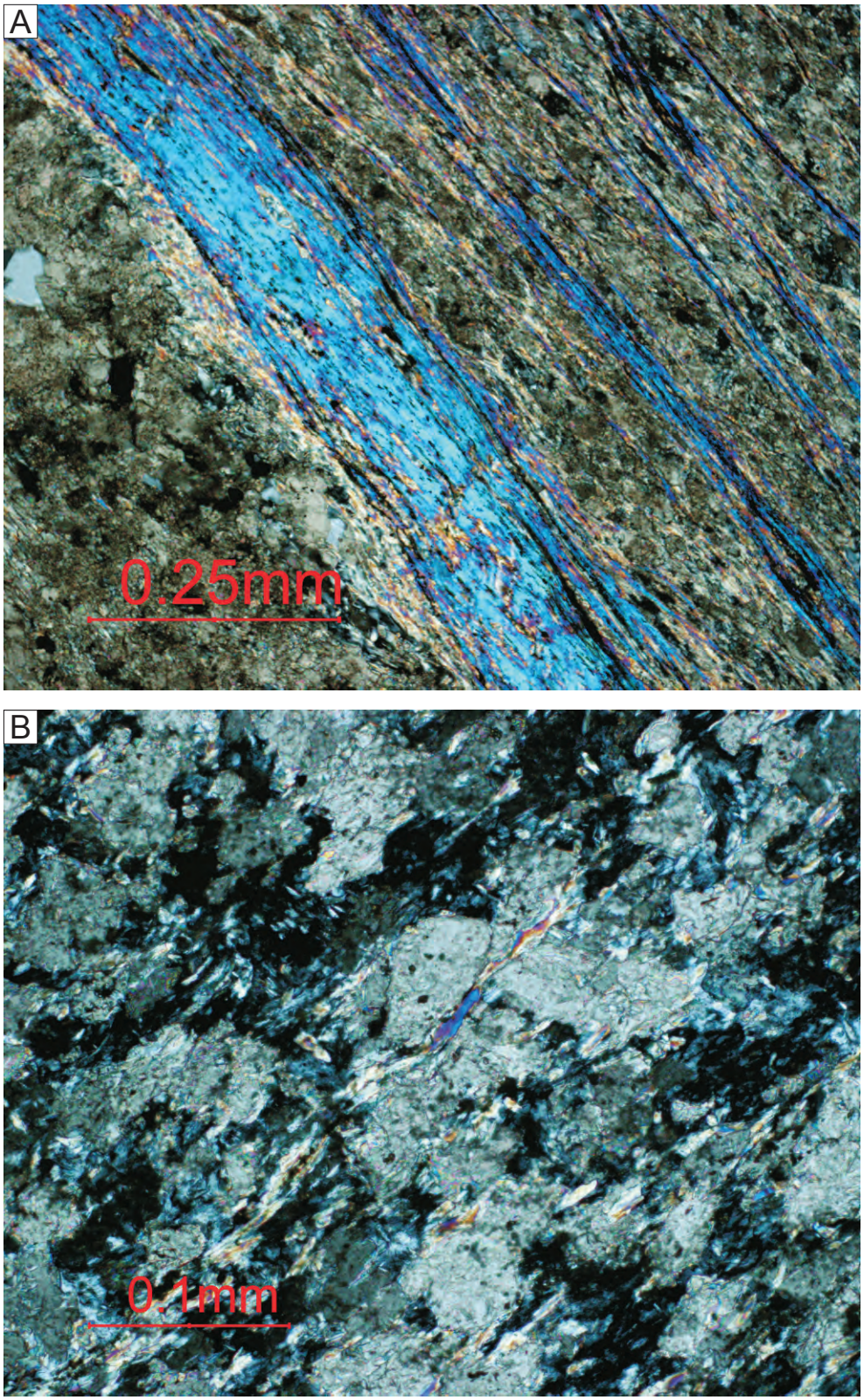

Plate 3.22 (A) Coarse bands of sericite separated by thicker bands of quartz-carbonate-oxide overprinting a quartz-feldspar-pyroxene groundmass; (B) Ankerite microporphyroblasts crosscut by sericite strands.

defined. They separate thicker bands of fine grained quartz-ankerite.

The Hope Bay Deformation Zone

The Hope Bay Deformation Zone is largely composed of altered and deformed quartz-feldspar phyric porphyry (Wolverine Porphyry), however, significant amounts of basalt and argillite are also recognized, especially in the Suluk area. The transition into the HBDZ can be gradual (over a few meters) or sharp. It is defined here as the point where primary textures of the basalt/porphyry are generally unrecognizable at the handsample scale and the rock takes on a banded appearance. This boundary coincides with the limit of mineralization, a sharp decrease in the pyrite content and an increase in sericite-ankerite alteration.

Fresh unaltered Wolverine Porphyry (Plate 3.23) contrasts markedly from strongly altered porphyry (Plate 3.23-3.24). Thin 2-3 mm segregations of yellow coloured sericite +/- green chlorite separate lozenge shaped portions of pink colored porphyry. In many cases phenocrysts (or porphyroclasts) can still be recognized. More intense alteration results in yellow mica segregations separating thicker bands (often veins) of quartz-ankerite. In this case only geochemistry can definitively identify the parent lithology. Plate 3.24 illustrates the progressive alteration and deformation of Wolverine Porphyry at the thin section scale from relatively fresh (A) to completely altered and mylonitized (C). As the alteration intensifies feldspars become completely replaced by sericite and carbonate. The end result is elongate and parallel coarse grained interstratified paragonitic mica +/- chlorite bands separated by thin linears of very fine grained Fe-oxides. Quartz phenocrysts can still be recognized, but have been stretched

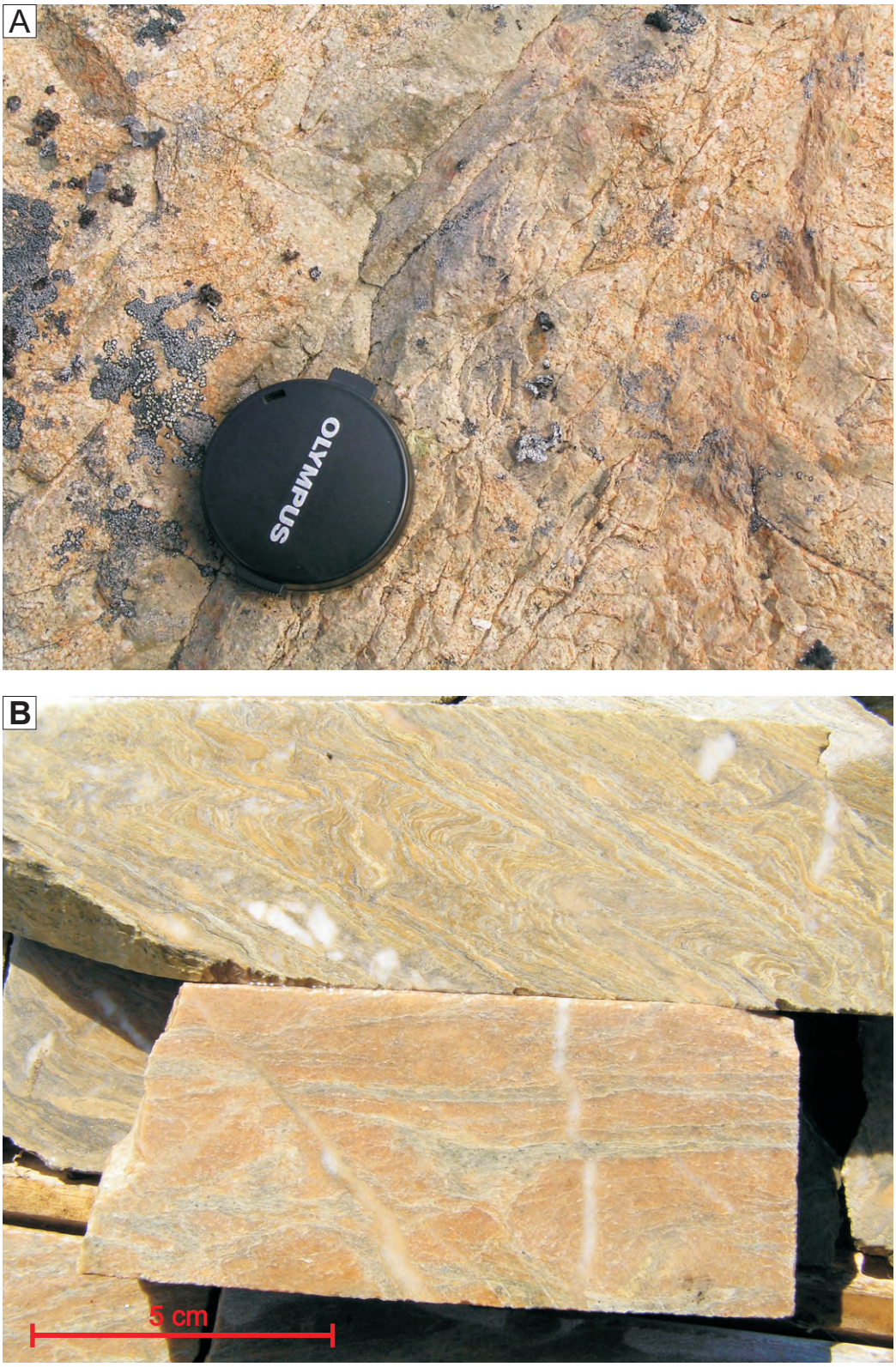

Plate 3.23 (A) Fresh quartz-feldspar phyric Wolverine Porphyry from north of Wolverine Lake; (B) Sericite-chlorite-ankerite altered, deformed and veined Wolverine Porphyry from the Hope Bay Deformation Zone.

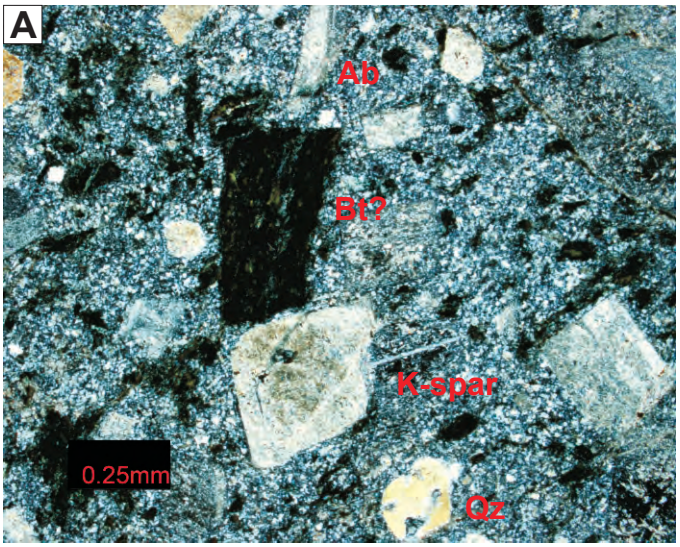

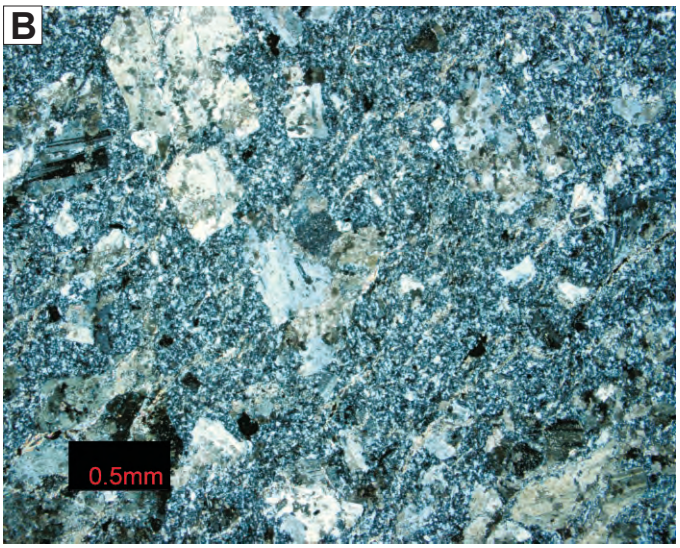

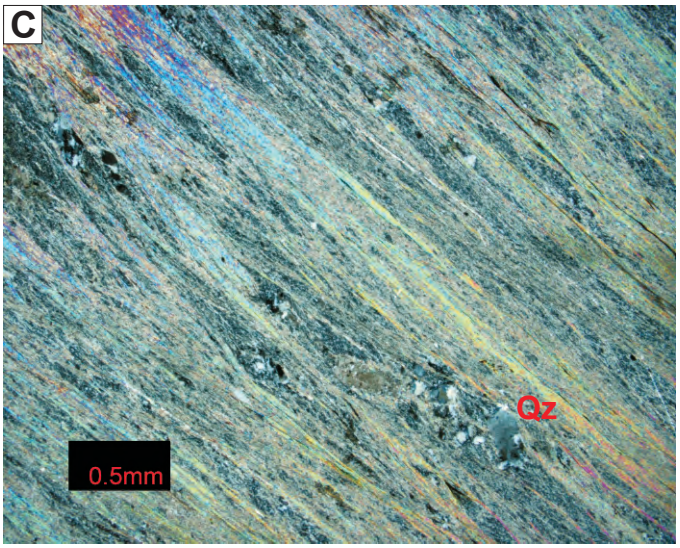

Plate 3.24 Progressive alteration and deformation of the Wolverine Porphyry: (A) Least altered and deformed porphyry with weakly altered euhedral phenocrysts of feldspar (albite and potassium feldspar) and rounded resorbed (embayed) quartz phenocrysts. Chlorite-oxide altered biotite occurs near center. Groundmass is composed of fine-grained quartz and feldspar; (B) Moderate sericite-chlorite-carbonate alteration of porphyry from the HBDZ. Feldspars are cloudy due to sericite replacement and carbonate overprint; (C) Strong sericite-carbonate altered porphyry. Mylonitized quartz phenocrysts at bottom right of photo. Foliation defined by well-aligned mica strands.

into lozenge shaped porphyroclasts with tails of fine grained quartz - a result of syntectonic recrystallization during mylonitization. The fine grained quartz-feldspar groundmass can still be recognized between mica bands, but has also undergone extensive recrystallization and been overprinted by carbonate alteration.

Basalts in the HBDZ are distinguished from porphyry by their darker colour and different alteration assemblage. The mica-chlorite segregations are various shades of yellow-green to tan in colour, but are still strongly paragonitic, similar to micas found in the Wolverine Porphyry. They are also finer grained. Dark coloured bands between the sericite layers contain stronger carbonate alteration and more Fe-Ti oxide material than the porphyry. It is nearly impossible to determine the specific basalt type in the HBDZ without the aid of geochemistry.

3.3.3 – Veining

As in most shear hosted quartz-carbonate Au deposits, veined and stockworked zones are the primary sites of gold. Veins within mineralized rock are composed of variable amounts of quartz (cryptocrystalline to 2mm crystals), Fe-carbonate (dolomite-ferroan ankerite and siderite-magnesite solid solutions), end-member albite, hematite (fine grained inclusions in the aforementioned minerals), sulphides (pyrite, chalcopyrite, gersdorffite, sphalerite, galena, pyrrhotite and arsenopyrite), electrum (high gold:silver ratios), monazite, altered basalt/argillite wall rock fragments, carbonaceous matter, and tourmaline. Crosscutting relationships and mineralogical variations have indicated at least three distinct generations of veining (Plate 3.25):

Type 1: Pervasive early thin (2-4 mm) grey quartz-dolomite veins and stockworks. These veins unquestionably pre/syndate D_2 deformation as they are strongly deformed and transposed into the orientation of S_2 as defined by thin sericite bands which border the veins. Pyrite is the primary sulphide association, occurring within veins or altered basaltic selvedges as fine to medium grained euhedrons or aggregates. This fluid event is presumably synchronous with the earliest sericite-quartz-ankerite alteration event. Gold is found as fine grained "pinpricks" within veins and as inclusions in pyrite.

Type 2: A later set of creamy-pink coloured quartz-ankerite-albite +/- hematite veins/stockworks crosscut the early Type 1 veins. The creamy-pink colour is due to the presence of albite. These veins are thicker and more irregular than the earlier variety. They are also less deformed. They often exhibit whispy indistinct margins as they grade outward into stockworked and silicified, ankeritized and albitized basalt. Wall rock fragments of sericite-ankerite altered basalt and brecciated argillite are common. Pyrite is the main sulphide association, occurring as fine to coarse euhedrons and aggregates. Thin dark coloured carbonaceous stylolitic-like segregations can be found perpendicular to vein margins and may be associated with visible gold. Visible gold commonly occurs as coarse flecks in clusters of multiple grains. This vein type is often present but not limited to lithological contacts and the HBDZ boundary.

Type 3: White coarse quartz-ankerite veins crosscut all other vein types. They are composed of quartz cores and coarse white ankeritic margins. Red hematite is commonly present. Chalcopyrite and gersdorffite with rare pyrite and arsenopyrite are the main sulphide association, occurring as mm-sized blebby clumps and intergrown crystal masses. Rarely, coarse visible gold is also present, however, these veins are not

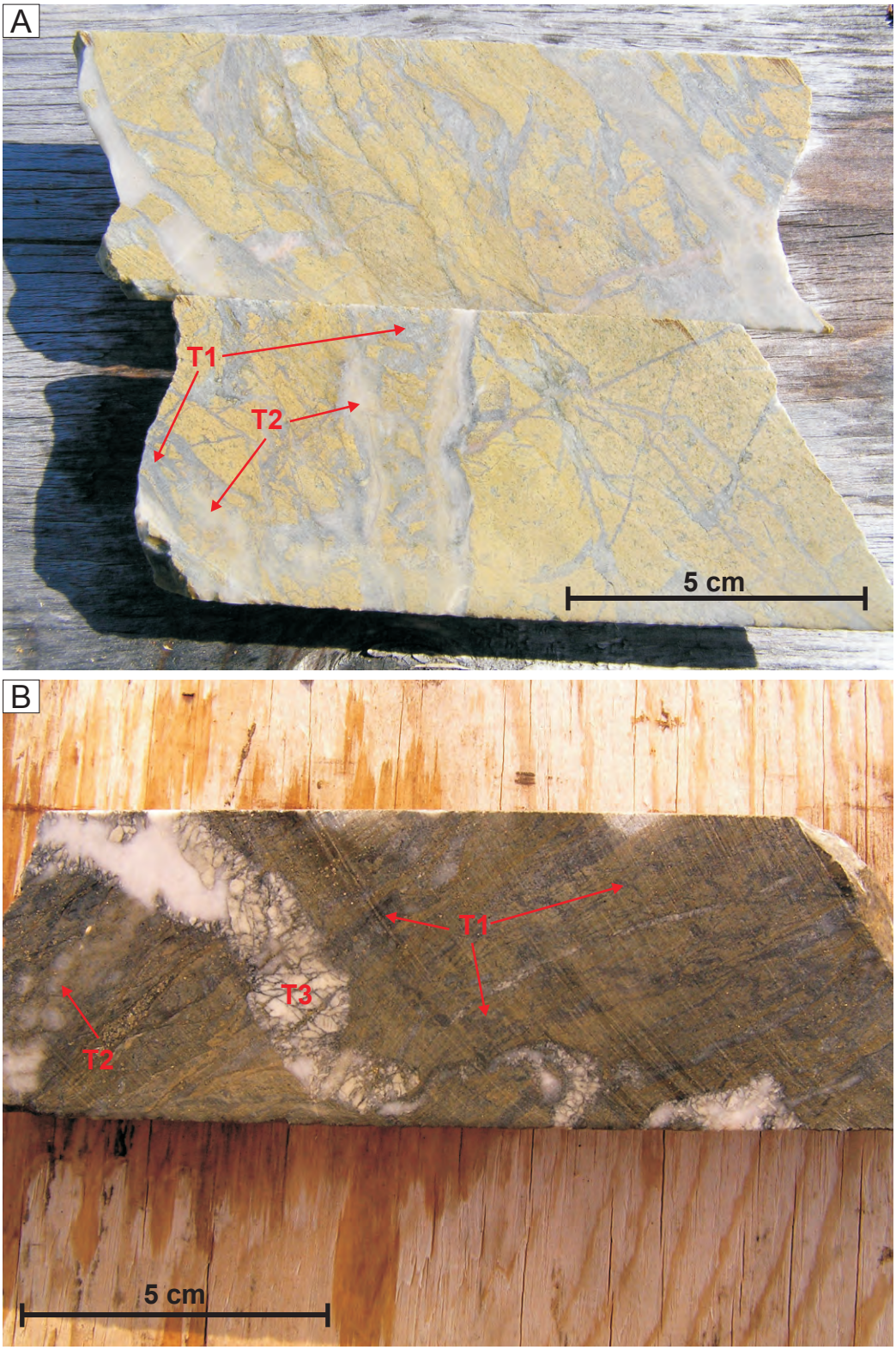

Fig 3.25 (A) Early thin grey quartz-ankerite veins (Type 1) crosscutting a komatiitic basalt. Type 1 crosscut by pink albitic Type 2 veins; (B) Thin grey quartz-ankerite veins (Type 1) bordered by yellow-green sericite. Crosscut by light cream coloured quartz-ankerite-albite veins (Type 2) crosscut by weakly deformed white quartz-coarse ankerite veins (Type 3).

especially prospective for mineralization. These veins appear to be late/post D_2 as they may be openly folded by F_2 (F_3?) folds. They are the only veinset that crosscuts the S_2 fabric of the HBDZ.

Outside of mineralized zones the veining intensity generally decreases and changes in composition to quartz + calcite +/- chlorite, pyrite, chalcopyrite, arsenopyrite and gersdorffite. These veins are typically straight and undeformed or lozenge-shaped, filling extensional tension gashes. They vary from white to light shades of pink and blue.

3.3.4 – Mineralization

Mineralization at Madrid may be classified under the umbrella term quartz-ankerite-pyrite vein/stockwork style mesothermal gold. Variations in veining density and composition, sulphide content, composition and textures, host rock and alteration intensity and type result in many different styles of mineralization. Plates 3.26 and 3.27 illustrate some of the more typical types of mineralization, which are described below:
1) Quartz-ankerite-albite-pyrite veined and stockworked Ti-rich komatiitic basalts. Veining can vary significantly from 5-10% to 75%. The hosting basalt is a yellow green colour resulting from (Cr)-phengitic muscovite and weakly paragonitic phengitic muscovite alteration. The typical alteration assemblage is sericite-ankerite with less common intervals of silicification. Preserved harrisitic and pseudocumulate textures are overprinted by sericite, ankerite, Fe-Ti oxides and sphene. Crosscutting veins are generally of Type 1 (thin grey quartz-ankerite stockworking veins) and 2 (thick chaotic creamy pink coloured albitic veins). Late Type 3 veins are locally present, carrying chalcopyrite and gersdorffite. Pyrite averages 5-10% of the rock but may comprise much

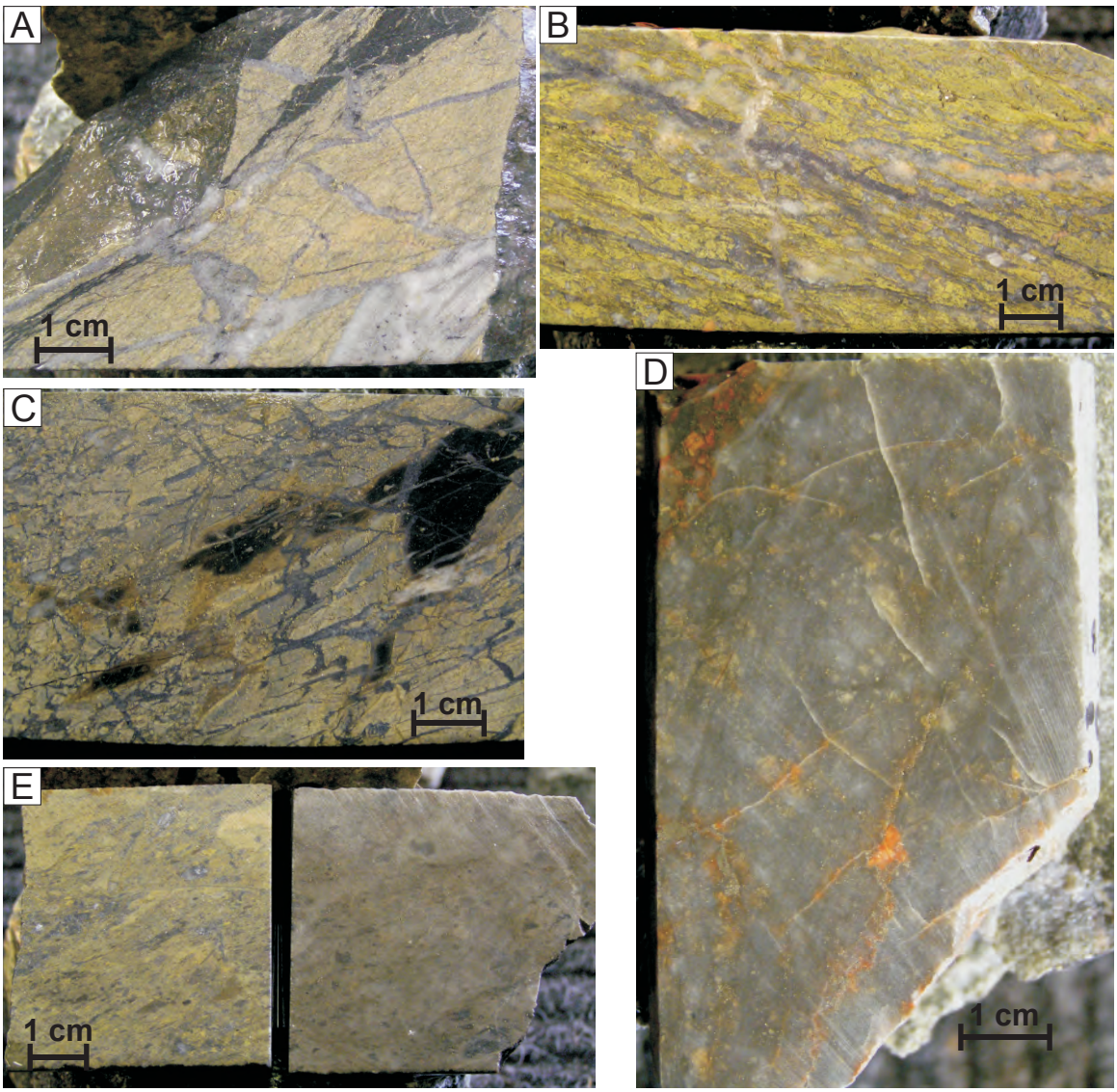

Plate 3.26 (A) Yellow-green sericite-ankerite altered peperitic komatiitic basalt. Creamy albitic (Type 2) veins crosscut minor Type 1 veins. 1-2% fine-medium grained pyrite-chalcopyrite in Type 2 veins and basalt; (B) Grey quartz-ankerite veins (Type 1) stockworking a yellow sericite-ankerite altered komatiitic basalt with weakly preserved harrisitic textures. Crosscut by chaotic pink albitic veins and patches (Type 2). 3-4% pyrite; C) Basalt-argillite breccia (secondary?) with moderate quartz-ankerite stockworking by thin grey veins (Type 1) overprinted by minor creamy white coloured albitic veins (Type 2) which recrystallize the Type 1. Coarse euhedral pyrite constitutes 15-20%; D) Strongly silica flooded basalt with bleached and hematitzed wallrock fragments. Pyrite is fine grained and disseminated (~3-4%). This style of veining is common on the margins of the HBDZ at Naartok; E) Heterolithic breccia with clasts of various basalts, argillite and veins. Left sample is predominately sericite ankerite altered, right sample is strongly silicified. Fine grained disseminated pyrite (2-3%) associated with silicified sample.

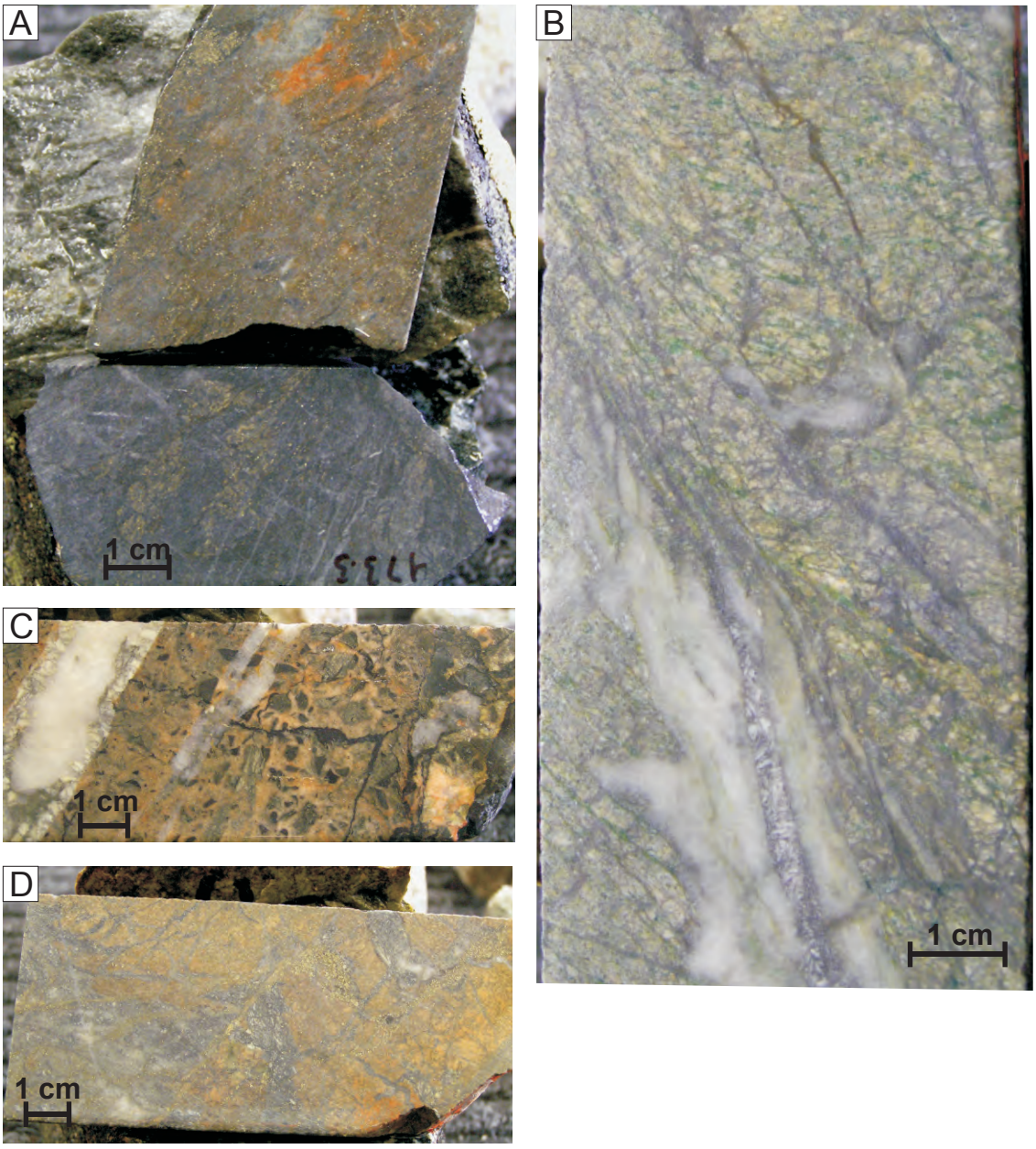

Plate 3.27 (A) Strong quartz-ankerite-hematite-pyrite stockworking of basalt-argillite breccia. The overall charcoal colour is caused by remobilized carbon. Medium-grained disseminated and clustered pyrite (10-15% in upper sample, 5% in lower); (B) Quartz-ankerite-fuchsite altered basalt cut by early generation of veining (Type 1) recut by later albitic veinset (Type 2) and minor Type 3. 1% pyrite; (C) Vein breccia ore with hematitic quartz-ankerite veins surrounding fragments of silicified argillite. Carbonaceous stylolites also present. Late crosscutting quartz-coarse ankerite vein. 2-3% pyrite; (D) Quartz-ankerite-sericite-hematite altered basalt cut by quartz-ankerite-albite veins. Clustered medium grained pyrite in basalt constitutes 5-7% of sample.

more. It occurs as medium grained euhedral cubes disseminated in the basalt and concentrated in veins and selvedges. Cubes often show quartz-ankerite pressure shadows and are wrapped by sericite segregations. Pyrite margins may be replaced by gersdorffite-chalcopyrite intergrowths. Gold occurs as inclusions in sulphide grains (pyrite and chalcopyrite-gersdorffite), as fine flecks in Type 1 veins, clustered coarse flecks in Type 2 veins and fine specks in vein adjacent altered basalt. Peperitic textures are common, but can be difficult to identify when strongly deformed or when dolomitized argillite is mistaken for ankeritic veins. This style of mineralization is the standard variety at Naartok-Perrin-Rand.

2) Strongly silica +/- albite and ankerite flooded basalt and associated Type 2 veins with fine-grained disseminated pyrite. Light coloured bleached (ankeritized) fragments, angular sericite-ankerite altered blocks of basalt and fragments of pyritized argillite are common in the fine grained silicious matrix. Albite commonly imparts a pinkish to creamy colour to the vein/rock. Fine grained disseminated hematite and thin dark coloured stylolitic fractures are relatively common. These quartz flooded/veined zones grade outward into Type 2 veins and stockworked basalt. This mineralization style is common near the border of the HBDZ at Naartok and along lithological contacts. It is strongly associated with multiple clustered coarse gold flecks.

3) Strongly pyritized basalt. Medium to coarse grained massive pyrite euhedrons and intergrown crystals can form up to 50% of the sericite-ankerite altered Ti-rich komatiitic basalt. These zones generally exhibit less stockworking and Type 2 veins than other ore horizons. This style of mineralization is a more pyritic variety of (1).

4) Some of the mineralized rocks at Suluk are distinguished from Naartok by being darker and more argillite rich basalt-argillite mixtures strongly overprinted by quartz-ankerite-albite stockwork veins. The larger proportion of argillite gives the basalt and veins a light-medium charcoal colour resulting from remobilized carbon. Brick red hematite is often present in significant amounts. Medium grained pyrite constitutes up to 20% of the basalt.

5) Fuchsite-magnesite-ankerite mineralization consists of slips of green coloured fuchsite and fuchsitic phengite between coarse blasts of magnesite/ankerite. The coarse carbonate is likely a result of alteration overprinting a coarse primary texture. Pyrite contents and gold values are generally low.

3.3.5 – Siting of Gold

Pyrite is ubiquitous to mineralized zones, but modal percents do not correlate well with Au values. Modal percents of pyrite in mineralized zones can vary from as little as 1-2% to as much as 45-50%. It varies in form from fine-grained (sub mm) disseminated grains, medium grained (1-2 mm) disseminated to clustered grains, larger clots and clumps of multiple intergrown crystals to coarse grained (>5 mm) cubic crystals (Plate 3.28-3.30). Pyrite crystals occur most often as euhedral grains, but may have strongly brecciated margins. Individual pyrite grains are often zoned compositionally and morphologically. Pyrite cores exhibit abundant inclusions of gangue material, whereas rims are comparatively inclusion free (Plate 3.30). The cores are also less arsenian as compared to their rims. Gersdorffite and chalcopyrite form the second most abundant sulphide species. Both may occur as disseminated blebby grains in basalt,

however, they are more commonly intergrown with each other. Gersdorffite-chalcopyrite intergrowths are commonly present replacing the margins of pyrite (Plate 3.28-3.30). Fe-Ti oxide phases (magnetite, ilmenite, leucoxene) are ubiquitous accessory phases in the Madrid system. Sphalerite, galena, arsenopyrite and pyrrhotite form accessory phases. Rarely, monazite occurs as isolated fine crystal clusters in veins.

Gold at Madrid is found in two dominant forms: coarse visible flecks within veins and enveloping wallrock, and microscopic sulphide-hosted grains. Coarse visible gold is typically sited in quartz-ankerite +/- albite veins (Type 1 and 2), but can also be found in the surrounding wallrock. Plate 3.31 illustrates some of the various sitings of visible gold in veins. In addition to the common pyrite association, multiple flecks of coarse grains are also found near dark coloured stylolitic-like fractures, along thin sericite strands and as free grains unassociated with sulphides. Microscopic gold exhibits a strong association with the various sulphide minerals (Plate 3.32). Small gold inclusions in pyrite are typically located toward the inclusion-free rims rather than the spongy cores (Plate 3.29). Several examples of intergrown gold-chalcopyrite-gersdorffite replace pyrite margins or crosscut pyrite grains in thin veinlets. Both gersdorffite and chalcopyrite are late in the system, suggesting gold has been remobilized or additional gold was introduced during this event.

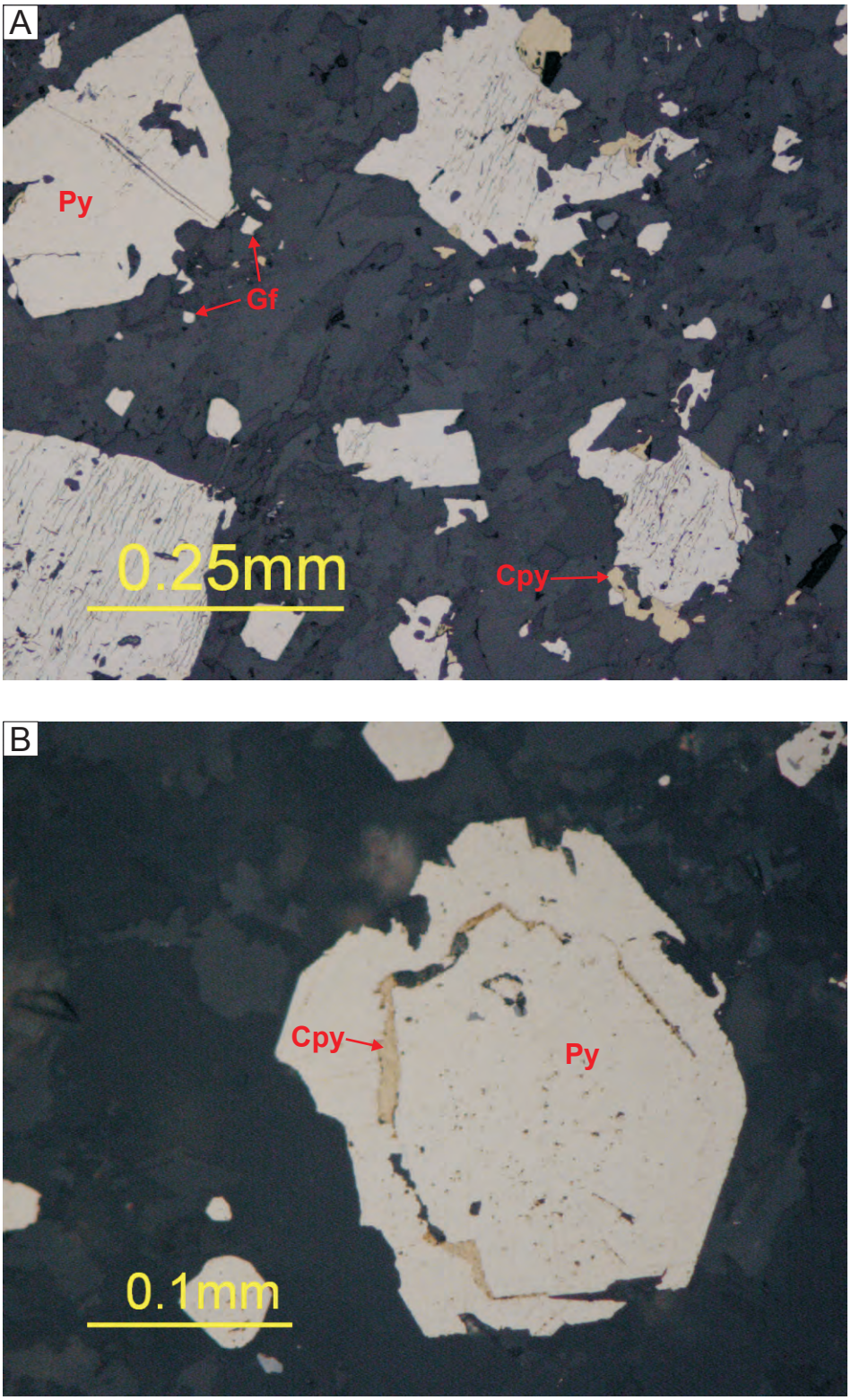

Plate 3.28 (A) Chalcopyrite and minor gersdorffite on the margins of embayed pyrite grains. Many of the pyrite crystals exhibit shear planes; (B) Chalcopyrite at the interface between inclusion-filled pyrite core and inclusion-free pyrite rim.

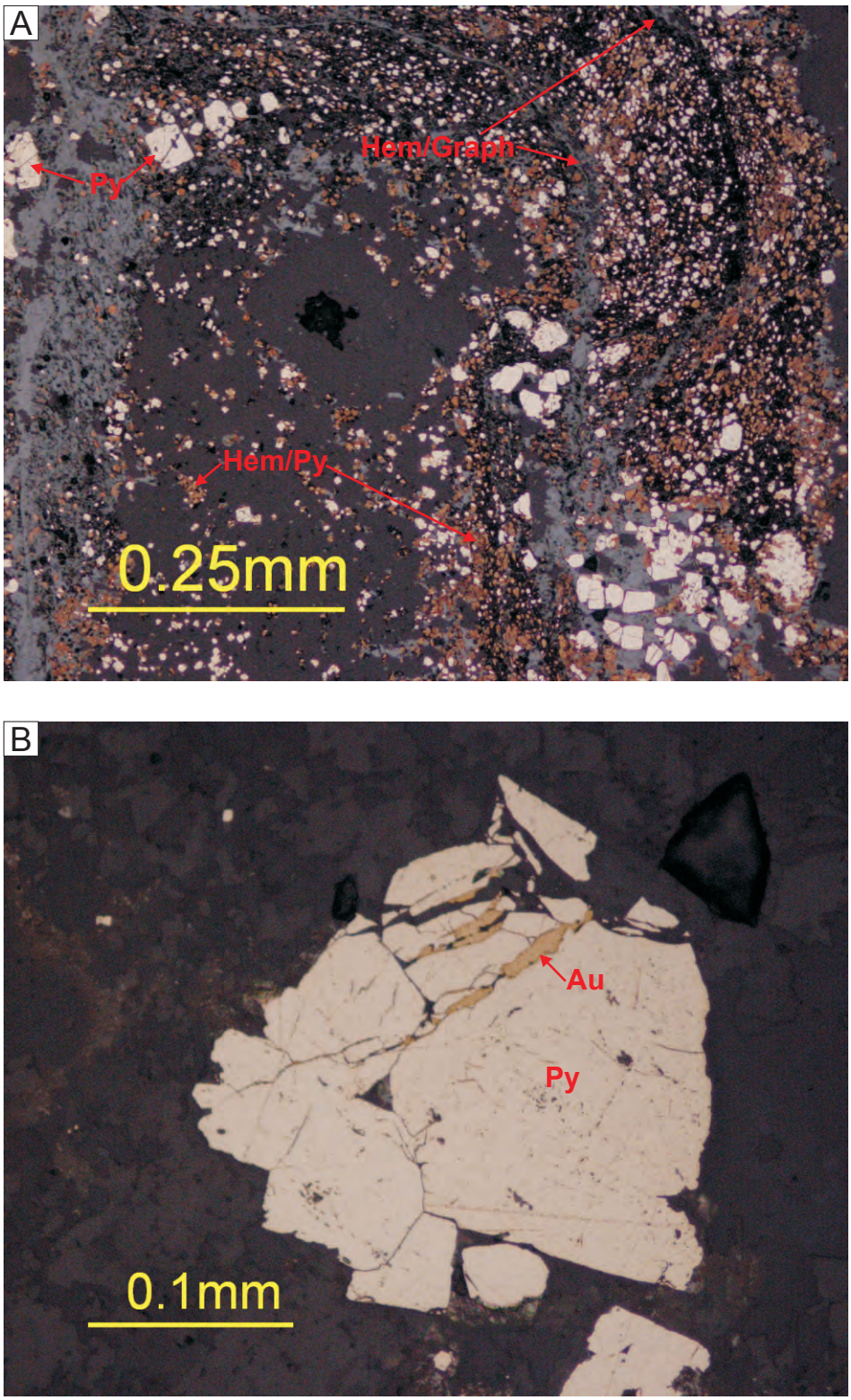

Plate 3.29 (A) Hematitic pyritic carbonaceous veinlet from mineralized basalt-argillite breccia at Suluk. The red colour is caused by hematite overprinting pyrite; (B) Thin gold veinlets in weakly brecciated pyrite crystal.

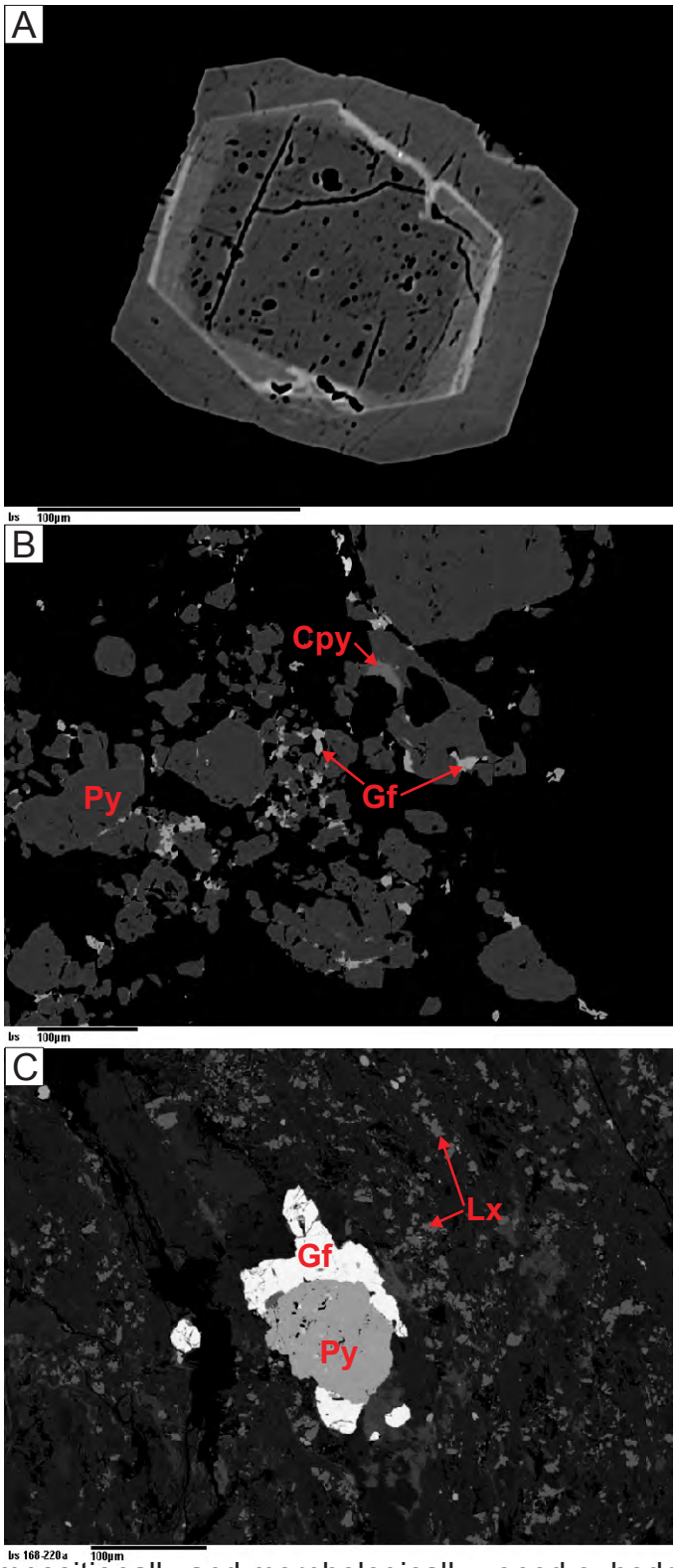

Plate 3.30 (A)Compositionally and morphologically zoned euhedral pyrite grain. Core region is arsenic poor and inclusion filled while rim overgrowth is more arsenian and inclusion free; (B) Pyrite replaced by gersdorffite and lesser chalcopyrite; (C) Light grey coloured pyrite rimmed by gersdorffite and surrounded by leucoxene (medium grey).

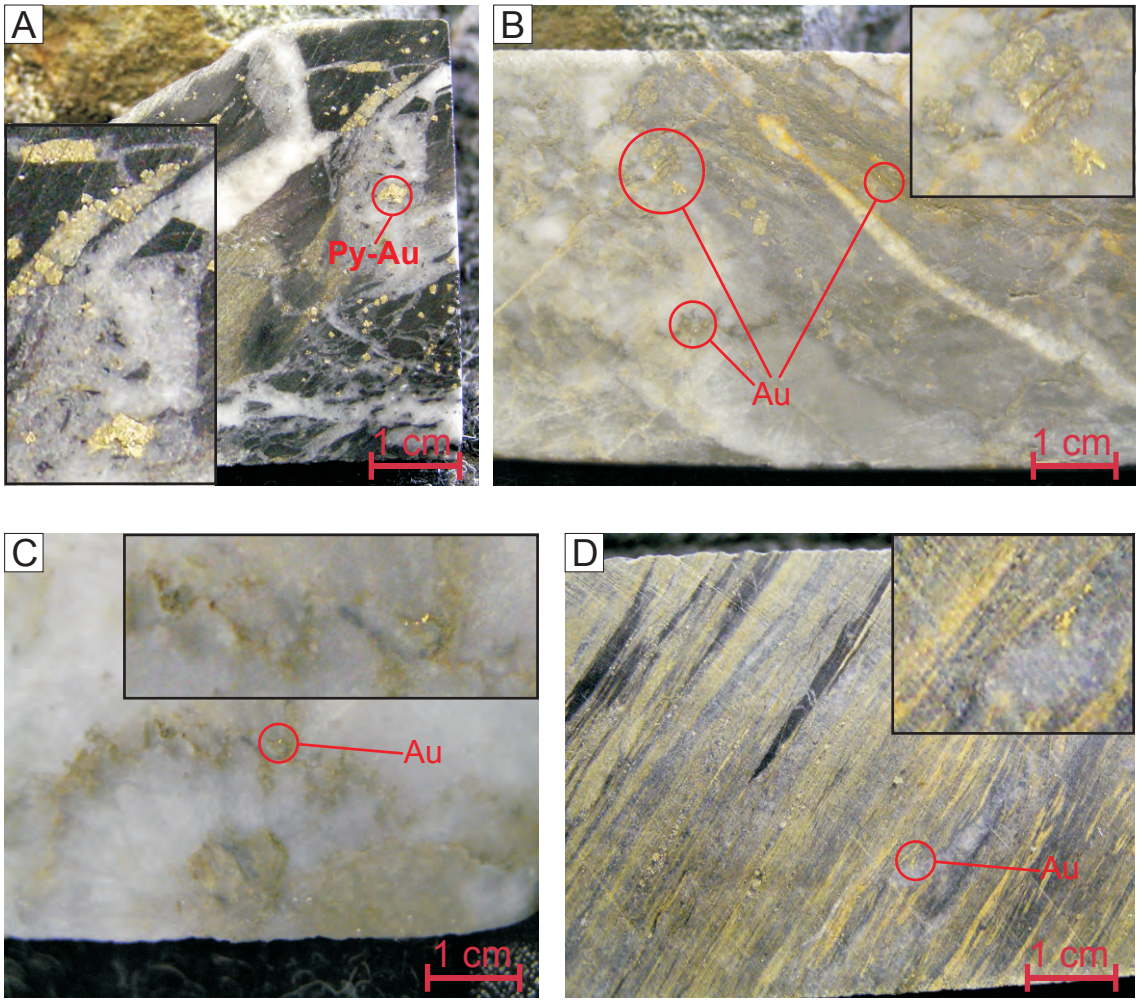

Plate 3.31 Textural relationships of coarse vein-hosted visible gold: (A) Coarse gold on the margins of a pyrite aggregate. The vein is composed of quartz-ankerite with subordinate albite, hematite, pyrite and gold. Brecciated wallrock clasts are predominately of black silicified argillite with lesser sericite-ankerite altered basalt; (B) Large gold flecks in a smokey quartz-ankerite vein. Gold is associated with large pyrite euhedrons (upper left), dark stylolitic-like partings (bottom) and sericite-pyrite bands (upper right); (C) White quartz vein with dark stylolitic structures with associated gold. Strongly bleached (silicified and ankeritized) wallrock clasts occur at the bottom of the photo. Note the lack of sulphides; (D) Strongly altered and deformed basalt-argillite breccia. Yellow-green sericite segregations are separated by parallel grey quartz- ankerite veinlets which host pyrite (and gold?). They are crosscut at a small angle by a creamier quartz-ankerite-albite vein which hosts a coarse gold fleck. Lozenge shaped argillite bands (upper left) have been strongly stretched parallel to veins and sericite laminae.

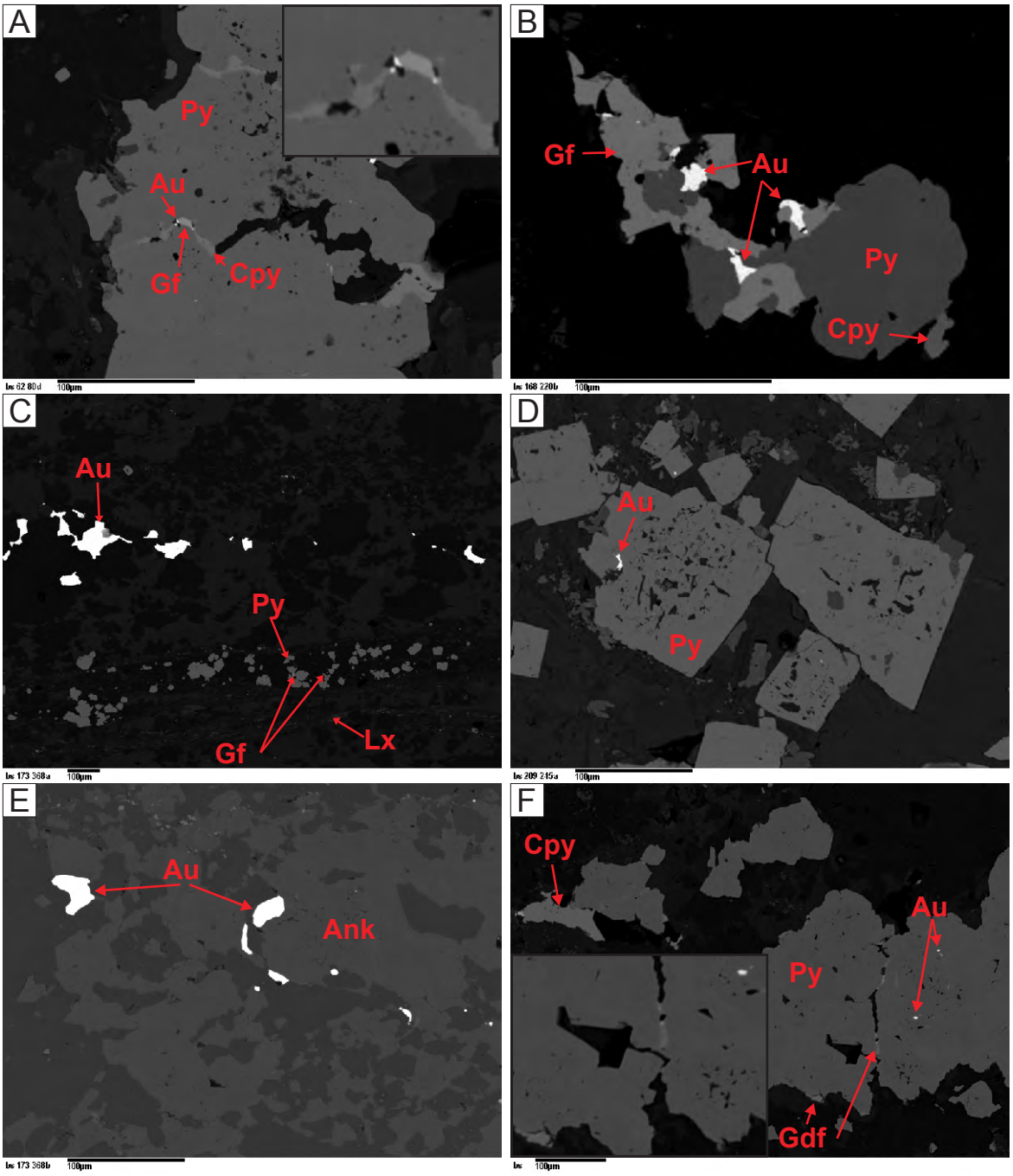

Plate 3.32 Relationship between Au and sulphides: (A) Chalcopyrite-gersdorffite-Au veinlet crosscutting pyrite; (B) Intergrown chalcopyrite-gersdorffite-Au replacing the margins of a pyrite grain; (C) Band of pyrite-leucoxene with minor gersdorffite. String of coarse Au grains associated with a quartz-ankerite vein; (D) Au inclusion on the outer margins of a spongy cored pyrite grain; (E) Coarse gold on the margins of ankerite grains in a quartz-ankerite vein; (F) Small Au inclusions within pyrite. Minor chalcopyrite and gersdorffite occur on pyrite margins.

CHAPTER 4

LITHOGEOCHEMISTRY IN THE MADRID AREA

4.1 – Introduction

Chapter 4 deals with the lithogeochemistry of rocks in the Madrid area of the HBVB. Major element data is presented from the entire Hope Bay Volcanic Belt, however, emphasis is placed on major and trace element data from the Madrid corridor and documents changes that occur during the hydrothermal alteration associated with the HBDZ. The majority of whole rock data was provided courtesy of the Miramar Mining Corporation and constitutes weakly to strongly altered surface and drillcore samples of predominately mafic volcanic rocks.

All samples have been overprinted by upper greenschist facies metamorphism and many have been altered hydrothermally to various degrees. Consequently only elements that are considered relatively immobile under these conditions (Ti, Al, Nb, Nd, Y, Zr) have been routinely used in the elemental plots throughout the chapter. The exception to this are least altered samples from Madrid which can be plotted with greater confidence on such diagrams as the Jensen cation plot which involve the more mobile elements Mg and Fe. The data used in the following graphs can be found in Appendix A.

4.2 – Lithogeochemistry of the HBVB

Several workers have written on the visual and geochemical differences between various lithotypes in the HBVB (Gebert, 1999; Hebel, 1999; Sherlock, 2002; 2003; Carpenter and Sherlock, 2001; Poulson , 2003). Poulson (2003) proposed a five-fold discrimination system (Suites A through E) useful for screening the various rock types on

a belt scale. This system is used here only to illustrate the variability of lithologies within the belt and to show where rocks of the Madrid area plot relative to rocks regionally. Suites A through E are shown on Figs 4.1 and 4.2. The TiO_2 vs Al_2O_3 plot (Fig 4.1) is useful for separating out gross differences in the mafic volcanic suites whereas Zr acts as a better monitor for the felsic rocks as seen in Fig 4.2. Although a great deal of the data is from altered samples, the elements Ti, Al and Zr are conserved and their ratios remain constant during alteration. Thus, the linear trends toward the origin in both the diagrams are largely a result of alteration and to a lesser degree, igneous processes such as fractionation. The TiO_2-Al_2O_3 plot in Fig. 4.1 clearly distinguishes the high-Ti suites from the low-Ti "normal" tholeiitic basalts. The characteristics of the various suites, initially defined by Poulson (2003) and modified by the author, are outlined below:

Suite A: Suite A comprises high Fe-Ti-Cr-Ni komatiitic and transitional basalts enriched in incompatible elements. These rocks have unusual chemistries as compared with other greenstone belts worldwide. The recognition of this unit is important as it is spatially associated with Au at each of the three major deposits in the belt (Doris, Madrid and Boston). This suite is examined in greater detail later in the chapter. The vast majority of mineralized basalts from the Madrid area plot as Suite A basalts.

Suite B: Suite B rocks are high-Fe basalts with elevated Ti. They are comparable to high-Fe basalts found in other greenstone belts but with a lower Mg content. Suite B rocks are associated with the Doris deposit and will not be discussed further.

Suite C: Samples from Suite C plot predominately as normal to high-Fe tholeiitic basalts and basaltic andesites and are similar to basalts found in many other greenstone belts. In the Madrid area rocks from the Windy Lake and Wolverine Mafics plot as C-type basalts and are discussed in more detail later in the chapter.

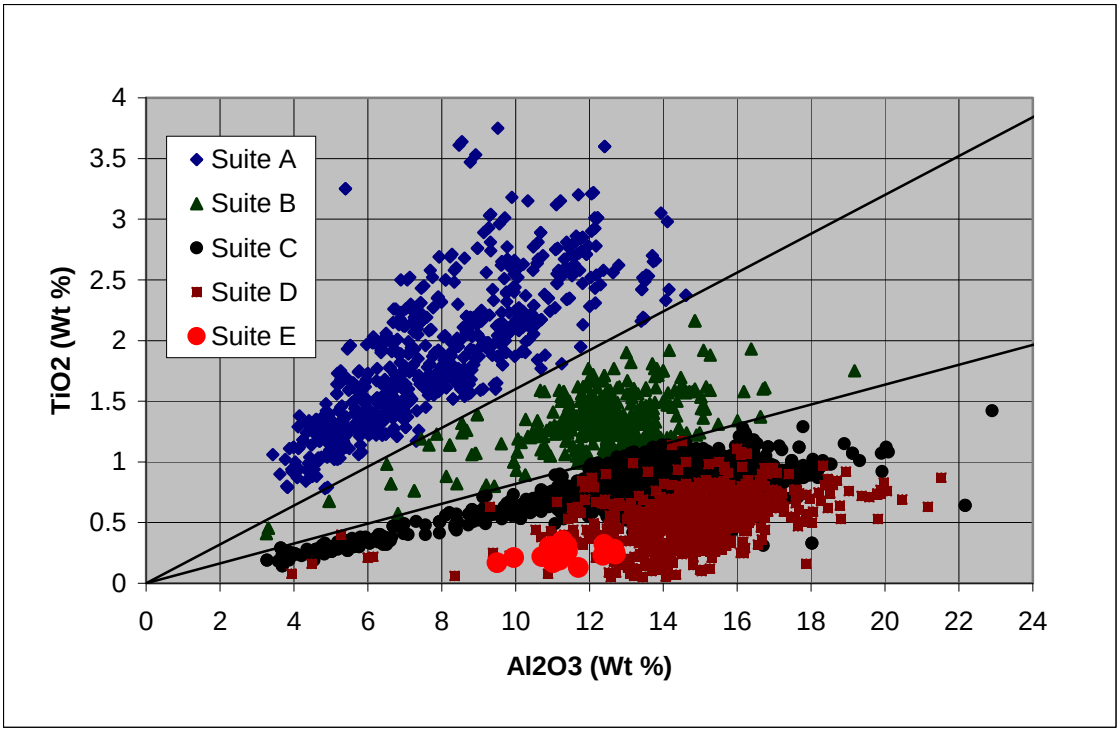

Fig. 4.1 Binary plot of wt % TiO_2 vs. Al_2O_3 for samples from the Hope Bay Volcanic Belt. High-Ti suites (A and B) can be distinguished from "normal" basalts and basaltic andesites (suite C) and various felsic rocks (suites D and E).

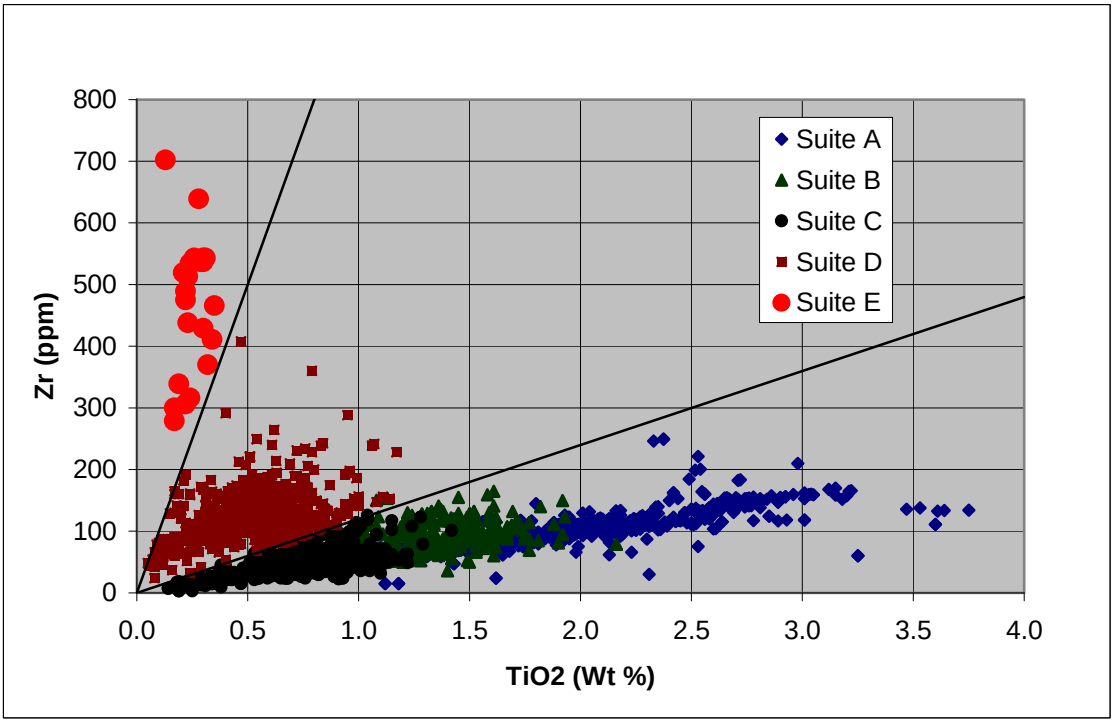

Fig. 4.2 Binary plot of ppm Zr vs. TiO_2 for samples from the Hope Bay Volcanic Belt. Mafic volcanic rocks (Suites A, B and C) can be distinguished from felsic rocks (Suites D and E).

Suite D: Suite D rocks are dacitic to rhyolitic in composition and include samples from the Windy and Koiknuk felsics as well as the Wolverine Porphyry.

Suite E: The limited number of samples which plot as Suite E belong to the Flake Lake rhyolites, identified by their high Zr and low TiO_2 values.

4.3 – Madrid Corridor Lithogeochemistry

4.3.1 – High-Ti Komatiitic and Transitional Basalts

Fig. 4.3 is an Al_2O_3 vs. TiO_2 binary plot for 337 samples of high-Ti mafics (Suite A) from the Madrid area. Each of the samples have been separated into one of seven subsuites based on petrographic analysis, Al_2O_3/TiO_2 ratios, trace element trends and least altered sample chemistries. Overall, two broad categories are recognized, corresponding well with the petrographic subdivision (Patch A and B) outlined in Chapter 3. The more primitive Patch A basalts comprise suites A2, A4 and A6 whereas Patch B basalts make up subsuites A3, A5 and A7. Samples in the A1 category are predominately coarse grained dark coloured flows that do not form a very coherent and homogenous group and so will not be discussed any further. Least altered samples of the Ti-enriched komatiitic basalt group (A2, A4 and A6) are dark green to black in colour and commonly show harrisitic, pseudocumulate and amygdaloidal textures as described in Chapter 3. Least altered high-Ti transitional basalts are consistently dark-medium green pillowed to flow brecciated units with abundant large white coalescing varioles. A fractionation trend is suggested between the komatiitic basalts (low TiO_2 and Al_2O_3) and the transitional basalts (high TiO_2 and Al_2O_3). The trend, however, does not form a continuous line on this plot - least altered samples tend to cluster in one of the two general areas suggesting bimodality. Variations in the Al_2O_3/TiO_2 ratio internal to these

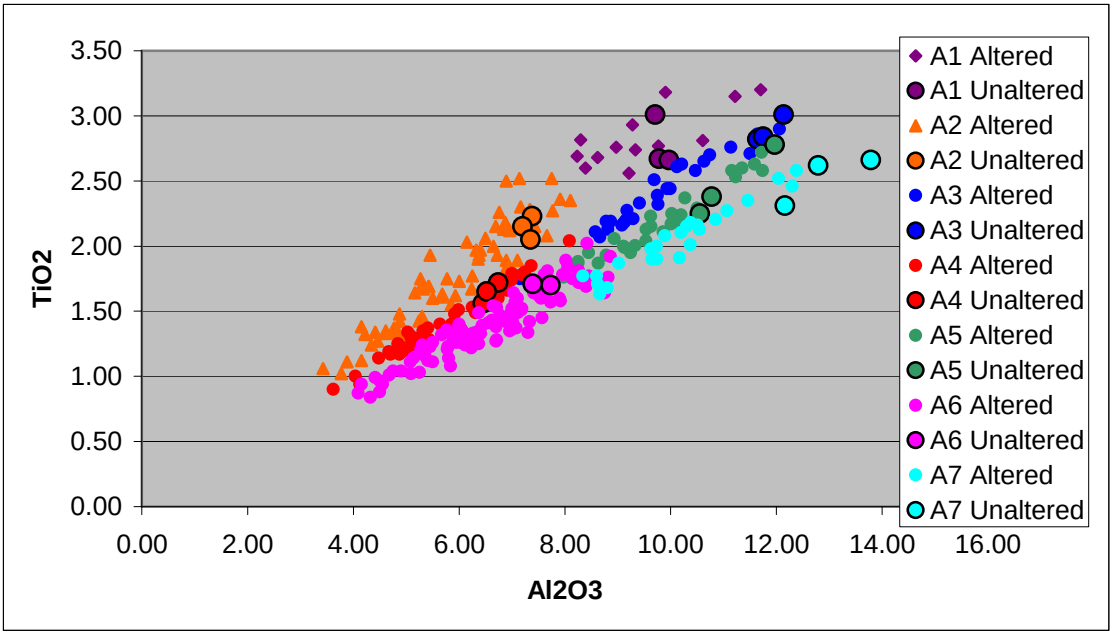

Fig. 4.3 TiO_2 vs. Al_2O_3 binary for 337 samples of high-Ti basalts from Madrid. Large dots represent least altered samples for each of the suites.

two groups (i.e. perpendicular to the fractionation trend) are related to within-plate basalt variations. This is discussed in more detail later in the chapter. They have been separated out to obtain more accurate results during mass balance calculations.

Representative major and trace element data for least altered samples of the high-Ti suites are shown in Table 4.1. The more primitive Patch A komatiitic basalts have elevated MgO, Fe_2O_3, Na_2O, K_2O, CaO, Cr and Ni and lower SiO_2, TiO_2, and Al_2O_3 relative to the Patch B basalts. The komatiitic basalts are also depleted in the incompatible elements Nb, Nd, Zr, Y and Yb relative to the Patch B basalts. The elevated TiO_2 values in the Patch B basalts are also associated with elevated Sm, Hf and Zr, i.e. Ti-associated elements. Al_2O_3/TiO_2 ratios are relatively consistent between suites, ranging from 3-6. This ratio is important when distinguishing between Al undepleted and Al depleted komatiites, i.e. Al depleted komatiites have Al_2O_3/TiO_2 ratios of about 11 whereas Al undepleted komatiites have ratios around 20 (Nesbitt *et al.*, 1979). Although

there are no samples of komatiitic basalt that plot as true komatiites on the Jensen ternary (Fig. 4.4), several least altered samples have >18 wt% MgO, the definition of a komatiitic rock according to Arndt and Nisbet (1982). When mass gains/losses of MgO are taken into account, approximately 20% of the high-Ti komatiitic basalts plot with >18% MgO. This suggests that the term 'Ti- enriched Al-depleted komatiite' is valid for at least some of the komatiitic basalts at Madrid. The trace element profiles (depleted HREE relative to Ti and LREE when normalized to MORB, low La/Yb_N normalized to chondrite) and major element geochemistry (low Al_2O_3/TiO_2) are comparable to other Ti-rich Al-depleted komatiitic rocks found elsewhere (Barnes and Often, 1990; Stone *et al*., 1987; Xie *et al*., 1993; Barley *et al*., 2000; Sharkov and Smolkin, 1997). The term TEAD (Ti-enriched Al-depleted) komatiite/komatiitic basalt is proposed for rocks of similar chemistry at Madrid and will be used in place of Patch A for the remainder of the thesis.

The Zr-Y magmatic affinity diagram of Barrett and MacLean (1994b) is shown in Fig. 4.5 for the high-Ti suites. Nearly all samples fall well within the transitional field at the boundary between tholeiitic and calc-alkaline. Samples plotting in the transitional field have characteristics in common with flanking tholeiitic and calc-alkaline fields. Their chondrite normalized REE patterns have intermediary slopes between tholeiitic ($La/Yb_n < 2.5$) and calc-alkaline ($La/Yb_n \geq 4$) suites (Barrett and MacLean, 1994b). Samples of the high-Ti basalt suites from Madrid have La/Yb_n values between 2.5-7.5 suggesting a transitional character. HFSE (Zr, Y, Nb, Th and REE) remain incompatible during fractionation of transitional rocks (similar to tholeiitic but dissimilar to calc-alkaline rocks), another feature noted in the high-Ti basalts at Madrid. Additional magmatic affinity diagrams including the Zr/P_2O_5 - TiO_2 of Winchester and Floyd (1976), the Y/Nb diagram of Pearce and Cann (1973) and the Ti/Y - Nb/Y diagram of Pearce

Suite	A1	A2	A3	A4	A5	A6	A7
Rock Type	FETI	TEAD	FETI	TEAD	FETI	TEAD	FETI
Si02	49.10	40.77	43.37	41.72	46.83	42.41	44.81
Al2O3	9.78	7.20	11.64	6.45	10.78	7.39	12.16
Fe2O3	16.65	19.31	16.65	18.40	13.92	18.48	16.02
CaO	8.86	7.95	11.35	4.43	11.28	8.26	10.62
MgO	6.54	16.59	6.39	20.75	7.66	15.39	7.67
Na2O	3.11	0.29	1.91	0.17	2.79	0.40	1.81
K2O	0.17	0.07	0.63	0.04	0.11	0.28	0.61
Cr2O3	0.17	0.18	0.04	0.24	0.04	0.24	0.15
TiO2	2.67	2.15	2.82	1.56	2.38	1.71	2.31
MnO	0.17	0.24	0.33	0.24	0.22	0.25	0.25
P2O5	0.20	0.17	0.28	0.12	0.19	0.12	0.17
BaO	0.03	0.01	0.06	0.01	0.03	0.01	0.09
Al2O3/TiO2	3.66	3.35	4.13	4.13	4.53	4.32	5.26
LOI	2.5	5.0	4.5	5.8	3.8	5.0	3.3
Ba	46.1	17.2	453.8	4.6	53.1	13.0	911.1
Co	170.9	102.6	72.3	129.5	59.6	110.8	115.5
Cr	1993.9	1420.9	428.3	1710.3	340.8	1884.5	1540.5
Cu	317.4	140.1	252.9	182.0	232.6	158.4	264.5
Ga	22.4	16.0	23.5	12.0	19.0	15.0	22.3
Ni	1002.0	862.5	177.4	1100.2	154.4	1032.5	821.9
V	399.8	357.2	448.7	251.1	419.0	308.7	431.7
Zn	220.8	116.1	150.9	150.0	124.3	120.3	181.4
Cs	0.7	0.5	0.8	0.3	0.1	1.7	1.3
Rb	1.6	1.2	9.6	0.7	1.5	11.0	12.8
Ta	1.3	1.1	1.5	0.6	1.4	0.6	1.0
Th	2.0	1.0	2.0	1.0	1.0	1.0	1.0
Nb	21.4	18.0	25.5	10.0	18.0	10.0	17.2
La	19.0	14.8	25.3	6.6	16.4	10.0	15.2
Ce	47.8	38.1	64.0	17.0	41.0	28.1	38.7
Pr	6.7	5.4	9.0	2.5	5.6	3.8	5.8
Sr	66.1	14.2	252.9	18.8	224.5	41.9	209.8
Nd	30.7	22.8	38.4	11.9	25.2	17.4	25.8
Sm	6.2	5.5	8.1	3.5	6.0	4.0	6.0
Zr	139.4	99.8	149.9	76.4	114.8	98.3	127.2
Hf	5.1	3.0	5.1	2.0	4.0	3.0	4.1
Eu	1.8	1.7	2.4	0.6	2.1	1.2	2.0
Gd	5.8	5.0	7.5	3.4	5.8	4.1	6.0
Tb	0.9	0.8	1.2	0.6	0.9	0.6	1.0
Dy	5.2	3.9	6.4	3.3	4.9	3.4	5.3
Y	24.3	18.6	30.2	14.2	23.4	17.0	26.2
Ho	0.9	0.8	1.1	0.6	0.9	0.6	1.0
Er	2.6	2.0	3.1	1.5	2.5	1.8	2.8
Tm	0.3	nd	0.4	nd	nd	0.2	0.4
Yb	2.2	1.7	2.5	1.3	2.0	1.5	2.1
Lu	0.3	0.2	0.4	0.2	0.3	0.2	0.3
W	2.0	1.0	1.0	1.0	32.1	17.0	2.0

Table 4.1 Major and trace element data for representative least altered high-Ti suite basalts from the Madrid area.

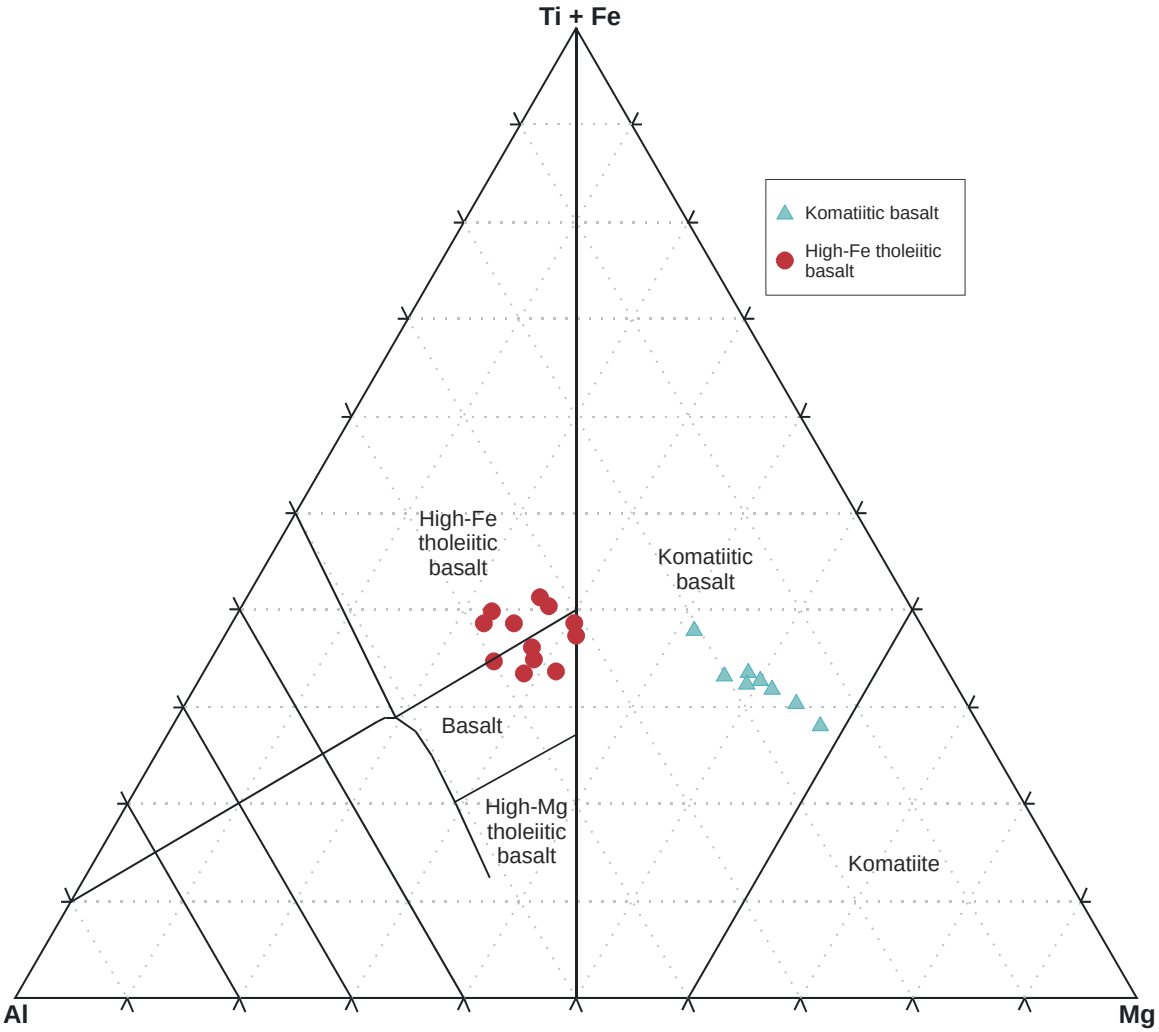

Fig. 4.4 Jensen cation plot of least altered TEAD komatiitic basalts and FETI basalts from the Naartok-Suluk area (from Jensen, 1976 and Grunsky *et al*., 1992).

(1982) yield similar results with samples plotting very close to the alkaline-tholeiite boundary, interior to the tholeiitic field on the Winchester and Floyd (1976) diagram (not shown) and within the transitional field of Pearce and Cann (1973) and Pearce (1982) (not shown). Madrid komatiitic and transitional samples also straddle the boundary between subalkaline and alkaline basalts on the Nb/Y - Zr/TiO_2 diagram of Winchester and Floyd (1977) in Fig 4.6. Consequently, the Patch B basalts will be referred to as FETI (Fe-Ti) transitional basalts or simply FETI basalts from this point forward.

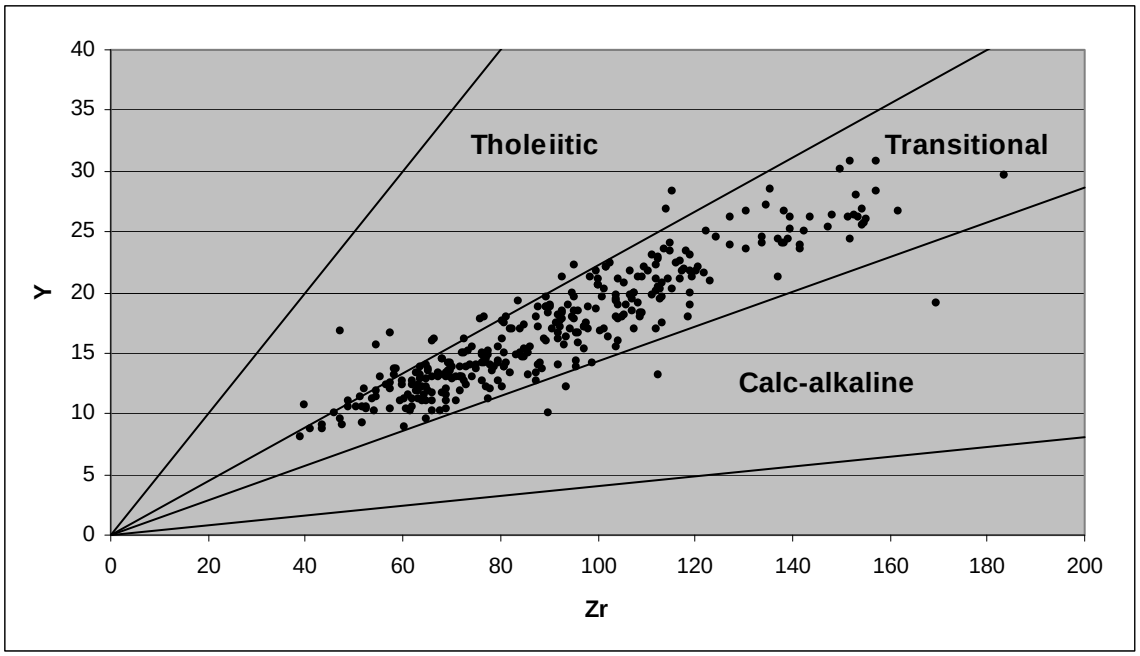

Fig. 4.5 Binary Zr vs. Y magmatic affinity diagram of Barrett and MacLean (1994) illustrating the transitional character of the high-Ti basalts from the Madrid area.

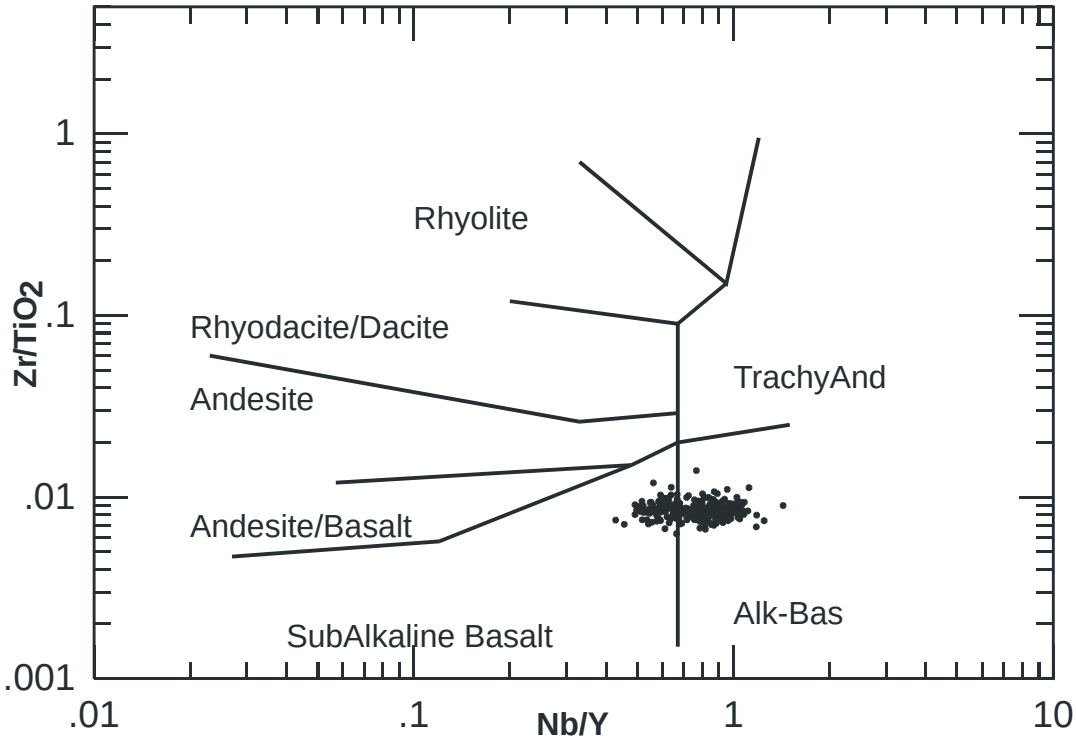

Fig. 4.6 Binary Zr/TiO_2 vs Nb/Y diagram of Winchester and Floyd (1976) for high-Ti basalts at Madrid. The suite straddles the boundary between alkaline and subalkaline basalts.

Least altered samples from the TEAD komatiitic and transitional basalt suites are shown on a MORB normalized multi-element diagram in Fig 4.7. TEAD komatiitic basalts clearly show increasing enrichment of all trace elements toward the FETI basalts. In both suites the more incompatible elements are significantly enriched relative to the less incompatible elements. Ti, Zr, Hf and Sm show significant enrichment relative to MORB in both Ti-enriched suites. Y and Yb are the only incompatible elements that are not enriched relative to MORB for these two suites. This trend is exactly comparable to Pearce's (1996) Fig. 4b (not shown) for within-plate basalts. Notably, samples from Madrid plot between Pearce's (1996) within plate tholeiitic basalt and within plate alkali basalt, further evidence of their transitional character. The elevated Ti/Y ratio and the depleted Y and Yb values likely relate to the melting of a plume-related garnet lherzolite source. With the right degree of partial melting, Y would be preferentially retained in the residual garnet (greater bulk distribution coefficient) while the more compatible Ti enters the melt (Pearce, 1996). Removal of garnet by fractional crystallization would also produce this trend. This interpretation is similar to that of Barnes and Often (1990), and Gale and Pierce (1982) for TEAD komatiites in Norway, for TEAD komatiites from the Boston Township (Xie *et al*., 1993) and general conclusions made by Green (1975), Nesbitt *et al*., (1979) Ohtani (1990), Polat and Kerrich (2001) and Sproule *et al*. (2002) for Ti-enriched Al-depleted komatiites. The implications of these results are discussed in more detail in Chapter 6.

The chondrite normalized REE diagram of Fig. 4.8 shows a moderate negative slope with a significant enrichment of all elements relative to chondritic values. The negative slope and range of La/Yb_n values (2.5-7.5) are similar to TEAD komatiites from Norway and Boston Township (Barnes and Often, 1990; Xie *et al*., 1993).

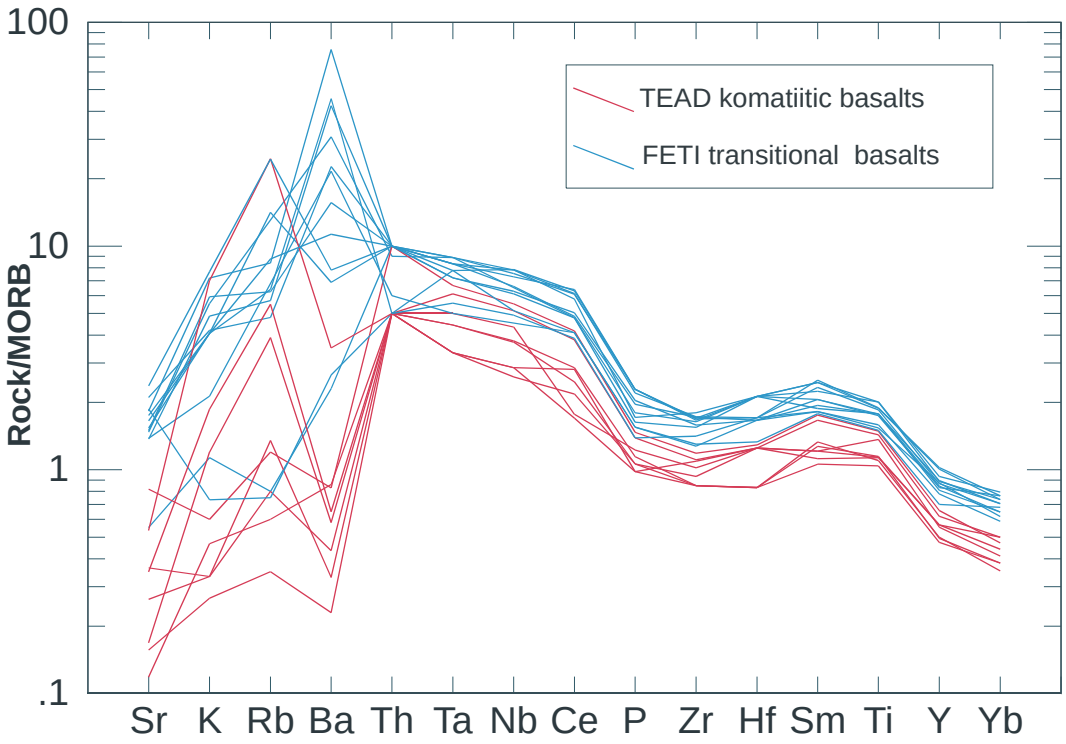

Fig. 4.7 MORB normalized multi-element variation diagram (Pearce, 1983) for least altered TEAD komatiitic basalts and FETI basalts at Madrid.

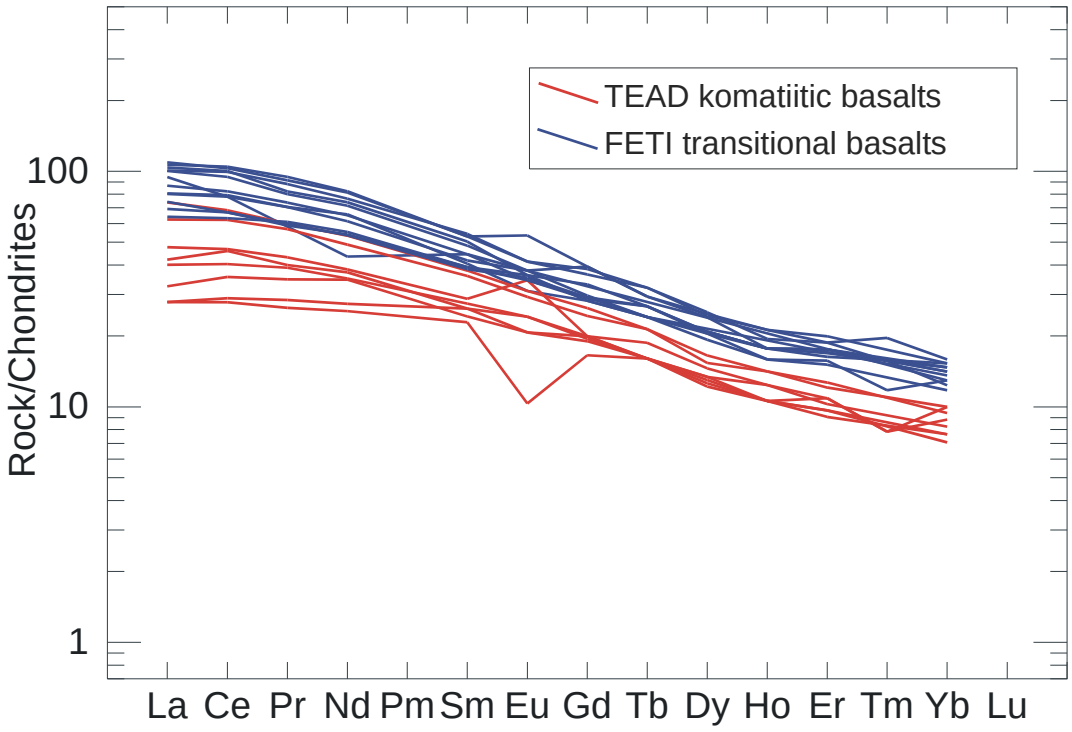

Fig. 4.8 Chondrite normalized REE diagram (Sun and McDonough, 1989) for least altered TEAD komatiitic basalts and FETI basalts from Madrid.

The Ti-Zr-Y tectonic discrimination diagram of Pearce and Cann (1973) has been used to determine the tectonic setting of the high-Ti komatiitic and tholeiitic suites. Fig. 4.9 suggests that these rocks are of within-plate origin, representing either continental or ocean island/plateau basalts. This is consistent with the MORB normalized multi-element diagrams discussed above and with other tectonic discrimination diagrams such as the Nb/Y - Ti/Y diagram of Pearce (1982) in Fig. 4.10 and the Nb-Zr-Y diagram of Meschede (1986) (not shown).

The Zr - Zr/Y tectonic discrimination diagram (Fig. 4.11) of Pearce and Norry (1979) shows that the vast majority of TEAD komatiitic basalts fall outside the field of within plate basalts whereas the majority of the FETI basalts fall well within this field.

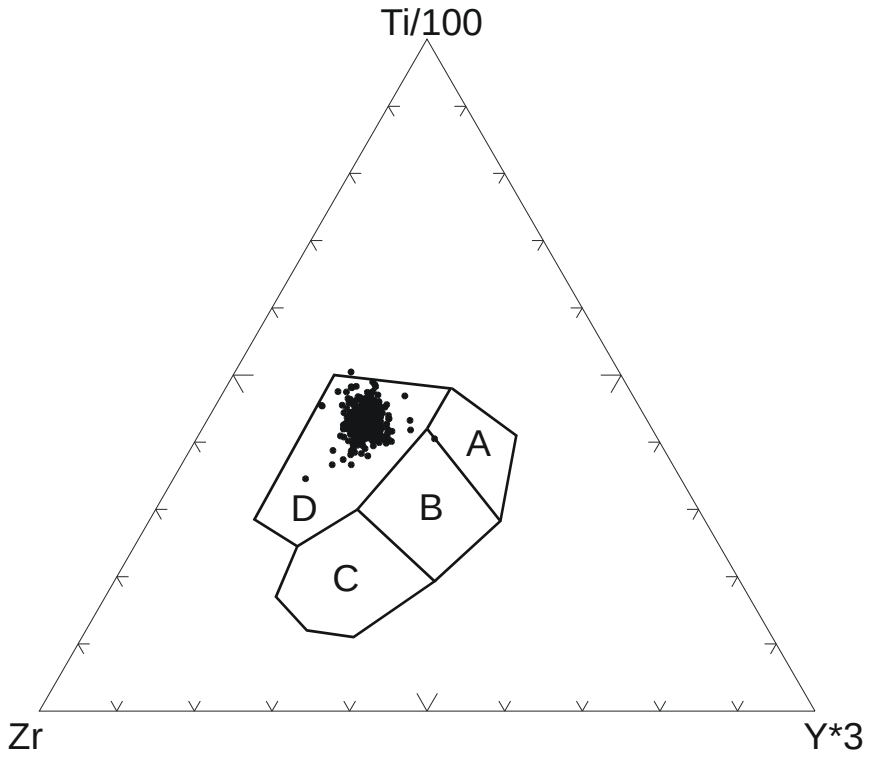

Fig. 4.9 Tectonic setting discrimination diagram of Pearce and Cann (1973) for TEAD komatiitic basalts and FETI basalts. A: Island arc tholeiites; B MORB, island arc tholeiites and calc-alkali basalts; C: Calc-alkali basalts; D: Within-plate basalts.

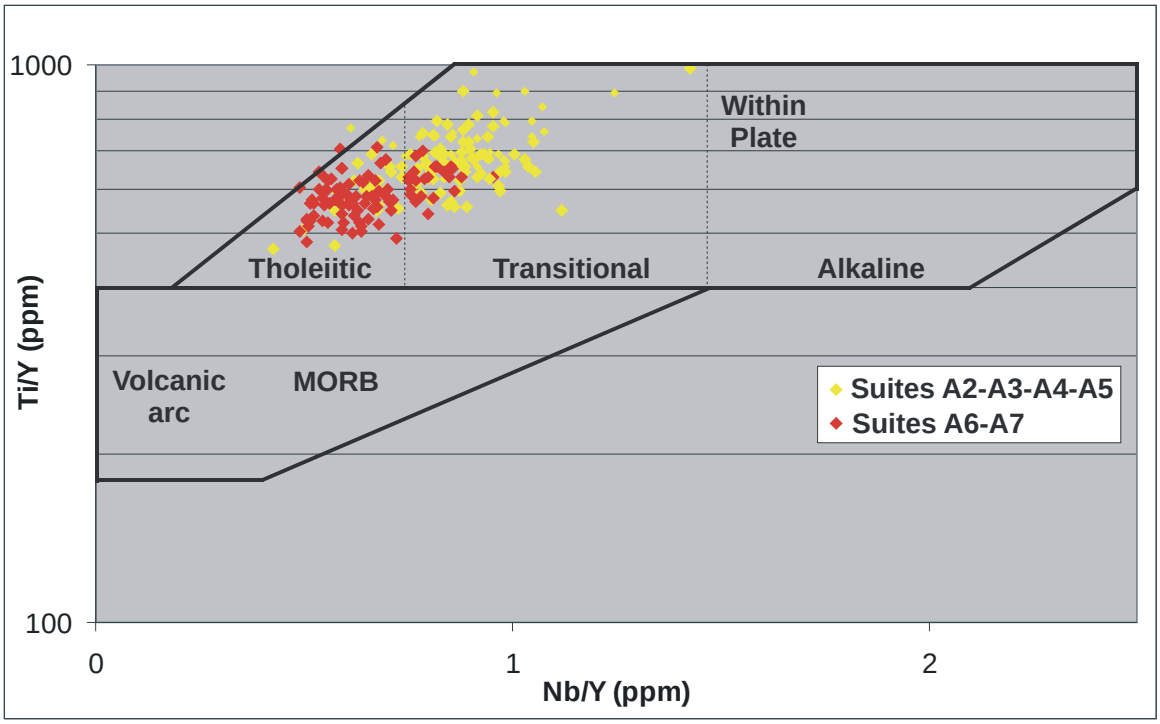

Fig. 4.10 Tectonic setting discrimination diagram of Pearce (1982) for TEAD komatiitic and transitional basalts from Madrid.

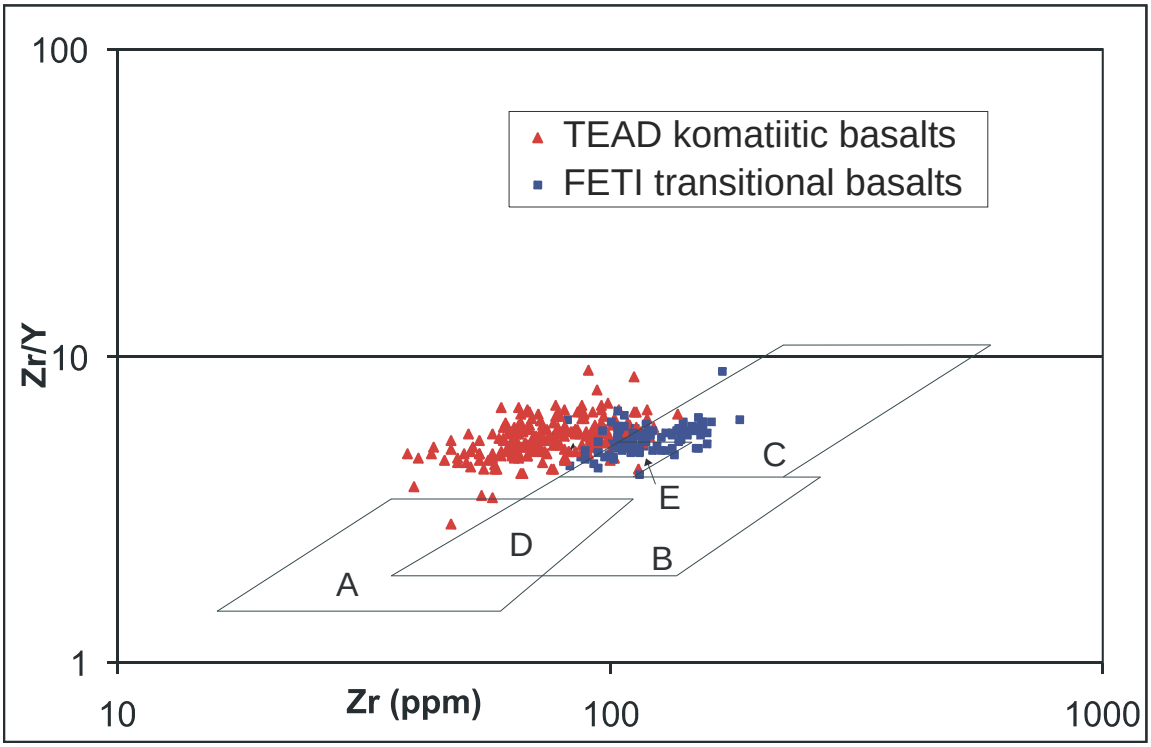

Fig. 4.11 Tectonic discrimination diagram of Pearce and Norry (1979) for TEAD komatiitic and transitional basalts. A: volcanic-arc basalts; B: MORB; C: within-plate basalts; D: MORB and volcanic-arc basalts; E: MORB and within-plate basalts.

The reason for this is not completely understood. Despite this apparent inconsistency, the diagram is useful for illustrating magmatic processes. The horizontal variation along this diagram can either be attributed to different degrees of partial melting or fractional crystallization (Pearce and Norry, 1979). In order to differentiate between these two processes, Cr and Ni may be used, as different degrees of partial melting will not strongly affect the Cr-Ni content of the melt. The relationship of the komatiitic vs. transitional basalt suites is shown on Figs 4.12 - 4.14 and suggests that fractional crystallization is the dominant process. Figs. 4.12 and 4.13 show a rapid decrease in Cr and Ni as Zr values progressively increase. Additional fractional crystallization related trends are illustrated in Fig. 4.14 which show an increase in the incompatible elements Nb, Y and Ti with fractionation (increasing Zr). This is consistent with the MORB and chondrite normalized multielement diagrams which show a relative increase in all immobile trace elements from the more primitive TEAD komatiitic basalts to the slightly more evolved FETI basalts.

An additional trend on which the fractionation trends are superimposed can be seen in Fig. 4.10. The overall path is toward increasing Ti/Y and Nb/Y ratios. As all three elements act incompatibly the ratios are not significantly affected by partial melting and fractional crystallization which led Pearce (1982; 1983) to suggest this trend is related to mantle heterogeneities. While variations due to fractionation are likely present on Fig. 4.10, the larger scale trend is between the *fractionation related couples* (i.e. A6/A7 toward A2/A3/A4/A5). As stated above, this also accounts for the changes in Al_2O_3/TiO_2 ratios on Fig. 4.3. The processes which may give rise to within-plate basalt enrichment are beyond the scope of this thesis, however, Pearce (1982) suggests it may involve enrichment by migrating incompatible-element enriched melts.

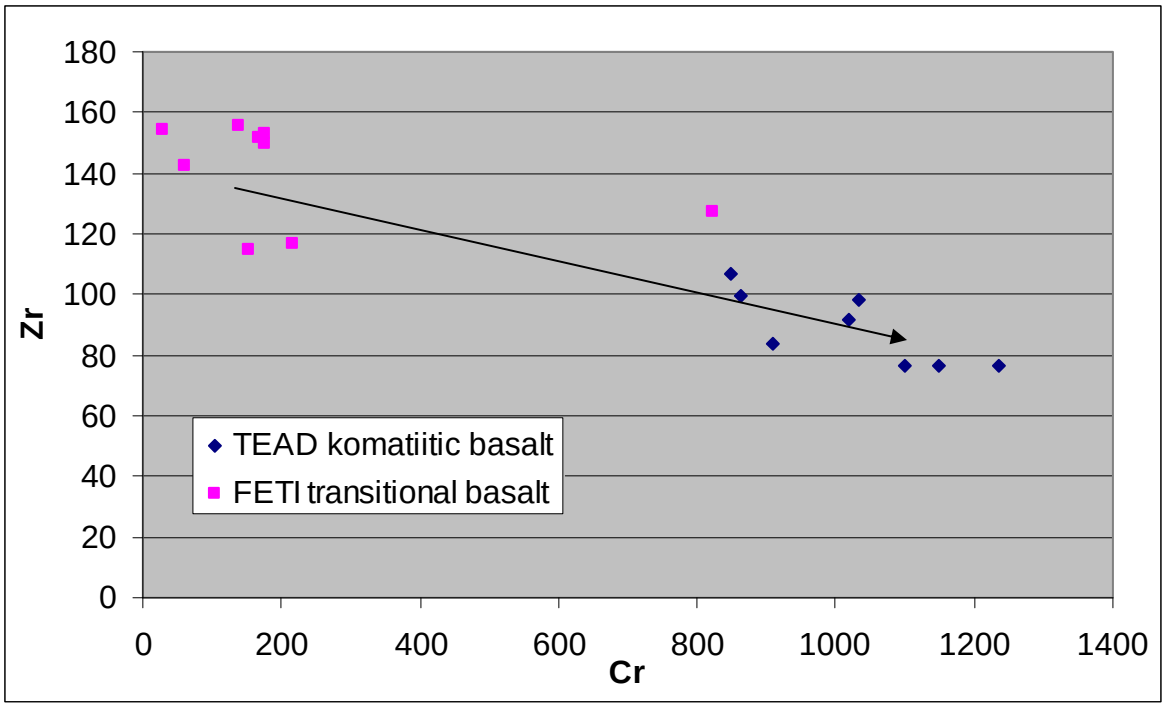

Fig. 4.12 Zr vs. Cr binary illustrating a dramatic decrease in Cr as the TEAD komatiitic basalt suite fractionates toward the FETI basalt suite marked by increasing Zr.

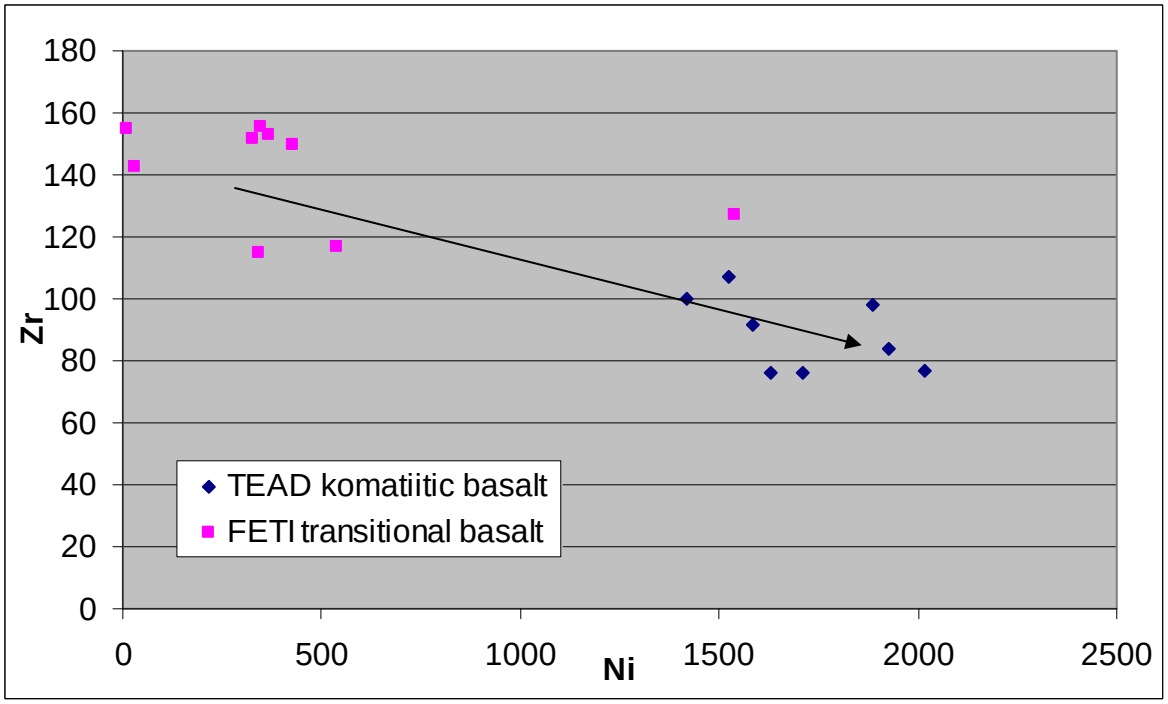

Fig. 4.13 Zr vs. Ni binary illustrating a dramatic decrease in Ni as the TEAD komatiitic basalt suite fractionates toward the FETI basalt suite marked by increasing Zr.

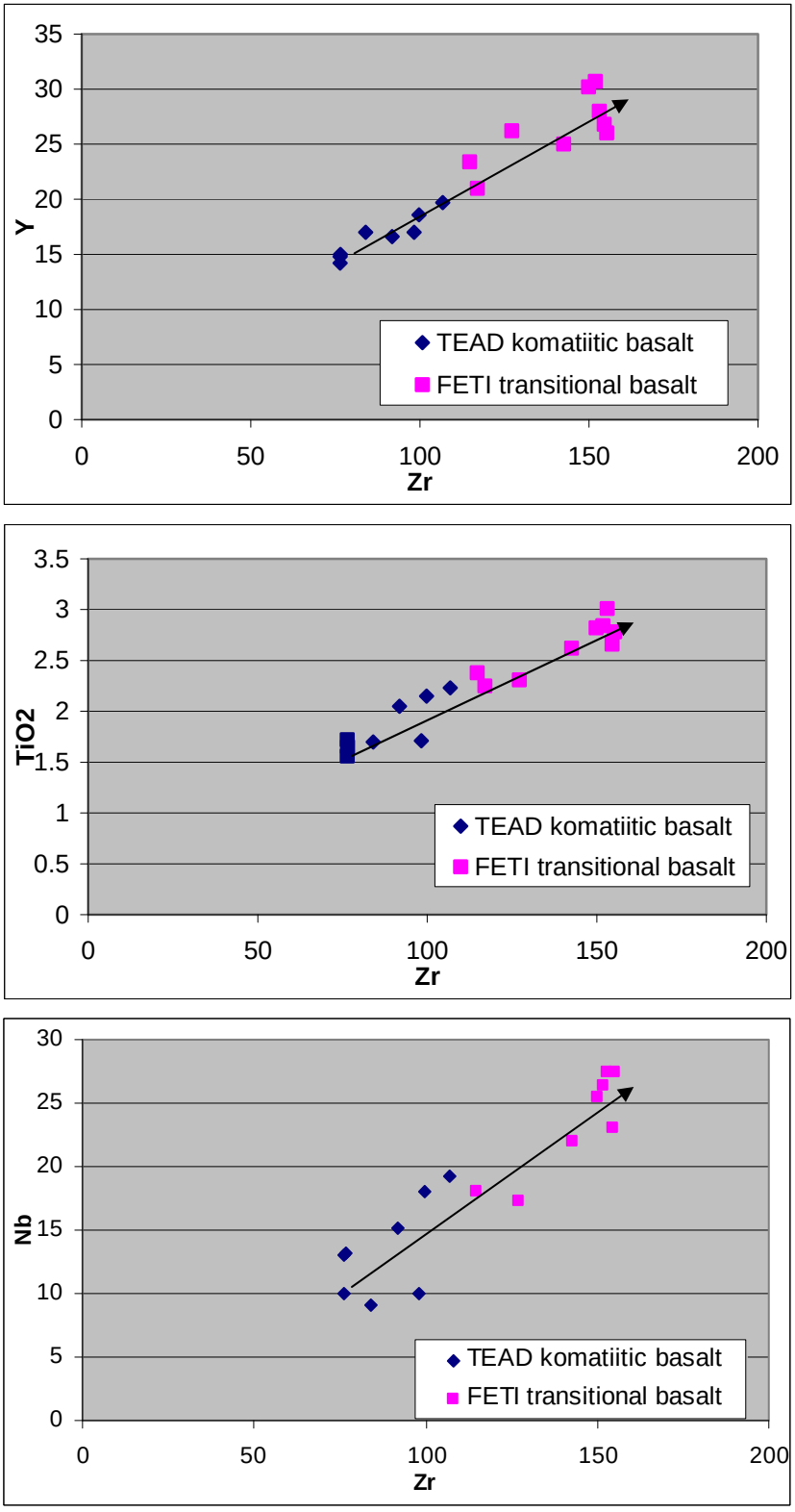

Fig. 4.14 Fractional crystallization trends between least altered TEAD komatiitic basalts and FETI basalts. TEAD komatiitic basalts fractionate toward the FETI basalts marked by increasing Zr, Y, Nb and TiO_2.

4.3.2 – Tholeiitic (high-Fe) Basalts and Basaltic Andesites

The remaining basaltic rocks from the Madrid area exhibit chemistries comparable to basalts found in other Archean greenstone belts (eg. the Superior Province: Grunsky *et al*., 1992). The magmatic affinity diagram (Fig. 4.15) of Barrett and MacLean (1994b) indicates that, in contrast to the high-Ti suite, the "normal" basalts are purely tholeiitic in nature. The same results are obtained from the Zr/P_2O_5 - TiO_2 of Winchester and Floyd (1976) and the Y/Nb diagram of Pearce and Cann (1973).

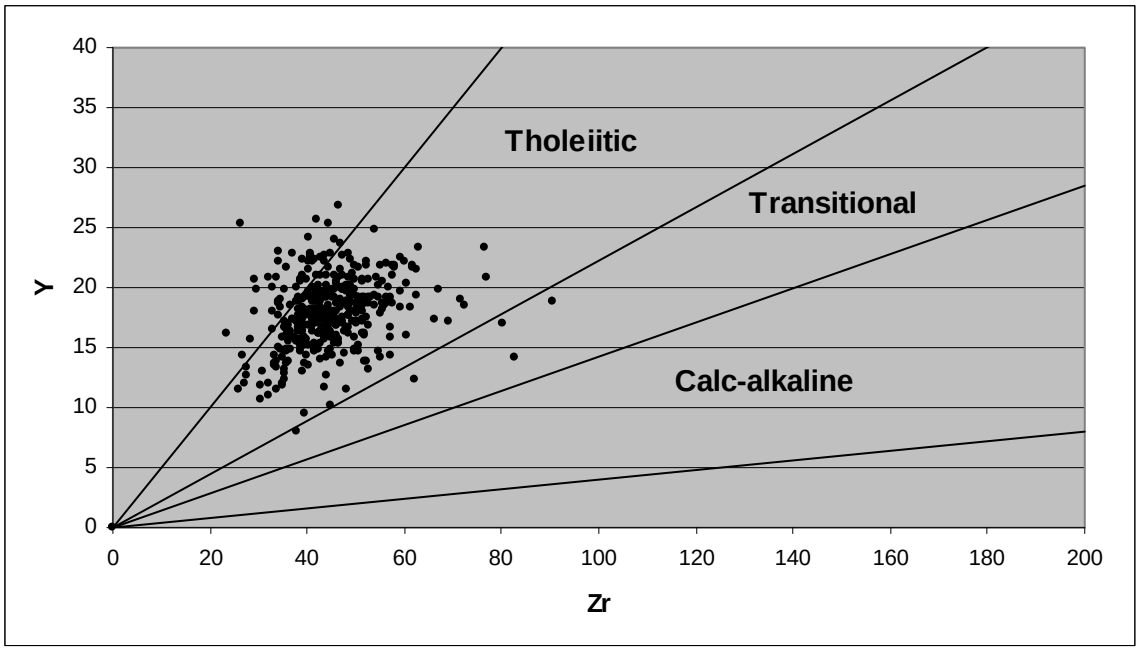

Fig. 4.15 Binary Zr vs. Y magmatic affinity diagram of Barrett and MacLean (1994b) illustrating the tholeiitic character of the "normal" to high-Fe basalts and basaltic andesites from the Madrid area.

For the purposes of this chapter the classification of the "normal" Ti basalts has been slightly modified from what was presented in Chapter 3. Variolitic high-Fe basalts (Windy Lake mafics) have been grouped together with their spatially (and temporally?) associated (but volumetrically less significant) gabbros and coarse flow bases, as their

geochemistries are nearly identical. The non-variolitic high-Fe basalts south of the HBDZ (Wolverine basalts) have been divided into two smaller groups of slightly different chemistry in order to obtain more accurate results during mass balance calculations presented later in this chapter. Basaltic andesites have been preserved as a single suite. Representative analyses of these rocks are shown in Table 4.2. Basaltic andesites have noticeably elevated SiO_2, Al_2O_3, Na_2O, Cr, Ni, Co and V values and lower Fe_2O_3, MgO and Zr values relative to the high-Fe basalts. Variolitic high-Fe basalts have elevated MgO and Cr and depleted Al_2O_3, TiO_2 and V relative to the non-variolitic high-Fe basalts. This suggests that the variolitic suite is the more primitive of the two. The major and trace element abundances of these rocks correspond closely to those presented by Pearce and Cann (1973) and Jakes and Gill (1970) for tholeiitic island arc rocks with the exception of the low Cr-Ni values (0-50 ppm) reported by Jakes and Gill (1970).

The separated suites for 301 samples are shown in Figs 4.16 and 4.17. C1 and C3 correspond to non-variolitic high-Fe basalts, C2 to variolitic high-Fe basalts and C4 to basaltic andesites. At first glance it appears that least-altered samples fractionate from the variolitic high-Fe basalts (C2) toward the non-variolitic suite (C1 and C3) with TiO_2 and Al_2O_3 acting incompatibly. This trend appears to then take a sharp downward turn toward the basaltic andesites (C4) as TiO_2 switches from incompatible to compatible. This conclusion, however, is contradictory to Fig. 4.16 which suggests fractionation toward decreasing Zr values, a trend that should not exist if these suites are related by fractional crystallization. Thus, other processes such as partial melting or source heterogeneity are likely involved.

Suite	C1	C3	C2	C2	C4	C4
Rock Type	NVT	NVT	VT	VT	BA	BA
Si02%	46.19	49.40	51.31	49.68	51.10	51.59
Al2O3%	15.26	16.48	13.06	13.47	17.65	17.77
Fe2O3%	14.02	11.49	11.69	13.02	8.72	8.68
CaO%	11.27	9.35	8.75	9.80	9.61	10.77
MgO%	6.63	5.19	7.93	7.93	3.80	3.95
Na2O%	2.21	3.73	2.45	2.39	5.50	3.73
K2O%	0.05	0.13	0.12	0.30	0.08	0.07
Cr2O3%	0.04	0.05	0.00	0.04	0.04	0.05
TiO2%	0.96	1.03	0.82	0.89	0.95	0.87
MnO%	0.22	0.20	0.20	0.19	0.15	0.19
P2O5%	0.07	0.07	0.07	0.05	0.06	0.06
BaO%	0.01	0.02	0.00	0.02	0.02	0.02
Al2O3/TiO2	15.90	16.00	15.93	15.13	18.58	20.43
LOI%	3.1	2.8	4.3	2.2	2.3	2.2
Ba ppm	23.7	41.6	39.1	83.0	43.1	85.8
Co ppm	55.8	56.7	47.0	49.9	58.4	65.3
Cr ppm	300.2	360.8	384.8	421.5	427.0	513.5
Cu ppm	144.1	153.3	112.9	105.4	143.4	143.0
Ga ppm	18.0	19.0	nd	15.1	16.3	17.1
Ni ppm	151.1	158.3	125.0	113.4	194.2	204.4
V ppm	346.2	340.7	256.6	274.0	385.3	350.4
Zn ppm	100.1	107.2	81.3	82.3	77.3	68.5
Rb ppm	0.6	1.7	nd	4.2	1.8	1.0
Ta ppm	0.5	nd	nd	nd	nd	nd
Th ppm	nd	nd	nd	nd	nd	nd
U ppm	nd	nd	nd	nd	nd	nd
Nb ppm	3.0	2.0	nd	2.0	2.0	2.0
La ppm	4.0	2.6	3.3	3.0	2.5	3.0
Ce ppm	8.1	8.0	5.3	8.5	7.7	8.2
Pr ppm	1.3	1.2	0.0	1.2	1.2	1.3
Sr ppm	164.1	102.7	106.2	114.4	120.5	213.5
Nd ppm	6.2	6.3	6.2	6.1	6.2	6.2
Sm ppm	2.0	2.1	2.0	1.9	2.5	2.1
Zr ppm	51.5	48.2	49.1	62.5	43.0	47.2
Hf ppm	2.0	2.0	2.0	2.0	1.0	2.0
Eu ppm	0.7	0.8	0.7	0.7	0.8	0.9
Gd ppm	2.5	2.5	nd	2.7	2.5	2.5
Tb ppm	0.5	0.5	nd	0.5	0.4	0.5
Dy ppm	3.3	3.5	nd	3.4	3.4	3.4
Y ppm	20.5	20.1	18.0	19.3	19.2	19.9
Ho ppm	0.7	0.8	nd	0.7	0.7	0.8
Er ppm	2.2	2.3	nd	2.1	1.9	2.3
Tm ppm	nd	nd	nd	0.3	nd	nd
Yb ppm	2.1	2.1	2.0	2.0	2.5	2.1
Lu ppm	0.4	0.4	0.3	0.3	0.3	0.3
W ppm	2.0	1.0	nd	2.0	nd	nd

Table 4.2 Major and trace element data for representative least altered high-Fe basalts and basaltic andesites from the Madrid area. NVT: non-variolitic tholeiite; VT: variolitic tholeiite; BA: basaltic andesite.

A significant amount of overlap exists between the variolitic and non-variolitic high-Fe suites on Fig. 4.16. This is related to the smearing of the two suites during metamorphism and hydrothermal alteration as indicated by a line that passes through the origin. However, the validity of the separation between C1-C3 can be seen on a Cr vs. Ni plot (Fig 4.18). Variolitic basalts have elevated Cr values relative to the non-variolitic suite. The basaltic andesite suite has elevated Cr and Ni values relative to the high-Fe basalts. The basaltic andesite suite may in fact be better classified as a calc-alkaline basalt, however, as it plots very near the boundary with tholeiitic andesites (Fig. 4.19), the term basaltic andesite is preserved. The remaining basalts plot as high-Fe and normal basalts on the Jensen ternary of Fig. 4.19. The protolith of these rocks is further confirmed using the immobile elements Nb-Y-Zr-Ti in Fig. 4.20.

The trace element geochemistry of the normal Ti tholeiitic basalts differs significantly from the Ti-enriched suite. A MORB normalized multi-element diagram for least altered high-Fe tholeiitic basalts and basaltic andesites is shown in Fig. 4.21. The depleted Nb values relative to Ce and the depletion of Nb, Zr, Ti and Y relative to MORB is characteristic of tholeiitic oceanic volcanic arc basalts (Pearce, 1996). Basaltic andesites show similar trends as the high-Fe-basalts, but with slightly lower ratios relative to MORB and a distinct P depletion which may be related to metamorphism/alteration. The chondrite normalized REE diagram (Fig. 4.22) shows a very flat trend (La/Yb_n ratios of 1-3) at approximately 10x chondritic values with very minor enrichments/depletions of various elements. This flat REE pattern can also be indicative of a tholeiitic volcanic arc setting (Jakeš and Gill, 1970; Jakeš and White, 1972).

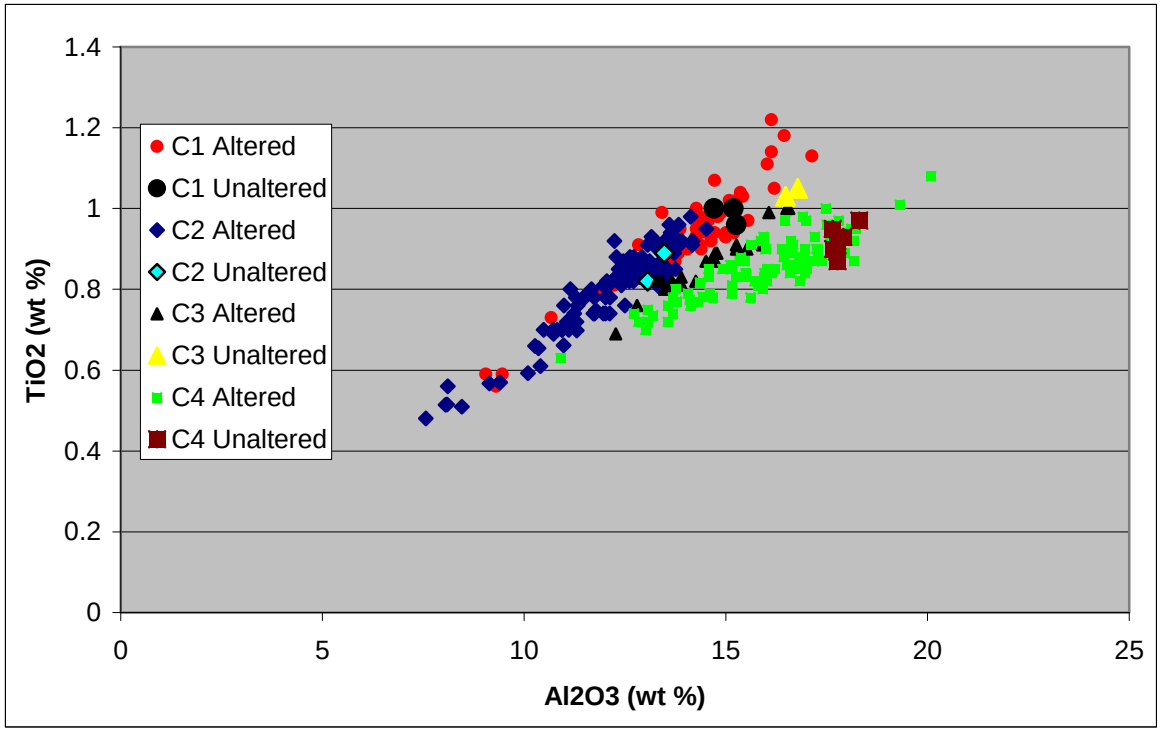

Fig. 4.16 TiO_2-Al_2O_3 binary plot separating high-Fe tholeiitic basalts and basaltic andesites. C1 and C3: non-variolitic high-Fe basalt; C2: variolitic high-Fe basalt and gabbro; C4: basaltic andesite.

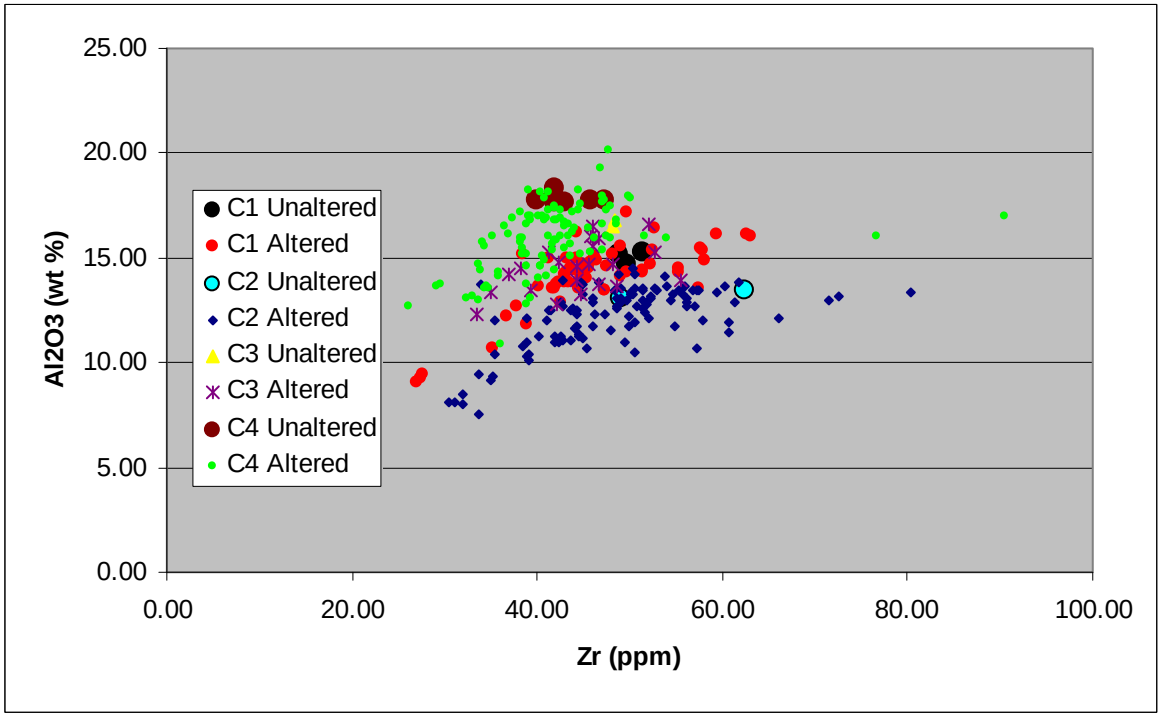

Fig. 4.17 Al_2O_3 vs. Zr binary of tholeiitic (high-Fe) basalts and basaltic andesites from Madrid.

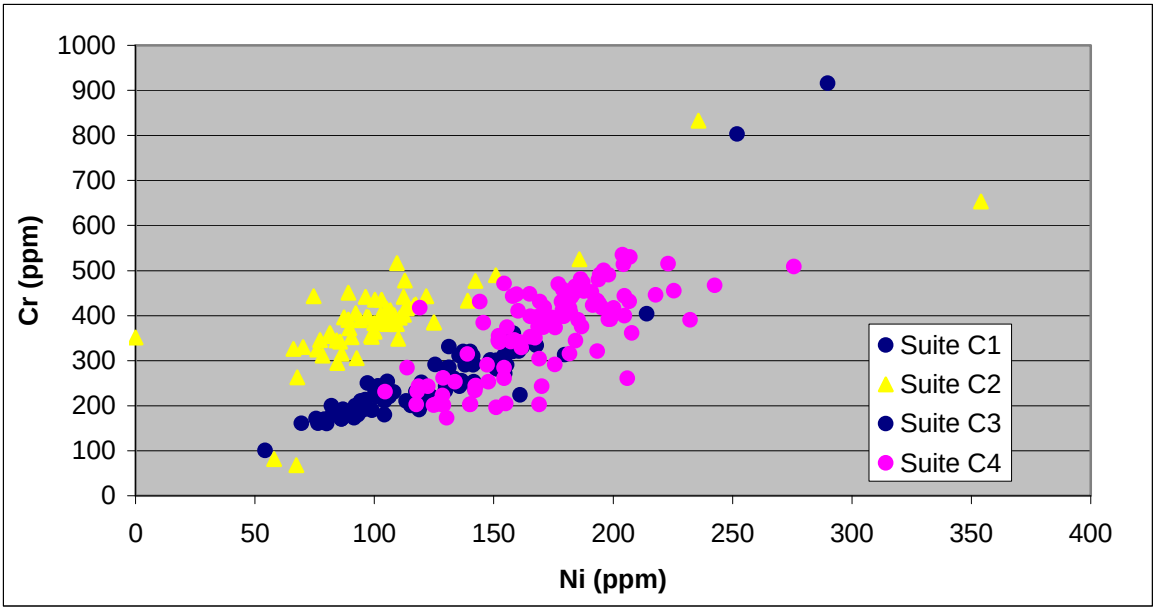

Fig. 4.18 Cr-Ni binary for suites C1-C4. Variolitic high-Fe basalts have significantly higher Cr values than their non-variolitic counterpart. Andesitic basalts are enriched in both Cr and Ni relative to the high-Fe basalts.

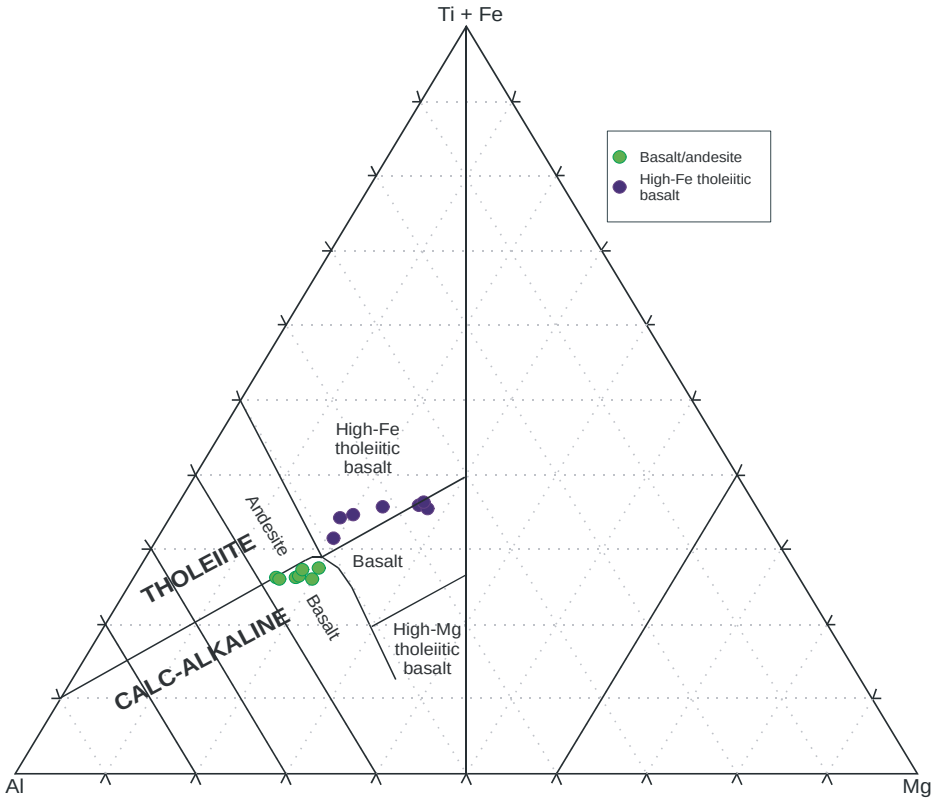

Fig. 4.19 Jensen cation plot of least altered high-Fe basalts and basaltic andesites from the Madrid area. A visually and chemically distinct cluster straddles the boundary between tholeiitic andesites and calc-alkali basalts while remaining samples plot as high-Fe and "normal" basalts.

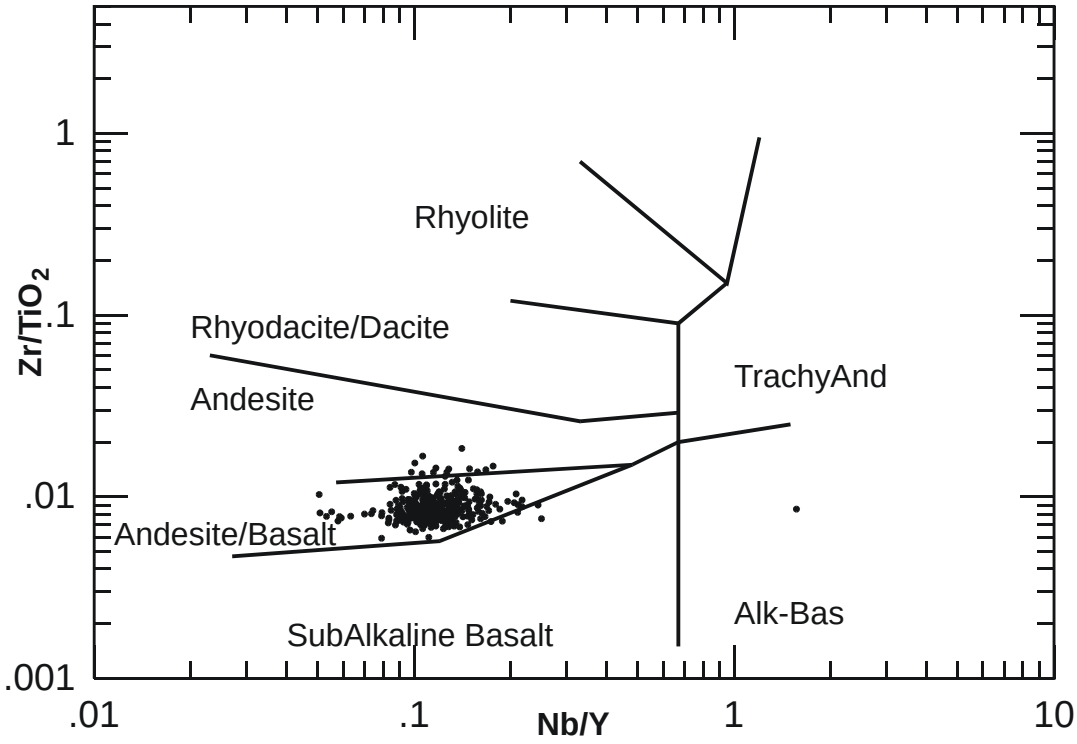

Fig. 4.20 Binary Zr/TiO_2 vs Nb/Y for "normal" basalts and andesites from the Madrid area (Winchester and Floyd, 1977).

The tectonic discrimination diagrams of Pearce and Cann (1973), Pearce and Norry (1979) and Pearce (1982) are shown in Figs. 4.23 - 4.26. On Figs 4.23 and 4.24 data falls in the MORB + island arc tholeiites + calc-alkali basalt field. Discrimination between these three settings is difficult, but based on the REE patterns discussed above these rocks likely represent an oceanic island arc. The tectonic discrimination diagrams in Figs. 4.25 and 4.26 also suggest that these rocks are tholeiitic arc related, with most of the data falling in the volcanic arc field. A more accurate discrimination can be made on a Ti-Zr-Sr ternary (not shown; Pearce and Cann, 1973). However, as Sr is likely to be a mobile element during metamorphism and alteration, this plot holds little significance. Nevertheless it is interesting to note that most of the least altered samples do fall in the tholeiitic volcanic arc field. The significance of a tholeiitic arc tectonic setting and its relationship to the intraplate high-Ti suite is discussed in more detail in Chapter 6.

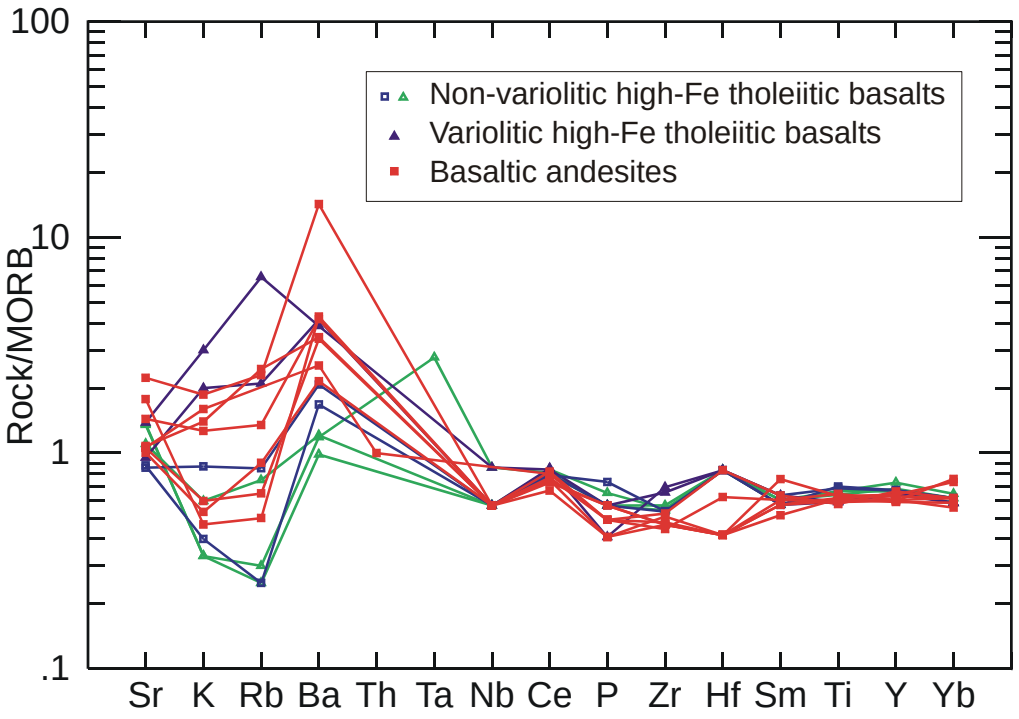

Fig. 4.21 MORB normalized multi-element variation diagram (Pearce, 1983) for least altered high-Fe basalts and basaltic andesites from Madrid. The significant negative Nb anomaly with respect to Ce and the depletion of Zr, Ti and Y are characteristic of volcanic arc basalts (Pearce, 1996).

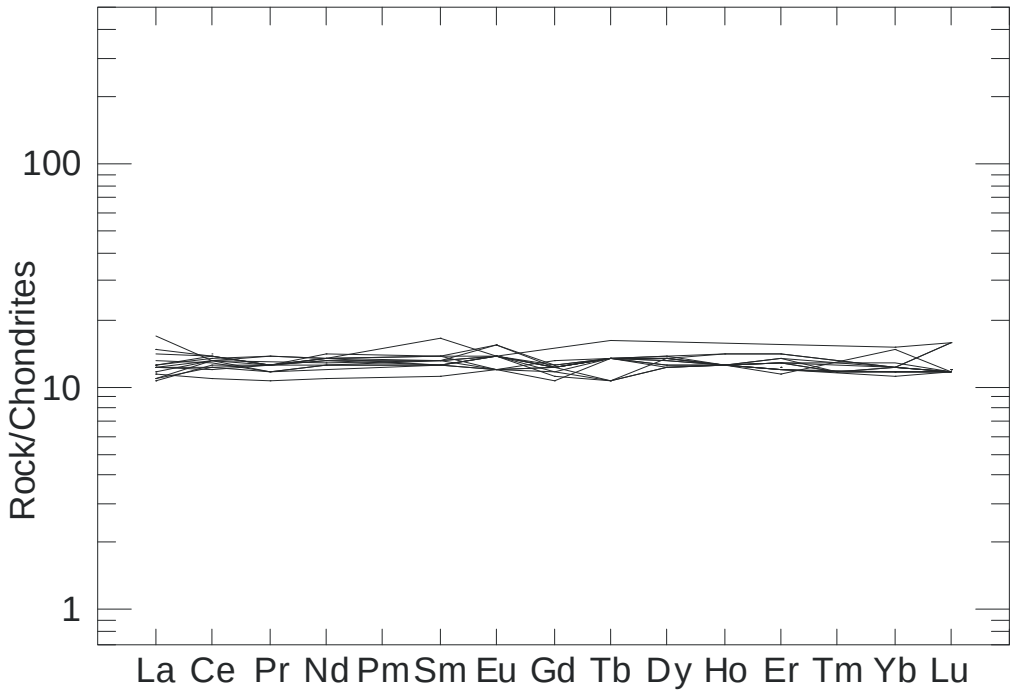

Fig. 4.22 Chrondrite normalized REE plot (Sun and McDonough, 1989) of least altered high Fe tholeiitic basalts and basaltic andesites from Madrid.

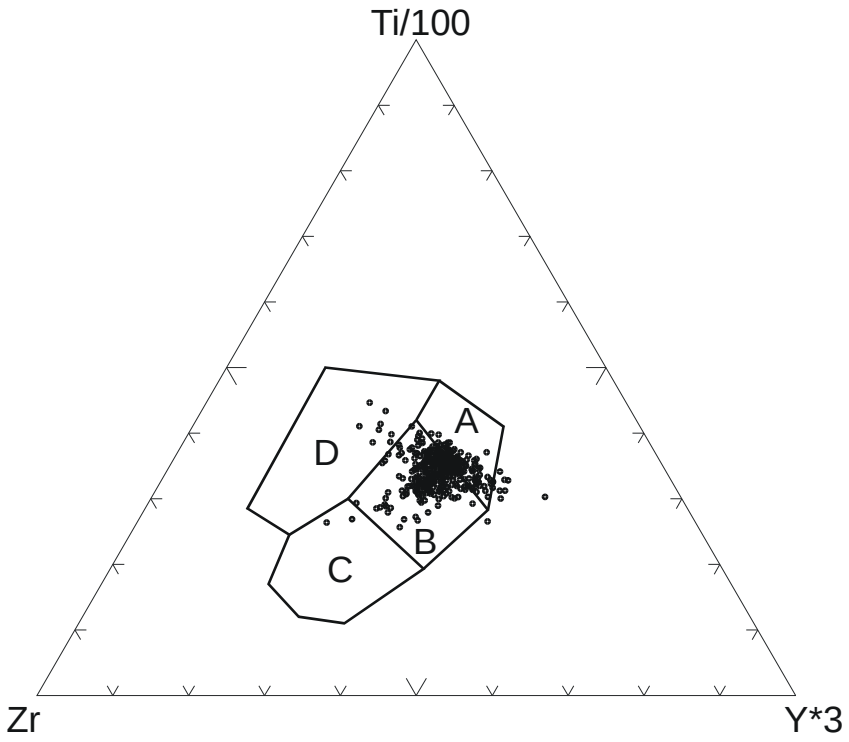

Fig. 4.23 Tectonic setting discrimination diagram from Pearce and Cann, 1973. A: Island arc tholeiites; B MORB, island arc tholeiites and calc-alkali basalts; C: Calc-alkali basalts; D: Within-plate basalts.

As mentioned above the high-Fe basalts and basaltic andesites do not appear to be related by simple fractional crystallization based on the relationships of their major and trace element geochemistry. Higher SiO_2, Al_2O_3 and Na_2O values in the basaltic andesites are not consistent with their elevated Cr, Ni and Co values relative to the more primitive high-Fe suites. Furthermore, their lower Zr values are not consistent with their lower Fe_2O_3 and MgO relative to the other suites. If equilibrium or progressive partial melting is invoked then increasing degrees of melting would trend toward lower Zr and higher MgO values i.e.) the first melt should have high Zr and low MgO-Cr-Ni while continued melting would yield the opposite. This is also inconsistent with the data. It is possible that the basaltic andesites represent the first phase of a fractionating calc-alkaline melt not directly related to the melts which give rise to the high-Fe suites. Comparison

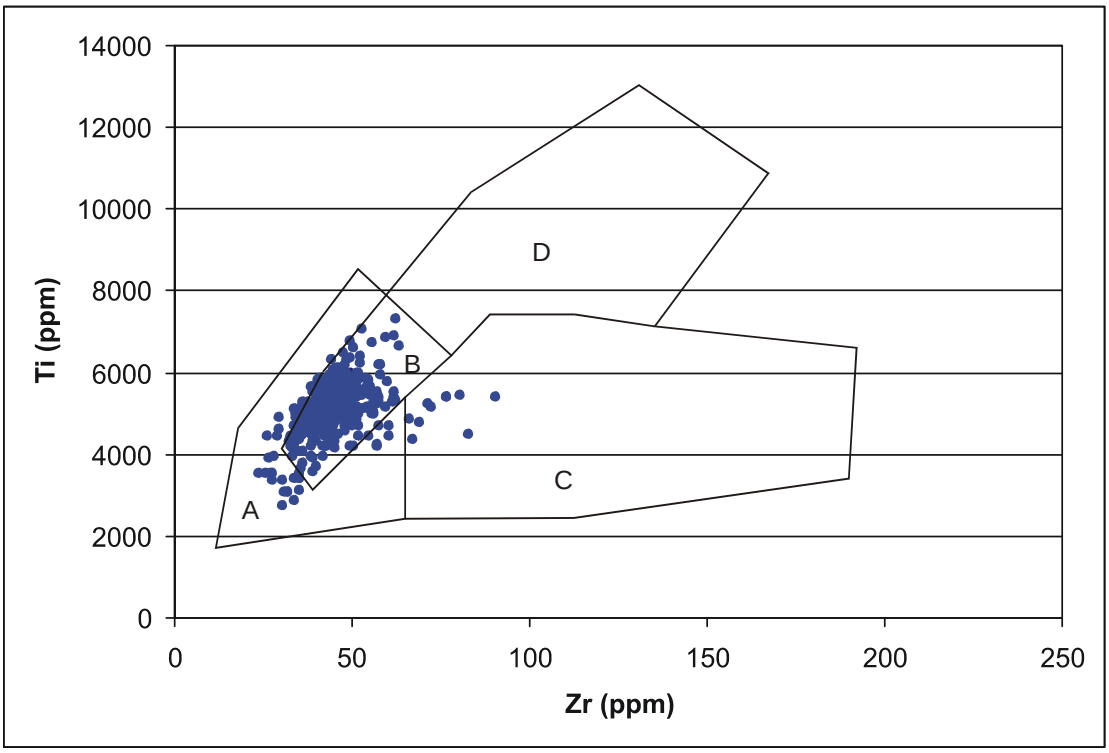

Fig. 4.24 Tectonic discrimination diagram of Pearce and Cann (1973) for high-Fe basalts and basaltic andesites from Madrid. A: Island arc tholeiites; B: MORB, calc-alkaline basalts and island arc tholeiites; C: calc-alkaline basalts; D: MORB

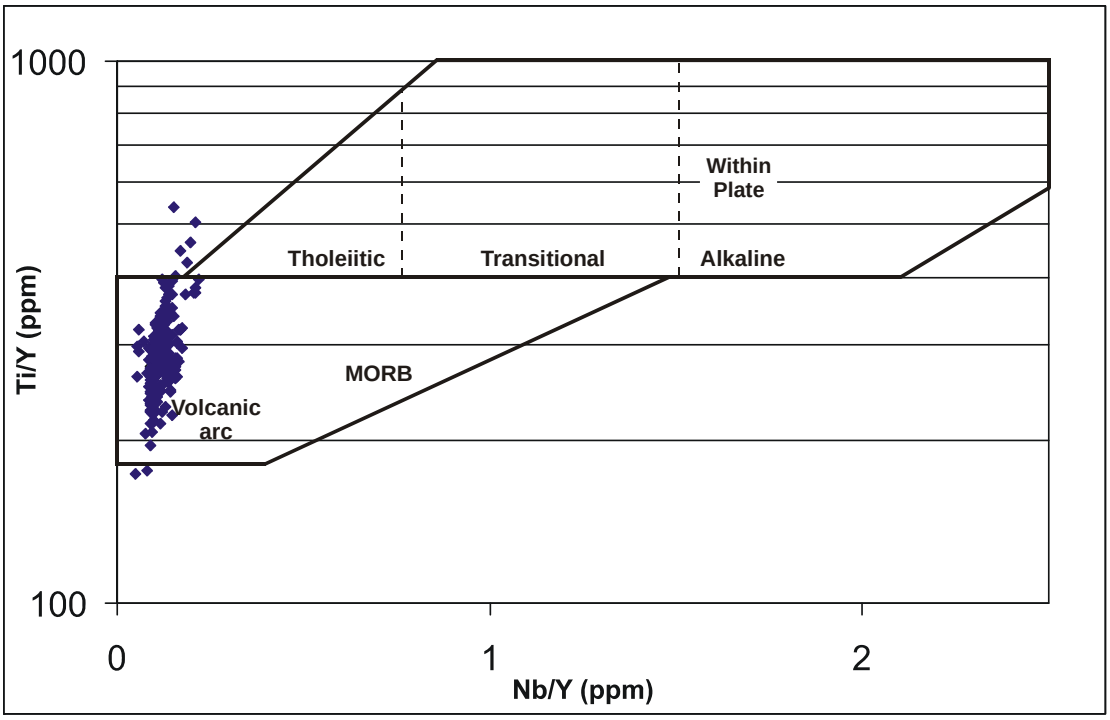

Fig. 4.25 Tectonic setting discrimination diagram of Pearce (1982) for high-Fe basalts and basaltic andesites from Madrid.

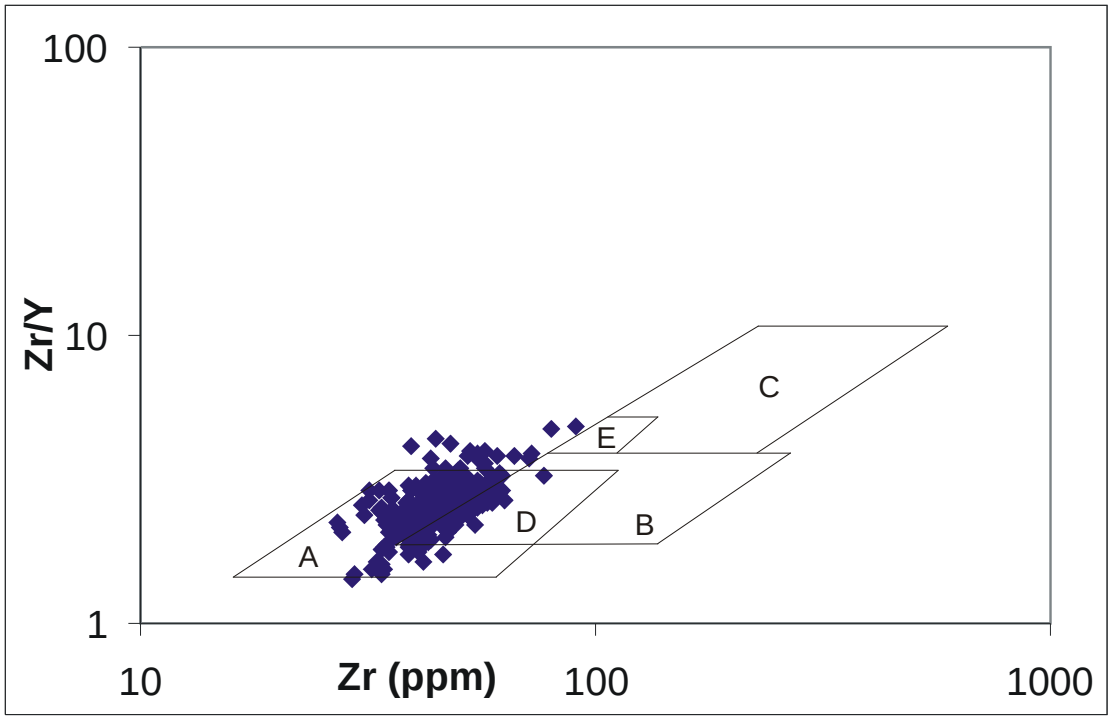

Fig. 4.26 Tectonic discrimination diagram of Pearce and Norry (1979). A: volcanic-arc basalts; B: MORB; C: within-plate basalts; D: MORB and volcanic-arc basalts; E: MORB and within-plate basalts.

of least altered high-Fe basalts show a similarly contradictory relationship. Variolitic high-Fe basalts have greater MgO-Cr values and lower Al_2O_3-TiO_2 values relative to the non-variolitic suite suggesting the variolitic suite is the more primitive of the two. However, Zr values are typically elevated in the variolitic high-Fe basalts. This also suggests that these suites are not related simply by fractional crystallization or degrees of partial melting. Nevertheless, the magmatic processes are likely complex and may involve variable contributions by subduction-derived fluids/melts, source heterogeneities, magma mixing and within-plate enrichment. Fractional crystallization and partial melting events would then be more difficult to distinguish and interpret. The genesis of these rocks is considered further in Chapter 6.

A classification scheme based on lithogeochemistry of rocks in the Madrid corridor is shown in Fig. 4.27. This arrangement varies only slightly from what was proposed in Chapter 3, but includes more formal terminology for the high-Ti suites in light of the geochemical results presented in this chapter. This terminology will be used throughout the remainder of the thesis.

4.4 Element Enrichment-Depletion Trends

4.4.1 Method

The method used to calculate element depletion-enrichment is based on Barrett and MacLean (1994a; 1994b) and is outlined below:

1) The immobility of various elements were calculated using the Pearson product moment correlation coefficient (r). Values range from -1 to 1 where values approaching 1 indicate a strong positive correlation (X increases with Y) and values approaching -1 indicate a strong negative correlation (Y increases as X decreases). High values (> 0.9) were yielded for Ti, Y and Zr and moderate values (> 0.8) for Al, Nb and Nd suggesting these elements are strongly immobile. Ti was found to be the most immobile element in the system and is used throughout the remaining calculations.

2) Several least altered (LA) examples were chosen to represent each of the suites defined in section 4.3. LA samples were chosen based on petrology and low (<3 %) loss on ignition (LOI) values.

3) All altered and LA data were normalized to 100% on a volatile-free basis. LA samples for each suite are averaged. Abnormal samples (sedimentary rocks, quartz veins and dyke rocks) were removed.

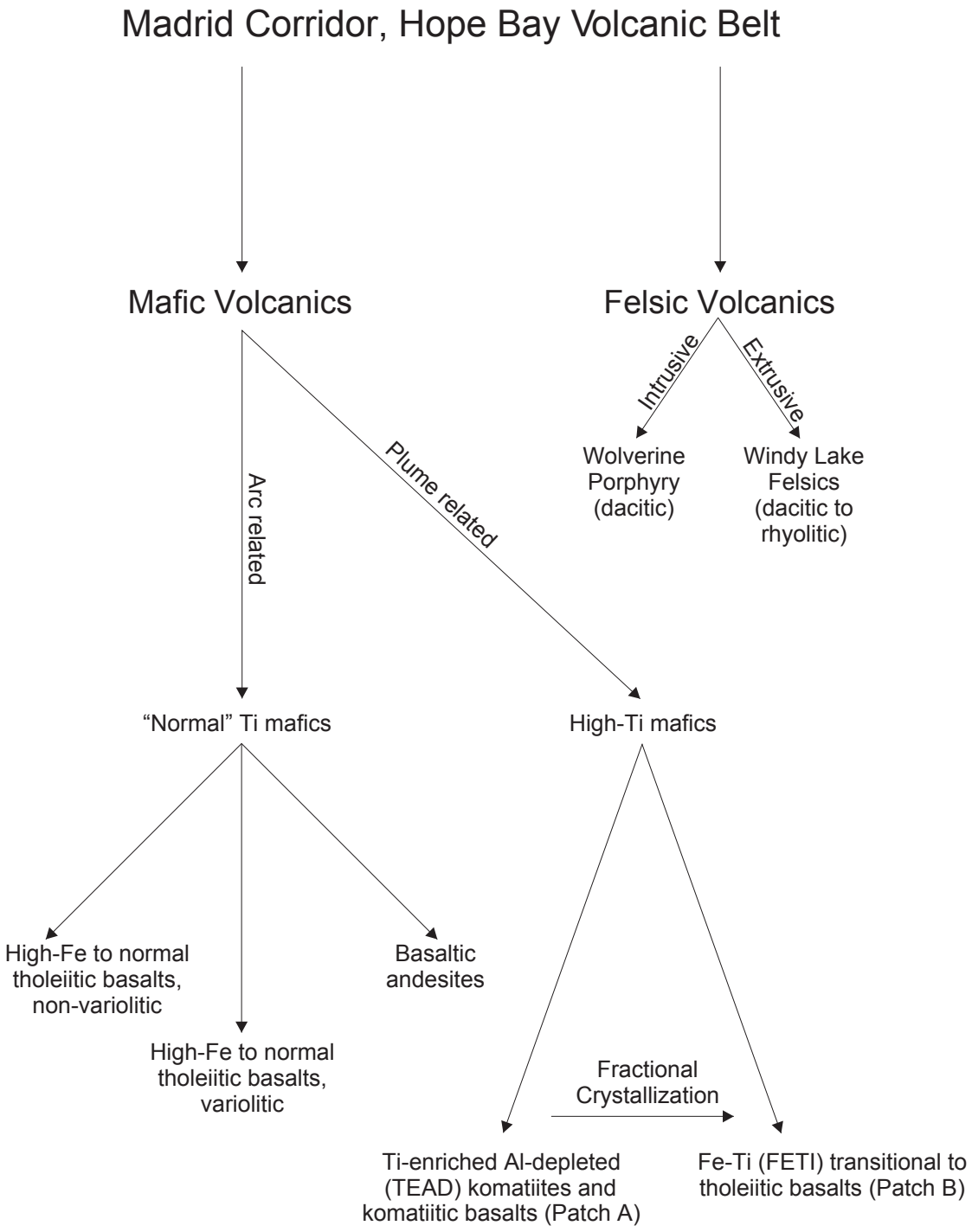

Fig. 4.27 Classification of lithologies from the Madrid area based on lithogeochemistry. This nomenclature varies only slightly from what was proposed in Chapter 3, but will be used in place of it for the remainder of the thesis.

4) Enrichment factors (EF) were calculated for each sample according to the formula:

$$EF = Ti_{(LA\ Average)}/Ti_{(altered\ sample)} \qquad \text{(Eq. 4.1)}$$

5) A reconstructed composition (RC) was calculated for each component of each sample according to the formula:

$$RC = EF \times Wt\%\ \text{or ppm (altered sample)} \qquad \text{(Eq. 4.2)}$$

6) Mass change (MC) for each component of each sample is calculated by

$$MC = RC - LA\ Average \qquad \text{(Eq. 4.3)}$$

A positive MC value indicates addition of a component relative to the LA average, while a negative MC corresponds to depletion. Note that the MC values are calculated as a weight percent rather than a percent gain/loss. Thus, an MC of 5% SiO_2 in a rock which originally contained 50% SiO_2 is less significant as compared to an MC of 1% Na_2O in a rock which contained 0.5% Na_2O in the LA precursor.

It should be noted that significant error is expected in the final results for a variety of reasons. Firstly, samples with quartz-carbonate veining will dilute immobile elements and make the sample appear more altered than it actually is. Secondly, samples with argillite or varioles will tend to drive a sample off the LA samples alteration line to different Al_2O_3 and TiO_2 values. Thirdly, fractionation within the subsuites will mean that the LA samples are not always the best estimate of precursor composition in some of the altered samples.

Another problem concerns the orientation of fractionation and alteration lines. Each of the elements Ti, Al, Nb, Nd, Y and Zr act incompatibly during fractionation within the high-Ti suites which yields a positive slope on binary plots. Superimposed on this are the alteration lines. This makes it difficult to determine which LA sample is most appropriate for each of the altered samples. Consequently, only altered samples which have a clear precursor (based on visual identification and lithogeochemistry) are used in the following graphs.

4.4.2 – Results

High-Ti suites

High-Ti komatiitic and tholeiitic basalts have been separated into seven subsuites (Fig. 4.3) each of which has a number of representative LA samples. The following figures illustrate the various enrichment and depletion trends of major and trace elements and how they relate to different alteration styles, intensities and lithologies. Figures 4.28 and 4.29 illustrate the processes of chloritization and sericitization. Mass gains of Fe_2O_3 and MgO (Fig. 4.28) and SiO_2 (Fig. 4.29) correspond to chloritization partly related to the breakdown of the ferromagnesian minerals. As alteration increases chlorite is progressively replaced by sericite (Eq. 4.4) resulting in the formation of ankerite and/or the loss of Fe_2O_3, MgO and SiO_2 to the fluid. Samples from the A3, A5 and A7 suites (FETI basalts) tend

$$3(Mg,Fe)_5Al_2Si_3O_{10}(OH)_8 + 15CaCO_3 + 2K^+ + 15CO_2 \rightarrow KAl_3Si_3O_{10}(OH)_2 + 15Ca(Mg,Fe)(CO_3)_2 + 3SiO_2 + 9H_2O + 2H^+$$

Chlorite + Calcite → Sericite + Ankerite (Eq. 4.4)

to define the chloritization trend. This is consistent with petrographic observations and

mineral chemistries, where the FETI basalts are predominately in the chlorite facies. Conversely, the better mineralized and more strongly white-mica altered TEAD komatiitic basalts (subsuites A2, A4 and A6) define the sericite alteration line. This is especially well illustrated by suite A6 which consists of some of the most altered and best mineralized samples. A sericite alteration line is also evident in Fig 4.30, where a vertical line from near the origin corresponds to mass gains in K. Once again the sericite line is defined by the more sericitized TEAD komatiitic basalts. The reason this line does not emanate from the origin is unclear. It may correspond to a slight overestimation of Na and K in the least altered precursor averages, or it may represent an early breakdown of feldspars causing Na and K depletions. Both Ba and Rb (feldspar associated elements) also show this early depletion trend suggesting that the Na-K depletions are associated with the breakdown of feldspars. This is corroborated by the fact that this Na-K-Ba-Rb depletion is seen between suites, i.e. different groups with different least altered precursors. Weakly defined trends with a negative slope can be seen emanating from the vertical K gain line on Fig. 4.30. This corresponds to a late albitization event as well as replacement of phengitic mica by paragonitic (sodic) mica as fluid temperatures drop (Eqs. 4.5 and 4.6; Kerrich, 1983). Since the sodic alteration lines emanate from the K alteration line, one can conclude that Na event postdates K alteration. Figures 4.31 and 4.32 illustrate that K gains during sericitization correspond to Ba and Rb enrichments.

$$KAl_3Si_3O_{10}(OH)_2 + 6SiO_2 + 3Na^+ \rightarrow 3NaAlSi_3O_8 + K^+ + 2H^+ \qquad \text{(Eq. 4.5)}$$

Sericite + Quartz → Albite

$$KAl_3Si_3O_{10}(OH)_2 + Na^+ \rightarrow NaAlSi_3O_{10}(OH)_2 + K^+ \qquad \text{(Eq. 4.6)}$$

Sericite → Paragonite

This relationship is expected as both Ba and Rb are accommodated in the phengite structure.

Figs. 4.33 and 4.34 are plots for TEAD komatiitic basalts from the A6 group. These two diagrams prove extremely useful for determining the relative ages of various alteration events:

1) Early feldspar destruction represented by losses in Na_2O and Rb.

2) Cr depletion, likely related to the breakdown of Cr-bearing pyroxenes or chromite. This is important as it indicates that Cr is a mobile element in the Madrid system. Note that this trend is not likely to be an inherited fractionation trend, as if this were the case, one would not expect the phengite alteration line to emanate from the terminus of the Cr-loss line.

3) (Fuchsitic) phengite formation marked by increases in Rb, Cr and K. Note that this results in horizontal movement at constant Na values in Fig. 4.34. Despite Cr gains, the rock still shows an overall depletion in Cr. Samples which have undergone early depletion in Cr are preferentially mica altered during this stage.

4) Sodium enrichments and Cr depletions during Na metasomatism associated with the formation of albite and paragonite. The most important consequence of this event is the introduction (or remobilization) of Au (Figs. 4.33 and 4.34).

Ten representative samples from four groups were chosen to further illustrate the alteration characteristics of the high-Ti rocks. The predominately chlorite-carbonate altered FETI basalts are shown in Figs. 4.35 and 4.36. In general there are large gains or small losses of SiO_2, Fe_2O_3, MgO, CaO, Cr and Ni. CaO, Fe_2O_3 and MgO gains correspond to carbonitization and chloritization. Na_2O and K_2O show significant

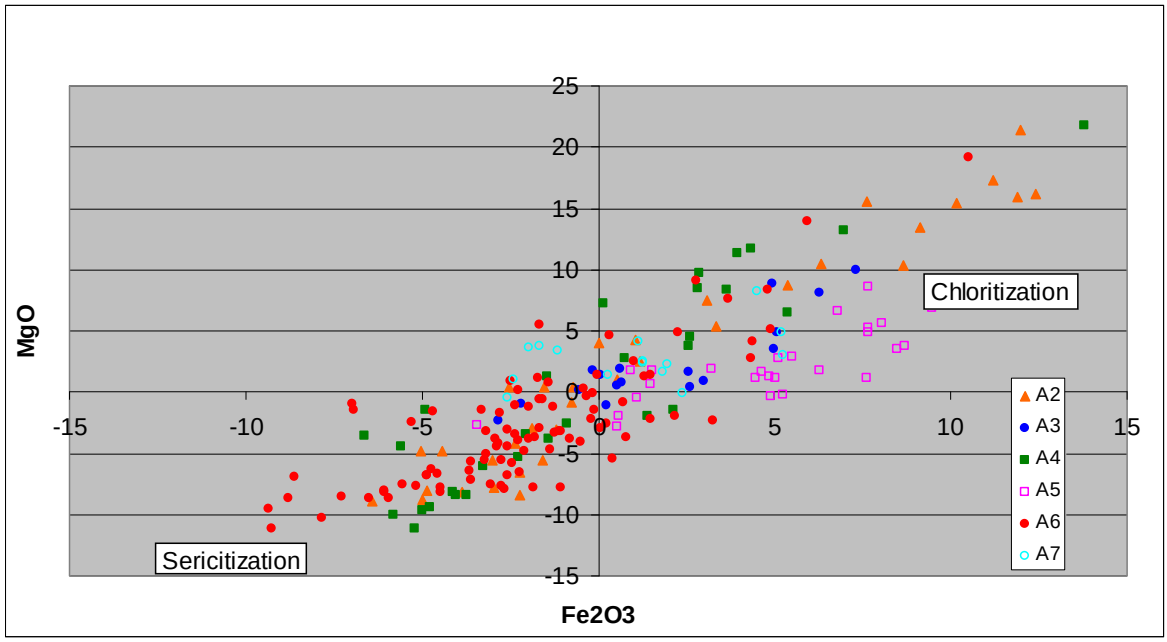

Fig. 4.28 Binary plot of total Fe_2O_3 vs. MgO gains/losses for TEAD and FETI basalts. Net gains of Fe_2O_3 and MgO represent chloritization while losses represent chlorite destruction during sericitization.

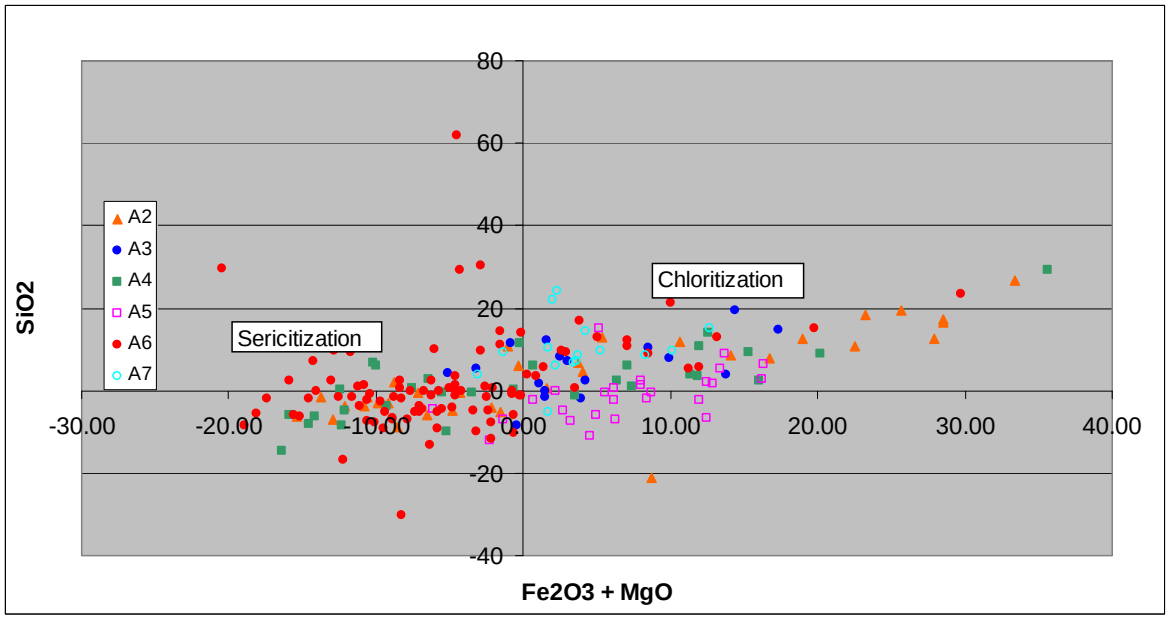

Fig. 4.29 Binary plot of total Fe_2O_3 + MgO vs. SiO_2 gains/losses for TEAD and FETI basalts. Net gains of Fe_2O_3 +MgO + SiO_2 represent chloritization (and potentially silicification) while losses represent sericitization and carbonate alteration.

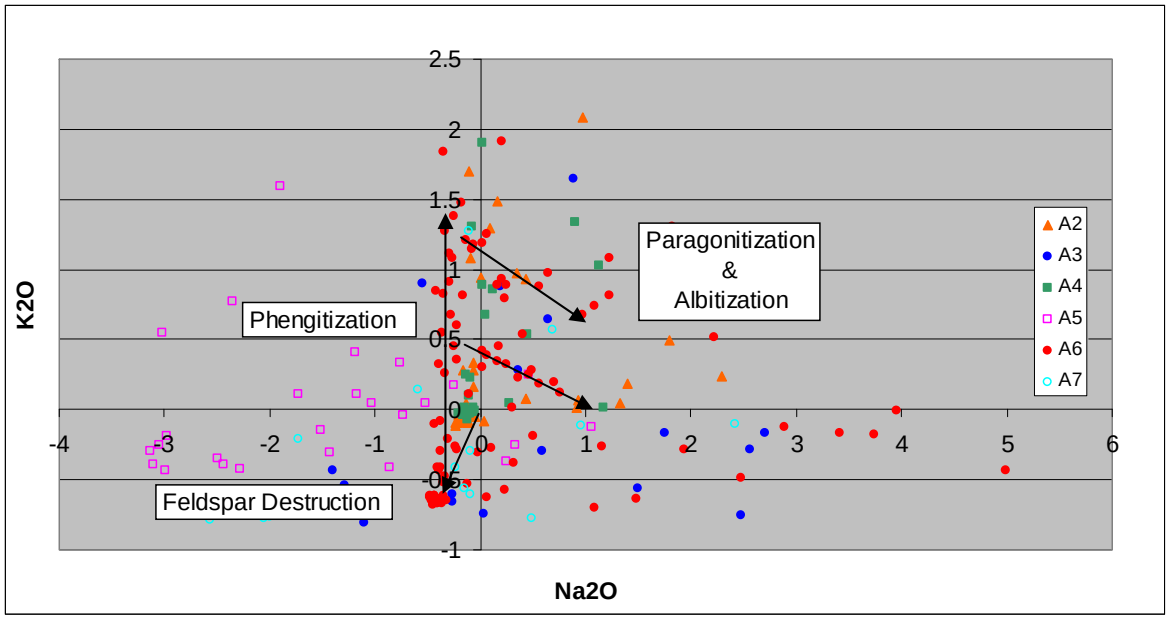

Fig. 4.30 Binary plot of Na_2O vs. K_2O gains/losses for TEAD and FETI basalts. The vertical trend from near the origin represents the formation of phengitic mica while splays off that trend indicate later paragonite alteration and albitization.

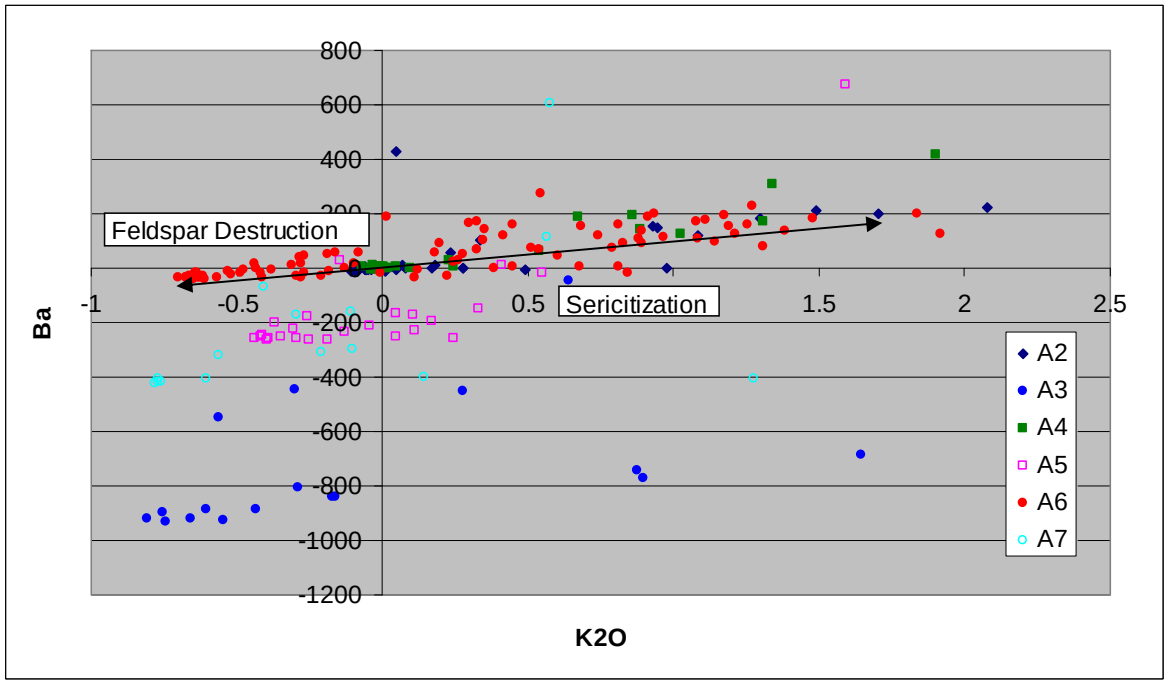

Fig. 4.31 Binary plot of Ba vs. K_2O gains/losses for TEAD and FETI basalts illustrating feldspar destruction (losses) followed by sericitization (gains).

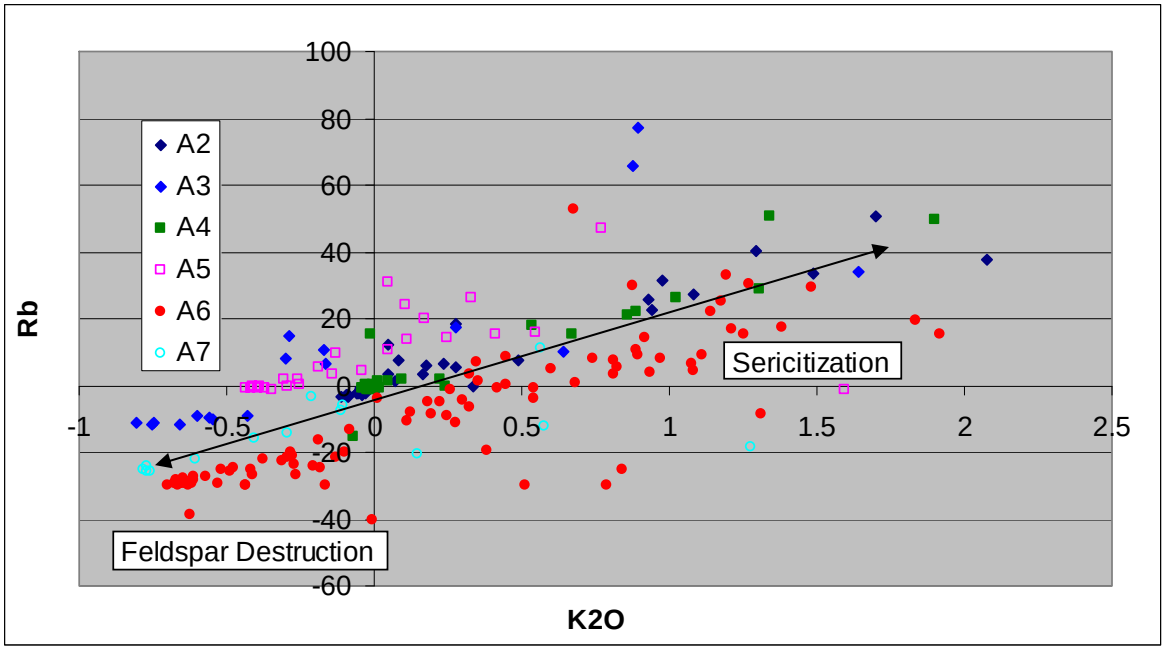

Fig. 4.32 Binary plot of Rb vs. K_2O gains/losses for TEAD and FETI basalts illustrating feldspar destruction (losses) followed by sericitization (gains).

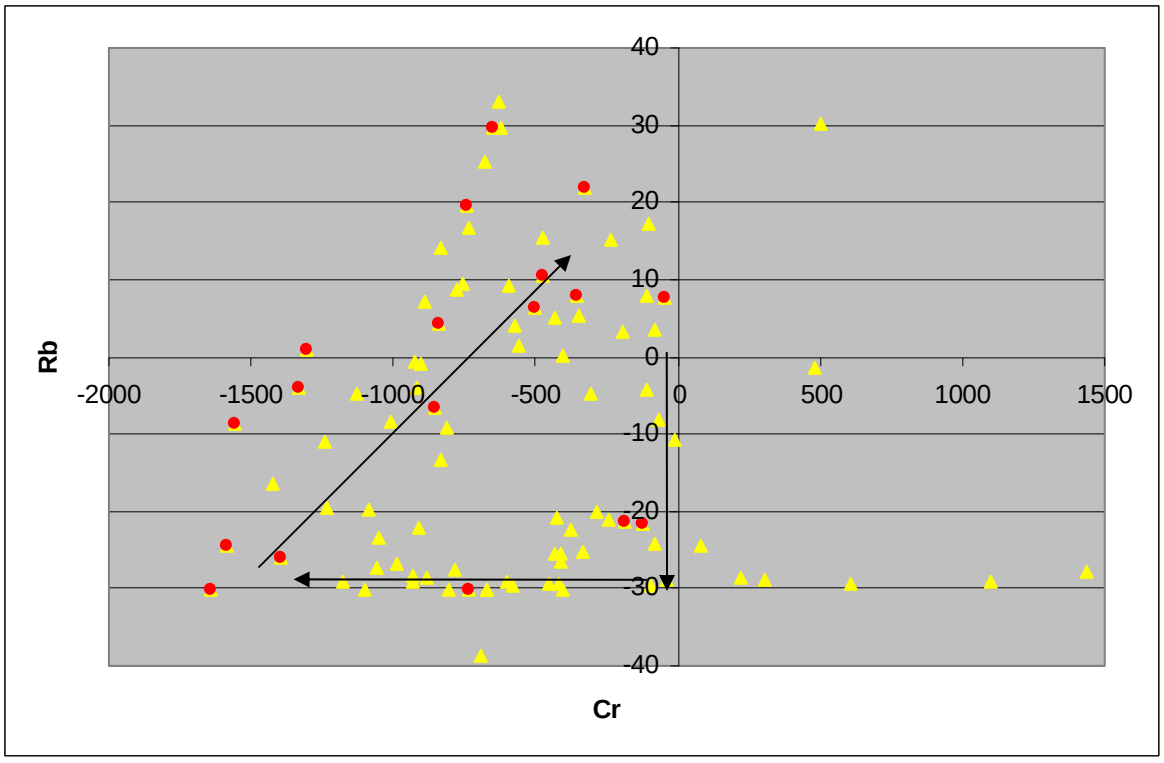

Fig. 4.33 Cr-Rb mass gain/loss diagram for Group 6 TEAD komatiitic basalts. Initial loss of Rb results from feldspar destruction. The Cr depletion is likely a result of pyroxene or chromite destruction. The gain in Rb and Cr corresponds to phengite formation. Red dots are samples with >0.5g/ton Au

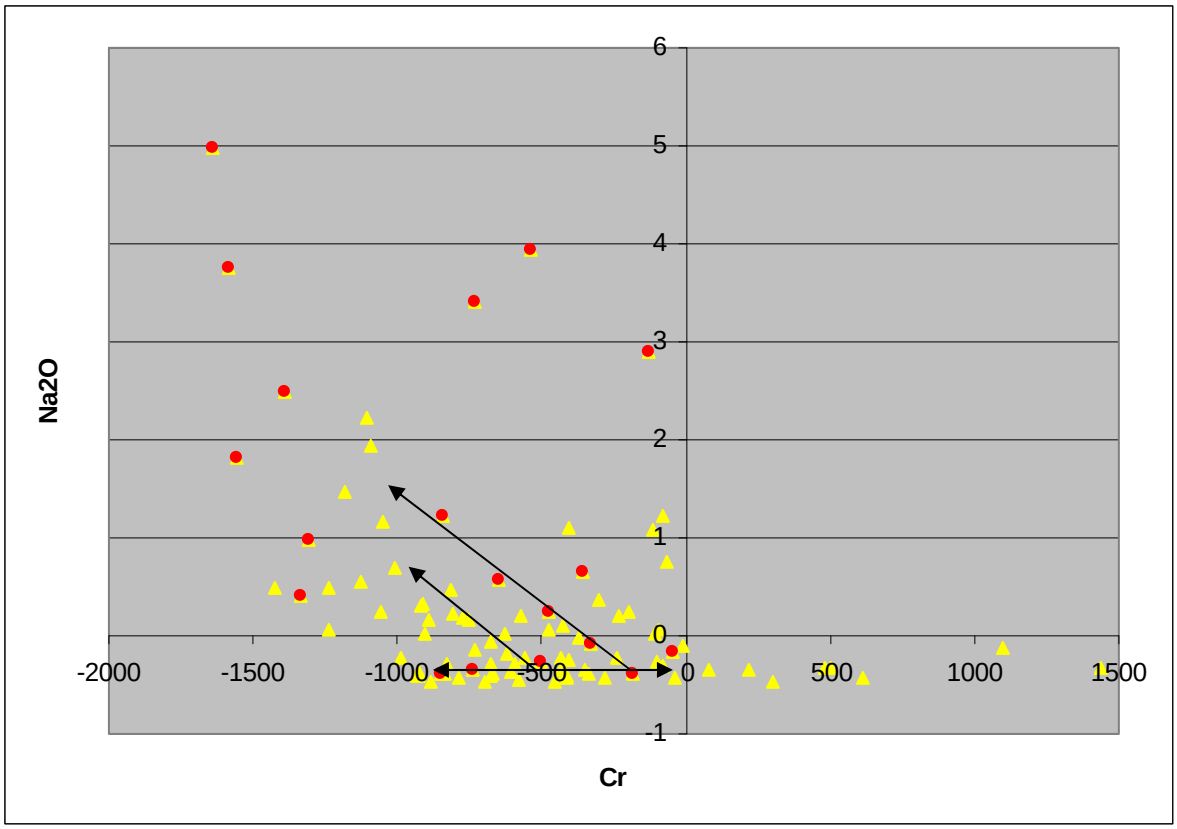

Fig. 4.34 Cr-Na_2O mass gain/loss diagram for Group 6 TEAD komatiitic basalts. Initial depletion in Na_2O during feldspar destruction followed by chromite destruction and phengite formation. This results in movement along the horizontal line. Red dots are samples with > 0.5g/ton Au.

but inconsistent gains/losses. As this package is often strongly variolitic, alkali gains/losses may relate to the amount of variolitic material sampled relative to the chosen LA precursors. Unmineralized basaltic komatiites (Figs. 4.37 and 4.38) show a comparable relationship with strong gains in SiO_2, Fe_2O_3, MgO, Ni and Cr and small enrichments of CaO. Both weakly and strongly mineralized samples (Figs. 4.39-4.42) show similar patterns of Fe_2O_3, MgO, Cr and Ni depletions and Na_2O, K_2O, CaO and Sr gains. Gains in Sr are probably related to carbonitization. SiO_2, CaO and Na_2O show greater enrichments in the strongly mineralized komatiitic basalts, likely a result of more

intense quartz-carbonate-albite alteration and stockworking. Conversely, greater gains in K within the weakly to moderately mineralized basalts are likely related to more widespread sericite alteration. A very obvious W anomaly can be seen in the strongly mineralized komatiitic basalts, and to a lesser extent in the weakly to moderately mineralized samples. Consequently, Na and W are considered to be useful pathfinder elements for Au at Madrid.

High-Fe tholeiitic basalts and basaltic andesites

The results obtained for the high-Fe tholeiitic basalts and basaltic andesites show less consistent trends as compared to the high-Ti suites. Despite this, the enrichment-depletion values show relatively minor fluctuations of Al_2O_3 (1-2%), Zr (5-7 ppm), and Y (2-3 ppm) suggesting that the results are significant. The slight changes in Al_2O_3 values may be attributed to small differences in LA precursor chemistry or to the amount of variolitic material sampled relative to the least altered precursor. Fig. 4.43 shows the effects of chloritization and potentially sericitization. Enrichments of Fe_2O_3 and MgO are related to chloritization and carbonitization as in the previous suite and is most obvious in the basaltic andesites (C4) and the non-variolitic high-Fe tholeiities (C1 and C3). This result is consistent with petrographic analysis of these suites. Unlike the high-Ti basalts, depletions in Fe_2O_3 and MgO of the C1 suite do not appear to be related to sericitization as most samples are dominantly chlorite altered. The majority of the samples which show these depletions also contain leucoxene and have TiO_2 values slightly larger than their LA precursors. Furthermore, samples from the C1 suite with large depletions in Fe_2O_3 and MgO show the strongest depletions in Al_2O_3. This indicates that variations in primary chemistry are a problem in at least some of the

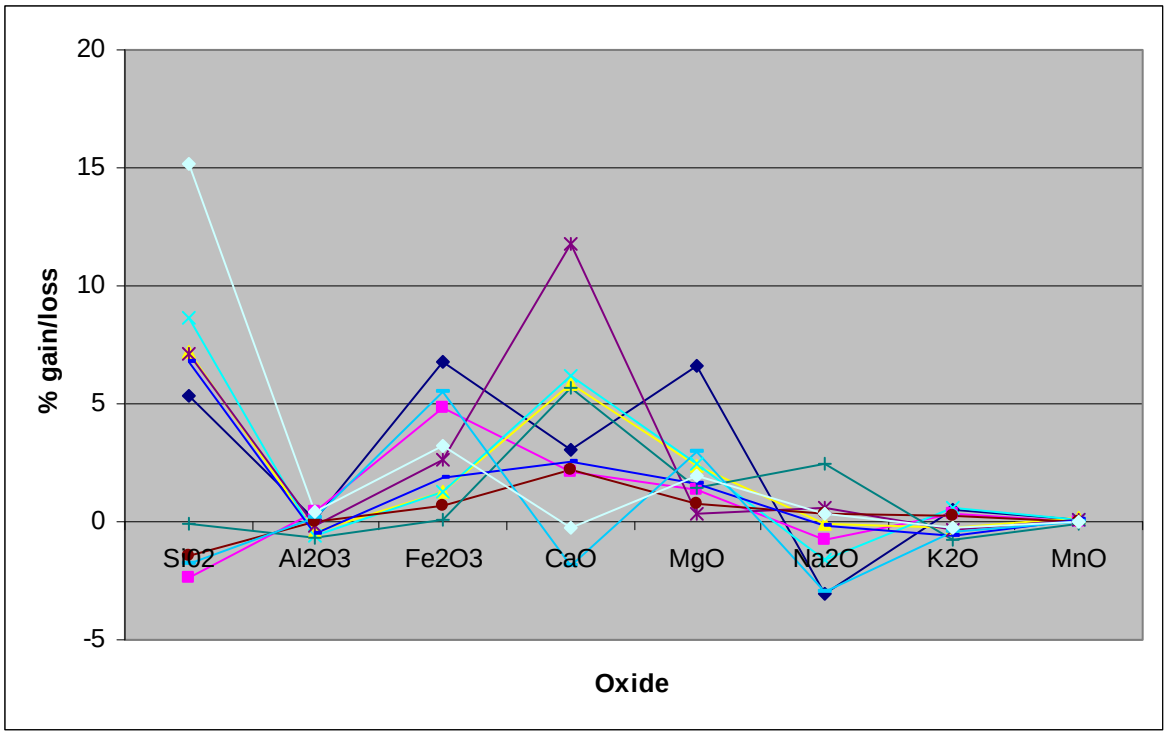

Fig. 4.35 Net gains/losses of major oxides for non-mineralized FETI basalts.

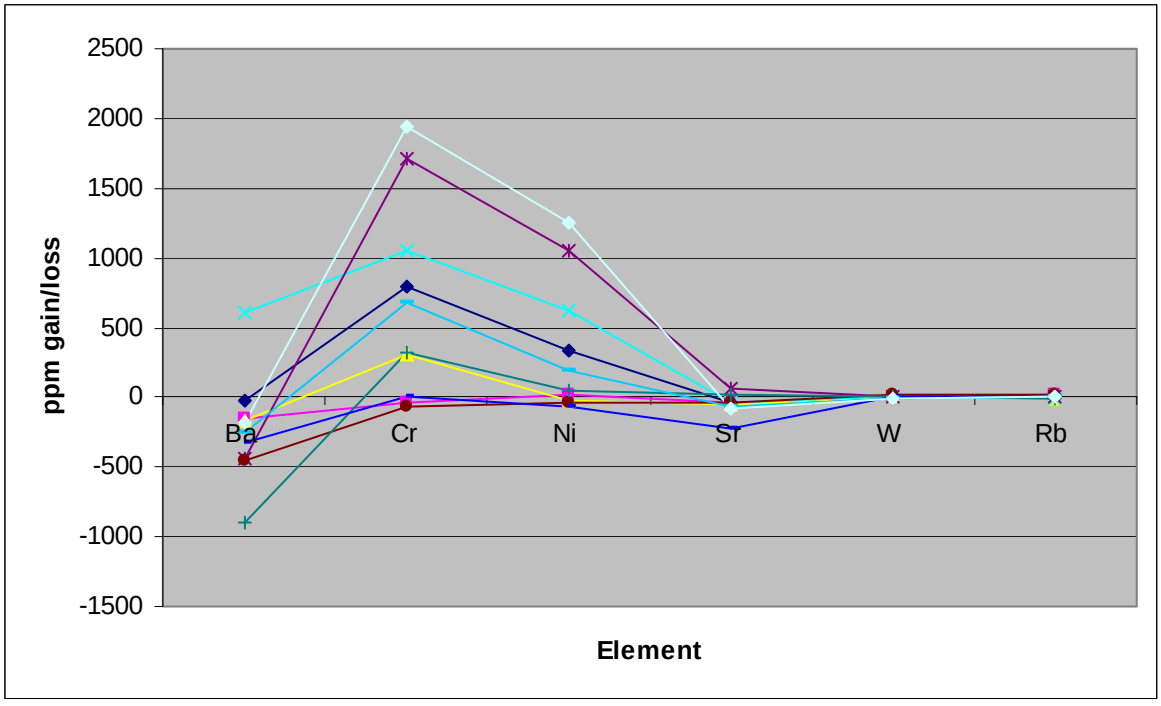

Fig. 4.36 Net gains/losses of trace elements for non-mineralized FETI basalts.

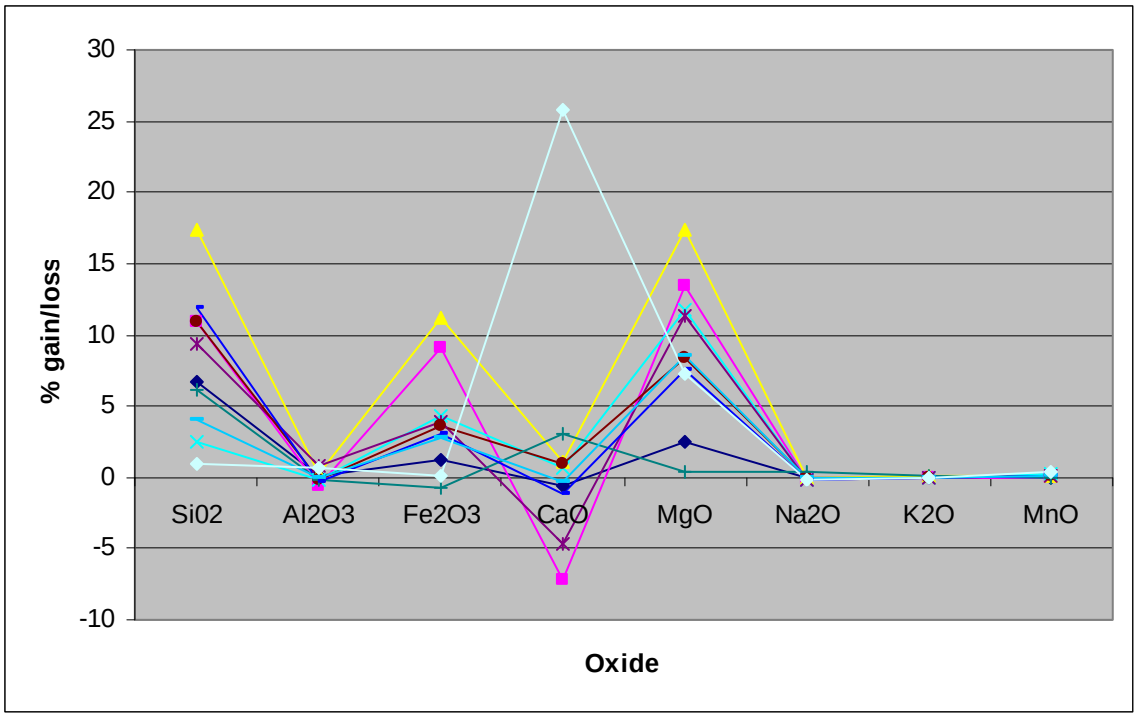

Fig. 4.37 Net gains/losses of major oxides for non-mineralized TEAD komatiitic basalts.

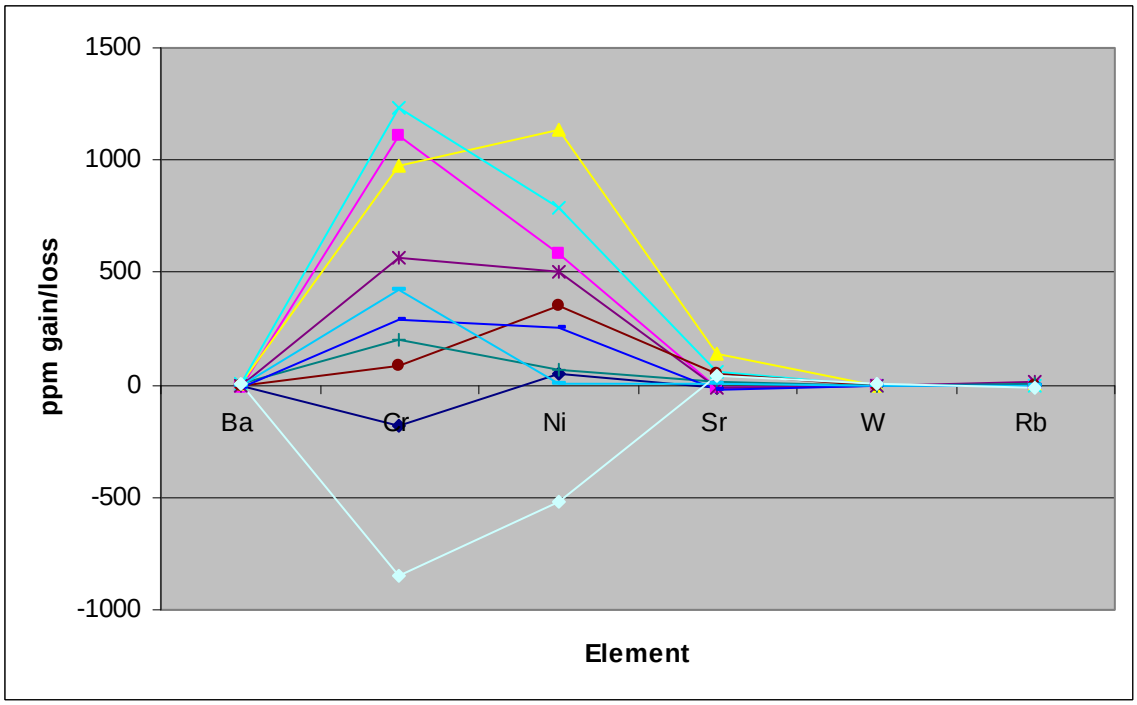

Fig. 4.38 Net gains/losses of trace elements for non-mineralized TEAD komatiitic basalts.

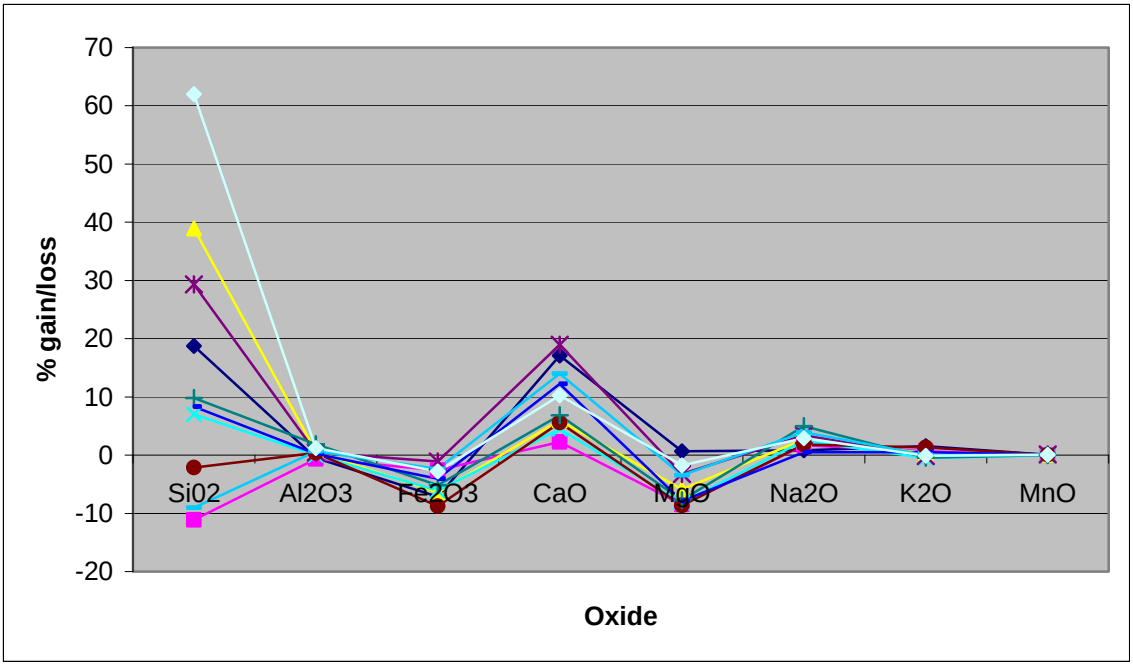

Fig. 4.39 Net gains/losses of major oxides for strongly mineralized TEAD komatiitic basalts.

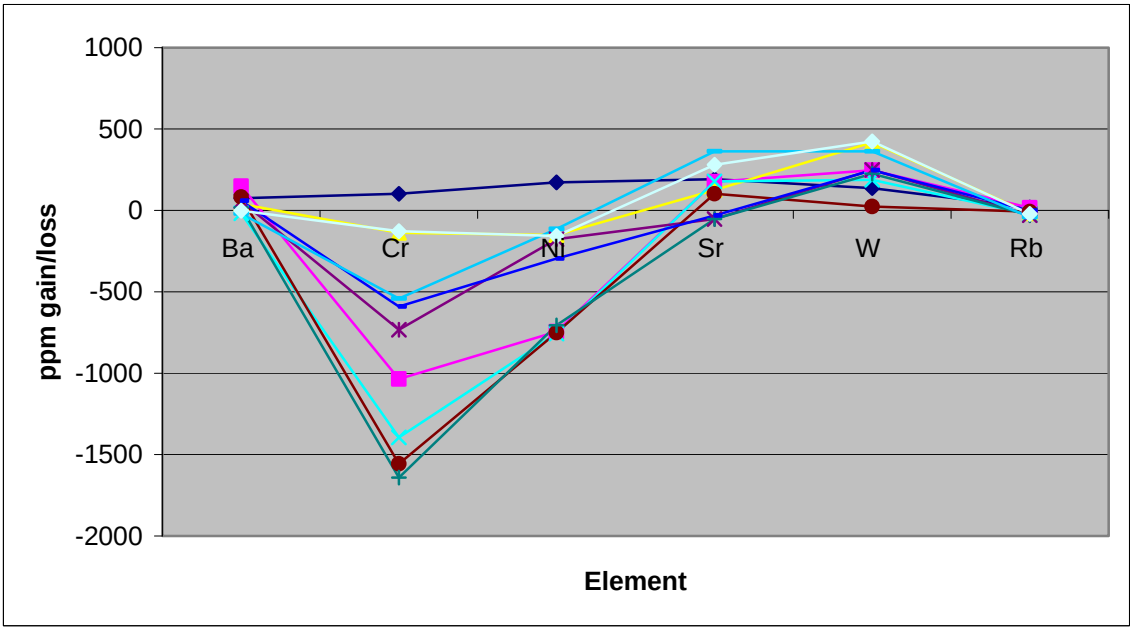

Fig. 4.40 Net gains/losses of selected trace elements for strongly mineralized TEAD komatiitic basalts.

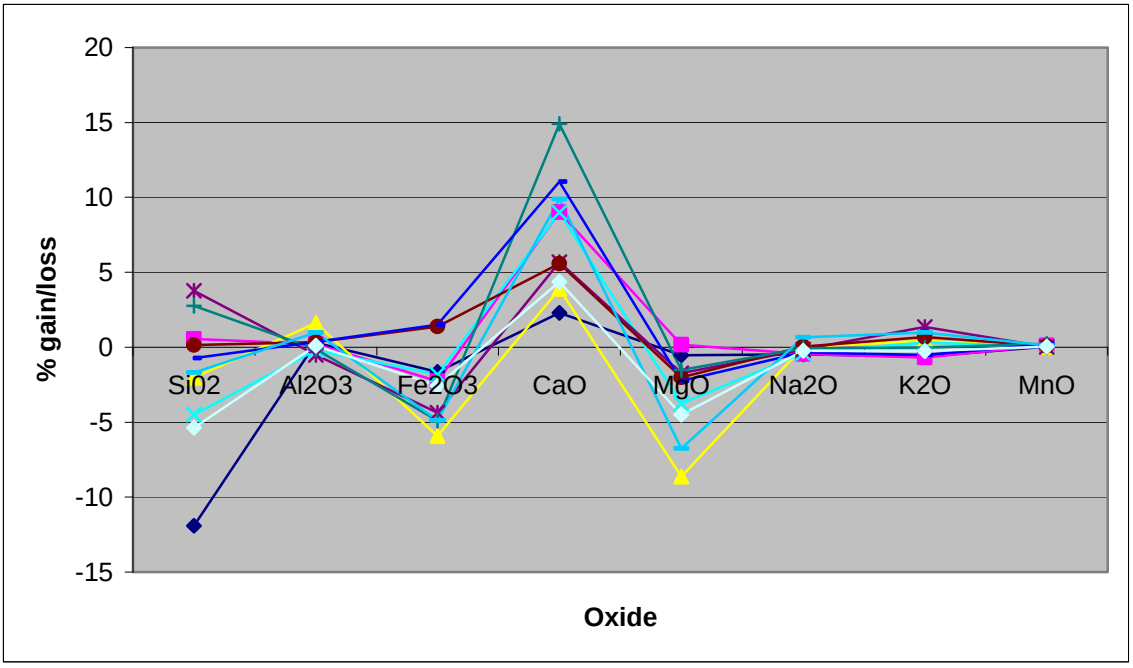

Fig. 4.41 Net gains/losses of major oxides for weakly/moderately mineralized TEAD komatiitic basalts.

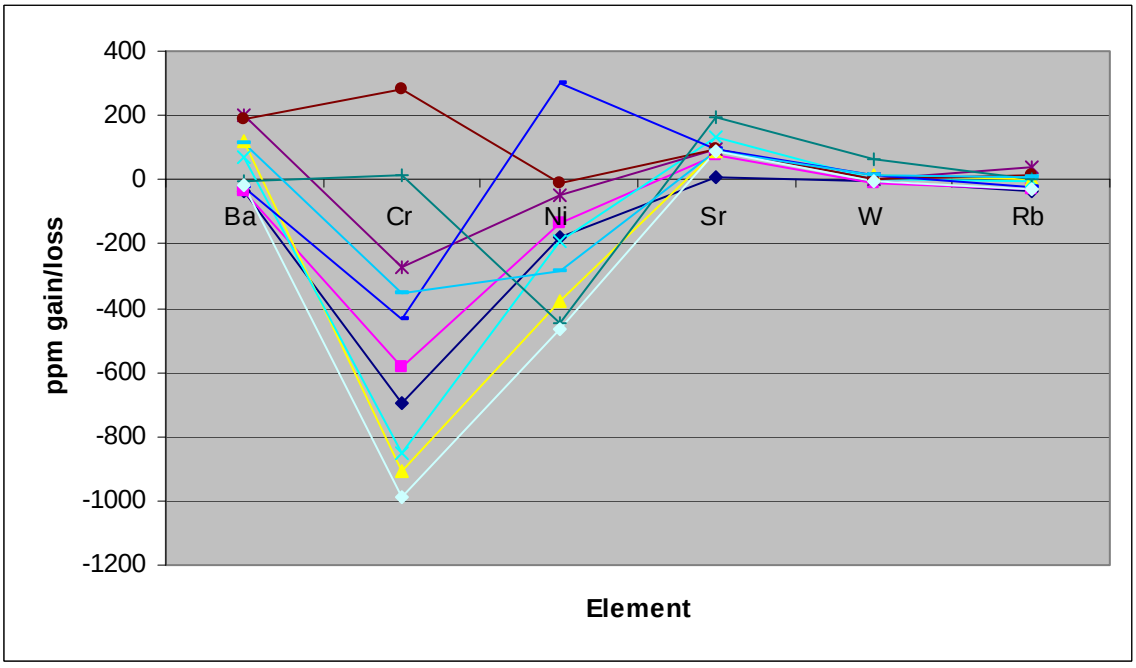

Fig. 4.42 Net gains/losses of trace elements for weakly/moderately mineralized TEAD komatiitic basalts.

samples. Similarly Fe_2O_3-MgO depletions are seen in some samples from the C4 suite and also do not appear to be related to sericitization. Despite this, the depletions are rather small and the majority of samples show relative gains, consistent with chloritization. A number of basaltic andesite samples from the Naartok-Perrin area show abnormally large Fe_2O_3-MgO gains relative to basaltic andesites from Suluk. These samples also show the strongest variability of Al_2O_3 (1-2% loss). Least altered samples for the C4 suite consist almost exclusively of samples from the Suluk area. This indicates that there are noticeable chemical variations in the primary chemistry of the basaltic andesites, i.e. basaltic andesites from Naartok have slightly higher Fe_2O_3 + MgO and lower Al_2O_3 relative to basaltic andesites from Suluk. Another interesting observation of C4 trends are the MgO and Fe_2O_3 changes relative to each other. The MgO gains/losses tend to show less variability than the Fe_2O_3 values, especially for depleted samples. This is related to the low MgO values of the LA precursor relative to their Fe_2O_3 contents. Many samples of variolitic high-Fe tholeiities (C2) also show depletions in Fe_2O_3 and MgO. This depletion may be related to:

1) Sericitization, which tends to cause depletions in Fe_2O_3, MgO and SiO_2 (Figs. 4.43 and 4.44; Eq. 4.4) as described previously. This is considered rather unlikely as the vast majority of these samples are chlorite altered.

2) A sampling problem, where the strongly variolitic cores of pillows are preferentially sampled. This makes it difficult to accurately characterize this suite as altered and least altered samples will have different proportions of pillow core and rim and thus mixed chemistries.

An interesting relationship exists between Rb/Ba, K_2O and the basaltic andesite suite. The trend on Fig. 4.45 shows that these elements have a positive correlation best

defined by the basaltic andesites. Furthermore, this K-enrichment is accompanied by Na depletion. Since most of this suite is chloritized rather than sericite altered, and K_2O does not form a component in the chlorite structure, this trend must be related to some other process. This trend may be explained by the partial breakdown of feldspar and the preferential removal of Na with the K component remaining in sericite. Alternatively, it may be related to the formation of small amounts of K-spar or white mica during hydrothermal alteration.

Figs. 4.46-4.48 further illustrate the trends discussed above. Within the C1, C3 and C4 suites SiO_2-Fe_2O_3-MgO act in similar ways, where all three are either enriched or depleted. Enriched SiO_2 values typically correspond to elevated CaO values, probably representing related silicification-carbonitization-epidotization processes. K_2O values from each of the suites show enrichment probably related to small amounts of sericite or K-feldspar. Variolitic high-Fe basalts show fairly consistent moderate/strong depletions

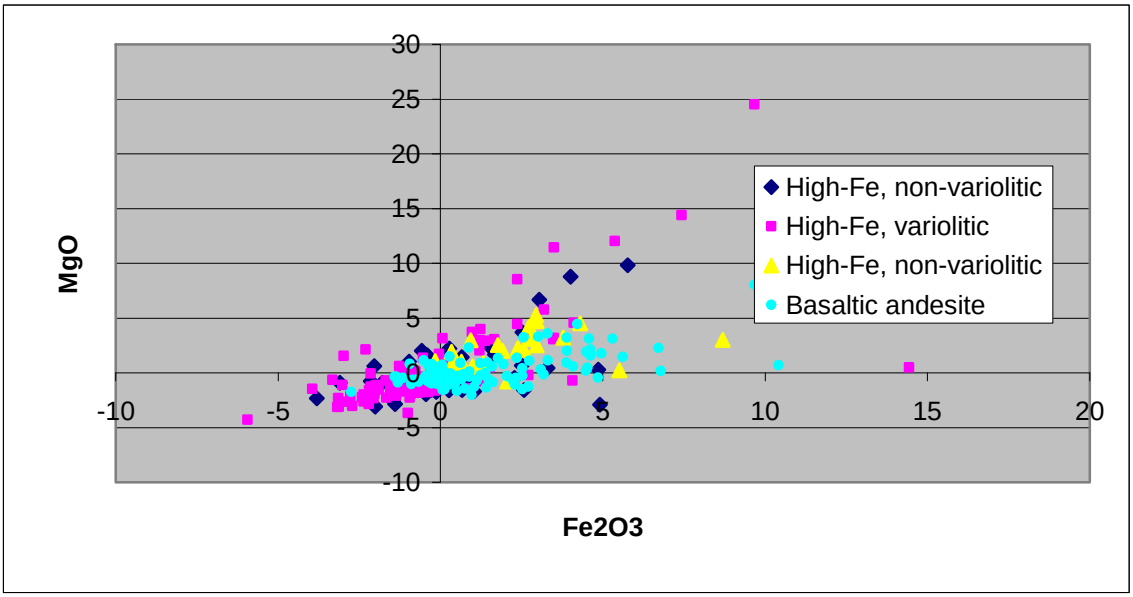

Fig. 4.43 Enrichment-depletion trends for Fe_2O_3 and MgO in the high-Fe tholeiitic basalts and basaltic andesites.

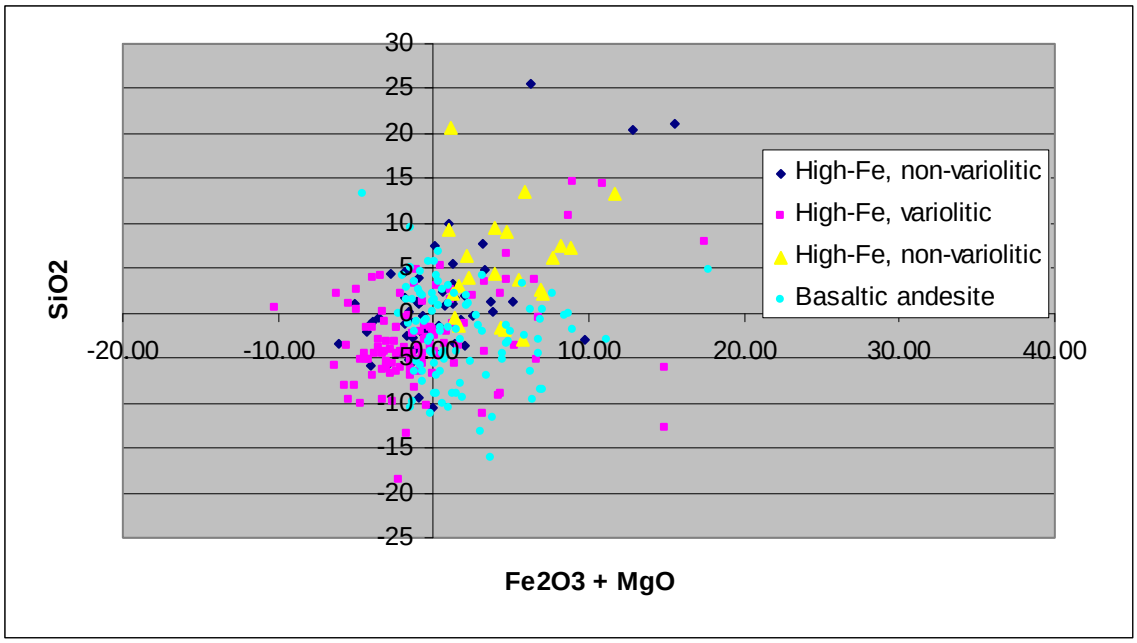

Fig. 4.44 Enrichment-depletion trends for Fe_2O_3 + MgO and SiO_2 for high-Fe tholeiitic basalts and basaltic andesites.

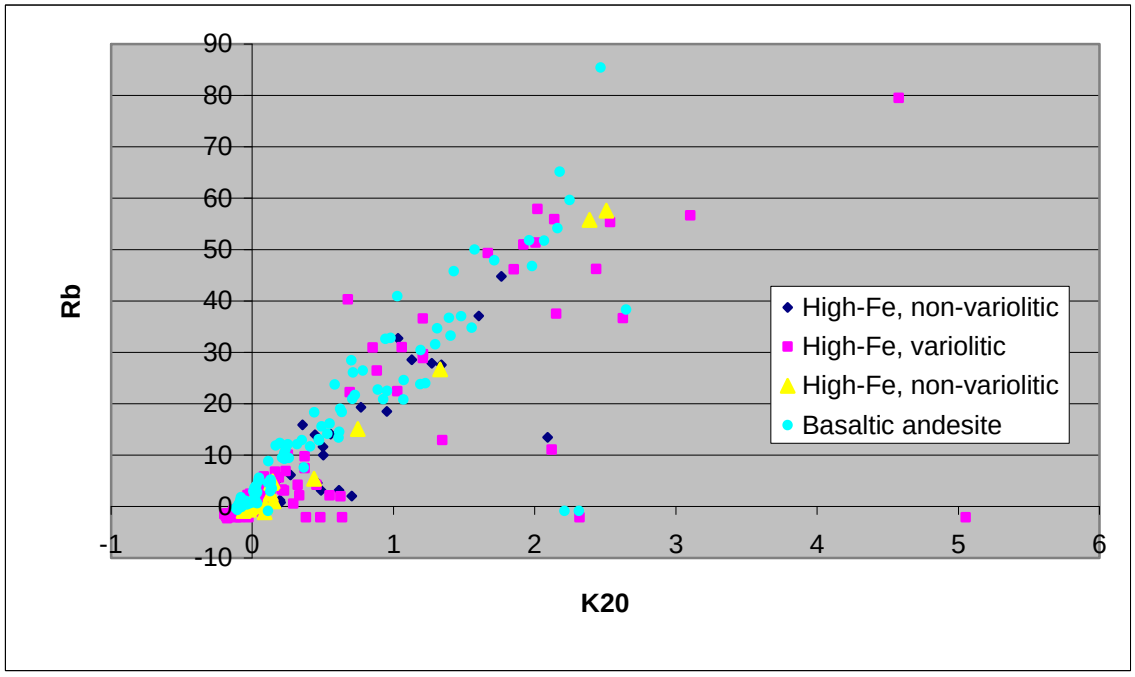

Fig. 4.45 Enrichment-depletion trends for K_2O and Rb for high-Fe tholeiitic basalts and basaltic andesites.

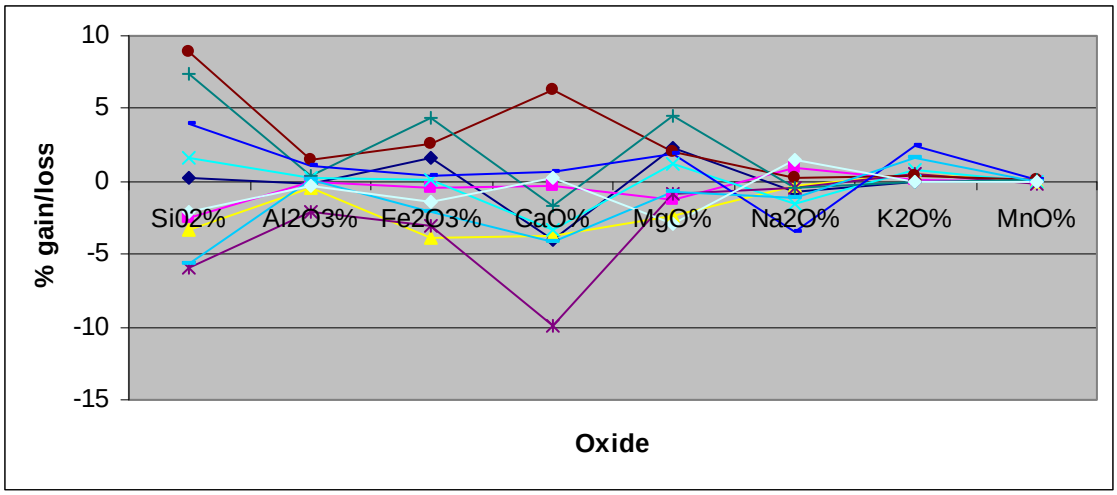

Fig. 4.46 Enrichment-depletion trends for non-variolitic high-Fe tholeiitic basalts (suites C1 and C3).

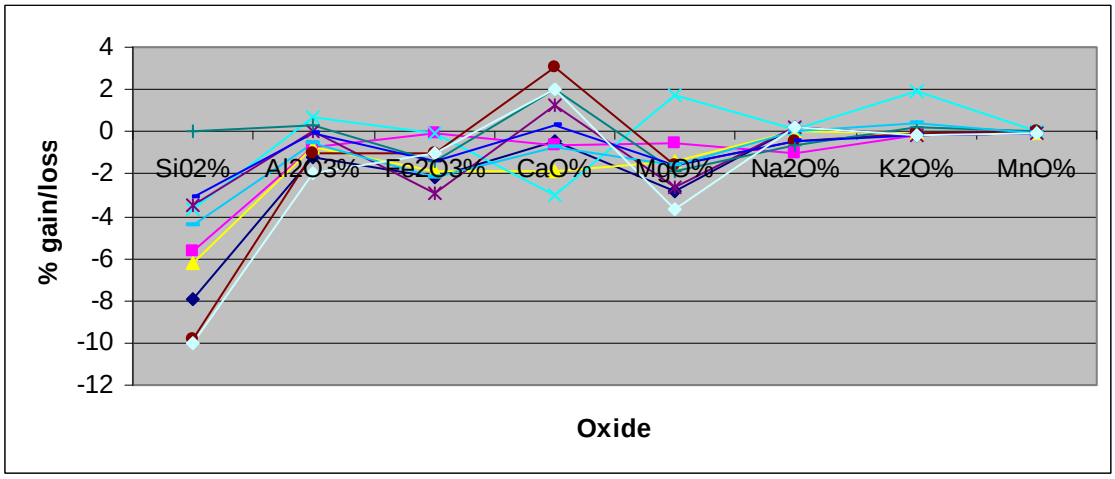

Fig. 4.47 Enrichment-depletion trends for variolitic high-Fe tholeiitic basalts (suite C2).

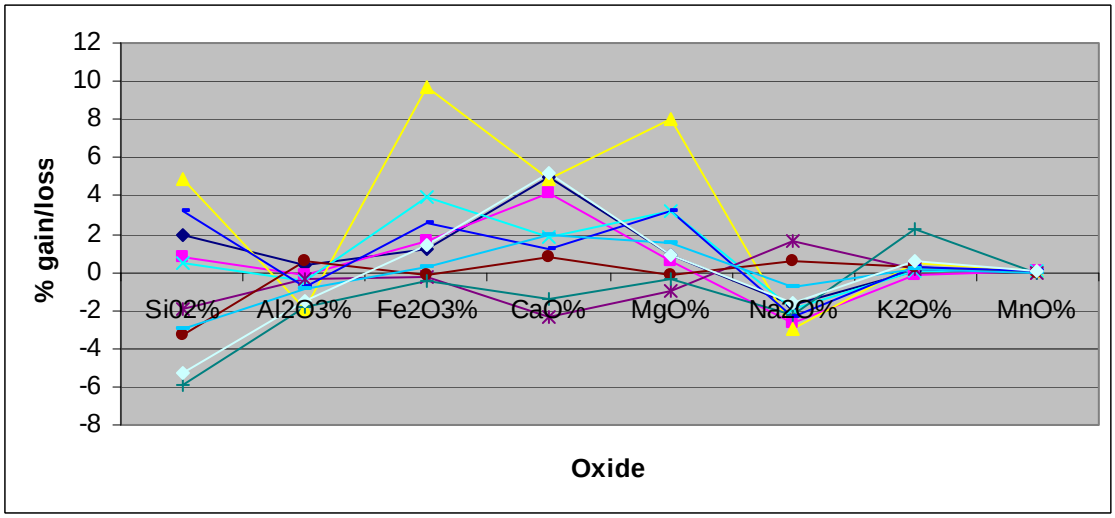

Fig. 4.48 Enrichment-depletion trends for basaltic andesites (suite C4).

in SiO_2, Fe_2O_3 and MgO. The significant scatter of the Al_2O_3 values is likely related to the variole content of the sampled interval.

In conclusion, it appears that results for the high-Fe basalts and basaltic andesites are less consistent than for the high-Ti rocks. Poor results are attributed mainly to parent rock heterogeneities and a low degree of alteration. Stronger degrees of alteration will result in larger absolute changes in elemental abundances which tend to mask small chemical variations in parent samples. Fluctuations of Al_2O_3 values of up to 2.5% are significant, especially when fluctuations of the mobile elements are small. Although the enrichment-depletion values for the high-Fe basalts and basaltic andesites do contain substantial error, identification of the source of this error is considered significant. It should also be noted that the accurate results obtained from the high-Ti suites are of far greater importance as they are the rocks associated with Au mineralization.

Wolverine Porphyry

A limited number of samples of Wolverine Porphyry were selected to assess elemental mass gains/losses. The most notable feature of altered porphyry is the consistent mass loss of Na_2O and mass gain of K_2O and CaO (Fig. 4.49). The loss of Na_2O is most likely related to the breakdown of feldspar and its replacement by sericite marked by gains in K_2O. Gains in CaO are attributed to carbonitization. Other elements do not show consistent results - SiO_2 and Fe_2O_3 are variable while MgO generally shows small enrichments related to the formation of dolomite-series carbonate. Significant variations in the Al_2O_3 values may relate to slight differences in primary chemistry (phenocryst composition and concentration) or to local remobilization of Al into sericite-rich bands. The latter option is considered correct because many samples of Wolverine

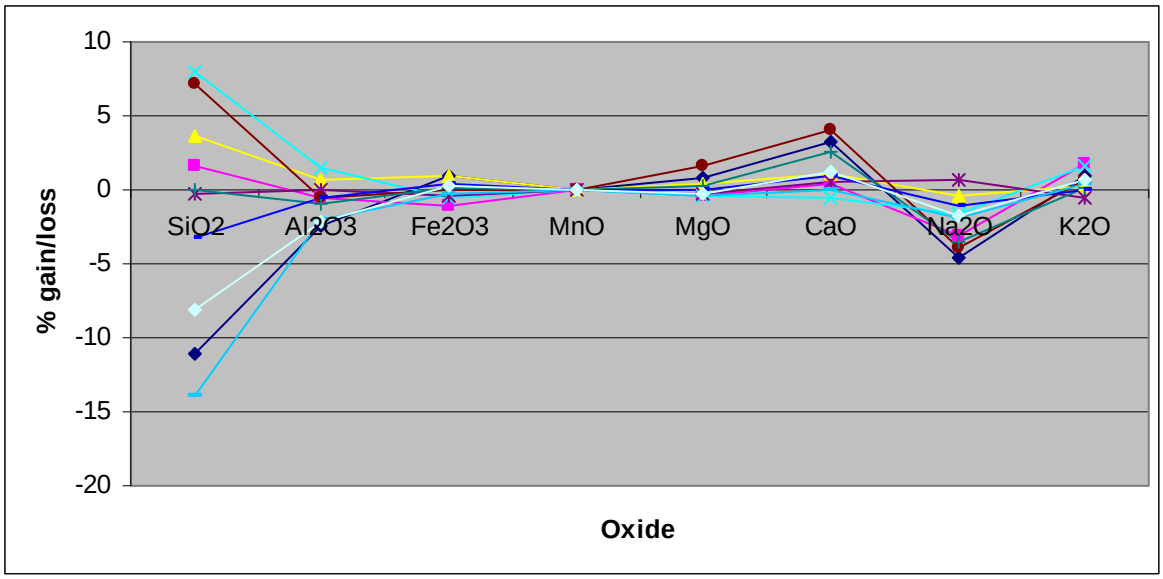

Fig. 4.49 Enrichment-depletion trends for the Wolverine Porphyry.

Porphyry contain a very high proportion of coarse grained sericite. Furthermore, the sericite occurs in bands separated by thicker domains of quartz-dolomite, giving the rock a strongly heterogeneous character.

CHAPTER 5

MINERAL CHEMISTRY

5.1 – Introduction

The composition of white micas in Au-bearing units and the HBDZ have been investigated extensively with the electron microprobe. Carbonate minerals interior to and bordering Au-bearing zones constitute the second most important focus of investigation. Quantitative analyses of chlorite, amphibole, pyroxene, epidote, feldspar and sulphides have also been completed on several samples from representative lithotypes in the Madrid area. Extensive qualitative work (EDS) has been completed on the sulphide phases to establish paragenetic relationships. Results of this work are presented below and interpreted in Chapter 6. Mineral chemistry data can be found in Appendix B.

5.2 – White Mica Chemistry

All white mica data reported below are presented in *afu* which have been calculated on the basis of 22 oxygens. Fe^{2+} and Fe^{3+} values can not be separated on the electron microprobe and so graphs involving iron are in terms of Fe_{Total}. The classification of white mica analyses is partly based on Guidotti (1984), however, boundaries between degrees of paragonitization and phengitization are defined here strictly for the purposes of this thesis.

Initial attempts at white mica analysis resulted in abnormally high oxide totals. Possible reasons for this likely involved one or more of the following:

1) The white micas at Madrid are extremely fine-grained and are compositionally interstratified with many analyses plotting within the 'paragonite gap', a region where natural homogenous micas should not plot (Guidotti, 1984). This is apparently a common problem and is not easily resolved on the EMP (Shau *et al*., 1991).

2) Chlorite intergrowths and Fe-Ti oxide inclusions in white mica strands are quite common in samples analyzed in the HBDZ and in mineralized zones. This could potentially explain the high totals.

3) Alkali decay related to a focused electron beam. In response to this problem a large beam size (5 nm) was used in conjunction with the coarsest and most homogenous looking micas (based on grey levels) and these modifications yielded results comparable with those in the literature.

5.2.1 – Preliminary Comments

White micas are di-octahedral phyllosilicates which consist of a layer of octahedrally coordinated Y cations sandwiched between two identical tetrahedral sheets and bound together by large positive cations (Deer *et al,* 1992). The generalized structural formula is:

$$X_2Y_4Z_8(OH,F)_2$$

where X = interlayer site (K, Na, Ca, Ba, Rb, Cs), Y = octahedral site (Al, Mg, Fe, Mn, Cr, Ti, Li) and Z = tetrahedral site (Si, Al, Fe^{3+},Ti) (Deer *et al*. 1992; Bailey, 1984). Variations in white mica chemistry relevant to this thesis include substitution of Na for K in the interlayer site to form paragonite:

MUSCOVITE (Mu): $\mathbf{K}Al_2(Si_3Al)O_{10}(OH,F)_2$

PARAGONITE (Pg): $\mathbf{Na}Al_2(Si_3Al)O_{10}(OH,F)_2$

The degree to which Na replaces K is quantified by the equation:

$$\% \text{ Paragonite Component} = (Na/Na+K)*100 \qquad \text{(Eq. 5.1)}$$

Experimental work has identified a wide immiscibility gap between the two species where muscovite generally does not exhibit a paragonitic component between 30% - 75% (Guidotti, 1984). Many analyses of fine-grained micas from the HBDZ fall within this gap. TEM, AEM and electron microprobe studies by Shau *et al*. (1991) have shown that paragonitic and phengitic micas as well as chlorite can be interstratified at a scale so fine that they can not be resolved with the electron microprobe. Consequently, a homogenous looking mica grain may in fact be composed of alternating layers of varying composition with the resulting analyses being an average of these compositions. For the sake of this thesis samples with a paragonitic component < 10% are described as *muscovite*, between 10-50% as *paragonitic muscovite* and >50% as *paragonite*.

The second important variation in chemistry of white micas at Madrid involves the phengite substitution. Deviation from the ideal white mica plane is caused by siderophile elements (Mg, Fe^{2+}, Cr, Mn, Ti, Li) replacing Al vi. In order to maintain charge balance, Si substitutes for Al iv (Guidotti, 1984). The phengitic component is quantified by the sum of the siderophile elements (in *afu*). Phengite is defined as white

mica with at least one of four octahedral sites occupied by a siderophile element (Guidotti, 1984; Stewart, 1992):

PHENGITE

$K_2[Al_3(Mg,Fe,Cr,Ti,Mn,Li)](Si_7Al)O_{20}(F,OH)_2$

For the sake of this thesis samples that have a phengite component between 0.25-0.5 are described as *weakly phengitic muscovites* and >0.5 as *phengitic muscovites*. Micas which contain a few tenths of the octahedral site filled by Cr typically take on a green colour and are termed fuchsite or fuchsitic phengites. Green micas at Madrid are somewhat common and have been analyzed to compare with other phengitic muscovites in the deposit. For the sake of this study samples with Cr values >0.1 (approximately 1% Cr_2O_3) are termed *weakly fuchsitic*. Sample with Cr >0.25 are termed *fuchsitic*. A slight overestimation of the phengite component is expected as Fe_{Total} has been used rather than Fe^{2+}.

Although it is not immediately intuitive there is a strong correlation between the amount of siderophile element replacement in the octahedral site and Na replacement in the interlayer site. With increasing phengitic substitution the ability for Na to replace K is inhibited. The reason for this is crystallochemical and involves a decreased ability of the interlayer site to distort and hold Na as the phengitic substitution increases (Guidotti, 1984).

5.2.2 – Results

White Micas at Madrid fall into two three broad groups:

1) Paragonites and paragonitic muscovites situated almost exclusively in the HBDZ. The phengitic component is generally quite low.

2) Phengitic micas seen in altered basalts in Au and non-Au bearing rocks outside the HBDZ. The paragonitic component of these micas is significantly lower than micas in the HBDZ.

3) Fuchsitic phengitic micas, a more rare form of Group 2 micas.

Representative analyses of these three mica groups are presented in Table 5.1.

Mica analyses from the HBDZ focused on the Wolverine porphyry, but did include a sample of basalt. The phengitic component of the vast majority of analyses falls below 0.2, presumably a result of the bulk chemistry of the porphyry. There is a clear boundary at Al vi = 3.8 separating the paragonitic micas in the HBDZ from the phengitic micas in Au-bearing lithologies (Fig. 5.1 & 5.2). The lack of phengitic substitution results in higher octahedral Al values, which varies with the paragonite value, i.e. as the phengitic substitution increases the paragonite component decreases (Fig. 5.3). Interestingly, the paragonitic component in mica altered porphyry carries over to adjacent basalt in the HBDZ. Notably some of the most paragonitic micas analyzed were from a basalt sample from the HBDZ. The progressive replacement of K by Na in the interlayer site can be seen in Fig. 5.4. Fig. 5.6 shows an overall increase in Ca with Na indicating that both Ca and Na are replacing K in the interlayer site with increasing paragonitization. It is likely that this relationship is related to feldspar destruction. Increasing tetrahedral Al is associated with increasing paragonitization, which is related

to the Si - Al iv substitution during phengitization (Fig. 5.7). Fig. 5.8 illustrates the relationship between Ba and Na: as Ba increases (increased phengite substitution), Na decreases.

	1	2	3	4	5	6	7	8
SiO2	47.26	49.73	48.11	49.62	46.61	46.70	48.64	45.84
TiO2	0.02	0.00	0.05	0.01	0.09	0.20	0.22	0.05
Al2O3	39.04	37.28	38.78	35.68	36.16	34.85	30.00	33.97
Cr2O3	0.02	0.00	0.02	0.00	0.55	0.22	1.04	3.25
FeO	0.24	0.25	0.31	0.31	0.56	1.00	1.17	0.61
MnO	0.03	0.00	0.03	0.00	0.06	0.00	0.00	0.06
MgO	0.12	0.23	0.10	0.22	0.48	0.87	2.68	0.74
CaO	0.05	0.08	0.06	0.15	0.07	0.02	0.06	0.01
BaO	0.14	0.07	0.08	0.13	0.03	0.23	0.17	0.29
Na2O	5.66	4.12	5.25	4.70	1.79	0.80	0.18	1.27
K2O	2.55	4.39	3.12	4.25	8.57	10.04	11.14	9.40
V2O5	0.13	0.00	0.09	0.03	0.23	0.21	0.17	0.16
Total	95.26	96.16	96.01	95.10	95.19	95.13	95.46	95.66
Label	209-90.3-7	173-96-3	173-75-2	173-96-5	144-122-4	173-368A-5	43-374-10	192-415-1
Si	6.06	6.33	6.13	6.41	6.15	6.21	6.50	6.11
Ti	0.00	0.00	0.01	0.00	0.01	0.02	0.02	0.00
Al (Total)	5.91	5.59	5.83	5.43	5.62	5.47	4.73	5.34
Al iv	1.94	1.67	1.87	1.60	1.85	1.79	1.50	1.89
Al vi	3.97	3.92	3.96	3.83	3.77	3.68	3.23	3.45
Cr	0.00	0.00	0.00	0.00	0.06	0.02	0.11	0.34
Fe	0.03	0.03	0.03	0.03	0.06	0.11	0.13	0.07
Mn	0.00	0.00	0.00	0.00	0.01	0.00	0.00	0.01
Mg	0.02	0.04	0.02	0.04	0.09	0.17	0.53	0.15
Ca	0.01	0.01	0.01	0.02	0.01	0.00	0.01	0.00
Ba	0.01	0.00	0.00	0.01	0.00	0.01	0.01	0.02
Na	1.41	1.02	1.30	1.18	0.46	0.21	0.05	0.33
K	0.42	0.71	0.51	0.70	1.44	1.70	1.90	1.60
V	0.01	0.00	0.01	0.00	0.02	0.02	0.01	0.01
O	22.00	22.00	22.00	22.00	22.00	22.00	22.00	22.00
CatTot	13.88	13.74	13.84	13.81	13.93	13.95	14.01	13.98
Total	35.88	35.74	35.84	35.81	35.93	35.95	36.01	35.98
Paragonite	77.10	58.78	71.85	62.71	24.04	10.79	2.35	16.99
Muscovite	22.90	41.22	28.15	37.29	75.96	89.21	97.65	83.01
Phengite	0.06	0.07	0.06	0.08	0.23	0.33	0.80	0.57

Table 5.1 Representative analyses of white micas from the Madrid deposit. Analyses 1-4 are paragonitic micas taken from the Hope Bay Deformation Zone. Analyses 5-6 are phengitic muscovites from mineralized samples. Analyses 7-8 are fuchsitic phengites.

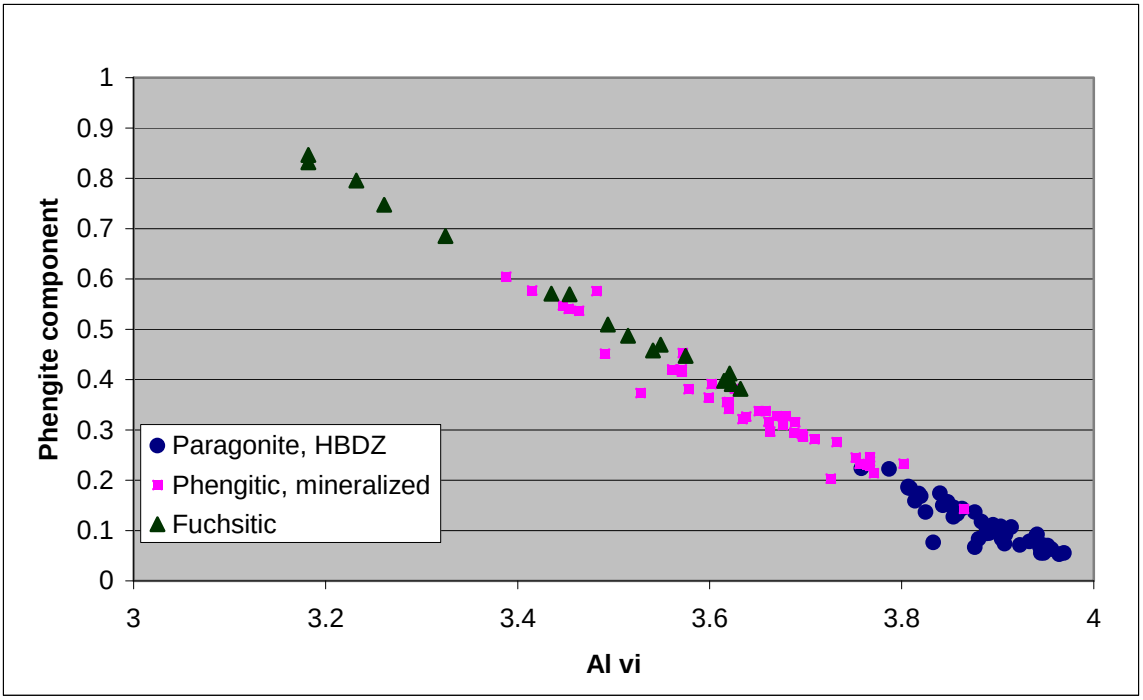

Fig. 5.1 Binary plot of phengitic component vs. octahedral Al for white mica analyses at Madrid. Phengite substitution in white micas interior to the HBDZ is low compared to Au-mineralized rocks, especially the fuchsitic variety.

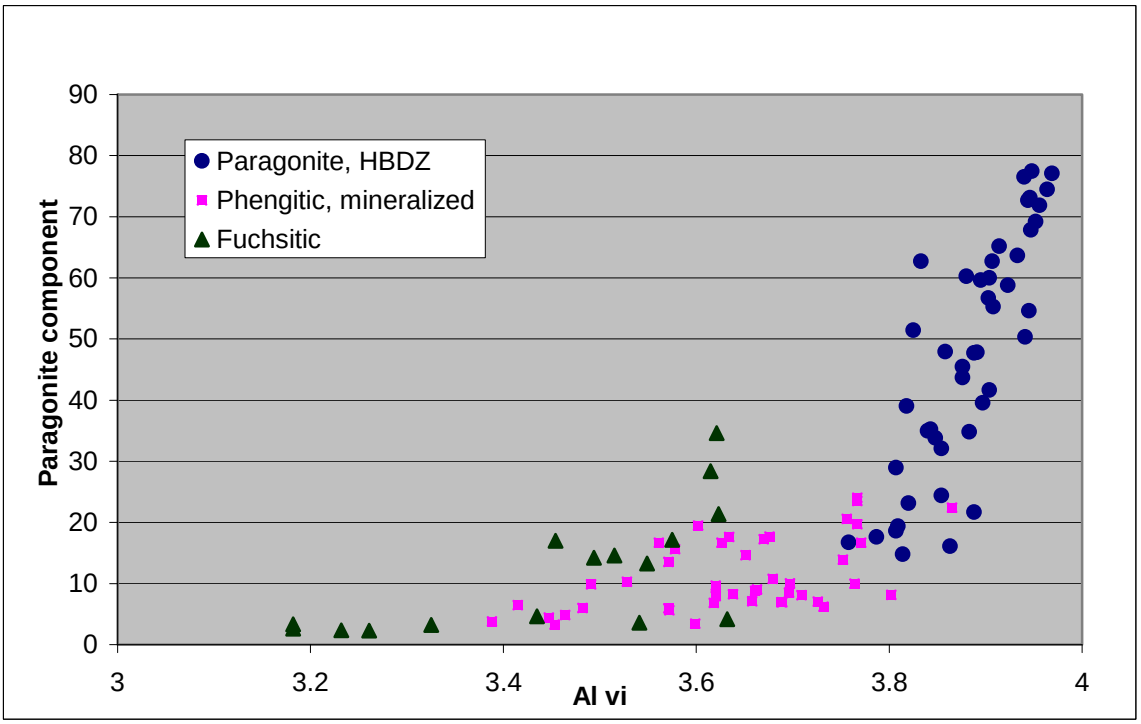

Fig 5.2 Binary plot of paragonite component vs. octahedral Al for white mica analyses at Madrid. Paragonitic muscovites and paragonites characterize micas in the HBDZ and contrast with weakly to non-paragonitic micas in Au-bearing horizons.

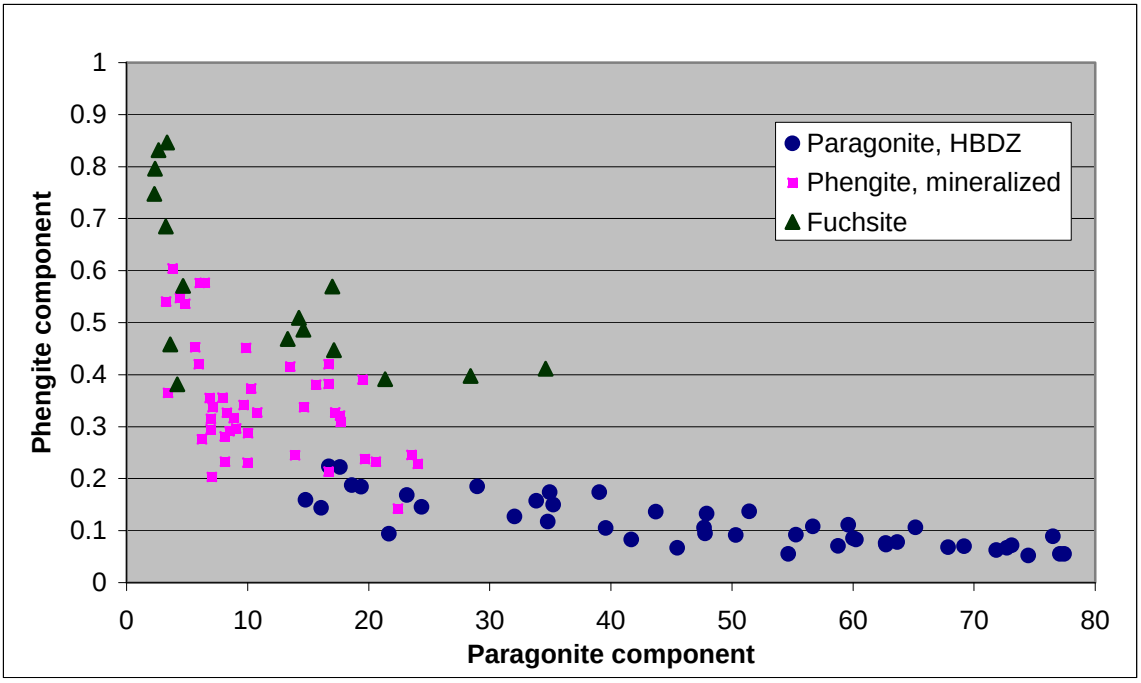

Fig. 5.3 Binary plot of paragonite vs. phengite component for white mica analyses at Madrid. As the phengitic substitution increases the paragonitic substitution decreases. The change in slope between white micas in the HBDZ and those in mineralized rocks is related to the influence of the paragonite and phengite substitutions in each group.

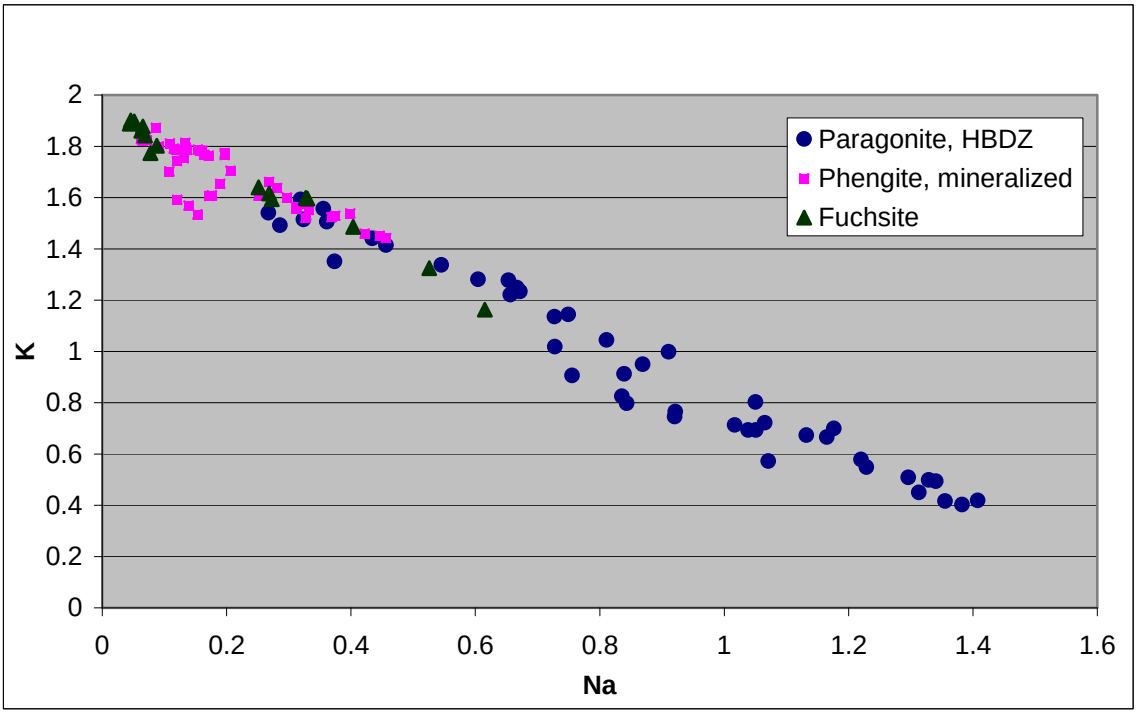

Fig. 5.4 Binary plot of Na vs. K for white mica analyses at Madrid showing progressive replacement of K by Na during paragonitization.

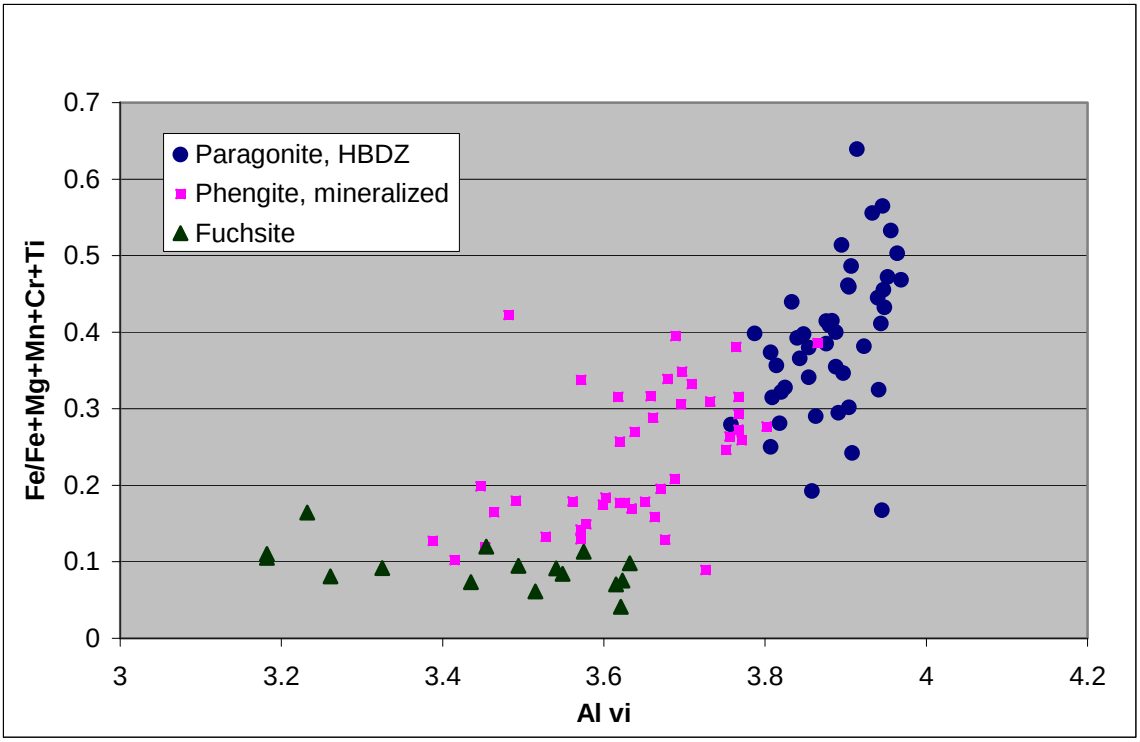

Fig. 5.5 Binary plot of Fe/Fe+Mg+Mn+Cr+Ti vs. Al vi for white mica analyses at Madrid showing the strongly phengitic character of fuchsitic micas contrasting with other phengitic micas and micas in the HBDZ.

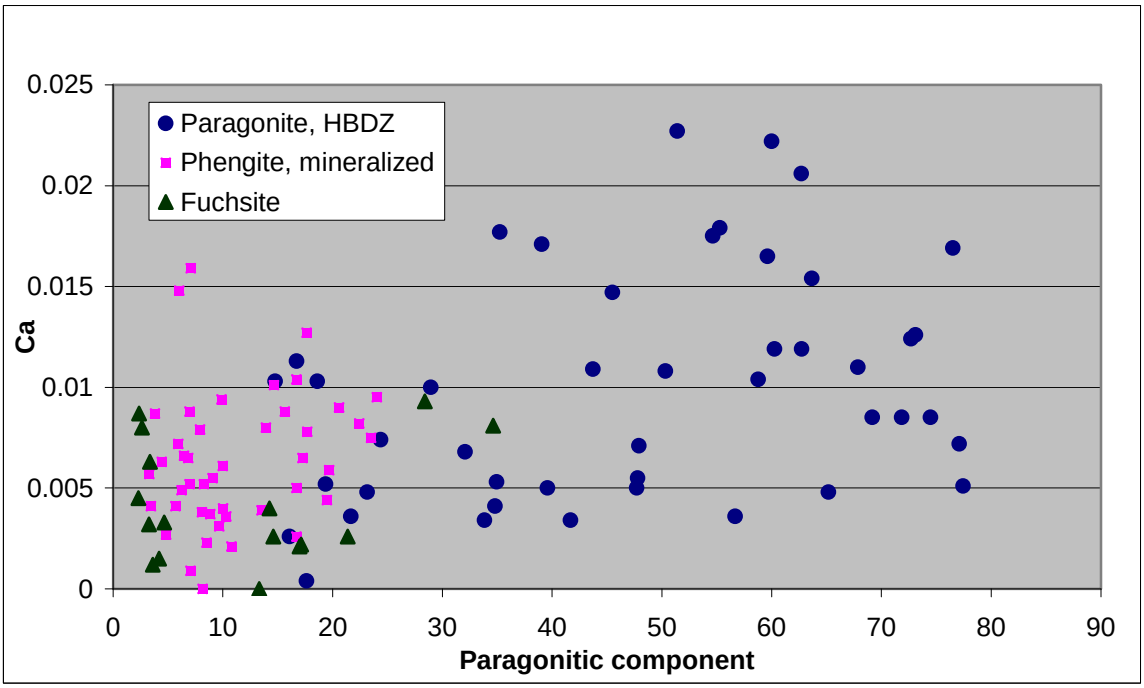

Fig. 5.6 Binary plot of Ca vs. paragonitic component for white micas at Madrid showing increasing Ca with Na.

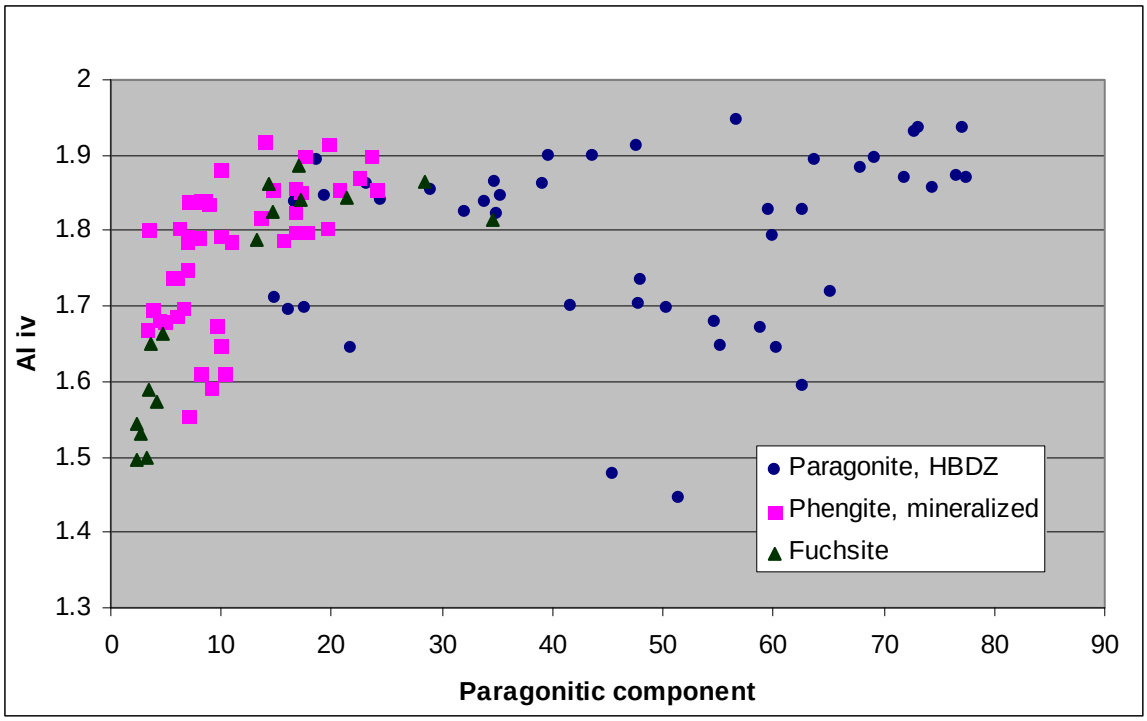

Fig. 5.7 Binary plot of Al iv vs. paragonitic component for white micas at Madrid. The amount of tetrahedral Al generally increases as the paragonitic component increases and the phengitic component decreases. This relationship is related to Si substituting for Al iv during phengite formation.

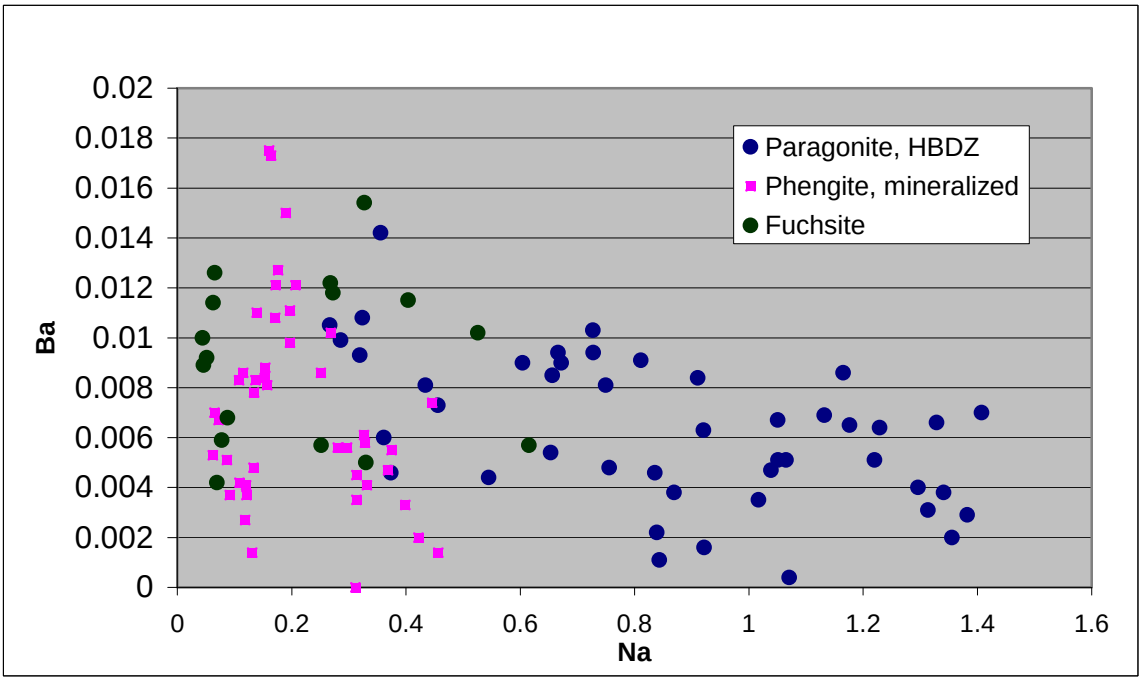

Fig. 5.8 Binary plot of Ba vs. Na for white micas at Madrid. Ba values increase with increasing phengite substitution in mineralized rocks and are only weakly influenced by Na. Ba values decrease with increasing paragonitization in the HBDZ.

Analyzed samples from outside the HBDZ are predominately of mineralized TEAD komatiites and komatiitic basalts. These samples show low paragonite values and elevated phengite values in comparison to analyses from the HBDZ. In terms of their paragonitic component Group 2 micas are classified as muscovites and paragonitic muscovites. In terms of their phengite component they fall under weakly phengitic to phengitic muscovites. Some samples from Group 2 contain enough Cr to be weakly fuchsitic to fuchsitic. Notably, the micas in these samples are not especially green (yellow to yellow-green), suggesting that colour alone is not the best method to identify Cr-micas at Madrid. Group 3 micas have the strongest phengite values owing to their elevated Cr. The change in slope between Group 1 and Group 2/3 micas on the paragonite vs. Al vi plot (Fig. 5.2) is because Group 2 and 3 micas are influenced by the paragonite and phengite substitution whereas Group 1 is affected almost exclusively by the paragonite substitution. Low Ca, Na and Al vi values and high K values are consistent with the phengite substitution being dominant over the paragonite substitution.

5.3 – Carbonate Chemistry

The chemistry of carbonates is relatively simple in comparison to the white micas. A complete solid solution exists between the siderite-magnesite join in the $CaCO_3$ - $MgCO_3$ - $FeCO_3$ system as discussed by Anovitz and Essene (1987), Deer *et al*., (1992) and the data presented in Fig. 5.9. The Mn substitution to form rhodochrosite is limited at Madrid (MnO < 1 wt%) and is not considered further. The dolomite series progresses from dolomite to ferrous dolomite to ankerite to ferrous ankerite with increasing Fe replacement of Mg.

Magnesitic carbonate (breunnerite) occurs together with phengitic (commonly fuchsitic) micas as an early fine-grained phase pseudomorphing cumulate and harrisitic textured pyroxenes. This phase is overprinted by ankerite +/- siderite and Fe-dolomite. Ankerite and siderite (sideroplesite and pistomesite) intergrowths commonly occur together in carbonitized basalt and veins as coarsely intergrown crystals which show contrasting paragenetic relationships. Ankerite and siderite may both show an outward zonation to more Fe rich rims. In a few instances ankerite grains are rinded by less Fe rich ankerite or ferrous dolomite. In one sample rims of siderite on ankerite were observed suggesting that siderite is a later phase replacing ankerite. Despite this, complex intergrowths between the two phases in most other samples suggests the two are similar in age. Representative carbonate analyses are given in Table 5.2.

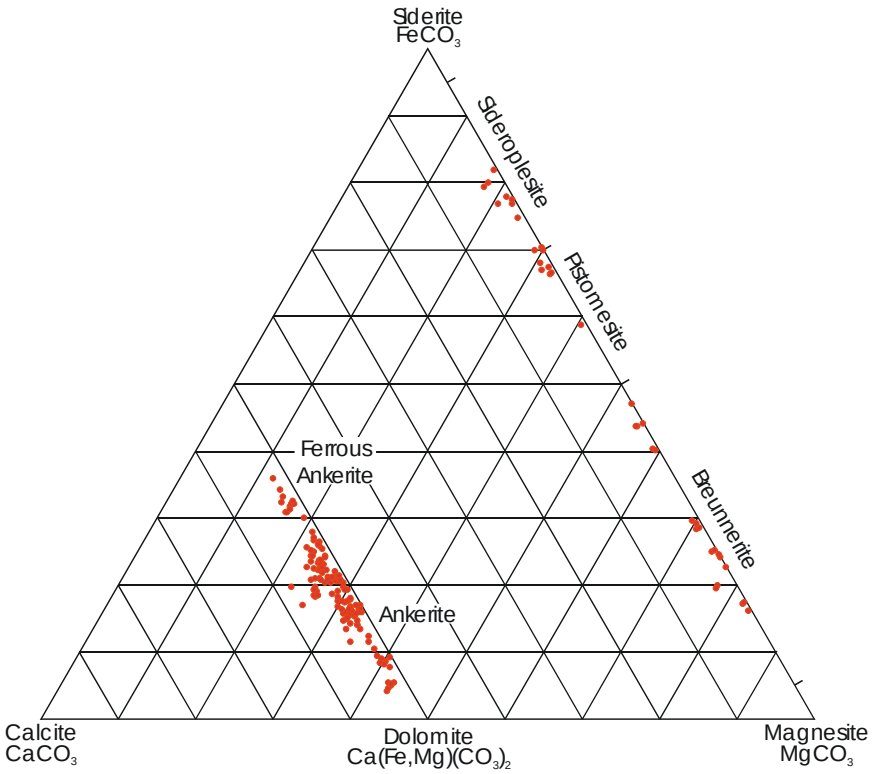

Fig. 5.9 Compositions of carbonate species from carbonitized basalt and veins from Madrid.

	1	2	3	4	5	6	7	8
FeO	43.74	44.19	21.06	21.22	15.44	14.59	30.55	30.77
MnO	1.06	0.39	0.53	0.44	0.98	0.50	0.66	0.22
MgO	12.04	11.55	6.21	6.28	9.28	10.29	21.72	21.67
CaO	0.47	0.90	28.08	28.30	28.73	28.18	0.10	0.70
CO2	44.26	44.26	44.26	44.26	44.26	44.26	44.26	44.26
Total	101.58	101.30	100.14	100.49	98.69	97.82	97.29	97.63
	144-122-8	144-110-18	123-55-1	123-55-7	108-103-1	168-220-8	62-80-9	62-80-5
Fe	4.97	5.03	2.37	2.38	1.73	1.64	3.42	3.44
Mn	0.12	0.05	0.06	0.05	0.11	0.06	0.07	0.02
Mg	2.44	2.34	1.25	1.26	1.85	2.06	4.33	4.31
Ca	0.07	0.13	4.05	4.07	4.12	4.05	0.01	0.10
C	8.20	8.23	8.14	8.12	8.09	8.10	8.08	8.07
O	24.00	24.00	24.00	24.00	24.00	24.00	24.00	24.00
CatTot	15.80	15.78	15.86	15.88	15.91	15.90	15.92	15.94
Total	39.80	39.78	39.86	39.88	39.91	39.90	39.92	39.94

Table 5.2 Representative carbonate analyses for samples from the Madrid area. Analyses 1-2 are siderite, 3-6 are ankerite and 7-8 are bruennerite.

5.3.1 – Carbonate Geothermometry

The compositions of equilibrated calcite-dolomite or siderite-ankerite pairs can be potentially useful as a geothermometer as discussed by Anovitz and Essene (1987) and Powell *et al*. (1984). The premise behind the carbonate geothermometers is that variations in the composition of coexisting carbonate *species* is governed by temperature, and independent of pressure or fluid/host rock composition (see Mumin and Fleet, 1995 and references therein). Mumin (1994) and Mumin and Fleet (1995) have shown that ankerite-siderite geothermometry can yield reasonable results, comparable with calcite-dolomite, arsenopyrite, carbon and oxygen stable isotope and fluid inclusion geothermometers. Despite this, the accuracy of the calibration is still in question and the geothermometer is better used to calculate relative temperature differences. The calibration, as proposed by Anovitz and Essene (1987) is as follows:

$$K_D = [(X^{FeCO_3}/X^{MgCO_3})\text{Ankerite}] \ / \ [X^{FeCO_3}/X^{MgCO_3}]\text{Siderite} = -0.691 + 0.00176\ T\ (T, K) \qquad \text{(Eq. 5.2)}$$

where,

K_D = Distribution constant for ankerite and calcite

X^{FeCO}_3 = Mole fraction $FeCO_3$

X^{MgCO}_3 = Mole fraction $MgCO_3$

T = Temperature in Kelvin

As shown in the previous section, ankerite-siderite intergrowths are commonly present in the mineralized rocks of Madrid. Geothermometry calculations have only been carried out for samples containing equilibrated carbonate pairs that were in *mutual contact*. Additional calculations were completed by estimating siderite compositions in samples where siderite was not present. The results of these calculations are comparable to the data presented, but are not included here. It should be noted that the absolute values obtained through these calculations is less important than the temperature differences between different styles of carbonate alteration. Fig. 5.10 displays the results of the ankerite-siderite data. Ideally the plot should follow the carbonate solvus for coexisting and equilibrated ankerite-siderite pairs. With increasing temperatures the mol % $FeCO_3$ in ankerite increases, while $FeCO_3$ in siderite decreases. This is the predicted result (Anovitz and Essene, 1987) and is identical to the trend observed by Mumin (1994). Additional analyses of vein related ankerite in samples without siderite generally yielded lower $FeCO_3$ values than ankerite overprinting basalt. This observation is consistent with vein temperatures being lower than the background pervasive carbonate alteration. The reasons for this are discussed in Chapter 6. Ankerite- siderite pairs within carbonitized basalt have calculated temperatures between 275-400 ^oC whereas carbonate

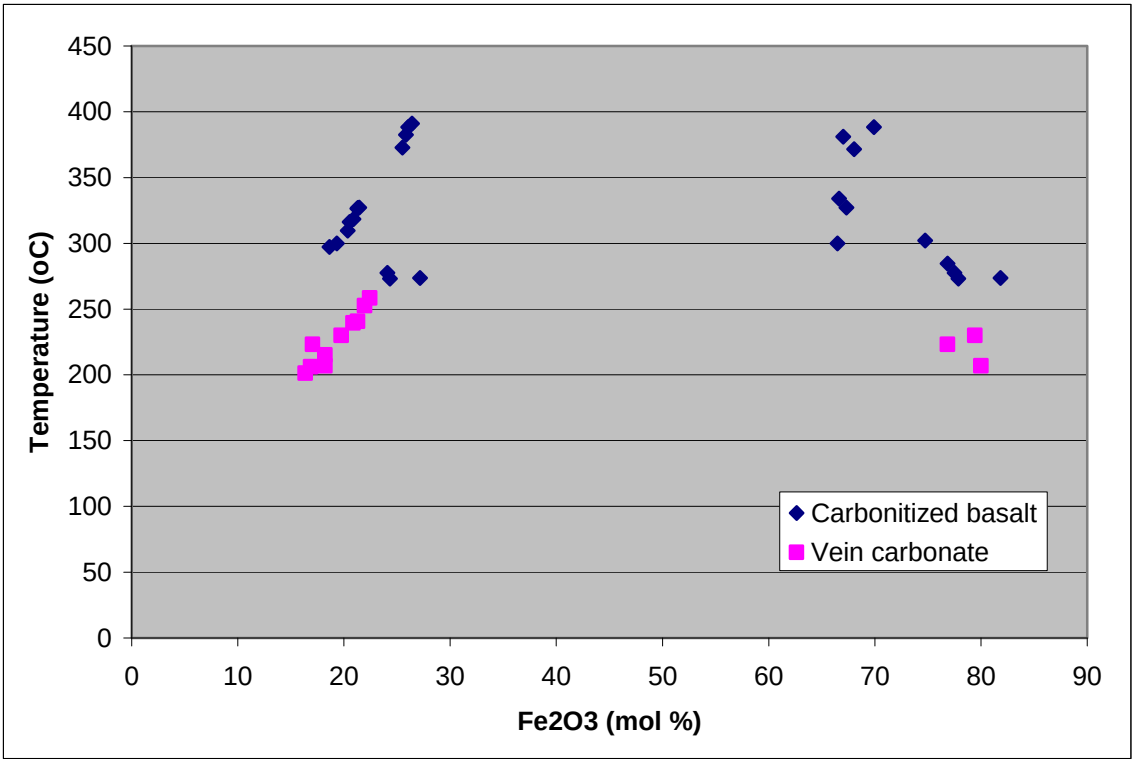

Fig. 5.10 Temperature calculations for equilibrated ankerite-siderite pairs in mutual contact at Madrid. Samples are from veins and carbonized basalt.

pairs in veins have temperatures between 200-250 ^{o}C.

5.4 – Chlorite Chemistry

Chlorite results have been calculated on the basis of 28 oxygens and have been presented based on the classification scheme of Hey (1954). Representative analyses are shown in Table 5.3. Analyses have been completed from several lithotypes including TEAD komatiitic basalts, FETI basalts, high-Fe tholeiitic basalts and basaltic andesites. Analyses were taken strictly from the quartz-carbonate-chlorite-amphibole-epidote facies i.e. no analyses were completed on samples with intergrown sericite and chlorite. Fe_{Total} values have been plotted on Fig 5.11 rather than Fe^{2+} values, however, the differences

between the two ratios is slight, and the more important result is where samples plot relative to each other rather than in which field.

Two samples of basaltic andesites both plot in the ripidolite field, but have considerably different Fe/(Fe+Mg) ratios. The sample with lower Fe/(Fe+Mg) is of a basaltic andesite from the Suluk area while the higher Fe/(Fe+Mg) ratio represents a sample of peperitic basaltic andesite from Perrin. Elevated Fe in the bulk rock chemistry of the latter sample explains the difference in the two ratios. Two samples of high-Fe basalt show similar chlorites defining a compositional trend which correspond to increasing Mg and Si related to Si and Mg replacing octahedrally coordinated Al and/or Mg replacing Fe in the octahedral layer. TEAD komatiitic basalts and FETI basalts show

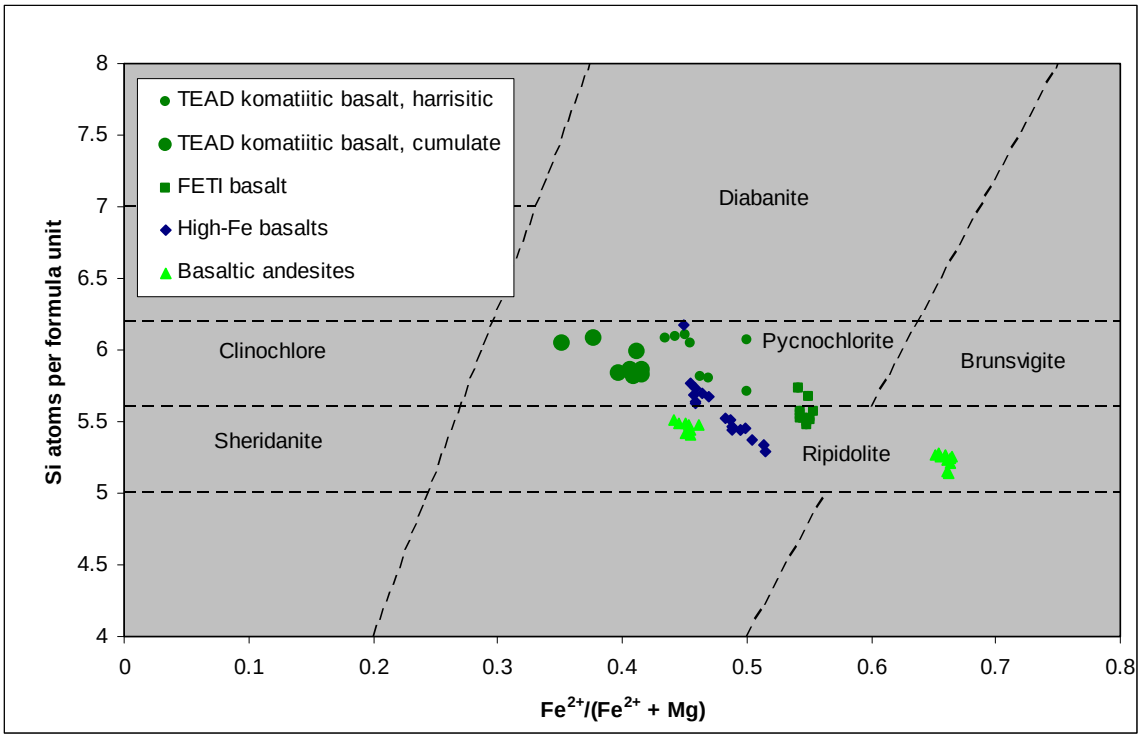

Fig. 5.11 Compositions of chlorite from unmineralized rocks at Madrid. Divisions from Hey (1954).

	1	2	3	4	5	6	7	8	9	10
SiO2	23.70	26.05	25.98	27.06	29.07	28.81	27.80	27.83	26.68	25.67
TiO2	0.05	0.05	0.05	0.01	0.10	0.18	0.06	0.04	0.11	0.06
Al2O3	22.23	21.56	21.68	18.61	15.69	16.07	17.22	17.44	18.95	19.30
Cr2O3	0.00	0.10	0.18	0.37	0.12	0.07	0.00	0.00	0.27	0.26
FeO	31.97	23.93	25.34	24.79	24.61	25.02	23.18	23.41	28.44	28.12
MnO	0.20	0.41	0.07	0.46	0.16	0.13	0.14	0.11	0.50	0.48
MgO	9.07	16.12	14.49	16.52	17.42	16.80	18.74	18.40	13.03	13.31
CaO	0.07	0.07	0.15	0.08	0.07	0.09	0.17	0.07	0.11	0.11
Na2O	0.13	0.04	0.00	0.00	0.20	0.19	0.00	0.02	0.06	0.10
K2O	0.07	0.00	0.03	0.00	0.48	0.76	0.01	0.07	0.73	0.13
NiO	0.01	0.05	0.04	0.04	0.09	0.09	0.15	0.12	0.15	0.11
Total	87.49	88.39	88.02	87.93	88.01	88.20	87.48	87.51	89.04	87.64
	23-71-6	173-247-4	007A-3	winchl7	K2-16	K2-17	108-88.7	108-88.8	23-197	23-197
Si	5.21	5.41	5.44	5.68	6.10	6.05	5.81	5.82	5.67	5.53
Ti	0.01	0.01	0.01	0.00	0.02	0.03	0.01	0.01	0.02	0.01
Al	5.76	5.27	5.35	4.61	3.88	3.98	4.25	4.30	4.75	4.90
Cr	0.00	0.02	0.03	0.06	0.02	0.01	0.00	0.00	0.04	0.05
Fe	5.87	4.15	4.44	4.36	4.32	4.40	4.05	4.10	5.06	5.07
Mn	0.04	0.07	0.01	0.08	0.03	0.02	0.02	0.02	0.09	0.09
Mg	2.97	4.99	4.53	5.17	5.45	5.26	5.84	5.74	4.13	4.27
Ca	0.02	0.02	0.03	0.02	0.02	0.02	0.04	0.02	0.03	0.03
Na	0.06	0.02	0.00	0.00	0.08	0.08	0.00	0.01	0.02	0.04
K	0.02	0.00	0.01	0.00	0.13	0.20	0.00	0.02	0.20	0.04
Ni	0.00	0.01	0.01	0.01	0.02	0.01	0.03	0.02	0.03	0.02
O	28.00	28.00	28.00	28.00	28.00	28.00	28.00	28.00	28.00	28.00
CatTot	19.95	19.95	19.86	19.98	20.04	20.07	20.06	20.04	20.03	20.03
Total	47.95	47.95	47.86	47.98	48.04	48.07	48.06	48.04	48.03	48.03

Table 5.3 Representative chlorite analyses from Madrid. Analyses 1-2 are basaltic andesites, 3-4 are Fe-rich tholeiites, 5-6 are harrisitic textured komatiitic basalts, 7-8 are coarse textured komatiitic basalts, 9-10 are FETI basalts.

a similar but less well defined trend. The lower Mg values from bulk rock chemistry in the FETI basalts are reflected by their chlorite compositions. Similarly, the higher Mg values of the TEAD komatiitic basalts are also reflected in their chlorite composition. Note the especially high Mg values corresponding to a coarser (cumulate?) phase of komatiitic basalt.

5.5 – Amphibole Chemistry

Amphibole compositions have been calculated on the basis of 23 oxygens and have been classified according to Leake (1978). Representative analyses are shown in Table 5.4. Although the diagrams (Fig. 5.13 and 5.14) presented below are intended to use Fe^{2+}, Fe_{Total} has been plotted. Estimations of Fe^{2+} and Fe^{3+} calculated by the method of Papike *et al*. (1974) show that using Fe_{Total} does not significantly affect the plotted ratio. Furthermore, for the purposes of this study the more important result is where samples plot relative to each other rather than in which field.

Amphiboles were encountered in several of the analyzed samples, occurring together with chlorite, epidote, carbonate and pyroxene. Their presence indicates one of two things:

1) The Madrid area is of higher metamorphic grade (epidote-actinolite facies, upper greenschist) and the epidote-actinolite assemblage is related to prograde metamorphism.

2) The Ca-rich minerals epidote and actinolite are hydrothermal in origin, related to the Ca-metasomatism event that has affected all the rocks in the Madrid area.

Evidence for the former is suggested by the distinct crystallinity of the epidote and amphibole as well as carbonate geothermometry temperatures up to 400 ^{o}C. Furthermore, amphibole and epidote is absent from strongly hydrothermally altered rocks, occurring with chlorite-facies rocks distal to mineralized units. Despite this it is difficult to prove conclusively considering the strong Ca-metasomatism overprint in the Madrid district. Additional work should involve sampling of the mafic volcanics well outside alteration zones and interpretation of the textures therein.

Amphibole analyses from a TEAD komatiitic basalt sample have not been plotted, but are included in Appendix B. The amphibole in this sample occurred as fine-grained acicular weakly pleochroic masses associated with elongate mats of chlorite. Analyses totals drifted around 90% suggesting poor results due to small grain size, chlorite

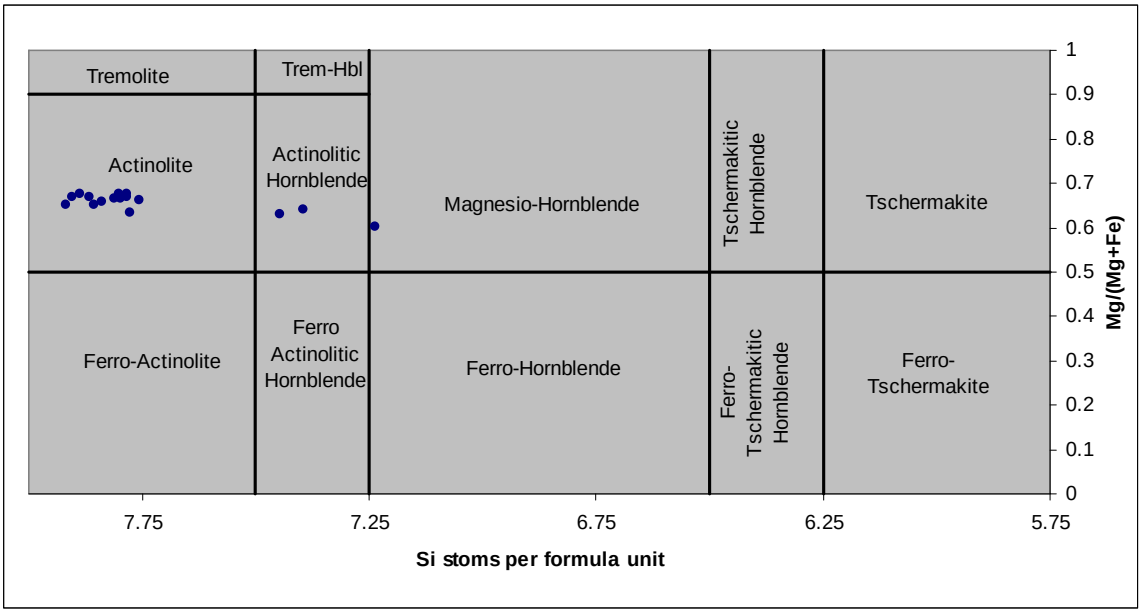

Fig. 5.12 Composition of amphiboles from high-Fe basalts at Madrid.

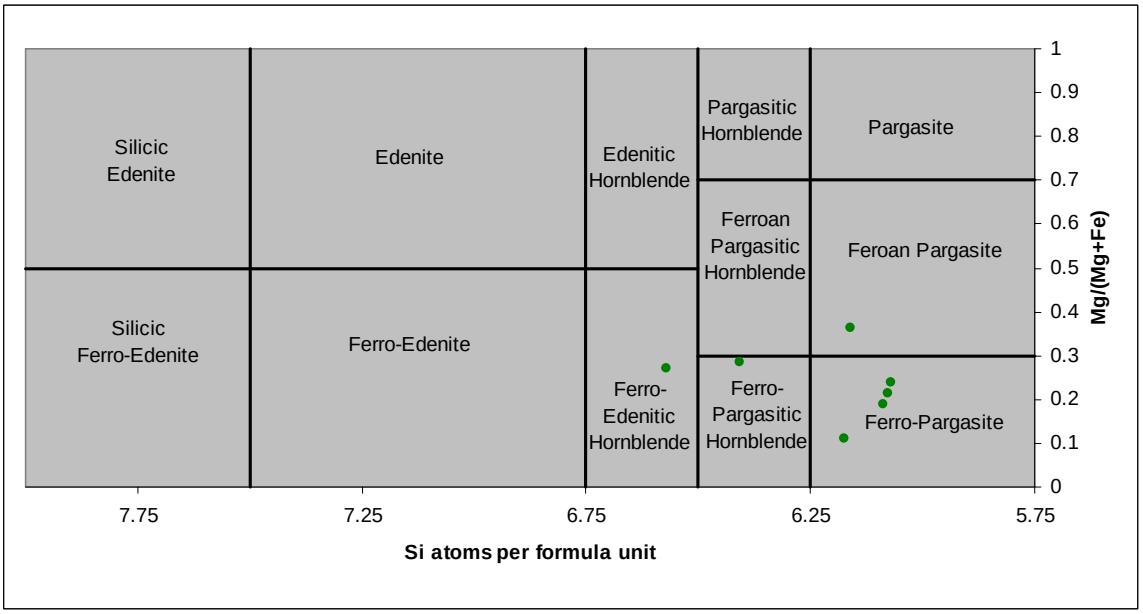

Fig. 5.13 Composition of amphiboles from high FETI basalts from Madrid.

	1	2	3	4	5	6
SiO2	53.69	53.98	54.55	38.81	38.23	38.41
TiO2	0.17	0.21	0.03	0.55	1.09	0.97
Al2O3	1.80	1.25	1.03	15.97	15.73	15.96
Cr2O3	0.04	0.00	0.00	0.03	0.00	0.04
FeO	13.27	13.21	13.19	24.42	24.00	24.56
MnO	0.35	0.33	0.23	0.39	0.36	0.52
MgO	15.01	15.43	15.38	4.25	3.65	3.19
CaO	12.84	13.20	12.89	9.38	9.42	8.48
Na2O	0.22	0.13	0.14	3.19	2.83	3.72
K2O	0.03	0.02	0.01	0.17	0.22	0.17
NiO	0.05	0.08	0.00	0.04	0.02	0.06
Total	97.47	97.84	97.46	97.22	95.55	96.09
Label	020-14	020-18	win-11	23-197-2	23-197-7	23-197-14
Si	7.78	7.80	7.89	6.07	6.08	6.09
Ti	0.02	0.02	0.00	0.06	0.13	0.12
Al	0.31	0.21	0.18	2.94	2.95	2.98
Cr	0.00	0.00	0.00	0.00	0.00	0.00
Fe	1.61	1.60	1.59	3.19	3.19	3.26
Mn	0.04	0.04	0.03	0.05	0.05	0.07
Mg	3.24	3.32	3.31	0.99	0.86	0.75
Ca	1.99	2.04	2.00	1.57	1.60	1.44
Na	0.06	0.04	0.04	0.97	0.87	1.14
K	0.01	0.00	0.00	0.03	0.05	0.04
Ni	0.01	0.01	0.00	0.01	0.00	0.01
O	23.00	23.00	23.00	23.00	23.00	23.00
CatTot	15.08	15.09	15.04	15.89	15.78	15.89
Total	38.08	38.09	38.04	38.89	38.78	38.89

Table 5.4 Representative amphibole compositions from Madrid. Analyses 1-3 are from Fe-rich tholeiitic basalts, analyses 4-6 are from FETI basalts.

contamination or a very water rich amphibole. Si values are too high for chlorite while Mg values are too low for serpentine.

Amphiboles from high-Fe basalts (Wolverine and Windy mafics) occur as fine feathery masses together with epidote, chlorite and carbonate. They are classified as calcic amphiboles and plot as actinolite and actinolitic hornblende (Fig. 5.12). In contrast, pleochroic green amphiboles from a FETI transitional basalt sample have elevated alkalis (Na + K) and plot as pargasites (Fig. 5.13). The Fe and Ti values are also

elevated relative to amphiboles from the high-Fe tholeiitic basalts. The reason for the higher Na-K in these amphiboles may relate to the bulk chemistry of the rock. The Na values in least altered samples of both groups are approximately the same, however, the K is slightly elevated in the bulk rock chemistry of the analyzed FETI basalt.

5.6 – Pyroxene Chemistry

Clinopyroxene compositions have been calculated on the basis of 6 oxygens. Representative analyses are included in Table 5.4. Euhedral clinopyroxene microphenocrysts were analyzed from a single sample of FETI basalt. A few grains were also analyzed from a sample of non-variolitic high-Fe tholeiitic basalt, however, most of these grains are strongly altered to epidote and amphibole. No strong zoning was noted, despite the fact that it was suggested in thin section (preferentially carbonate altered

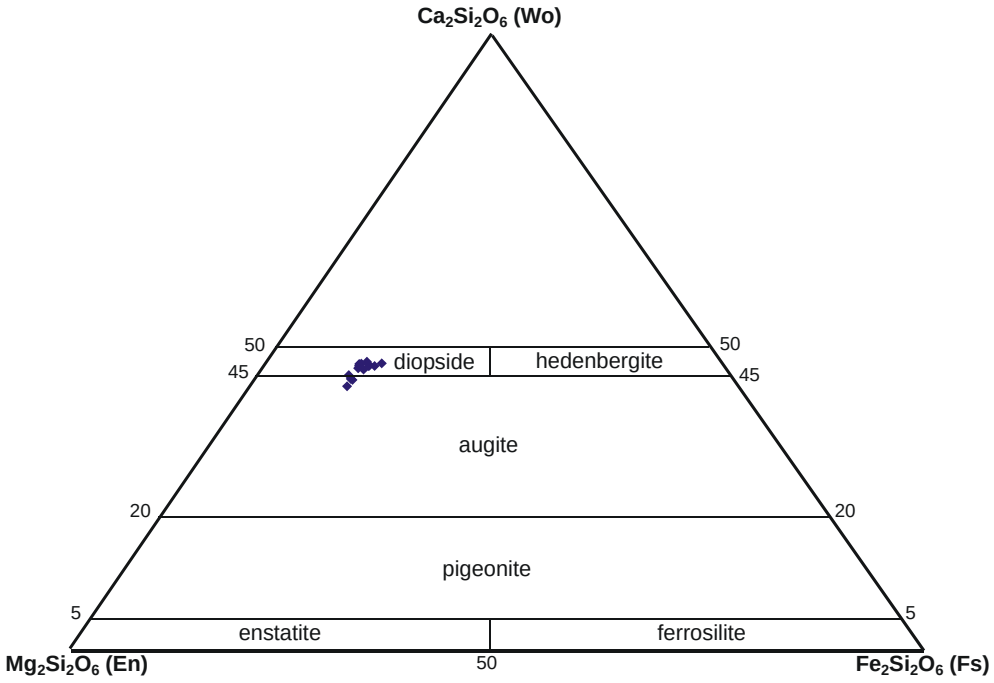

Fig. 5.14 Composition of pyroxene grains from a sample of FETI basalt.

	1	2	3	4
SiO2	50.24	50.72	48.03	52.12
TiO2	0.86	0.86	1.89	0.57
Al2O3	3.56	3.28	5.03	1.76
Cr2O3	0.73	0.70	0.50	0.55
FeO	7.28	6.74	8.07	6.63
MnO	0.13	0.13	0.12	0.12
MgO	14.77	14.79	13.51	15.83
CaO	22.07	22.20	21.99	22.03
Na2O	0.35	0.29	0.42	0.35
K2O	0.02	0.02	0.03	0.01
Total	100.01	99.72	99.59	99.98
	23-197-4	23-197-9	23-197-11	23-197-1
Si	1.87	1.89	1.81	1.93
Ti	0.02	0.02	0.05	0.02
Al Total	0.16	0.14	0.22	0.08
Al iv	0.03	0.03	0.03	0.01
Al vi	0.13	0.11	0.19	0.07
Cr	0.02	0.02	0.02	0.02
Fe	0.23	0.21	0.25	0.21
Fe2+	0.07	0.07	0.09	0.12
Fe3+	0.15	0.14	0.16	0.09
Mn	0.00	0.00	0.00	0.00
Mg	0.82	0.82	0.76	0.87
Ca	0.88	0.89	0.89	0.87
Na	0.03	0.02	0.03	0.02
K	0.00	0.00	0.00	0.00
O	6.00	6.00	6.00	6.00
CatTot	4.03	4.02	4.04	4.02
Total	10.03	10.02	10.04	10.02

Table 5.5 Representative analyses of clinopyroxene crystals from a sample of FETI basalt.

cores). Many of the analyzed clinopyroxenes show partial replacement by amphibole, epidote, chlorite, sphene and Fe-Ti-oxides.

Pyroxene compositions plot consistently as aluminian-chromian augite/diopside (Fig. 5.14), an expected result considering the bulk rock chemistry of the sample. The low Ti values in the pyroxenes (0.5-1.5%) suggest that most of the Ti in this sample is hosted within sphene and various Fe-Ti oxides.

5.7 – Epidote Chemistry

Epidote crystals were analyzed from three samples of chlorite altered basalt. The number of ions have been calculated on the basis of 12.5 oxygens. Representative analyses are shown in Table 5.6. Epidote occurs as fine-grained feathery masses with Ca-amphiboles, chlorite and carbonate. The main chemical variation occurs between epidotes from high-Fe tholeiitic basalts and basaltic andesites. Elevated Fe, Mg and Mn occur in the high-Fe suite which corresponds to lower Al values related to Fe^{3+} replacing Al in the octahedral site (Fig. 5.15). Increases in Ca with decreases in Fe are related to Fe^{2+} replacing Ca (Fig. 5.16). Epidote analyses from basaltic andesites have lower Fe, Mg and Mn values and correspondingly higher Al contents.

5.8 – Feldspar Chemistry

Two varieties of feldspars have been analyzed from the Madrid deposit. Primary igneous feldspar crystals in a basaltic andesite were examined; however, focus was

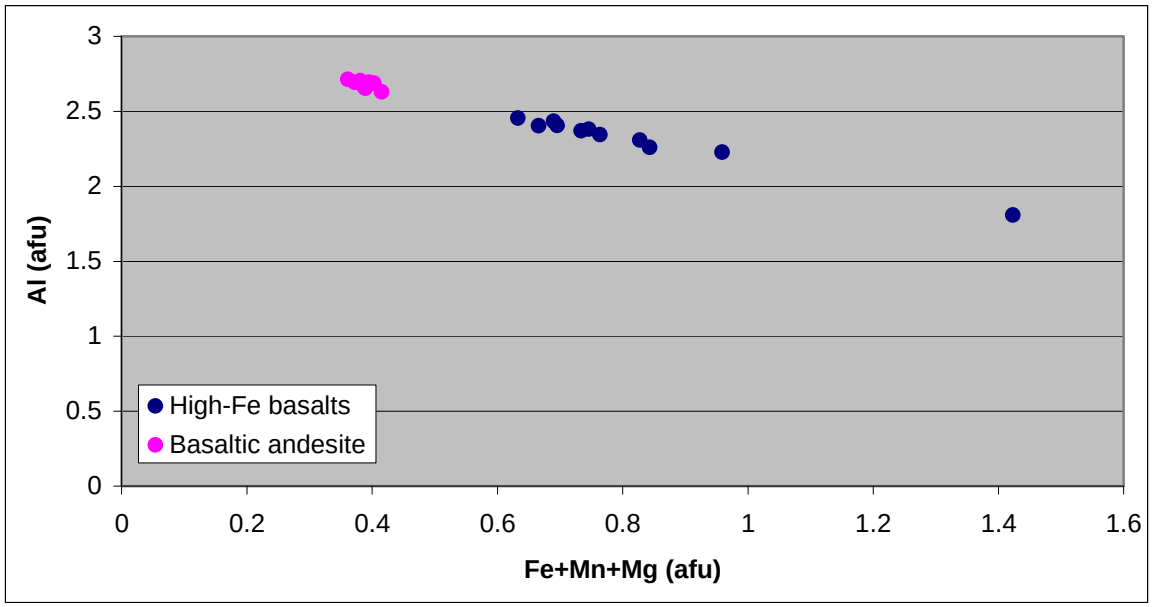

Fig. 5.15 Variations in Al and Fe+Mn+Mg for epidotes at Madrid.

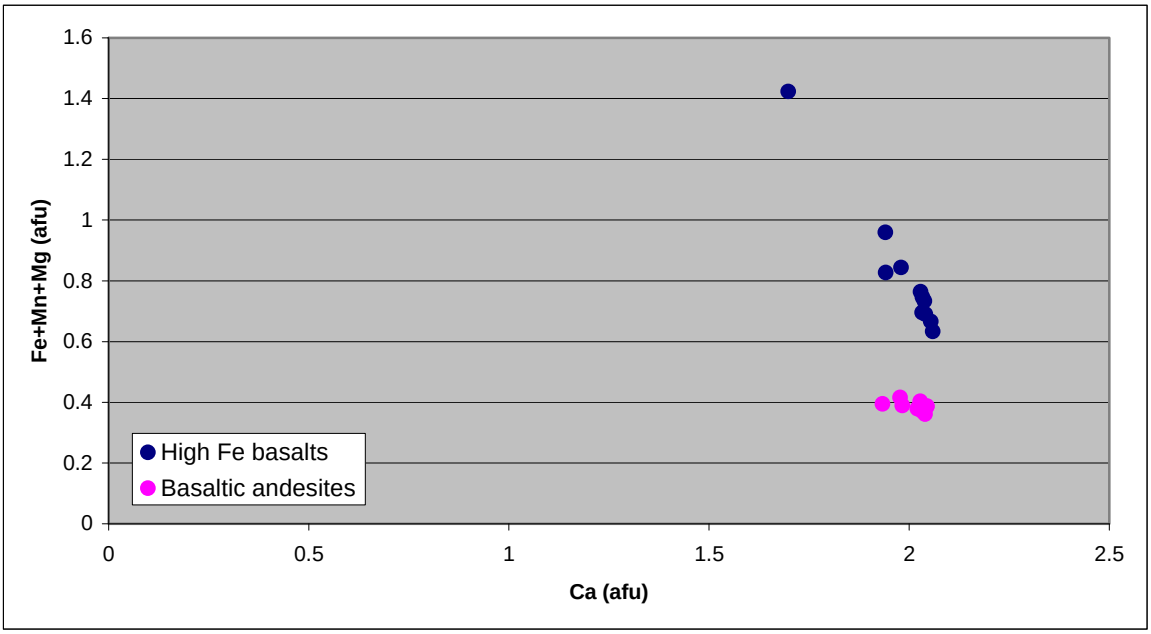

Fig. 5.16 Variations in Ca and Fe+Mn+Mg for epidotes at Madrid.

	1	2	3	4
SiO2	38.66	40.17	38.12	37.65
TiO2	0.04	0.79	0.31	0.08
Al2O3	29.45	18.78	25.34	23.58
Cr2O3	0.12	0.02	0.04	0.00
FeO	5.79	14.85	9.50	11.62
MnO	0.06	0.34	0.14	0.16
MgO	0.00	3.17	0.14	0.07
CaO	24.23	19.41	23.83	21.82
Na2O	0.00	0.09	0.00	0.05
K2O	0.01	0.01	0.01	0.02
Total	98.36	97.63	97.44	95.06
Label	173-247-6	020-8	020-12	23-197-5
Si	3.01	3.28	3.07	3.13
Ti	0.00	0.05	0.02	0.01
Al	2.71	1.81	2.40	2.31
Cr	0.00	0.00	0.00	0.00
Fe	0.38	1.01	0.64	0.81
Mn	0.00	0.02	0.01	0.01
Mg	0.00	0.39	0.02	0.01
Ca	2.02	1.70	2.05	1.94
Na	0.00	0.01	0.00	0.01
K	0.00	0.00	0.00	0.00
O	12.50	12.50	12.50	12.50
CatTot	8.13	8.27	8.21	8.22
Total	20.63	20.77	20.71	20.72

Table 5.6 Analyses of epidote from Fe-rich tholeiitic basalts and basaltic andesites.

placed on secondary hydrothermal albites hosted predominately in veins and stockworks. Both varieties of feldspar are similar (Table 5.7), with the former being slightly more calcic than the near-endmember vein associated albites. This is illustrated in Fig 5.17. Insufficient study prevents any major conclusions from being drawn, except that the albite component is slightly greater in the hydrothermal feldspars.

	1	2	3	4	5
SiO2	66.57	64.66	67.91	68.32	68.31
Al2O3	19.86	19.83	18.67	18.43	18.37
Fe2O3	0.45	1.40	0.05	0.05	0.01
CaO	0.83	1.60	0.08	0.03	0.09
Na2O	10.96	10.39	11.62	11.40	11.60
K2O	0.04	0.00	0.03	0.03	0.00
MgO	0.20	0.60	0.00	0.00	0.00
SrO	0.01	0.16	0.00	0.00	0.00
BaO	0.01	0.03	0.05	0.00	0.05
Total	98.93	98.67	98.42	98.26	98.43
Label	177-221-3	177-221-4	173-202.9-1	58-189-3	209-257.3-4
Si	2.95	2.89	3.01	3.03	3.03
Al	1.04	1.05	0.98	0.96	0.96
Fe	0.02	0.05	0.00	0.00	0.00
Ca	0.04	0.08	0.00	0.00	0.00
Na	0.94	0.90	1.00	0.98	1.00
K	0.00	0.00	0.00	0.00	0.00
Mg	0.01	0.04	0.00	0.00	0.00
Sr	0.00	0.00	0.00	0.00	0.00
Ba	0.00	0.00	0.00	0.00	0.00
O	8.00	8.00	8.00	8.00	8.00
CatTot	5.00	5.01	5.00	4.98	4.99
Total	13.00	13.01	13.00	12.98	12.99
Alb	95.77	92.14	99.46	99.71	99.55
Anor	4.03	7.86	0.38	0.15	0.44
Ortho	0.20	0.00	0.16	0.14	0.01

Table 5.7 Representative feldspar compositions for samples from Madrid. Analyses 1-2 are igneous feldspars from a basaltic andesite. Analyses 3-5 are hydrothermal albites from veins.

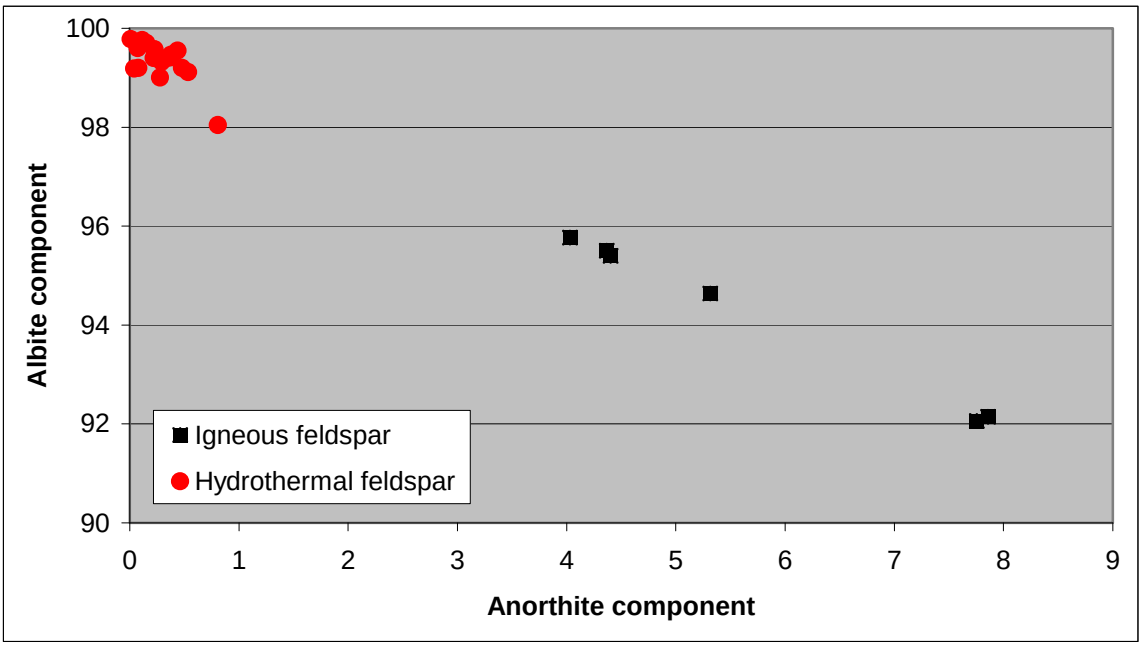

Figure 5. 17 Comparison of primary igneous plagioclase with vein-related hydrothermal plagioclase.

5.9 – Sulphide Chemistry

Both WDS and EDS analyses were completed on the various sulphide species at Madrid. Quantitative results were obtained for only pyrite and gersdorffite, an As-Ni-Co sulphide (Yund, 1962). The results are shown in Figures 5-18, 5-19, 5-20 and Table 5.8. Many of the pyrite grains showed textural and compositional differences between the core and rim (Fig. 5.19). Pyrite cores are commonly spongy textured and amoeboidal in shape. The spongy texture is a result of abundant fine-grained gangue inclusions while the shape is likely a result of resorbtion or replacement related to disequilibrium conditions. In contrast rims were typically free of inclusions and texturally mature (sub to euhedral). Compositionally, many of the pyrites exhibit pseudozoning from a homogenous arsenic poor core to a relatively homogenous arsenian rim. Rather than zoning smoothly outward, there are sharp contrasts, morphologically and chemically, between the rim and core. Cobalt and nickel contents are less consistent, but also tend to

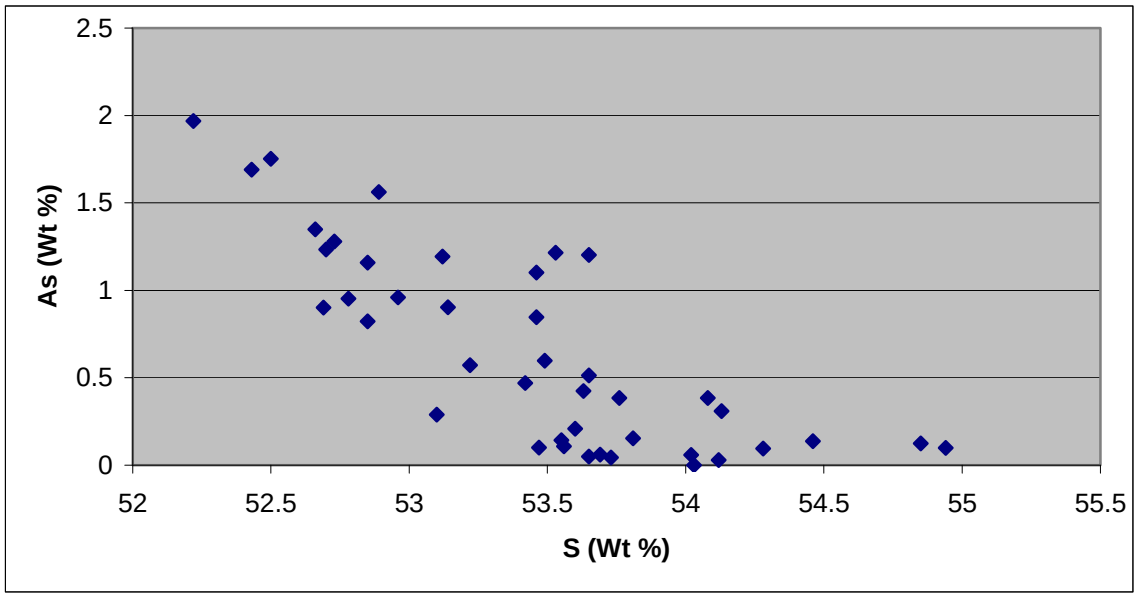

Fig. 5. 18 Binary plot showing variation in As and S for arsenian and non arsenian pyrite

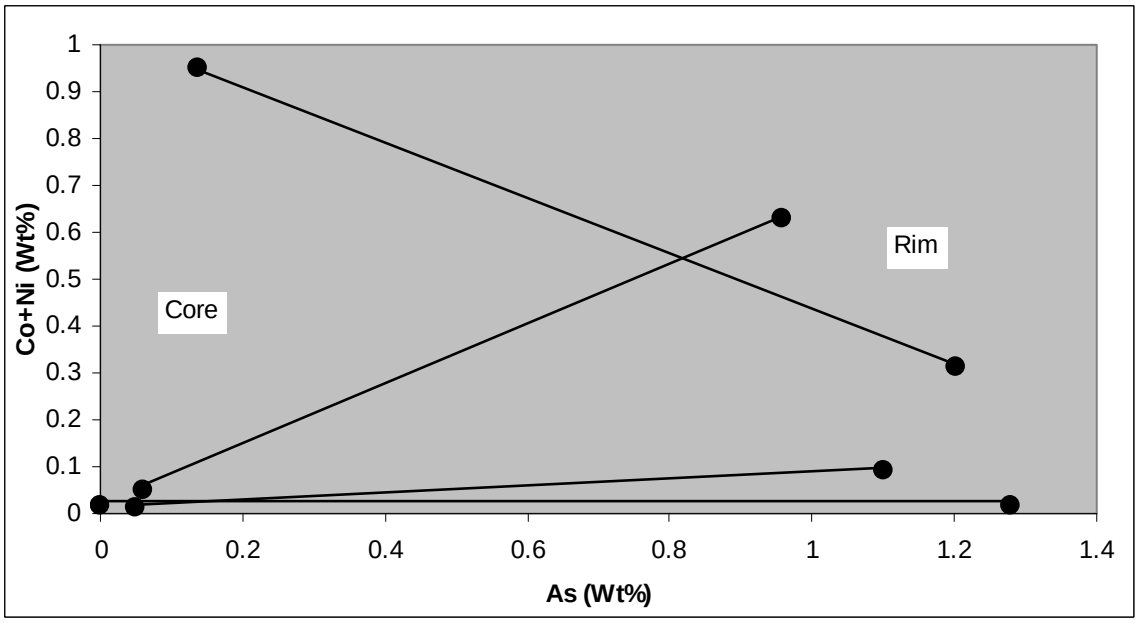

Fig. 5. 19 Binary plot showing arsenic variation between pyrite cores and rims.

	1	2	3	4	5	6	7
Fe	46.60	45.58	45.93	45.27	9.43	7.94	5.75
Co	0.00	0.01	0.00	0.04	2.99	1.23	5.00
Ni	0.01	0.62	0.00	0.00	23.40	26.01	24.91
As	0.05	0.96	0.15	0.03	43.01	42.90	43.99
S	54.03	53.11	53.68	53.48	20.28	20.73	20.56
Total	100.69	100.28	99.76	98.83	99.11	98.80	100.21
Label	58-189-4	58-189-5	209-257.3-3	173-202.9-1	173-202.9-5	58-189-11	58-113.5-5
Fe	0.99	0.98	0.99	0.98	0.28	0.23	0.17
Co	0.00	0.00	0.00	0.00	0.08	0.03	0.14
Ni	0.00	0.01	0.00	0.00	0.66	0.73	0.69
As	0.00	0.02	0.00	0.00	0.94	0.94	0.96
S	2.01	1.99	2.01	2.02	1.04	1.06	1.05
Total	3.00	3.00	3.00	3.00	3.00	3.00	3.00

Table 5.8 Representative compositions of sulphides from Madrid. Analyses 1-2 are of the same pyrite grain, 1 is the core, 2 is the rim. Analyses 3-4 are representative pyrite grains. Analyses 5-7 are gersdorffite.

be higher in the rim relative to the core. Many pyrite grains exhibit oscillatory banding in their rims. The bands do not consistently change in chemistry either toward or away from the rim contact. Instead they are quite random based on contrasting grey levels on a backscatter image. The banding is probably a consequence of slight changes in P-T-fluid chemistry conditions during the growth of pyrite rims.

Gersdorffite grains occur as fine grained blebs intergrown with chalcopyrite and more rarely Au as individual blebs between quartz-carbonate grains and on the rims of pyrite. Both gersdorffite and chalcopyrite are late in the system, predominately associated with Type 3 veins. Its association with Au is interesting and probably results from late Au remobilization. Its presence is not entirely unexpected considering the elevated Ni values in the TEAD komatiites and komatiitic basalts. It also adds support to the previous comment on the mobility of Ni in the Madrid system. Table 5.8 and Fig. 5.20 illustrate the chemical features of this mineral.

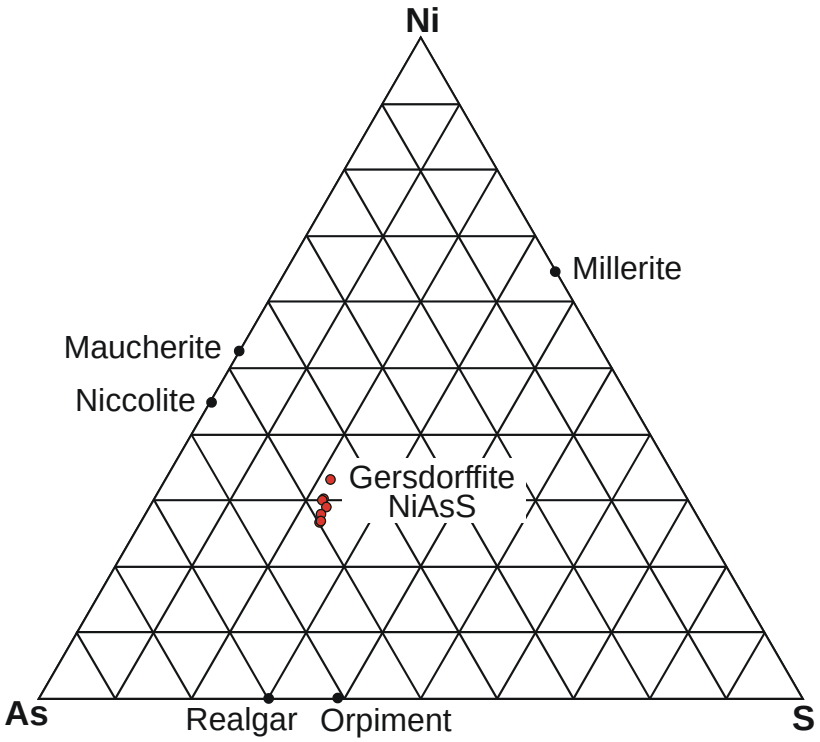

Fig. 5. 20 Ternary plot of gersdorfite from mineralized zones at Madrid (Yund, 1962)

CHAPTER 6

DISCUSSION

6.1 – Introduction

The goal of this thesis is to characterize the metallogenic framework of the Madrid Au system in the Hope Bay Volcanic Belt. This has been accomplished through documentation of the geology (field mapping, core logging and petrography) and the geochemistry (major/trace element, mass balance fluctuations and mineral chemistry) of mineralized and non-mineralized assemblages.

The features of the Madrid system discussed in the earlier chapters are here brought together into a comprehensive interpretation of the deposit genesis and the regional setting in which it formed. The first part of this chapter (section 6.2) discusses the results from Chapters 3.0 and 4.0 concerning how the primary igneous major and trace element geochemistry relates to magmatic processes and tectonic environment. This is an important consideration when interpreting the genesis of the deposit, as primary features (autoclastic and magma-sediment breccia textures, primary geochemistry of the mineralized units and structural elements) which are key controls on Au mineralization have ties to their environment of formation. The second part of this chapter (section 6.3) discusses the relationships of various features of the gold mineralized rocks at Madrid including alteration assemblages, mass balance fluctuations and mineral chemistries. The final part of this chapter (section 6.4) presents a metallogenic model to account for the gold concentration at Madrid.

6.2 – Magmatic Setting and Tectonic Evolution

6.2.1 – High-Ti Suites

Komatiites and komatiitic basalts at Madrid are classified as Al-depleted rather than the more common Al-undepleted type (Purvis, 1978; Nesbitt *et al*., 1979). However, unlike most Al-depleted komatiites, the rocks at Madrid have unusually elevated TiO_2 values and strong incompatible element enrichment. Rocks of similar chemistry are rare worldwide, suggesting that different magmatic processes/sources are involved in the genesis of the TEAD komatiites than those that give rise to the usual Al-depleted or Al-undepleted varieties. A few examples of TEAD komatiites and their interpreted genesis are described below.

TEAD komatiites documented from northern Norway by Barnes and Often (1990) are interpreted to have formed by 10-20% partial melting of garnet lherzolite at pressures >40 kb where garnet was a residual phase. TEAD komatiites from the Boston Township are thought to be derived from the undepleted portions of a plume from depths of approximately 300 km (80-100 kb) where majoritic garnet is either a residual or crystallizing phase (Stone, 1985; Stone *et al*., 1987; 1995; Xie *et al*., 1993). TEAD komatiites documented in the Wawa greenstone belt are interpreted by Polat *et al*. (1999) to be plume sourced oceanic plateau rocks derived from partial melting at depths of >400 km with garnet as a residual phase. Schaefer and Morton (1991), Tomlinson *et al*. (1999) and Hollings and Wyman (1999) describe TEAD komatiites in the Steep Rock and Lumby Lake area of the Western Superior Province. Tomlinson *et al*. (1999) suggest that the TEAD komatiites result from high degrees of deep partial melting derived from the

core/tail of a plume system. Barley *et al*. (2000) reported on TEAD komatiites from the Murchison Terrane of Western Australia. Based on their Ti-enriched Al-depleted character they suggest that the komatiites were derived from partial melts at depths >250 km with residual garnet. Textural features indicative of a hydrous melt (porphyritic textures, amygdules and volcaniclastic intervals) are explained by melt interaction with metasomitized or subduction modified mantle lithosphere rather than a primary hydrous mantle (Barley *et al*., 2000). Finally, Sproule *et al*. (2002) distinguishe between the Ti-enriched and Al-depleted varieties. The former are interpreted as melts derived from a plume head involving a dunite-harzburgite source at 20-80 kb while the latter are derived from a plume tail involving a garnet peridotite source at pressures of 60-90 kb.

TEAD komatiites and komatiitic basalts in the HBVB are interpreted to have formed by similar processes as described above. Alteration is not believed to be responsible for producing the unique geochemistry of these rocks as one would have to invoke mobility of elements that are traditionally viewed as strongly immobile. The smooth patterns exhibited by the incompatible elements on normalized multi-element diagrams and the well-separated groups on an Al_2O_3 vs. TiO_2 diagram also suggest alteration does not play a role. Contamination of the TEAD basalts by continental crust is not likely for a variety of reasons. Firstly, the SiO_2 values are lower than would be expected from a melt contaminated by continental crust. Secondly, the contaminating material would have to have a low Al_2O_3/TiO_2 ratio (<20) in order to explain the Al depleted character of the rock. Thirdly, contamination by continental crust does not explain the enrichment in Ti and other incompatible elements. Finally, the presence of

thick (up to several meters) argillite and chert beds and laminations are indicative of an oceanic, not continental, environment.

Thus, partial melting involving a residual garnet source is considered to be the most likely explanation for the genesis of these rocks. As noted by Pearce and Parkinson (1993), and Pearce (1996), garnet is an important phase in explaining the genesis of plume related within plate basalts. If garnet is either left as a residue or fractionated out, the resulting melt would have low Al values and high Ti (and Ti-associated elements) relative to the HREE's Y and Yb as these are preferentially retained in the garnet. This same logic is used in the interpretation of TEAD komatiites (Green, 1975; Nesbitt, 1979; Gale and Pearce, 1982; Ohtani, 1984; 1990**;** Ohtani *et al*. 1989; Barnes and Often, 1990; Xie *et al*., 1993; Arndt, 1994; Barley *et al*., 2000; Sproule *et al*., 2002). Although there is some dispute as to the exact depth and degree of partial melting, it is generally accepted by the various authors that TEAD komatiites are derived from a comparatively deep source (>250 km) in the stability field of majoritic garnet. The degrees of partial melting are debatable, but are probably sufficiently low so as not to melt all of the garnet and to cause significant enrichment in the incompatible elements. In contrast, Barley *et al*. (2000) argues for higher degrees of partial melting with the incompatible element enrichment (and a hydrous component) derived primarily from metasomatically altered or subduction modified mantle lithosphere.

The suggestion by Stone *et al*. (1995; 1997), Schaefer and Morton (1991), Capdevila *et al*. (1999) and Barley *et al*. (2000) that certain volcanological and geochemical features of the TEAD komatiite series may indicate the presence of a volatile phase may have relevance to the HBVB. Each of these authors describe the

presence of amygdules/vesicles, phenocryst phases and volcaniclastic rocks which are indicative of volatile phases escaping from the melt. Additionally, Stone *et al*., (1995; 1997) reports primary igneous amphibole in the TEAD komatiites of the Boston Township. Notably, amygdules are a relatively common texture found in the komatiites/komatiitic basalts at Madrid. Furthermore, the previously discussed harrisitic textured pyroxene in the TEAD komatiites may have formed by crystallization from a supercooled liquid brought on by degassing (Arndt *et al*, 1998). The presence of comminuted basalt clasts in flow breccias and peperitic sequences may or may not relate to escaping volatiles and associated explosive activity. Although these volcanic features may indicate the presence of volatile phases, it does not necessitate a primary hydrous mantle. As suggested by Barley *et al.* (2000) the source of volatiles may be related to a subduction component in the form of metasomatized or subduction modified mantle lithosphere. Given the interpreted tectonic environment at Madrid (plume influenced subduction zone) this conclusion is quite reasonable.

Whereas the above discussion accounts for the high-Ti and incompatible element enrichment character in the TEAD komatiitic and FETI transitional basalts, superimposed chemical variations due to source heterogeneities and fractional crystallization can also be detected. The elements Y and Yb are both elements that do not participate significantly in the processes that cause mantle heterogeneity. This may be because mantle enrichment/depletion only involves elements that are incompatible with the garnet lherzolite source. As the elements Ti-Y-Nb-Yb all act incompatibly during partial melting and fractional crystallization, their ratios (Ti/Y vs. Nb/Y) are useful for defining mantle heterogeneities. Fig. 4.10 illustrated significant variations between fractionation

related pairs i.e. the A6/A7 suites show less enrichment than the A2/A3/A4/A5 suites. In addition to chemical variations due to source heterogeneities, the effects of fractional crystallization can also be observed. A great deal of evidence was presented to suggest that the FETI transitional basalts are related to the TEAD komatiites/komatiitic basalts by fractional crystallization. This included fractionation paths involving Zr vs. Cr, Zr vs. Ni, Zr vs. Y, Zr vs. TiO_2 and Zr vs. Nb. Higher MgO values and lower SiO_2 and TiO_2 values in the TEAD komatiitic basalts relative to the FETI basalts also attest to the two being related by fractional crystallization. Furthermore, on MORB and chondrite normalized multi-element and REE diagrams the TEAD komatiitic basalts clearly fractionate smoothly upward toward increasing incompatible element enrichment in the FETI transitional basalts.

6.2.2 – Tholeiitic Basalts

The high-Fe tholeiitic basalts and basaltic andesites are well interpreted as primitive island arc tholeiites. The Nb anomaly relative to Ce on a MORB normalized diagram is characteristic of volcanic arc basalts. Its depletion relates to the conservative-non conservative behavior of these elements: Nb acts conservatively remaining in the subducting slab while Ce is transported from the slab to the sub-arc melting column (Pearce, 1996). Elements of low ionic potential (K, Rb, Sr, Ba) should also be elevated relative to high ionic potential elements, however, these trends are not reliable since low ionic potential elements are also mobile during metamorphism and hydrothermal metasomatism. The lack of high Ti/Y ratios characterized by the within-plate basalts relates to higher degrees of partial melting due to addition of water from the subducting

slab. The low absolute abundance of high ionic potential elements relative to MORB is similar to other tholeiitic volcanic arc basalts, however, their elevated Cr-Ni is significantly higher than values reported by Pearce (1982), Jakeš and Gill (1970) and Jakeš and White (1972). The depletion of the incompatible elements and Cr relative to MORB in most island arc tholeiites is explained by the presence of stable incompatible-element hosting phases in the melt residue, higher degrees of partial melting or melting of an already depleted source. As the Cr-Ni values are significantly elevated relative to MORB (assuming a normalizing value of Cr=250 ppm; Pearce, 1982) the tholeiitic rocks at Madrid are more primitive than N-MORB. This more than likely reflects a depleted source in the upper mantle related to the earlier extraction of melts (Pearce, 1995).

It has been stated in Chapter 4 that the high-Fe tholeiitic basalt suites and basaltic andesites do not relate to each other by simple fractionation or degrees of partial melting for a variety of reasons. This is especially evident on a Cr-Ni binary plot where the variolitic high-Fe tholeiites define a separate trend from the non-variolitic tholeiites and basaltic andesites. Furthermore, Zr values in the basaltic andesites do not match with their more evolved bulk rock chemistry relative to the high-Fe tholeiites. If the oddities in chemistry were a result of crustal contamination, then one would expect different shapes on the multi-element plots. However, only the absolute abundances change between the suites suggesting crustal contamination is not a realistic explanation. The juxtaposition of the basaltic andesites with the high-Ti series rocks may explain their elevated Cr-Ni as these elements were shown earlier to be somewhat mobile. The lower Zr values in the basaltic andesites may be explained by greater interaction with subduction derived metasomatic *fluids* (marked by increases in non-conservative

elements) or less interaction with subduction derived *melts*, in which Zr can act non-conservatively (Pearce and Parkinson, 1993; Pearce, 1995) as compared with the high-Fe tholeiites.

The chemistry of arc rocks may be influenced to different degrees by a variety of sources and processes. The fertility of the mantle wedge, composition of subducting slab, composition and amount of subduction-derived fluids and melts, interaction of melts with the mantle lithosphere and influence of temporally overlapping plume related processes may have all played a role making for a very complex system. Tholeiitic arc volcanism brackets plume related volcanism, with chemistries that indicate a depleted source influenced by subduction derived fluids. Basaltic andesites at Madrid are spatially associated with the high-Ti suites and contain abundant argillite. This indicates they were deposited into a similar tectonic setting at a similar time. They may be a sort of compositional bridge marking the transition back to high-Fe tholeiite volcanism.

6.2.3 – Discussion

The high-Ti suites and the tholeiitic basalts are geochemically and genetically distinct suites which overlapped in time with each other. Arc volcanism, represented by the tholeiitic basalts, was interrupted by plume-related volcanism represented by the high-Ti suites. Plume related volcanism was likely sporadic and long lived as evidenced by the abundance of argillite throughout. The within-plate affinity and abundance of sedimentary rocks indicate an extensional basinal setting; potentially rifting of the developing arc. Felsic volcanism partially overlapped with mafic volcanism in the Madrid Corridor as is evident by interbedded 2689.4 +4.0/-3.6 Ma (Sherlock and

Carpenter, 2003) dacitic volcaniclastics in the Wolverine Mafics. The intrusion of the Wolverine Porphyry at 2686 Ma and its subsequent venting gave rise to the Windy Lake Felsics. The porphyry sill was to a large extent controlled by the stratigraphic contact between the plume-related high-Ti basalts and the arc-related tholeiitic basalts along its north-south limb. The east-west segment of the HBDZ may have followed the primary volcanic contact between the variolitic and non-variolitic high-Fe tholeiites which has subsequently been structurally modified. These events occurred before significant deformation as the volcanic stratigraphy was still horizontal. Based on clasts of altered and veined basalt in the Windy Lake Felsics and other evidence presented below an alteration event must have occurred near the time of the intrusion of the Wolverine Porphyry. This alteration event most likely marks the start of D_1. Alteration and deformation related to this event helped to structurally soften the rocks within and bordering the HBDZ which would later become preferentially mineralized, altered and overprinted by D_2 deformation.

6.3 – Mineralization

As discussed in previous chapters gold is situated predominately in Types 1 & 2 veins and their associated quartz-ankerite-sericite altered basalt/argillite selvedges. It occurs as coarse free flecks visible to the naked eye and as microscopic grains either isolated in silicates or as inclusions in sulphides. Coarse clusters of gold grains may be found associated with sulphides (pyrite +/- chalcopyrite and gersdorffite), stylolitic fractures or clast/vein margin contacts. Au is also found as inclusions in sulphide minerals (pyrite, chalcopyrite and gersdorffite) at the microscopic scale. In pyrite it

typically occurs as high Au low Ag blebs toward the more arsenian - less inclusion filled rims of grains. The textural and chemical differences between the core and rim of pyrite grains may relate to changing P-T-fluid chemistry conditions during the growth of pyrite. Alternatively they may represent a second stage of pyrite growth onto previously formed pyrite grains. Textural relationships between pyrite and chalcopyrite-gersdorffite indicate that the latter two sulphides are late in the system. This suggests that either new gold was introduced into the system after the first event or Au has been remobilized and reprecipitated with gersdorffite + chalcopyrite during late/post D_2.

6.3.1 – *Controls on Gold Mineralization*

Several mechanical and chemical controls on Au mineralization and associated alteration occur at a variety of scales in the Madrid system and are detailed below:

1) The HBDZ is considered to be the primary conduit for migrating hydrothermal fluids which gave rise to Au mineralization in adjacent mechanically and chemically amenable rocks. Smaller scale S_1 shear structures which are likely splays off the HBDZ also structurally controlled mineralization, as is evident on the southern tip of Patch Peninsula and north of Patch Thumb. Alteration and mineralization is spatially related to the hangingwall region in the north-dipping Naartok area and the western side of the steeply dipping Suluk deposit. Evidence for an early alteration-deformation-(mineralization?) event is presented below and suggests that the mineralized rocks were structurally prepared early on, making them more amenable to mineralizing fluids. There is no argument that all other controls on mineralization at Madrid are secondary to the HBDZ.

2) Lithological contacts play a significant role in the distribution of alteration and mineralization at Madrid. This is especially evident at the Perrin deposit. Although still spatially related to the HBDZ, the Perrin deposit occurs in hangingwall TEAD komatiitic basalts which overlie FETI transitional basalts. The contact between the two lithologies is marked by the sharp truncation of mineralization, alteration and deformation. Other contacts in the Madrid system have also acted as fluid migration pathways. In the Naartok area, auriferous Type 2 veins can commonly be found at major lithological contacts and paralleling the HBDZ. Contacts between basalt and interbedded argillite have a significant effect on the distribution of deformation, alteration and mineralization. This is particularly evident in the Suluk area where the intensity of sericite-ankerite alteration, deformation and usually suphidization + Au mineralization increases toward argillite beds. This observation attests to strain partitioning into the argillite beds with their margins acting as pathways for mineralizing hydrothermal fluids.

3) Primary textural heterogeneities played a significant but smaller scale role during mineralization. Field mapping and core logging has shown that a large component of the TEAD komatiitic basalts are primary (autoclastic) breccias. Such units would tend to take on a greater proportion of deformation via strain partitioning and conceivably be more permeable to hydrothermal fluids. Furthermore, the more mafic TEAD komatiitic basalts would take on a greater proportion of deformation relative to other, less mafic units. Magma-wet sediment interaction textures (peperitic textures) are common in the TEAD komatiitic basalts and typically host Au mineralization. The peperitic units are thought to be preferentially mineralized for a variety of reason, both mechanical and chemical. As with the flow breccias, peperitic units would be more prone to deformation

and have greater permeability than massive basalt units. In several cases the contact between matrix argillite and juvenile basalt fragments are more strongly sericitized and sulphizided than the rest of the basalt. This indicates that the basalt-argillite contact was preferentially exploited by hydrothermal fluids, even on a handsample scale. Significantly, the peperitic basalts at Madrid and in other Au deposits are not well documented or described. Although argillaceous peperites on their own are not likely to be prospective gold targets, their mechanical and chemical attributes make these rocks more permeable to migrating fluids and probably more chemically amenable to mineralization as their argillaceous component would reduce auriferous fluids. When combined with the structural features of the Madrid deposit, peperitic units in TEAD komatiitic basalts can be regarded as an important exploration target.

4) The primary geochemical characteristics of mineralized lithotypes have an important role in the precipitation of gold at Madrid. Considering the elevated pyrite contents, its association with gold, and the lack of base metal signatures Au was likely transported as a bisulphide ($Au\text{-}(HS)_2$) complex rather than a chloride complex. Various physiochemical changes may take place which causes Au to precipitate from solution and include changes in pressure, temperature, oxygen activity, Ph and fluid composition. When Au is transported as a bisulphide complex, changes in Ph do not significantly alter the fluid to cause gold deposition (Romberger, 1990), whereas decreases in temperature usually lead to lowering of the bisulphide complexes solubility (Seward, 1973). However, many consider oxidation of the fluid to be the most effective way to promote Au precipitation (Seward, 1973, 1984, 1991; Romberger, 1986a/b, 1990; Shenberger and Barnes, 1989). Oxidation of the fluid may be promoted in a variety of ways. Abundant

Fe-Ti oxides in the mineralized TEAD komatiitic basalts at Madrid are thought to be involved in Au deposition by exchanging oxygen with the fluid resulting in oxygenation of the fluid and destabilization of the Au-bisulphide complex (Romberger, 1990). Sulphidization of wallrock made possible by H_2S in the fluid and available Fe in the rock to form pyrite will also destabilize the bisulphide complex by lowering the activity of S and causing Au to precipitate (Romberger, 1986a; 1990; Shenberger and Barnes, 1989). The frequent appearance of fine grained hematite in the Madrid system, especially at Suluk suggests the presence of an oxidized fluid. Hematite commonly overprints pyrite, indicating the deposition of pyrite and gold was followed by hematite as the fluid became progressively more oxidized.

The presence of carbonaceous material and its role in gold precipitation has been described and debated by a number of authors (Springer, 1983; Downes *et al*., 1984; Springer, 1985; Wilson and Rucklidge, 1986; 1987; Cox *et al*., 1991; Coad *et al*, 2000; Bierlein and Cartwright, 2001). Amorphous carbonaceous material best observed in the Suluk area constitutes a minor component in mineralized rocks at Madrid. The source of the carbon is likely from the abundant (carbonaceous) argillite units. Remobilization during hydrothermal metasomatism deposited it in quartz-carbonate veins as dark material in stylolites and as fine grained dustings in the volcanic flows. The light grey charcoal colour of some of the basalts at Suluk are a result of this remobilized carbon, and are reminiscent of the so-called 'grey zones' in the Hoyle Pond and Owl Creek deposits of the Timmins area (Downes *et al*., 1984; Wilson and Rucklidge, 1986; 1987; Coad *et al*, 2000).

The importance and exact role of carbonaceous material in gold deposition continues to be debated, however, the chemical attributes of carbon and its occurrence at several gold deposits suggest it is involved. The following section is only a cursory examination at some of the ways carbon may be directly involved in gold precipitation at Madrid and makes no definitive statements on precise reactions or fluid evolution pathways.

Carbonaceous material is known to cause fluid reduction which some author's believe is an important mechanism for destabilizing the Au-bisulphide complex (Shenberger and Barnes, 1989; Hayashi and Ohmoto, 1991). Consequently, this may be a mechanism for Au precipitation in parts of Madrid. However, the evidence presented earlier suggests that fluids were predominately oxidizing. Alternatively, the formation of methane from C (Eq. 6.1; Naden and Shepherd, 1989) may be involved. Removal of the methane and H_2S, probably by phase separation/immiscibility, is an efficient mechanism

$$C + 2H_2O \text{ --> } CH_4 + 2[O] \qquad \text{Eq. 6.1}$$

for Au precipitation as the oxygen activity of the residual solution becomes progressively greater thus destabilizing the Au-bisulphide complex (Naden and Shepherd, 1989; Drummond and Ohmoto, 1985). The low solubility of methane in aqueous solutions also suggests that very little fluid-wallrock interaction needs to be invoked to reach fluid immiscibility (Naden and Shepherd, 1989). The gold bisulphide complex may also be destabilized by direct reaction with the C-derived methane (Eq. 6.2; Norman and Blamey,

2005). Increases in methane fugacity will tend to drive the reaction to the right destabilizing the Au complex.

$$8AuHS + 5CH_4 + 3CO_2 = 8C + 8Au + 8H_2S + 6H_20 \qquad \text{Eq. 6.2}$$

Thus, the primary bulk rock chemistry of the Au-bearing lithologies at Madrid played a significant role in their mineralization. It is interesting to speculate why the TEAD komatiitic units are preferentially mineralized over the FETI transitional basalts as their overall chemistries are quite similar. It is likely that the elevated MgO values in the komatiitic basalts acted as a sink for CO_2. Decarbonization and decreasing temperatures of the hydrothermal fluids then promoted preferential gold precipitation in these rocks.

6.3.2 – *Timing of Mineralization*

Au has been shown to exhibit a positive correlation with mass gains in Na which are clearly related to the Type 2 albitic veinset. Type 2 veins at Madrid have been partially deformed and folded by D_2 but may also contain clasts of unoriented foliated basalt/argillite and crosscut foliations at small angles. This is suggestive of syn D_2 emplacement. However, the basaltic rocks that they overprint are typically already stockworked by auriferous Type 1 veins and altered to quartz-ankerite-sericite. This is indicative of an earlier alteration-mineralization event that pre/syndates the 2686 Ma Wolverine Porphyry. Thus, Type 2 veins may either represent another Au event or remobilization of gold already present in the system. Further evidence for an earlier alteration event includes:

1) The rare bomb-sized clasts of quartz-ankerite altered and veined basalt found in the Windy Felsics suggests a pre/syn 2686 Ma alteration and veining event. Minute quartz-ankerite altered and veined fragments occur interior to the Windy Lake felsics immediately overlying the mafic-felsic break in the western Madrid area. Although difficult to prove, it is interesting to speculate how much of the supposed ankerite alteration in the immediate Windy Felsics is detrital, derived from alteration marginal to the HBDZ before/during the intrusion of the Wolverine Porphyry.

2) "Cleavage zones" in the Naartok hangingwall of the HBDZ are interpreted as areas that have been preferentially overprinted during D_2 deformation. If the reason they are preferentially deformed is related to earlier alteration which structurally softened the rock, this further suggests a pre D_2 alteration event.

3) A mafic dyke in the Naartok area crosscuts the surrounding quartz-ankerite alteration and veining, but is foliated by S_2. This is evidence to suggest pre D_2 mineralization but could also be interpreted as syn D_2.

4) East-west trending (110^0-120^0) structures are interpreted as D_1 shears related to the main HBDZ structure as the associated S_1 and quartz-ankerite veins are folded by F_2 folds and exhibit S_2 foliations. Such structures are known to concentrate and bound quartz-ankerite-sericite alteration zones. One of these structures north of Patch Thumb marks the transition from E-W trending stratigraphy and quartz-ankerite-sericite alteration/veining to northwest striking stratigraphy with minimal alteration. This is evidence to suggest a D_1 structural control on mineralization.

5) Mass balance calculations identify elemental mobility accompanying an early K-metasomatic event and later Na-metasomatic event associated with much of the Au mineralization. Samples which contain albite also contain micas with a larger paragonitic component whereas those that do not have albite have micas with low paragonite values. This suggests that the albitization and paragonitization event were both caused by the same Na event. Since the albite occurs predominately in Type 2 stockwork systems which crosscut the main S_2 foliation (but are still deformed by it) then the mica-defining foliations formed early. This suggests that the phengitic micas were later paragonitized during the Na-metasomatism event. This is consistent with mass balance trends and can be interpreted in one of two ways: a progressive hydrothermal system, beginning with K-metasomatism and ending with Na-metasomatism as temperatures drop (Kerrich, 1983) or the phengitic micas represent an earlier phase of alteration not directly related to the Na-metasomatism event. The existence of Type 1 veining, which have phengitic mica rich selvedges combined with the evidence above lends credence to the latter interpretation.

6.3.3 – *Mass Balance Considerations*

Very consistent results for elemental gains/losses were obtained via mass balance calculations for the TEAD komatiitic and FETI transitional basalts. As the TEAD komatiitic basalts constitute >90% of the mineralized rocks at Madrid, they are the only ones discussed in detail below. The variations of each of the discussed elements are thought to be accurate and not influenced by within-flow fractional crystallization based on several lines of evidence:

1) The Al_2O_3 values show very little fluctuation in least altered samples for each of the individual subsuites. If within-flow primary chemical variations were involved, one would expect to see changes in the Al content as Al will vary from the top of a fractionated flow (high Al) to the bottom of the flow (low Al).

2) Fluctuations in Fe_2O_3 and MgO are positively correlated in both mineralized and unmineralized units. If within flow crystallization were a major issue, than these two elements should show a negative correlation, especially in the least altered unmineralized samples. The positive correlation is better explained by progressive sericite, carbonate and/or chlorite alteration.

3) Weakly and strongly mineralized units show very comparable elemental gains/losses. Non-mineralized units also show consistent results. Within each of these two groups, different LA precursors (A2-A7) were used. If within flow crystallization were an issue, one would expect to see these primary variations in the LA samples and the resultant elemental gains/losses of their associated subsuites. For example, one would not expect consistent results between mineralized samples of the A2-A4-A6 suites if their LA precursors had different primary chemistries relative to their altered equivalents.

Variable gains and losses of major and trace elements were used to characterize the different styles, intensities and timing of alteration mineralogy overprinting the mafic volcanics at Madrid. Fluctuations in the major elements SiO_2, Fe_2O_3, MgO, Na_2O and K_2O and the trace elements Rb, Ba, Cr and Ni proved most useful for defining sericitization, chloritization and carbonitization trends. Non-mineralized TEAD and

FETI basalts showed quite consistent gains in Fe_2O_3, MgO, SiO_2 and CaO and minor gains/losses in Na_2O and K_2O owing to the processes of chloritization, carbonitization and potentially silicification. Mineralized TEAD komatiites showed consistent gains in CaO, Na_2O, K_2O, SiO_2 and W and losses in Fe_2O_3 and MgO owing to the processes of sericite replacing chlorite, ankeritization, albitization/paragonitization and silicification/quartz vein stockworking.

Elevated Au values at Madrid generally do not correlate *directly* with elevated sulphides, however, sulphidized rocks correspond to higher gold grades than non-sulphidized rocks. In contrast, Au does show a well defined positive correlation with mass gains in Na and W. The W gains correlate with both Au and Na. It is likely present in the form of scheelite as in most other Archean mesothermal gold systems, but was not identified in thin section, possibly because of its small grain size and modal abundance. The source of the Na-W-Au bearing fluids are unknown, but similar metal associations have been noted in other Archean Au deposits (Bell *et al.*, 1989; Jones, 1992; Anglin *et al.*, 1996; Armstrong, 1997). At least some portion of the Na budget was provided by the breakdown of plagioclase in the Wolverine Porphyry. A mass loss of Na in the porphyry and a mass gain in Na in mineralized zones suggests this interpretation is correct. Despite this, the Wolverine Porphyry is volumetrically too small to supply all the Na to the system, thus, Na was already present in the mineralizing fluid.

One of the interesting results obtained from the mass balance calculations was the behavior of Cr-Ni, elements that are generally thought to be immobile. Mineralized units show consistent losses of these two elements while non-mineralized units show consistent gains. The loss of these elements in mineralized zones probably relates to the

breakdown of Cr-bearing phases such as pyroxene, spinel or chromite. It is possible that these rocks are the source of Cr-Ni gains in the non-mineralized units. Cr and Ni can both be accommodated in the chlorite structure, which happens to be the most abundant alteration mineral in the non-mineralized units. Based on data presented in Chapter 4.0 the Cr-Ni loss event occurred early in the systems alteration history.

6.3.4 – Mineral Chemistry Considerations

The variation in mineral chemistry of the white mica species proved to be most useful in defining the detailed paragenetic relationships of the gold mineralization. The distribution of Na in paragonitic micas is strongly spatially controlled with true paragonite occurring only within basalt and porphyry in the HBDZ. Paragonitic values decrease rapidly outward into the mineralized zones. The different mica compositions are likely reflecting both the chemistry of the host rock and the chemistry of the hydrothermal fluids. As the porphyry contains phenocrysts of sodic plagioclase, it is likely that the paragonitic character of their micas is related to the breakdown of feldspar. The progressive replacement of sodic feldspar by white mica was shown in Plate 3.24 suggesting this conclusion is accurate. An overall mass loss of Na in the porphyry indicates that not all the available Na was retained in the mica structure. Samples of basalt in the HBDZ also have micas with a strongly paragonitic character. In this case the mica chemistry likely relates to the composition of the fluid with the Na in part being sourced from the adjacent Wolverine Porphyry. The phengitic micas in the mineralized units formed during an early K-metasomatism event. Their elevated phengitic components are reflective of the primary chemistry of the mineralized basalt indicating

that both fluid and wall rock composition contributed to their chemistry. Subsequent paragonitization of the phengitic micas coincides with later Na-metasomatism, albite veining and Au mineralization.

An interesting feature noted in core is that samples with especially green (fuchsitic) mica are commonly less sulphidized/mineralized than samples with less chromian mica. Possible explanations for this observation are:

1) Rocks containing the Cr-bearing micas may be indicative of a more Mg-Cr rich flow base. The bases of komatiitic flows would presumably be lower in Fe-Ti, be more massive and not have any argillite. This may make these portions of the flow less chemically and mechanically amenable to sulphidization and (presumably) mineralization. It would also explain the preponderance of fuchsitic phengites. However, as was discussed above, there does not appear to be significant variation in the primary chemistry of individual subsuites. Despite this, it is acknowledged that small chemical fluctuations related to fractional crystallization are likely present, but are masked by the larger fluctuations occurring during intense hydrothermal alteration. Thus, this explanation may partly account for the presence of the fuchsitic phengites.
2) The green micas may be reflecting different P-T conditions, probably during the same K-metasomatic event that formed the non-Cr phengitic micas. These micas may represent a higher temperature expression of alteration after Cr-bearing mafic minerals with further alteration and fluid interaction upgrading them to lower Cr values, i.e. a more muscovitic phengite, during K-metasomatism. Subsequent Na metasomatism resulted in paragonitization of the phengites. As discussed earlier, samples of phengitic

mica, including the Cr-rich variety, only show elevated paragonitic components when albite is present in related Type 2 veins. Further proof of this can be seen in the mass balance calculations where phengitization (fluxes of Ba-Rb-Cr) were shown to predate Na fluctuations related to albitization and paragonitization. The reason why these two mica species are not resolvable at the thin section scale and on the EMP relate to extremely small scale interstratification of the micas of differing composition. This has important implications for the timing of mineralization as well as explaining why the mineralization is situated where it is i.e. the site was already structurally prepared during D_1 by carbonate-mica alteration.

The results and limitations of carbonate geothermometry were discussed in Chapter 4 and are here interpreted. Two distinct groups of temperatures were identified, one relating to carbonate alteration in the mafic volcanics distal to veins (275-400 ^{o}C) and one related to the veins themselves (200-250 ^{o}C). These results may be interpreted in a variety of ways, however, in light of the evidence presented above, the higher temperature values are thought to represent the earlier alteration event (K-metasomatism) while the lower temperatures represent the later Na-metasomatism event and associated D_2 veins. The higher temperature values were gathered predominately from samples that contained fuchsite and magnesitic carbonate. The magnesitic carbonate was typically partially replaced by late ankerite suggesting an earlier origin for the magnesite, likely coincident with the formation of (fuchsitic) phengite.

The P-T conditions for Cr versus non Cr phengites are not well documented in the literature, however, a few relevant examples do exist. Morata *et al.* (2001) report on fuchsitic micas from the Almadén mercury mining district in Spain where they define

two separate alteration events. The earliest phase is defined by the formation of fuchsitic micas at the expense of Cr-spinel and the precipitation of ankerite from relatively hot CO_2 - K rich fluids. $^{40}Ar/^{39}Ar$ dates of fuchsitic micas range from 365 to 427 Ma. The second event is marked by the progressive destabilization of fuchsitic micas as overprinting argillic alteration results in illite (a form of sericite) formation. Fluid temperatures are suggested to be sub 270 ^{o}C. $^{40}Ar/^{39}Ar$ dating of illites yield an age of 361 ± 2 Ma. Thus, two temporally and chemically distinct alteration events have been identified, with the earlier, higher temperature phase coinciding with fuchsite formation. The second example comes from the geochemically and mineralogically zoned hangingwall of the polymetallic Hellyer VHMS deposit in Tasmania. The hangingwall is zoned outwards from a high temperature fuchsitic core to a distal lower temperature sericite zone (Gemmell and Fulton, 2001). Cr, Ba, V and Ni all increase toward the core of the deposit. Thus, in both systems, the fuchsitic altered zones are considered to be the higher temperature phase relative to the non fuchsitic phengites.

Based on this information fuchsitic phengites at Madrid are interpreted to be a higher temperature phase which was strongly influenced by the primary chemistry of the TEAD komatiites. In contrast non fuchsitic weakly phengitic muscovites characteristic of the Au-bearing units appear to be more influenced by the fluid chemistry. These differences can be attributed to degrees of fluid-wall rock interaction with the more phengitic micas being progressively muscovitized as K-rich fluids continue to compositionally mature the micas.

6.4 – Genetic Model for the Madrid Gold System

The following sequence of events is proposed to explain the genesis of the Madrid gold system:

1) Initial stages of primitive tholeiitic arc volcanism related to a subducting oceanic plate resulted in the deposition of high-Fe tholeiites.

2) Emplacement of the plume-related TEAD komatiites/komatiitic basalts and FETI transitional basalts derived from depths in excess of 250 km with majoritic garnet as a residual or fractionating phase. Plume volcanism was likely sporadic, within an arc rift setting and coincided with argillite sedimentation. Amygdules, autoclastic breccias and harrisitic textures suggest the presence of a volatile phase which may be related to subduction derived metasomatic fluids. Deposition of volcanics onto tholeiitic flows was likely related to rifting of the arc system.

3) Basaltic andesite volcanism occurred toward the end of the TEAD komatiitic and FETI transitional basalt volcanism. This stage of volcanism probably occurred in a similar setting as evidenced by the abundance of argillite. It appears to mark the transition from plume related volcanism back to tholeiitic arc volcanism.

4) Continuation of arc-related volcanism with the variolitic tholeiites overlain by the non-variolitic tholeiites. Felsic volcanism overlaps with mafic volcanism as evidenced by 2689 Ma felsic volcaniclastic intervals in the non-variolitic tholeiites.

5a) Early alteration event mostly affecting the TEAD komatiitic basalts proximal to the komatiitic-tholeiitic contact (HBDZ) marked by (fuchsitic) phengite, magnesite and

potentially the spongy arsenic poor pyrite. This alteration phase may be coincident with Type 1 veining and stockworking and possibly the first stage of Au mineralization. Carbonate geothermometry suggests temperatures around 300-400 ^{o}C.

5b) Intrusion of the Wolverine porphyry, venting, and deposition of the Windy Lake Felsics at 2686 Ma. The intrusion of the porphyry is likely coincident with the earliest stage of alteration (D_1). This would explain the presence of quartz-ankerite-sericite altered and veined clasts interior to the Windy Felsics and other evidence presented earlier.

6a) Belt-wide D_2 deformation marked by north-south trending foliation and fold axes accompanied by upper greenschist facies (epidote-actinolite) metamorphism.

6b) Au-related Na-alteration and veining event characterized by Type 2 quartz-ankerite-albite-sericite-pyrite-Au assemblages with temperature around 200-250 ^{o}C. Introduction of paragonitic component to phengitic micas. Overgrowth of previously formed pyrite grains by arsenian inclusion-free rims with Au inclusions near the end of D_2.

7) Formation of coarse quartz-ankerite-chalcopyrite-gersdorffite Type 3 veins and remobilization or reintroduction of gold. Non-penetrative D_3 deformation marked by crenulated S_2.

The Madrid gold system therefore comprises protracted multistage structurally controlled alteration and vein sets related to K-metasomatism during early porphyry intrusion and late D_2 Na-metasomatism and Au deposition. Future work in the Madrid system should focus on better defining the stratigraphy of the mineralized TEAD komatiitic basalts, especially where they come into contact with the FETI transitional

basalts (i.e. northern Perrin). A study of other potentially economic metals in the Madrid system may also be warranted. Although Ni values are an order of magnitude lower than economic concentrations, the potential for PGE mineralization does exist.

CHAPTER 7

CONCLUSIONS

7.1 – Final Remarks

The important features of the Madrid deposit which have been identified in this study are:

1) The mafic volcanic rocks in the Madrid Corridor comprise two genetic types: (i) Ti-rich Al-depleted (TEAD) komatiites and komatiitic/transitional basalts are dark green to black in colour, show harrisitic and pseudocumulate textures, are Fe-Ti-Cr-Ni enriched, have elevated incompatible elements with preferential enrichment in the LREE's (La/Yb_n = 2.5-7.5) and plot as within-plate basalts; and (ii) High-Fe tholeiitic basalts and basaltic andesites are by comparison lighter in colour, have lower Fe-Ti-Cr-Ni values, flat chondrite normalized REE patterns (La/Yb_n = 1-3) and exhibit a primitive tholeiitic island arc signature. Together, these two lithogeochemically distinct groups represent different tectonic environments. TEAD komatiitic basalts were likely derived from the lower levels of a plume system (>250 km) in the stability field of majoritic garnet. The incompatible element enrichment may be explained by low degrees of partial melting of an enriched source, or mixing with incompatible-element enriched melts. The presence of amygdules, harrisitic textures, flow breccias and peperitic units may be indicative of a volatile phase which could be derived from fluids shed off of a subducting oceanic plates. The abundances of peperitic textures and interflow argillite suggests that volcanism was synsedimentary, sporadic and within a basinal setting. The high-Fe tholeiitic basalts and

basaltic andesites relate to subduction and associated arc volcanism. The depletion in incompatible elements and enrichment in Cr-Ni relative to MORB indicate a more primitive composition than MORB likely related to melting of a depleted source. The lack of argillite throughout this succession suggest a different depositional environment than the Ti-rich suites or higher rates of volcanism. The oddities in chemistry between the tholeiitic units suggests a complicated magmatic history, probably involving variably enriched-depleted source rocks and variable contributions by subduction derived fluids and melts. Basaltic andesites, which occur interlayered and at the upper boundary with the high-Ti suites likely represent a transition from plume volcanism back into arc volcanism. The relative timing of these events based on stratigraphic relationships indicates that arc volcanism was interrupted by plume volcanism for a period of time. The plume related mafics may correspond to rifting of the primitive arc setting. Subsequent arc volcanism gave rise to the variolitic and non-variolitic high-Fe tholeiites respectively.

2) The N-S contact between the TEAD komatiites and high-Fe tholeiites served as a magma conduit for the Wolverine Porphyry. Similarly, the E-W contact between the variolitic and non-variolitic high-Fe tholeiites was exploited by the porphyry. Its subsequent venting circa 2686 Ma gave rise to the Windy Lake Felsics which overlie the mafic volcanic succession. The intrusion of the porphyry and deposition of its associated felsic volcaniclastics likely initiated D_1 in the mafic platform.

3) Au deposits in the Madrid Corridor are situated adjacent to the HBDZ and in subsidiary D_1 splays. In addition to a magma conduit, the HBDZ also acted as a conduit for mineralizing hydrothermal fluids and is considered the primary control on gold

mineralization. Adjacent mineralized rocks are almost exclusively TEAD komatiites and komatiitic basalts. They have been preferentially mineralized for a number of reasons relating to their mechanical and chemical attributes.

4) Numerous lines of evidence were given to show that an early alteration event pre/syn dates the intrusion of the porphyry. This event appears to be responsible for shearing along the HBDZ and subsidiary splays, a large portion of the fuchsite-phengite-magnesite alteration and foliation parallel dark coloured quartz-ankerite veins, an early porous stage of pyrite formation, and potentially the earliest stage of gold mineralization within the TEAD komatiitic basalts. This early event is characterized by hot (275-400 ^{o}C) CO_2 and K rich metasomatic fluids. Postdating this event the main stage of gold mineralization is marked by Na metasomatism, quartz-ankerite-albite veining/stockworking, coarse gold deposition and second stage pyrite growth with Au inclusions occurring late D_2. This second event is characterized by lower temperature (200-250 ^{o}C) fluids. Mass balance calculations for mineralized rocks indicate consistent gains in CaO, Na_2O, K_2O, SiO_2, W and S and losses in Fe_2O_3 and MgO corresponding to sericitization, albitization, carbonitization, silicification and sulphidization. Post D_2 quartz-ankerite veining is partly responsible for remobilizing gold into chalcopyrite and gersdorffite.

5) Regional metamorphism is marked by upper greenschist (epidote-amphibole) facies conditions. The regional D_2 deformation produced a N-S fabric preferentially developed in previously altered and deformed areas i.e. strongly overprinting the HBDZ and adjacent TEAD komatiitic basalts.

REFERENCES

Agnerian, H. 2003. Report on the Hope Bay Project. Miramar internal report, Roscoe Postle Associations Inc. September 2, 2003. 206p.

Amstutz, G.C. 1968. Spilites and spilitic rocks. *In* Basalts - The Poldervaart Treatise on Rocks of Basaltic Composition. *Edited by* H.H. Hess and A. Poldervaart. Interscience Publishers, New York and London, International. pp. 737-753.

Anglin, C. D., Jonasson, I. R. and Franklin, J. M. 1996. Sm-Nd dating of scheelite and tourmaline; implications for the genesis of Archean gold deposits, Val d'Or, Canada. Economic Geology and the Bulletin of the Society of Economic Geologists, **91:** 1372-1382.

Anovitz, L.M. and Essene, E.J. 1987. Phase Equilibria in the system $CaCO_3$-$MgCO_3$-$FeCO_3$. Journal of Petrology, **28:** 389-414.

Armstrong, 1997. Variations in silicate and sulphide mineral chemistry between free-milling "metallic" and refractory "invisible" gold ores, Con Mine, Yellowknife, N.W.T. Unpublished Ph.D. thesis, The University of Western Ontario, 317p.

Arndt, N.T., Naldrett, A.J. and Pyke, D.R. 1977. Komatiitic and iron-rich tholeiitic lavas of Munro Township, Northeast Ontario. Journal of Petrology, **18:** 319-369.

Arndt, N., Ginibre, C., Chauvel, C., Albarede, F., Cheadle, M., Herzberg, C., Jenner, G., and Lahaye, Y. 1998. Were komatiites wet? Geology, **26:** 739–742.

Arndt, N. T. 1994. Archaean komatiites. *In* Archaean Crustal Evolution. *Edited by* K.C. Condie. Elsevier, Amsterdam, pp. 11–44.

Bailey, S.W. 1984. Classification and structures of the micas. Reviews in Mineralogy, **13:** 1-12.

Barley, M.E., Kerrich, R., Reudavy, I. and Xie, Q. 2000. Late Archaean Ti-rich, Al-depleted komatiites and komatiitic volcaniclastic rocks from the Murchison Terrane in Western Australia. Australian Journal of Earth Sciences, **47:** 873-883.

Barnes, S.J. and Often, M. 1990. Ti-rich komatiites from northern Norway. Contributions to Mineralogy and Petrology, **105:** 42-54.

Barrett, T.J. and MacLean, W.H. 1994a. Mass changes in hydrothermal alteration zones associated with VMS deposits of the Noranda area. Exploration and Mining Geology, **3:** 131-160.

Barrett, T.J. and MacLean, W.H. 1994b Chemostratigraphy and hydrothermal alteration in exploration for VHMS deposits in greenstones and younger volcanic rocks. *In* Alteration and Alteration Processes Associated With Ore-Forming Systems. *Edited by* D.R. Lentz. Geological Association of Canada, Short Course Notes, v. 11, pp. 433-467.

Bell, K., Anglin, C. D. and Franklin, J. M. 1989. Sm-Nd and Rb-Sr isotope systematics of scheelites; possible implications for the age and genesis of vein-hosted gold deposits. Geology, **17:** 500-504.

Bevier, M.L. and Gebert, J.S. 1991. U-Pb geochonology of the Hope Bay-Elu Inlet area, Bathurst Block, northeastern Slave Structural Province, Northwest Territories. Canadian Journal of Earth Sciences, **28:** 1925-1930.

Bierlein, F.P. and Cartwright, I. 2001. The role of carbonaceous "indicator" slates in the genesis of lode gold mineralization in the western Lachlan Orogen, Victoria, Southeastern Australia. Economic Geology, **96:** 431-450

Blackburn, W.H. and Dennen, W.H. 1969. Harrisitic structure in the gabbro at Nahant, Massachusetts. The Canadian Mineralogist, **10:** 126-127.

Bleeker, W., Ketchum, J.W.F. 1998. Central Slave Basement Complex, Northwest Territories: its autochthonous cover, d´ecollement, and structural topology. *In* Current Research, 1998-C. Geological Survey of Canada, pp. 9–19.

Bleeker, W., Ketchum, J.W.F., Jackson, V.A., Villeneuve, M.E. 1999a. The Central Slave Basement Complex, Part I: its structural topology and autochthonous cover. Canadian Journal of Earth Sciences, **36**: 1083–1109.

Bleeker,W., Ketchum, J.W.F., Davis,W.J. 1999b. The Central Slave Basement Complex, Part II: age and tectonic significance of high-strain zones along the basement/cover contact. Canadian Journal of Earth Sciences, **36:** 1111–1130.

Bleeker, W. 2002. Archean tectonics: a review, with illustrations from the Slave craton. *In* The Early Earth: Physical, Chemical and Biological Development. *Edited by* C.M.R. Fowler, C.J. Ebinger and C.J. Hawkesworth. Geological Society Special Publications 199, pp. 151-181.

Bleeker, W. 2003. The late Archean record: a puzzle in ca. 35 pieces. Lithos, **71:** 99-134.

Bleeker, W., Ketchum, J., Davis, B., Sircombe, K., Stern, R., and Waldron, J. 2004. The slave craton from on top: the crustal view. *In* The Lithoprobe Celebratory Conference: From Parameters to Processes - Revealing the Evolution of a Continent. Abstract, 5p.

Callan, N.C. and Spooner, E.T.C. 1989. Archean Au quartz vein mineralization hosted in a tonalite-trondhjemite terrane, Renabie Mine area, Wawa, North Ontario, Canada. Economic Geology Monographs, **6:** 9-18.

Campbell, F.H.A. 1978. Geology of the Helikian rocks of the Bathurst Inlet area, Northwest Territories. *In* Current Research, Part A. Geological Survey of Canada, paper 78-1A, pp. 97-106.

Campbell, F.H.A. 1979. Stratigraphy and sedimentation in the Helikian Elu Basin and Hiukitak Platform, Bathurst Inlet-Melville Sound, Northwest Territories. Geological Survey of Canada, paper 79-8, 18p.

Campbell, F.H.A and Cecile, M.P. 1976a. Geology of the Kilohigok Basin, Goulburn Group, Bathurst Inlet, District of Mackenzie, N.W.T. *In* Report of Activities, Part A, Geological Survey of Canada, paper 76-1A, pp. 369-377.

Campbell, F.H.A. and Cecile, M.P. 1976b. Geology of the Kilohigok Basin. Geological Survey of Canada, Open File Map 332, 1:500 000 scale, 1 sheet.

Campbell, F.H.A and Cecile, M.P. 1981. Evolution of the early Proterozoic Kilohigok Basin, Bathurst Inlet-Victoria Island, Northwest Territories. *In* Proterozoic Basins of Canada. *Edited by* F.H.A. Campbell. Geological Survey of Canada, paper 81-10, pp. 103-131.

Carpenter, R.L. 2001. Summary of geological work on the Naartok gold deposit and environs (July-August 2001), Hope Bay Greenstone Belt, Kitikmeot District, Nunavut. Prepared for Adrian Fleming, Hope Bay Joint Venture, 14p.

Carpenter, R.L. and Sherlock, R.S. 2001. Preliminary geochemical analysis of volcanic rocks in the Wolverine-Madrid corridor. Department of Indian and Northern Affairs Canada - Nunavut Minerals Section, 12p.

Carpenter, R.L., Sherlock, R.S., Quang, C., Kleespies, P. and McLeod, R. 2003. Geology of the Doris North gold deposits, northern Hope Bay volcanic belt, Slave Structural Province, Nunavut. Geological Survey of Canada, Current Research 2003-C6, 10p.

Capdevilar, R., Arndt, N., Letendre, J. and Sauvage, J.F. 1999. Diamonds in volcaniclastic komatiite from French Guiana. Nature, **399:** 456–458.

Clark, D.B. 1996. The geology of the Boston deposit, Hope Bay Volcanic Belt, Northwest Territories, Canada. Unpublished M.Sc. thesis, Queen's University, Kingston, Ontario, 94p.

Coad, P.R., Brisbin, D.I., Labine, R.J., and Roussain, R. 2000. Geology of the Owl Creek gold mine, Timmins, Ontario. Exploration and Mining Geology, **7:** 271-286.

Cox, S.F., Wall, V.J., Etheridge, M.A., Potter, T.F. 1991. Deformation and metamorphic processes in the formation of mesothermal vein-hosted gold deposits - examples from the Lachlan Fold Belt in central Victoria, Australia. Ore Geology Reviews, **6:** 391-423
.
Davis W.J. and Hegner E. 1992. Neodymium isotopic evidence for the tectonic assembly of Late Archean crust in the Slave province, northwest Canada. Contributions to Mineralogy and Petrology, **111:** 493-504.

Davis, W.J. and Bleeker, W. 1999. Timing of plutonism, deformation, and metamorphism in the Yellowknife Domain, Slave Province, Canada. Canadian Journal of Earth Sciences, **36:** 1169–1187.

Deer, W.A., Howie, R.A. and Zussman, J. 1992. An Introduction to the Rock Forming Minerals. Pearson Education Limited, Essex, England.

Donaldson, C.H. 1982a. Origin of the Rhum harrisite by segregation of intercumulus liquid. Mineralogical Magazine, **45:** 201-209.

Donaldson, C.H. 1982b. Spinifex-textured komatiites: a review of textures, compositions and layering. *In* Komatiites. *Edited by* N.T Arndt and E.G. Nisbet. George Allen and Unwin, pp. 213-245.

Downes, M.J., Hodges, D.J. and Derweduwen, J. 1984. A free carbon-and carbonate-bearing alteration zone associated with the Hoyle Pond gold occurrence, Ontario, Canada. *In* Gold '82. The Geology, Geochemistry and Genesis of Gold Deposits. *Edited by* R.P. Foster. Rotterdam, A.A. Balkema, pp. 435-448.

Drummond, S.E. and Ohmoto, H. 1985. Chemical evolution and mineral deposition in boiling hydrothermal systems. Economic Geology, **81:** 979-983.

Fiala, F. 1974. Some notes on the problem of spilites. *In* Spilite and Spilitic Rocks. *Edited by* G.C. Amstutz. Springer-Verlag, pp. 9-22.

Fraser, J.A.1964. Geological notes on northeastern District of Mackenzie, Northwest Territories. Geological Survey of Canada, Paper 63-40, 20p.

Fyson, W.K., and Helmstaedt, H. 1988. Structural patterns and tectonic evolution of supracrustal domains in the Archean Slave Province. Canadian Journal of Earth Sciences, **25:** 301-315.

Gale, G.H. and Pearce, J.A. 1982. Geochemical patterns in Norwegian greenstones. Canadian Journal of Earth Sciences, **19:** 385-397.

Gebert, J.S. 1989a. Preliminary mapping in the Hope Bay metavolcanic belt, Bathurst block, Slave province, NWT. Canada-NWT Mineral Development Agreement, 8p.

Gebert, J.S. 1989b. The geology of the Hope Bay and Elu Inlet metavolcanic belts northeastern Slave province, NWT. *In* Northwest Territories Geology Division Department of Indian Affairs and Northern Development, Exploration Overview 1989. Mining, Exploration and Geological Investigations, pp. 33-34.

Gebert, J.S. 1990a. Geology of the Hope Bay and Elu Inlet metavolcanic belts, Bathurst Block, northeastern Slave Province, N.W.T. *In* Northwest Territories Geology Division Department of Indian Affairs and Northern Development, Exploration Overview 1990: Mining, Exploration and Geological Investigations, pp. 26-27.

Gebert, J.S. 1990b. Hope Bay project. *In* GNWT-DIAND Geoscience Projects 1989, Annual Report, March 1990, Canada-Northwest Territories Mineral Development Agreement, pp. 21-27.

Gebert, J.S. 1992. Geology of the Hope Bay and Elu Inlet metavolcanic belts, northeastern Slave province, NWT. *In* Project Summaries, Canada-Northwest Territories Mineral Development Subsidiary Agreement 1987-1991. *Edited by* D.G. Richardson and M. Irving. Geological Survey of Canada Open File 2484, pp. 15-17.

Gebert, J.S. 1993. Geology and mineral potential of the Archean Hope Bay and Elu Inlet volcanic belts, Northeastern Slave Structural Province, District of Mackenzie, N.W.T. Northern Affairs Program, Northwest Territories Geology Division, EGS Paper 1993-1, 103p

Gebert, J.S. 1999. Hope Bay project, exploration overview. Unpublished summary report, BHP minerals, 367p.

Gemmell, J.B. and Fulton, R. 2001. Geology, genesis, and exploration implications of the footwall and hanging-wall alteration associated with the Hellyer volcanic hosted massive sulfide deposit, Tasmania, Australia. Economic Geology, **96:** 1003-1035.

Getsinger, J.S. 1997. Petrographic report on ten samples from the Madrid project area, Northwest Territories. Unpublished report for BHP Minerals Canada Ltd., 36p.

Gibbons, W.A. 1987. Preliminary geology of the central Hope Bay Volcanic Belt, northern portions of NTS 77A/3, 6. Northern Affairs Program, Northwest Territories Geology Division, EGS Paper 1987-12, 1:50,000 scale geology map with marginal notes.

Green, D.H. 1975. Genesis of Archean peridotitic magmas and constraints on Archean geothermal gradients and tectonics. Geology, **3:** 15-18.

Grunsky, E.C., Easton, R.M., Thurston, P.C. and Jensen, L.S. 1992. Characterization and statistical classification of Archean volcanic rocks of the Superior Province using major element geochemistry. *In* Geology of Ontario. *Edited by* P.C. Thurston, H.R. Williams, R.H. Sutcliffe and G.M. Stott. Ontario Geological Survey Special Volume 4, 1397-1438.

Guidotti, C.V. 1984. Micas in metamorphic rocks. Reviews in Mineralogy, **13:** 357-467.

Hayashi, K.I. and Ohmoto, H. 1991. Solubility of gold in NaCl- and H_2S-bearing aqueous solutions at 250-350^{o}C. Geochimica et Cosmochimica Acta, **55:** 2111-2126.

Hebel, M.U. 1999. U-Pb geochonology and lithogeochemistry of the Hope Bay greenstone belt, Slave Structural Province, Northwest Territories, Canada. Unpublished M.Sc. thesis, University of British Columbia, 95p.

Helmstaedt, H., Padgham, W.A. and Brophy, J.A. 1986. Multiple dykes in lower Kam Group, Yellowknife Greenstone Belt: Evidence for Archean seafloor spreading? Geology, **14:** 562-566.

Henderson, J.B. 1970. Stratigraphy of the Archean Yellowknife Supergroup, Yellowknife Bay-Prosperous Lake area, District of MacKenzie (85 J/8, J/9). Geological Survey of Canada, Paper 70-26, 12p.

Henderson, J.B. 1981. Archean basin evolution in the Slave Province, Canada. *In* Precambrian Plate Tectonics. *Edited by* A. Kroner A. Elsevier, Amsterdam, pp. 213-235.

Henderson, J.B. 1985. Geology of the Yellowknife-Hearne Lake area, District of Mackenzie: a segment across an Archean basin. Geological Survey of Canada Memorandum, **414:** 135p.

Henderson, J.B., McGrath, P.H., Theriault, R.J. and van Breeman, O. 1990. Intracratonic indentation of the Archean Slave Province into the Early Proterozoic Thelon Tectonic Zone of the Churchill Province, northwestern Canadian Shield. Canadian Journal of Earth Sciences, **27:** 1699-1713.

Hey, M.H. 1954. A new review of the chlorites. The Mineralogical Magazine, **30:** 277-292.

Hoffman, P.F. 1988. United plates of America, the birth of a craton. early Proterozoic assembly and growth of Laurentia. Annual Review of Earth and Planetary Sciences, **16:** 543-603.

Hoffman, P.F. and Bowring, S.A. 1984. Short-lived 1.9 Ga continental margin and destruction, Wopmay orogen, northwest Canada. Geology, **12:** 68-72.

Hollings, P. and Wyman, D. 1999. Trace element and Sm–Nd systematics of volcanic and intrusive rocks from the 3 Ga Lumby Lake greenstone belt, Superior Province: evidence for Archaean plume–arc interaction. Lithos, **46:** 189–213.

Isachsen, C.E. and Bowring, S.A. 1994. Evolution of the Slave craton. Geology, **22:** 917-920.

Isachsen, C.E. and Bowring, S.A. 1997. The Bell Lake group and Anton Complex: a basement-cover sequence beneath the Archean Yellowknife greenstone belt revealed and implicated in greenstone belt formation. Canadian Journal of Earth Sciences, **34:** 169–189.

Jakes, P and Gill, J. 1970. Rare earth elements and the island arc tholeiitic series. Earth and Planetary Science Letters, **9:** 17-28.

Jakes, P. and White, A.J.R. 1972. Major and trace element abundances in volcanic rocks of orogenic areas. Geological Society of America Bulletin, **83:** 29-39.

Jemiellta, R.A., Callan, N.J. and Spooner, E.T.C. 1988. Grant 288; Petrogenesis of Archean trondhjemite-tonalite-granodiorite (TTG) intrusions and their relationships to gold mineralization, Renabie and Magino areas, Wawa. Summary of Research 1987-1988, Ontario Geological Survey Miscellaneous Paper, 78-93.

Jensen, L.S. 1976. A new cation plot for classifying subalkalic volcanic rocks. Ontario Division of Mines, Miscellaneous Paper 66, 22p.

Jones, M.I. 1992. Variolitic basalts; relations to Archean epigenetic gold deposits in the Abitibi greenstone belt. Unpublished M.Sc. thesis, University of Ottawa, 320p.

Kerrich, R. 1983. Geochemistry of gold deposits in the Abitibi greenstone belt. Canadian Institute of Mining and Metallurgy, Special Volume 27, 75p.

Ketchum, J.W.F., Bleeker, W. 2000. New field and U–Pb data from the Central Slave Cover Group near Yellowknife and the Central Slave Basement Complex at Point Lake. *In* Slave-Northern Cordillera Lithospheric Experiment (SNORCLE) Transect Meeting, University of Calgary. *Compiled by* F. Cook and P. Erdmer. LITHOPROBE Report No. **72:** 27–31.

Ketchum, J.W.F., Bleeker, W. and Stern, R.A. 2004. Evolution of an Archean basement complex and its autochthonous cover, southern Slave Province, Canada. Precambrian Research, **135:** 149-176.

Kleespies, P. and Mercer, B. 2001. Naartok core re-examination memorandum. Unpublished summary report, Hope Bay Joint Venture.

Kusky, T.M., 1989. Accretion of the Archean Slave province. Geology, **17:** 63–67.

Leake, B.E. 1978. Nomenclature of amphiboles. Canadian Mineralogist, **16:** 501-520.

Leclair, S.G. 1990a. Interactions of granitoids and the gold mineralization Ida Point,

N.W.T. *In* GNWT-DIAND Geoscience Projects 1989, Annual Report, March 1990, Canada-Northwest Territories Mineral Development Agreement, pp. 21-27.

Leclair, S.G. 1990b. The Ida Point gold showing, Hope Bay greenstone belt, NWT. *In* Northwest Territories Geology Division-Department of Indian Affairs and Northern Development, Exploration Overview 1990, Mining, Exploration and Geological Investigations, pp. 35-36.

Leclair, S. G. 1990c. Tonalites and gold mineralization in an Arctic Archean Greenstone Belt, Hope Bay, NWT. Yellowknife Indian and Northern Affairs Canada, NWT Geology Division, 25p.

Leclair, S.G. 1991. Mineralization at the margin of a tonalitic intrusion: the Ida Point gold showing, Hope Bay greenstone belt, NWT. Yellowknife Indian and Northern Affairs Canada, NWT Geology Division, 58p.

Leclair, S.G. 1992. The Ida Point gold showing, Hope Bay greenstone belt, Northwest Territories. *In* Project Summaries, Canada Northwest Territories Mineral Development Subsidiary Agreement 1987-1991. *Edited by* D.G. Richardson and M. Irving. Geological Survey of Canada, Open File 2484, pp. 61-63.

Leol, H.B. 1985. Ocean-floor hydrothermal metamorphism as represented by spilites from Cyprus. Unpublished B.Sc. thesis, The University of Western Ontario, 113p.

Lindsay, D., Mercer, B., Kleespies, P., Light, J., Poulton, L., Figueiredo, M. Chang, F., Beck, R., Mann, R., McCartney, I., Kemp, R., Wakeford, J. 2003. Hope Bay Project, Miramar Hope Bay Ltd., Program Summary. Unpublished Miramar Report, 40p.

Lindsay, D.W. 1997. Madrid Deposit: Ore petrography of selected samples from the Discovery Zone. Unpublished BHP report, Jan 13, 42p.

Mann, R.K. 2003. Patch Lake project - Report on alteration and lithology derived from drillhole. Unpublished report to Miramar Hope Bay Ltd, 37p.

McGlynn, J.C. and Henderson, J.B. 1970. Archean volcanism and sedimentation in the Slave Structural Province. *In* Symposium on Basins and Geosynclines of the Canadian Shield. *Edited by* A.J. Baer. Geological Survey of Canada, Paper 70-40, pp. 31-44.

McGlynn, J.C. and Henderson, J.B. 1972. The Slave Province. *In* Variations in Tectonic Styles in Canada. Edited by R.A. Price and J.W. Douglas. Geological Association of Canada Special Paper 11, pp. 505-526.

Miramar Mining Corporation. 2003. Hope Bay Project. Retrieved August 15, 2005, from http://www.miramarmining.com/s/HopeBayProject.asp.

Morata, D., Higueras, P., Dominguez-Bella, S., Parras, J., Velasco, F. and Aparico, P. 2001. Fuchsite and other Cr-rich phyllosilicates in ultramafic enclaves from the Almadén mercury mining district, Spain. Clay minerals, **36:** 345-354.

Mueller, W.U., Corcoran, P.L. and Pickett, C. 2005. Mesoarchean continental breakup; evolution and inferences from the >2.8 Ga Slave Craton-cover succession, Canada. Journal of Geology, **113:** 23-45.

Mueller, W.U. and Pickett, C. 2005. Relative sea level change along the Slave Craton coastline; characteristics of Archean continental rifting. Sedimentary Geology, **176:** 97-119.

Mumin, A.H. and Fleet, M.E. 1995. Evolution of gold mineralization in the Ashanti Gold Belt, Ghana: evidence from carbonate compositions and parageneses. Mineralogy and Petrology, **55:** 265-280.

Mumin, A.H. 1994. Early Proterozoic Birimian gold mineralization of the Bogosu and Prestea districts of the Ashanti Gold Belt, Ghana, West Africa. Unpublished M.Sc. thesis, The University of Western Ontario, 312 p.

Naden, J. and Shepherd, T.J. 1989. Role of methane and carbon dioxide in gold deposition. Nature, **342:** 793-795.

Nesbitt, R.W. 1971. Skeletal crystal forms in the ultramafic rocks of the Yilgarn block, Western Australia: Evidence for an Archaean ultramafic liquid. Special Publication - Geological Society of Australia, **3:** 331-347.

Nesbitt, R.W., Sun, Shen-Su and Purvis, A.C. 1979. Komatiites: geochemistry and genesis. Canadian Mineralogist, **17:** 165-186.

Norman, D.I. and Blamey, N. 2005. Methane in Carlin-type gold deposit fluid inclusions. Goldschmidt Conference Abstracts 2005, p. A124.

Ohtani, E. 1984. Generation of komatiite magma and gravitational differentiation in the deep upper mantle. Earth and Planetary Science Letters, **67:** 251-272.

Ohtani, E. 1990. Majorite fractionation and the genesis of komatiites in the deep mantle. Precambrian Research, **48:** 195-202.

Ohtani, E., Kawabe, I., Moriyama, J. and Nagata, Y. 1989. Partitioning of elements between majorite garnet and melt and implications for petrogenesis of komatiite. Contributions to Mineralogy and Petrology, **103:** 263-269.

Padgham, W.A. 1992. The Slave Structural Province, North America: a discussion of tectonic models. *In* The Archean: Terranes, Processes and Metallogeny. *Edited by* J.E. Glover and S.E. Ho. University of Western Australia Publication, **22:** 381-394.

Padgham, W.A. and Fyson, W.K. 1992. The Slave Province; a distinct Archean craton. Canadian Journal of Earth Sciences, **29:** 2072-2086.

Papike, J. J., Cameron, K.L. and Baldwin, K. 1974. Amphibole and pyroxenes: Characterization of other than quadrilateral components and estimates of ferric iron from microprobe data. Abstracts with Programs, Geological Society of America, **6**: 1053-1054.

Pearce, J.A. and Cann, J.R. 1973. Tectonic setting of basic volcanic rocks determined using trace element analysis. Earth and Planetary Science Letters, **19**: 290-300.

Pearce, J.A. and Norry, M.J. 1979. Petrogenetic implications of Ti, Zr, Y, and Nb variations in volcanic rocks. Contributions to Mineralogy and Petrology, **69**: 33-47.

Pearce, J.A. 1982. Trace element characteristics of lavas from destructive plate boundaries. *In* Andesites. *Edited by* R.S. Thorpe. John Wiley and Sons, pp. 525-548.

Pearce, J.A., 1983. Role of the sub-continental lithosphere in magma genesis at active continental margins *In* Continental Basalts and Mantle Xenoliths. *Edited by* C.J. Hawkesworth and M.J. Norry. Shiva Geology Series, pp. 230-249.

Pearce, J.A. and Parkinson, I.J. 1993. Trace element models for mantle melting: application to volcanic arc petrogenesis. *In*. Magmatic Processes and Plate Tectonics. *Edited by* H.M. Prichard, T. Alabaster, N.B.W. Harris and C.R. Neary. Geological Society Special Publication No. 76, 373-403.

Pearce, J.A. 1995. Tectonic implications of the composition of volcanic arc magmas. Annual Review of Earth and Planetary Sciences, **23:** 251-285

Pearce, J.A. 1996. A user's guide to basalt discrimination diagrams. *In* Trace Element Geochemistry of Volcanic Rocks: Applications for Massive Sulphide Exploration. *Edited by* D.A. Wyman. Geological Association of Canada, Short Course Notes, v. 12, 79-113.

Polat, A., Kerrich, R. and Wyman, D.A. 1999. Geochemical diversity in oceanic komatiites and basalts from the late Archean Wawa greenstone belts, Superior Province, Canada: trace element and Nd isotope evidence for a heterogeneous mantle. Precambrian Research, **94:** 139-173.

Polat, A. and Kerrich, R. 2001. Geodynamic processes, continental growth, and mantle evolution recorded in late Archean greenstone belts of the southern Superior Province, Canada. Precambrian Research, **112:** 5-25.

Poulson, K.H. 2002a. Estimation of minimum CO_2 content of metamorphic and metasomatic rocks using whole rock analyses reporting only loss-on-ignition. Unpublished geological report to Hope Bay Joint Venture, February 4, 2002, 6p.

Poulson, K.H. 2002b. Structural geology field-work, northern Hope Bay belt, Unpublished memorandum to the Hope Bay Joint Venture, January 17, 2002, 4p.

Poulson, K.H. 2002c. Overview of 2002 geological work in the Hope Bay gold belt, Nunavut, Canada. Unpublished report to the Hope Bay Joint Venture, December 20, 2002, 18p.

Poulson, K.H. 2003a. March 18-22, 2003 site visit to the Hope Bay Project, Nunavut and the issue of lithogeochemical mapping. Unpublished report to Miramar Hope Bay Ltd., 21p.

Poulson, K.H. 2003b. Summer 2003 field work in the Hope Bay Gold Belt, Nunavut, Canada. Unpublished report to Miramar Hope Bay Ltd., 12p.

Poulson, K.H. 2004. An assessment of the structural geology in the area around the Madrid Gold Deposit, Hope Bay Belt, Nunavut, Canada. Unpublished report to Miramar Mining Corporation, 7p.

Powell, R., Condliffe, D.M. and Condliffe, E. 1984. Calcite-dolomite geothermometry in the system $CaCO_3$-$MgCO_3$-$FeCO_3$: an experimental study. Journal of Metamorphic Geology, **2:** 33-41.

Purvis, A.C. 1978. The geochemistry and metamorphic petrology of the southern Cross-Forrestania greenstone belt at Digger's Rocks, Western Australia. Unpublished Ph.D thesis, University of Adelaide, Australia.

Pyke, D.R., Naldrett, A.J. and Eckstrand, A.R. 1973. Archean ultramafic flows in Munro Township, Ontario. Bulletin of the Geological Society of America, **84:** 955-978.

Reid, D.F. 1987. Final report on the Hope Bay Project 1987 Exploration Program, NTS sheets 77 A-3/A-6, District of Mackenzie, Northwest Territories. Report No. 16-87, December, 1987.

Reid, W. and Gerakiteys, C. 1998. The Hope Bay Volcanic Belt alteration atlas. Unpublished report for BHP minerals, 172p.

Robert, F. 1997. A preliminary geological model for syenite-associated disseminated gold deposits in the Abitibi Belt, Ontario and Quebec. Geological Survey of Canada, Current Research, 1997-C, 10p.

Robert, F. 2001. Syenite-associated disseminated gold deposits in the Abitibi greenstone belt, Canada. Mineralium Deposita, **36:** 503-516.

Romberger, S.B. 1986a. The solution geochemistry of gold applied to the origin of hydrothermal deposits. *In* Gold in the Western Shield. *Edited by* L.A. Clark. Montreal, Canadian Institute of Mining and Metallurgy Special Volume 38, pp. 168-186.

Romberger, S.B. 1986b. Ore deposit models No. 9. Disseminated gold deposits. Geoscience Canada, **13**: 23-31.

Romberger, S.B. 1990. Transport and deposition of gold in hydrothermal systems. *In* Greenstone Belts and Crustal Evolution. *Edited by* F. Robert, P.A. Shearan and S.B. Green. NUNA conference volume, Val d'Or, Montreal. Geological Association of Canada, p. 61-66.

Schaefer, S.J. and Morton, P. 1991. Two komatiitic pyroclastic units, Superior Province, northwestern Ontario: their geology, petrography, and correlation. Canadian Journal of Earth Sciences, **28:** 1455-1470.

Seward, T.M. 1973. Thiocomplexes of gold and the transport of gold in hydrothermal solutions. Geochemica et Cosmochimica Acta, **37:** 379-399.

Seward, T.M. 1984. The transport and deposition of gold in hydrothermal systems. *In* Gold '82. The Geology, Geochemistry and Genesis of Gold Deposits. *Edited by* R.P. Foster. Rotterdam, A.A. Balkema, pp. 165-182.

Seward, T.M. 1991. The hydrothermal geochemistry of gold. *In* Gold Metallogeny and Exploration. *Edited by* R.P.Foster. Blackie, London, pp. 37-62.

Sharkov, E.V. and Smolkin, V.F. 1997. The early Proterozoic Pechenga-Varzuga Belt: a case of Precambrian back-arc spreading. Precambrian Research, **82:** 133-151.

Shau, Y.H., Feather, M.E., Essene, E.J. and Peacor, D.R. 1991. Genesis and solvus relations of submicroscopically intergrown paragonite and phengite in a blueschist from northern California. Contributions to Mineralogy and Petrology, **106:** 367-378.

Shenberger, D.M. and Barnes, H.L. 1989. Solubility of gold in aqueous sulfide solutions from 150 to 350^{o}C. Geochimica et Cosmochimica Acta, **53:** 269-278.

Sherlock, R.L., Carpenter, R.L., Bardoux, M., Flood, E. and Kleespies, P. 2002. Volcanic relationships and gold mineralization in the Wolverine-Madrid corridor, Hope Bay Volcanic Belt, Nunavut. Geological Survey of Canada, Current Research 2002-C9, 11p.

Sherlock, R.S. and Lindsay, D.W. 2002. Volcanic stratigraphy of the QSP area, Hope Bay volcanic belt, Nunavut. Geological Survey of Canada, Current Research 2002-C8, 9p.

Sherlock, R.L. and Carpenter, R.L. 2003. Bedrock geology of the Wolverine-Doris corridor, northern Hope Bay Volcanic Belt. GSC open file 1553, 1 sheet.

Sherlock, R.L., Carpenter, R.L., and Quang, C. 2003. Volcanic stratigraphy, structural geology, and gold mineralization in the Wolverine-Doris corridor, northern Hope Bay Volcanic Belt, Nunavut. Geological Survey of Canada, Current Research 2003-C7, 11p.

Sherlock, R.L. and Sandeman, H.A. 2004a. Volcanic stratigraphy and structural geology of the area of the Boston gold deposit, Hope Bay Volcanic Belt, Nunavut. Geological Survey of Canada, Current Research, no. 2004-C2, 11p.

Sherlock, R.L. and Sandeman, H.A. 2004b. Volcanic stratigraphy and structural geology of the Boston area, Hope Bay Volcanic Belt, Nunavut. Geological Survey of Canada, Open File 4601, 1 sheet.

Simpson, R. 2001. 2001 oriented core memo. Unpublished memorandum to the Hope Bay Joint Venture, July 11, 159p.

Skilling, I.P., White, J.D.L., McPhie, J. 2002. Peperite: a review of magma-sediment mingling. *In* Peperite: Processes and Products of Magma-Sediment Mingling. *Edited by* I.P. Skilling, J.D.L. White and J. McPhie. Journal of Volcanology and Geothermal. Research, **114:** 1-17.

Springer, J.S. 1983. Invisible Gold. *In* The Geology of Gold in Ontario. *Edited by* A.C. Colvine. Ontario Geological Survey Miscellaneous Paper 110, 240-250.

Springer, J.S. 1985. Carbon in Archean rocks of the Abitibi belt (Ontario-Quebec) and its relation to gold distribution. Canadian Journal of Earth Sciences, **22**: 1945-1951.

Sproule, R.A., Lesher, C.M., Ayer, J.A., Thurston, P.C. and Herzberg, C.T. 2002. Spatial and temporal variations in the geochemistry of komatiites and komatiitic basalts in the Abitibi greenstone belt. Precambrian Research, **115:** 153-186.

Stemler, J.U. 2000. A fluid inclusion and stable isotopic examination of the Boston greenstone belt hosted, Archean lode gold deposit, Hope Bay volcanic belt, Nunavut, Canada. Unpublished M.Sc. thesis, University of Alberta, 212p.

Stewart, P. 1992. The origin of the Hope Brook Mine, Newfoundland; a shear zone-hosted acid sulphate gold deposit. Unpublished Ph.D. thesis, The University of Western Ontario, 752p.

Stone, W.E. 1985. Geochemistry of the Boston Flow Fe-rich komatiite, Kirkland Lake area, northeastern Ontario. Unpublished M.Sc. thesis, The University of Western Ontario, 199p

Stone, W.E., Jensen, L.S. and Church, W.R. 1987. Petrography and geochemistry of an unusual Fe-rich basaltic komatiite from Boston Township, northeastern Ontario. Canadian Journal of Earth Sciences, **24:** 2537-2550.

Stone, W.E. 1988. Nature and significance of metamorphism in gold concentration, Bousquet Township, Abitibi greenstone belt, Northwest Quebec. Unpublished Ph.D. thesis, The University of Western Ontario, 441p.

Stone, W.E., Crocket, J.H. and Fleet, M.E. 1995. Differentiation processes in an unusual iron-rich alumina-poor Archean ultramafic/mafic igneous body, Ontario. Contributions to Mineralogy and Petrology, **119:** 287-300.

Stone, W.E., Deloule, E., Larson, M.S. and Lesher, C.M. 1997. Evidence for hydrous high-MgO melts in the Precambrian. Geology, **25:** 143-146.

Stubley, M. 2002. Bedrock geology of the Discovery-Twin Peaks area, Hope Bay Volcanic Belt, Slave craton. Unpublished report to Miramar Hope Bay Ltd., December 2002, 39p.

Sun, S.S. and McDonough, W.F. 1989. Chemical and isotopic systematics of oceanic basalts; implications for mantle composition and processes. Geological Society Special Publications, **42:** 313-345.

Theriault, R.D. and Fowler, A.D. 1995. Harrisitic textures in the Centre Hill complex, Munro Township, Ontario: product of diffusion limited growth. Mineralogy and Petrology, **54:** 35-44.

Therriault, R.G. 2003. The metallogeny of gold-bearing banded iron formation on the margins of the Crazy Bear Metamorphic Complex, Bathurst Inlet, Nunavut. Unpublished B.Sc. thesis, The University of Western Ontario, 73p.

Thompson, P.H. 1978. Archean regional metamorphism in the Slave structural province – A new perspective on some old rocks. *In* Metamorphism in the Canadian Shield, Geological Survey of Canada, Paper 78-10, pp. 85-102.

Thompson, P.H. and Henderson, J.B. 1983. Polymetamorphism in the Healey Lake map area - implications for the Thelon Tectonic Zone. *In* Geological Survey of Canada, Current Activities Forum 1983, Program with Abstracts, Geological Survey of Canada, Paper 83-8, pp. 2.

Thompson, P.H. and Ashton, K. 1984. Preliminary report on the geology of the Tinney Hills-Overby Lake (west half) map area, District of Mackenzie: a look at the Thelon Tectonic Zone northeast of the Bathurst Fault. *In* Current Research, Part A, Geological Survey of Canada, paper 84-1A, pp. 415-423.

Thompson, P.H., Culshaw, N., Thompson, D.L. and Buchanan, J.R. 1985. Geology across the western boundary of the Thelon Tectonic Zone in the Tinney Hills-Overby Lake (west half) map area, District of Mackenzie. *In* Current Research, Part A, Geological Survey of Canada, paper 85-1A, pp. 555-572.

Thompson, P.H., Culshaw, N., Buchanan, J.R. and Manojlovic, P. 1986. Geology of the Slave Province and Thelon Tectonic Zone in the Tinney Hills-Overby Lake (west half) map area, District of Mackenzie. *In* Current Research, Part A, Geological Survey of Canada, paper 86-1A, pp. 275-289.

Thompson, P.H. 1996. Regional geology of Archean granitoid rocks adjacent to the Hope Bay Volcanic Belt, northeastern Slave province, Canadian Shield. Unpublished report to BHP Minerals, 39p.

Thompson, P. H. 1997. Regional geology of Archean granitoid rocks adjacent to the Hope Bay and Elu Inlet volcanic belts, northeastern Slave structural province, Canadian Shield. Unpublished report to BHP Minerals, November 12, 1997, 58p.

Thorpe, R.I. 1972. Interpretation of lead isotope data for base metal and gold deposits, Slave Province, Northwest Territories. *In* Report of Activities, Geological Survey of Canada, Paper 72-1B, pp. 72-77.

Thorpe, R.I. 1982. Lead isotope evidence regarding Archean and Proterozoic metallogeny in Canada. Revista Brasileira de Geociencias, **12:** 510-521.

Thorpe, R.I., Cumming, G.L. and Mortensen, J.K. 1992. A significant Pb-isotope boundary in the Slave province and its probable relation to ancient basement in the western Slave province. *In* Project Summaries, Canada-Northwest Territories Mineral Development Subsidiary Agreement 1987–1991. *Edited by* D.G. Richardson and M. Irving. Geological Survey of Canada, Open File 2484, pp. 179–184.

Tomlinson, K.Y., Hughes, D. J., Thurston, P. C. and Hall, R. P. 1999. Plume magmatism and crustal growth at 2.9 to 3.0 Ga in the Steep Rock and Lumby Lake area, Western Superior Province. Lithos, **46:** 103–136.

Tourigny, G., Doucet, D., Bourget, A. 1993. Geology of the Bousquet 2 mine; an example of a deformed, gold-bearing, polymetallic sulfide deposit. Economic Geology, **88:** 1578-1597.

Tyler, T. 1997. The lithogeochemical and petrographic analysis of altered Archean greenschist rocks associated with three gold-bearing vein systems in the Hope Bay volcanic belt, northeastern Slave Structural Province, Northwest Territories. Unpublished B.Sc. thesis, University of Calgary, 33p.

van Breemen, O., Davis, W.J. and King, J.E. 1992. Temporal distribution of granitoid plutonic rocks in the Archean Slave Province, northwest Canadian Shield. Canadian Journal of Earth Sciences, **29:** 2186–2199.

van Breeman, O., Thompson, P.H., Hunt, P.A. and Culshaw, N. 1987. U-Pb zircon and monazite geochronology from the northern Thelon Tectonic Zone, District of Mackenzie. *In* Radiogenic age and isotope studies: Report 1. Geological Survey of Canada Paper 87-2, pp. 81-93.

Wadsworth, W.J. 1961. The layered ultrabasic rocks of south-west Rhum, Inner Hebrides. Philosophical Transactions of the Royal Society of London, Series B: Biological Sciences, **244:** 21-64.

Wilson, G.C and Rucklidge, J.C. 1986. Grant 262: Lithological features and economic significance of reduced carbonaceous rocks in gold deposits. Ontario Geological Survey Miscellaneous Paper 130, 177-189.

Wilson, G.C. and Rucklidge, J.C. 1987. Mineralogy and microstructures of carbonaceous gold ores. Mineralogy and Petrology, **36:** 219-239.

Winchester, J.A. and Floyd, P.A. 1976. Geochemical magma type discrimination: application to altered and metamorphosed basic igneous rocks. Earth and Planetary Science Letters, **28**: 459-469.

Winchester, J.A. and Floyd, P.A. 1977. Geochemical discrimination of different magma series and their differentiation products using immobile elements. Chemical Geology, **20:** 325-343.

Wright, G.M. 1957. Geological notes on eastern District of Mackenzie, Northwest Territories. Geological Survey of Canada, paper 56-10, 23p.

Wright, G.M. 1967. Geology of the southeastern barren grounds, parts of the Districts of Mackenzie and Keewatin (Operations Keewatin, Baker, Thelon). Geological Survey of Canada, Memoir 350, 91p.

Xie, Q., Kerrich, R. and Fan, J. 1993. HFSE/REE fractionations recorded in three komatiite-basalt sequences, Archean Abitibi greenstone belt: Implications for multiple plume sources and depths. Geochimica et Cosmochimica Acta, **57:** 4111-4118.

Yund, R.A. 1962. The system Ni-As-S: phase relations and mineralogical significance. American Journal of Science, **260**: 761-782.